UNIVERSIDADE FEDERAL DE MINAS GERAIS
INSTITUTO DE CIÊNCIAS BIOLÓGICAS

DEPARTAMENTO DE MICROBIOLOGIA

PROGRAMA DE PÓS-GRADUAÇÃO EM MICROBIOLOGIA

TESE DE DOUTORADO

INTERAÇÕES ENTRE VÍRUS GIGANTES E PROTOZOÁRIOS: CARACTERIZAÇÃO DO TUPANVIRUS SODA LAKE E DO CEDRATVIRUS GETULIENSIS

LUDMILA KAREN DOS SANTOS SILVA

Belo Horizonte
2018

LUDMILA KAREN DOS SANTOS SILVA

INTERAÇÕES ENTRE VÍRUS GIGANTES E PROTOZOÁRIOS: CARACTERIZAÇÃO DO TUPANVIRUS SODA LAKE E DO CEDRATVIRUS GETULIENSIS

Tese de doutorado apresentada ao Programa de Pós-Graduação em Microbiologia do Instituto de Ciências Biológicas da Universidade Federal de Minas Gerais, como requisito parcial para a obtenção do **título de Doutor em Microbiologia.**

Orientador: Dr. Jônatas Santos Abrahão

Coorientadores: Dr. Cláudio Antônio Bonjardim e Dr. Jonas Dutra Albarnaz

Belo Horizonte
2018

043 Silva, Ludmila Karen dos Santos.
Interações entre vírus gigantes e protozoários: caracterização do tupanvirus soda lake e do cedratvirus getuliensis [manuscrito] / Ludmila Karen dos Santos Silva. – 2018.

226 f. : il. ; 29,5 cm.

Orientador: Dr. Jônatas Santos Abrahão. Coorientadores: Dr. Cláudio Antônio Bonjardim, Dr. Jonas Dutra Albarnaz.
Tese (doutorado) – Universidade Federal de Minas Gerais, Instituto de Ciências Biológicas.

1. Microbiologia. 2. Mimiviridae. 3. Vírus - Isolamento. 4. Replicação Viral. 5. Interações Hospedeiro-Patógeno. I. Abrahão, Jônatas Santos. II. Bonjardim, Cláudio Antônio. III. Albarnaz, Jonas Dutra. IV. Universidade Federal de Minas Gerais. Instituto de Ciências Biológicas. V. Título.

CDU: 579

Ficha Catalográfica elaborada pela Biblioteca do Instituto de Ciências Biológicas

DEDICATÓRIA

Aos meus pais,

pelo amor, pela paciência e

pela sabedoria que não se encontra em livros.

EPÍGRAFE

"— Adeus, disse ele...

— Adeus, disse a raposa. Eis o meu segredo. É muito simples: só se vê bem com o coração. O essencial é invisível para os olhos.

— O essencial é invisível para os olhos, repetiu o principezinho, a fim de se lembrar.

— Foi o tempo que perdeste com tua rosa que fez tua rosa tão importante.

— Foi o tempo que eu perdi com a minha rosa... repetiu o principezinho, a fim de se lembrar.

— Os homens esqueceram essa verdade, disse a raposa. Mas tu não a deves esquecer. Tu te tornas eternamente responsável por aquilo que cativas. Tu és responsável pela rosa...

— Eu sou responsável pela minha rosa... repetiu o principezinho, a fim de se lembrar."

Antoine de Saint-Exupéry

AGRADECIMENTOS

À Deus, que esteve comigo em todas as horas que precisei;

À minha família pelo amor incondicional;

À minha mãe pela motivação constante, pelas palavras de carinho e por ser meu exemplo de força e determinação;

Ao meu pai por sempre acreditar em mim e por nunca medir esforços para me ajudar a alcançar meus sonhos;

Aos meus irmãos, meus exemplos de luta e sucesso na vida;

À Julinha, que acabou de chegar para fazer meu mundo ter mais gosto de inocência;

Ao Greg e meus amigos, pelo amor e companheirismo;

Ao meu orientador, Jônatas, por ter me dado a oportunidade de realizar esse trabalho e por acreditar no meu potencial. Obrigada pelo café e pelo croissant após toda reunião de quarta-feira em Marseille. O seu apoio foi essencial para me ajudar a vencer os osbtáculos impostos;

Ao professor Bernard La Scola, pela supervisão durante o doutorado sanduíche e aos colegas do Laboratório de Culturas Especias da Aix-Marseille Univesrité;

Aos meus coorientadores, Cláudio e Jonas, pelo apoio durante o desenvolvimento dessa tese;

Aos amigos do GEPVIG, por me ensinarem o verdadeiro significado de trabalho em grupo.

Aos colegas de profissão do Laboratório de Vírus;

Aos professores do Laboratório de Vírus, Erna, Paulo, Giliane e Betânia, pelo aprendizado;

Ao Centro de Microscopia da UFMG pelo ótimo trabalho prestado e pela excelente qualificação profissional de todos os funcionários;

À banca avaliadora pela disponibilidade e por colaborar na fase final desse trabalho.

Às agências de fomento, CAPES, CNPq E FAPEMIG pelo auxílio financeiro que permitiu a realização desse trabalho;

Obrigada!

SUMÁRIO

LISTA DE FIGURAS **12**

LISTA DE TABELAS **15**

LISTA DE SIGLAS E ABREVIATURAS **16**

RESUMO..... ..... **18**

ABSTRACT.... ..... **19**

1. INTRODUÇÃO **20**

1.1. Vírus Grandes Núcleo-citoplasmáticos de DNA (NCLDVs) 20

1.2. Descoberta dos mimivírus e a família *Mimiviridae* 24

1.3. Acanthamoeba polyphaga mimivirus (APMV) 26

1.3.1. Estrutura 27

1.3.2. Genoma 28

1.3.3. Ciclo de multiplicação 29

1.4. Diversidade de outros vírus gigantes 31

1.5. Isolamento de vírus gigantes no Brasil 38

1.6. Cedratvirus getuliensis 40

1.7. Tupanvírus 41

1.7.1. Descoberta 41

1.7.2. Estrutura 43

1.7.3. Espectro de hospedeiros e ciclo de multiplicação 44

1.7.4. Genoma e aparato traducional 45

1.8. Amebas de vida livre e outros protozoários 47

1.9. Interações entre vírus gigantes e protozoários 50

1.10. Ribofagia: autofagia de ribossomos 52

2. JUSTIFICATIVA **54**

3. OBJETIVOS **55**

3.1. Objetivo geral 55

3.2. Objetivos específicos..... 55

3.2.1. Investigação do shutting down do RNA ribossomal e da presença de sequências ribossomais em tupanvírus..... 55

3.2.2. Caracterização do ciclo de multiplicação do cedratvirus getuliensis..... 55

4. FLUXOGRAMA 57

5. MATERIAIS E MÉTODOS 58

5.1. Investigação do shutting down do RNA ribossomal e da presença de sequências ribossomais em tupanvírus..... 58

5.1.1. Investigação do shutting down do RNA ribossomal..... 58

5.1.1.1. Sistema celular 58

5.1.1.2. Vírus 59

5.1.1.3. Multiplicação e purificação viral..... 59

5.1.1.4. Titulação viral 60

5.1.1.5. Ensaios para reprodução e avaliação da ocorrência do shutting down 60

5.1.1.6. Extração de RNA e fracionamento eletroforético em gel de agarose 61

5.1.1.7. Transcrição reversa e qPCR..... 61

5.1.1.8. Ensaios com inibidores de acidificação..... 62

5.1.1.9. Silenciamento gênico do gene Atg8..... 62

5.1.1.10. Análise da acidificação celular..... 63

5.1.1.11. Análise das mudanças celulares ocorridas durante o *shutdown*..... 64

5.1.2. Investigação da presença e caracterização de sequências ribossomais em tupanvirus..... 64

5.1.2.1. Avaliação dos Best hits..... 65

5.1.2.2. Análise de vizinhança e de regiões imediatamente adjacentes 65

5.1.2.3. Avaliação da expressão..... 65

5.2. Caracterização do ciclo de multiplicação do cedratvirus getuliensis..... 67

5.2.1. Sistema celular 67
5.2.2. Vírus 67
5.2.3. Multiplicação e purificação viral 67
5.2.4. Infecção para análise do ciclo de multiplicação 68
5.2.5. Microscopia eletrônica de transmissão 68
5.2.6. Microscopia eletrônica de varredura 69
5.2.7. Ensaios de penetração viral 69
5.2.8. Ensaio de tráfego de membrana 70
6. RESULTADOS 71
6.1. Investigação do shutting down do RNA ribossomal e da presença de sequências ribossomais em tupanvírus 71
6.1.1. Investigação do shutting down do RNA ribossomal 71
6.1.1.1. Avaliação da reprodução e ocorrência do *shutdown* 71
6.1.1.2. Avaliação da ação de inibidores na ocorrência do *shutdown* 74
6.1.1.3. Análise do papel do gene Atg8 no *shutdown* 75
6.1.1.4. Investigação de alterações no pH amebiano durante a infecção por tupanvírus 78
6.1.1.5. Investigação de alterações citoplasmáticas e nucleares durante o *shutdown* 80
6.1.2. Investigação da presença e caracterização de sequências ribossomais em tupanvírus 84
6.1.2.1. Presença de sequências 18S-like em tupanvirus 84
6.1.2.2. Avaliação dos best hits 84
6.1.2.3. Análise de vizinhança e de regiões imediatamente adjacentes 88
6.1.2.4. Análise da expressão das cópias 1 e 2 89
6.2. Caracterização do ciclo de multiplicação do cedratvirus getuliensis 92
6.2.1. Ação de diferentes inibidores na penetração de cedratvirus getuliensis 93

6.2.2. Caracterização da fábrica viral de cedratvirus getuliensis e observação de outras mudanças celulares..... 94

6.2.3. Morfogênese das partículas virais de cedratvirus getuliensis..... 95

6.2.4. Caracterização da progênie viral..... 97

6.2.5. Liberação das partículas virais ao final do ciclo de multiplicação 99

7. DISCUSSÃO..... 101

8. CONCLUSÕES 112

9. REFERÊNCIAS BIBLIOGRÁFICAS 114

10. ANEXOS..... 126

10.1. Anexo I – Preparação de solução PAS..... 126

10.2. Anexo II – Preparação de meio NEFF 126

10.3. Anexo III – Preparação do meio PYG 127

10.4. Anexo IV – Tabela best hits das cópias 1 e 2 127

10.4.1. Cópia 1 127

10.4.2. Cópia 2 134

11. DISCIPLINAS E PRODUÇÃO CIENTÍFICA 138

11.1. Disciplinas cursadas durante o doutorado 136

11.2. Trabalhos apresentados em eventos científicos.....136

11.3. Artigos publicados relacionados a tese de doutorado 139

11.4. Outros artigos publicados durante o doutorado 185

LISTA DE FIGURAS

Figura 1: Ilustração esquemática evidenciando a retenção de vírus gigantes por filtros de 0,2 μm..... 23
Figura 2: Redefinição da classificação dos vírus. 23
Figura 3: APMV, inicialmente chamado de Coco de Bradford, no interior de uma ameba de vida livre..... 24
Figura 4: Imagem de microscopia eletrônica de transmissão do mimivírus. 25
Figura 5: Gêneros e linhagens que compõem a família *Mimiviridae*..... 26
Figura 6: Organização das camadas da partícula viral de APMV. 27
Figura 7: Estrutura do star-gate dos mimivírus..... 28
Figura 8: Ciclo de multiplicação do APMV em ameba..... 30
Figura 9: Imagens de microscopia eletrônica de transmissão evidenciando fusão da membrana interna viral com a membrana do fagossomo e a semente viral..... 30
Figura 10: Imagens de microscopia eletrônica das fábricas virais dos mimivírus..... 31
Figura 11: Imagens de microscopia eletrônica de partículas de Marseillevirus marseillevirus. 32
Figura 12: Partículas virais de pandoravírus, pithovírus e mollivírus..... 33
Figura 13: Imagens de microscopia eletrônica de transmissão de kaumoebavírus e pacmanvírus. 35
Figura 14: Partículas de cedratvírus. 36
Figura 15: Imagens de microscopia confocal de *A. castellanii* infectadas com cedratvirus laussanensis evidenciando a presença da fábrica viral. 37
Figura 16: Imagens de microscopia eletrônica de transmissão do Orpheovirus IHUMI-LCC2..... 38
Figura 17: Vírus isolados pelo Grupo de Estudo e Prospecção de Vírus Gigantes. 40
Figura 18: Imagem de microscopia eletrônica de transmissão de cedratvirus getuliensis. 41
Figura 19: Partículas virais de tupanvírus observadas por microscopia eletrônica de varredura. 42
Figura 20: Estrutura da partícula viral do tupanvírus..... 43
Figura 21: Estrutura da cauda do tupanvírus 44
Figura 22: Ciclo de multiplicação de tupanvirus soda lake em *A. castellanii*. 45

Figura 23: Árvore filogenética baseada no gene da DNA polimerase B..... 46
Figura 24: Estágios do ciclo de vida de amebas do gênero *Acanthamoeba*.. 48
Figura 25: Imagem de microscopia óptica de *Tetrymena* sp. 49
Figura 26: Teoria do Gato Risonho expandida para o universo dos vírus gigantes e amebas..... 51
Figura 27: *Shutdown* ribossomal em amebas *A. castellanii*..... 72
Figura 28: Ocorrência do *shutdown* em amebas infectadas por tupanvírus inativado.. 73
Figura 29: *Shutdown* em *T. hyperangularis*..... 73
Figura 30: O tratamento com cloroquina não altera a ocorrência do *shutdown* em *A. castellanii*. 74
Figura 31: O tratamento com bafilomicina A não altera a ocorrência do *shutdown* em *A. castellanii*..... 75
Figura 32: O *shutdown* ocorre mesmo após o silenciamento do gene Atg8..... 76
Figura 33: Controle de transfecção dos siRNAs marcados com FITC em amebas *A. castellanii.* 77
Figura 34: Controle biológico da ocorrência do silenciamento. 78
Figura 35: Tupanvírus induz uma intensa acidificação do citoplasma de amebas *A. castellanii* 79
Figura 36: Medida da intensidade de fluorescência de amebas tratadas com lysotracker e infectas por tupanvírus 80
Figura 37: Formação de vesículas contendo ribossomos em amebas *A. castellanii* infectadas por tupanvírus 81
Figura 38: Alterações citoplasmáticas observadas em *T. hyperangularis* infectadas por tupanvírus..... 82
Figura 39: Alterações nucleares observadas em *A. castellanii* e *T. hyperangularis* infectadas por tupanvírus. 83
Figura 40: Análise dos best hits das cópias de regiões intrônicas de 18S em tupanvirus soda lake..... 86
Figura 41: Árvore filogenética das sequências intrônicas de 18S presentes em mimivírus, phycodnavírus, fungos e mitocôndrias de fungos..... 87
Figura 42: Análise da vizinhança das cópias 1 e 2 de tupanvirus soda lake..... 88
Figura 43: Análise das regiões imediatamente adjacentes às cópias de 18S-like em mimivírus 89

Figura 44: Análise da expressão das cópias de 18S-like de tupanvirus soda lake por FISH..... 91
Figura 45: Análise da expressão das cópias de 18S-like de tupanvirus soda lake por qPCR..... 92
Figura 46: Penetração do cedratvirus getuliensis em amebas *A. castellanii* 93
Figura 47: Fábrica viral de cedratvirus getuliensis e outras alterações celulares observadas durante a multiplicação viral. 94
Figura 48: A morfogênese de cedratvirus getuliensis envolve a ocorrência de estruturas complexas subsequentes 96
Figura 49: Espessamento do capsídeo viral de cedratvirus getuliensis..... 97
Figura 50: Partículas de cedratvirus getuliensis apresentam um formato ovóide e um capsídeo estriado 98
Figura 51: Imagens de microscopia eletrônica de varredura de partículas de cedratvirus getuliensis evidenciando a plasticidade dessas estruturas 98
Figura 52: Estruturas de morfologia incomum observadas em meio à progênie viral.. 99
Figura 53: Partículas de cedratvirus getuliensis podem ser liberadas por lise celular ou exocitose..... 100
Figura 54: Representação esquemática do ciclo de multiplicação do cedratvirus getuliensis.....108

LISTA DE TABELAS

Tabela 1: Famílias e membros do grupo dos vírus grandes núcleo-citoplasmáticos de DNA e suas principais características. 21

LISTA DE SIGLAS E ABREVIATURAS

AMAV: Amazônia virus

APMV: Acanthamoeba polyphaga mimivirus

aaRS: aminoacil-tRNA-sintetase

ASFV: African Swine fever virus

AT: Adenina-Timina

ATCC: American Type Culture Collection

Atg: genes relacionados a autofagia (autophagy-related genes)

AVL: Amebas de vida livre

BrMSV: Brazilian Marseillevirus

CEOs: organismos codificadores de capsídeo

CroV: Cafeteria roenbergensis virus

DAPI: 4',6-Diamidine-2'-phenylindole dihydrochloride

DNA: Ácido Desoxi-ribonucléico

EhVS: Emiliania huxleyi virus

EIPA: 5-(*N*-ethyl-*N*-isopropyl) amiloride

EUA: Estados Unidos da América

FISH: Fluorescence In Situ hybridization

FITC: isotiocianato de fluoresceína

GC: Guanina-Citosina

GEPVIG: Grupo de Estudos e Prospecção de Vírus Gigantes

ICTV: Comitê Internacional de Taxonomia de Vírus (International Committee on Taxonomy of Viruses)

Kb: Kilo pares de bases

kDa: kilodalton

KROV: Kroon virus

Mb: Mega pares de bases

MET: Microscopia Eletrônica de Transmissão

mL: mililitros

mM: milimolar

MOI.: Multiplicidade de Infecção

MSV: Marseillevirus

NCBI: Centro nacional de informação em biotecnologia (do ingles, "National Center for Biotechnology information")

NCLDV: Vírus Grandes Núcleo-citoplasmáticos de DNA (Nucleo-Citoplasmatic Large DNA Virus)

nm: nanômetros

NYMV: Nyemeyer virus

ORFs: Janelas Abertas de Leitura

PAS: Salina para amebas

PCR: Reação em Cadeia da Polimerase (Polimerase Chain Reaction)

PYG: Protease Peptona Extrato de Levedura e Glicose

REOs: organismos celulares codificadores de ribossomos

RNA: Ácido Ribonucléico

rRNA: RNA ribossomal

siRNA: pequenos RNAs de interferência

SMBV: samba virus

TEM: Microscopia Eletrônica de Transmissão

TGH: Transferência gênica Horizontal

TGL: Transferência gênica Lateral

TPV: tupanvirus

tRNA: RNA transportador

UFMG: Universidade Federal de Minas Gerais

UV: Ultravioleta

µL: microlitros

µm: micrômetros

µM: micromolar

RESUMO

Tese de Doutorado
Programa de Pós-Graduação em Microbiologia-Universidade Federal de Minas Gerais
INTERAÇÕES ENTRE VÍRUS GIGANTES E PROTOZOÁRIOS: CARACTERIZAÇÃO DO TUPANVIRUS SODA LAKE E DO CEDRATVIRUS GETULIENSIS
LUDMILA KAREN DOS SANTOS SILVA
ORIENTADOR: Dr. Jônatas Santos Abrahão
COORIENTADORES: Dr. Cláudio Antônio Bonjardim e Dr. Jonas Dutra Albarnaz
Belo Horizonte, maio de 2018

Após o isolamento do mimivírus, vários outros vírus tão ou mais complexos foram identificados, apresentando diferenças notáveis em relação a estrutura, genoma, ciclos de multiplicação e, consequentemente, interação com seus hospedeiros. Recentemente, um amplo trabalho de prospecção viral, a partir de amostras de diversos ambientes, foi realizado pelo nosso grupo de pesquisa, possibilitando o isolamento de dois novos vírus, tupanvirus soda lake e cedratvirus getuliensis. A caracterização inicial do tupanvírus evidenciou uma curiosa interação determinada pelo *shutdown* do RNA ribossomal em células hospedeiras e não hospedeiras, quando inoculadas com tupanvírus. Já a descoberta do cedratvirus getuliensis representou o isolamento do terceiro cedratvírus no mundo, revelando a ascensão de um novo grupo viral e evidenciando o nosso ainda limitado conhecimento acerca da biologia desses vírus. Diante disso, o presente trabalho teve como objetivo analisar as interações entre esses vírus e protozoários a partir da caracterização do *shutdown* e da presença de sequências ribossomais em tupanvirus soda lake, assim como da descrição do ciclo de multiplicação do cedratvirus getuliensis. Com o intuito de elucidar se o canônico processo de ribofagia/autofagia estaria relacionado à degradação ribossomal promovida pelo tupanvírus, alguns experimentos foram conduzidos. O tratamento de *A. castellanii* com cloroquina e bafilomicina A, assim como o silenciamento do gene Atg8, não preveniram a ocorrência do *shutdown*. Ademais, foi possível observar que a infecção por tupanvírus induz uma notável acidificação do citoplasma de amebas, assim como uma progressiva degradação do núcleo/nucléolo temporalmente associada ao *shutdown*. Imagens de microscopia eletrônica de transmissão também revelaram a presença de pequenas vesículas, em sua maioria com uma única membrana, contendo ribossomos, próximas ao núcleo. Essas vesículas, posteriormente, se agregam formando grandes estruturas que são depletadas do citoplasma no mesmo tempo que o *shutdown* pode ser detectado. Em conjunto, esses dados sugerem que o *shutdown* não é diretamente relacionado ao processo de ribofagia. Além disso, embora a formação de vesículas contendo ribossomos e a degradação do nucléolo possam estar relacionadas a ocorrência desse fenômeno, os mecanismos envolvidos no *shutdown* ainda precisam ser melhor investigado. Em paralelo aos experimentos da caracterização do *shutdown*, investigações sobre a presença de sequências ribossomais presentes no genoma do tupanvírus também foram conduzidas. Nossas análises revelaram a presença de duas cópias similares a partes de regiões intrônicas de 18S, mais especificamente a íntrons self-splicing do grupo I, no genoma de tupanvírus. Sequências similares também foram encontradas nos genomas de outros mimivírus, embora nunca antes descritas. A análise filogenética dessas duas cópias evidenciou que elas apresentam origens separadas, e, apesar de estarem localizadas em regiões intergênicas, são altamente expressas durante o ciclo de multiplicação. No entanto, a real função dessas cópias nos genomas virais ainda é obscura. A outra seção dessa tese foi destinada ao estudo aprofundado do ciclo de multiplicação do cedratvirus getuliensis. Inicialmente, o uso de diferentes inibidores de endocitose demonstraram que a penetração desses vírus em *A. castellanii* ocorre principalmente por fagocitose. Imagens de microscopia eletrônica de transmissão evidenciaram que, em seguida, ocorre a formação de uma fábrica viral elétron-lucente perinuclear, no interior da qual ocorre a morfogênese de cedratvirus getuliensis envolvendo estruturas subsequentes, complexas e elétron-densas. Além disso, alterações celulares, como recrutamento de mitocôndrias, polarização de lisossomos e intenso tráfego de membranas também foram observadas ao longo da multiplicação de cedratvirus getuliensis. O final do ciclo de multiplicação foi marcado pela liberação da progênie viral principalmente pela lise celular, mas também por exocitose. Os dados aqui apresentados revelaram características peculiares de ambos os isolados virais e contribuíram para um melhor entendimento das relações entre esse vírus e seus hospedeiros.

Palavras chave: tupanvirus, cedratvirus getuliensis, interação vírus hospedeiro, degradação ribossomal, ciclo de multiplicação.

ABSTRACT

Doctoral Thesis
Programa de Pós-Graduação em Microbiologia-Universidade Federal de Minas Gerais

INTERACTIONS BETWEEN GIANT VIRUSES AND PROTOZOANS: CARACTERIZATION OF TUPANVIRUS SODA LAKE AND CEDRATVIRUS GETULIENSIS

LUDMILA KAREN DOS SANTOS SILVA
ADVISOR: Dr. Jônatas Santos Abrahão
CO-ADVISORS: Dr. Cláudio Antônio Bonjardim e Dr. Jonas Dutra Albarnaz

Belo Horizonte, May 2018

Following the isolation of mimivirus, many other viruses as or more complex than APMV were identified, revealing notable differences related to structure, genome, replication cycle, and, consequently, host interactions. Recently, a extensive work of viral prospection using samples from diverse environments was performed by our research team, enabling the isolation of two new viruses, tupanvirus soda lake and Cedratvirus getuliensis. The initial characterization of tupanvirus showed a curious relationship determined by the ribosomal shutdown of host and non-host cells when inoculated with tupanvirus. Also remarkably, the discovery of cedratvirus getuliensis has represented the isolation of the third cedratvirus in the whole world, revealing the ascension of a new viral group and evidencing our limited knowledge about the biology of these viruses. Faced with this, the main goal of this thesis was to analyze the protozoan-viruses interactions based on the ribosomal RNA shutdown characterization and the presence of ribosomal sequences in tupanvirus soda lake, as well as the description of cedratvirus getuliensis replication cycle. Initially, to elucidate whether the canonical process of ribophagy/autophagy would be related with the observed ribosomal degradation promoted by tupanvirus, some experiments were conducted. The obtained results showed that the *A. castellanii* treatment with chloroquine and bafilomycin A, as well as the Atg8 gene silencing do not prevent the occurrence of tupanvirus induced shutdown in *A. castellanii* cells. Moreover, it was possible observe that the tupanvirus soda lake infection induces a remarkable acidification of amoebas cytoplasm and as a progressive degradation of the nucleus/nucleoli that was temporally associated with shutdown. Transmission electron microscopy also revealed the presence of small vesicles, in majority composed of just one membrane, containing ribosomes next to nuclear membrane. These vesicles, posteriorly, suffer aggregation and constitute growing structures that were depleted from the cytoplasm at the same time that shutdown could be detected. Taken together, these data suggest that the shutdown is not directly related to the ribophagy. Moreover, although the formation of vesicles containing ribosomes and the degradation of the nucleolus may be related to the occurrence of this phenomenon, the mechanism involved in the ribosomal degradation still need to be further investigated. In parallel to the experiments developed on the characterization of the ribosomal RNA shutdown, the presence of ribosomal sequences in tupanvirus were also investigated. Our analyzes revealed the presence of two copies that presented similarity with parts of 18S intronic regions, more specifically to group I self-splicing introns, in the genome of tupanvirus. Similar copies were also found in genomes of other mimiviruses, although never reported before. The phylogenetic analyzes of these two copies present evidenced that they had separated origins and, although they are located in intergenic regions, they are highly expressed during the replication cycle. However, the possible role of these copies in viral genomes still unclear. The other section of this thesis was devoted to the in-depth study of cedratvirus getuliensis replication cycle. Initially, the use of different endocytosis inhibitors evidenced that the entry of these viruses into *A. castellanii* occurs mainly by phagocytosis. Transmission electron microscopy images showed the formation of a perinuclear electron-lucent viral factory. Inside and on the periphery of this structure occurs the morphogenesis that involved subsequent, complex and electron-dense structures. In addition, cellular alterations, such as mitochondria recruitment, lysosomes polarization, and intense membrane traffic were also observed along the replication of cedratvirus getuliensis. The end of the replication cycle was marked by the release of viral progeny mainly by cells lysis, but also by exocytosis. These data presented here revealed peculiar characteristics of both viral isolates and contribute to a better understanding about the host-virus interactions.

Key words: tupanvirus, cedratvirus getuliensis, host-virus interaction, ribosomal degradation, replication cycle.

1. INTRODUÇÃO

1.1. Vírus Grandes Núcleo-citoplasmáticos de DNA (NCLDVs)

O final do século XIX foi marcado por um crescimento notável do campo da microbiologia, principalmente pelos estudos desenvolvidos por Louis Pasteur e Robert Koch que associaram uma etiologia microbiana a algumas doenças que acometiam o homem e outros animais (ARTENSTEIN, 2012; LECOQ, 2001). No final do mesmo século, três pesquisadores botânicos (Adolf Mayer, Dimitri Ivanovsky e Martinus Beijerinck), envolvidos no estudo da doença do mosaico do tabaco, tiveram um papel essencial na origem da virologia (LECOQ, 2001; LUSTIG; LEVINE, 1992). Baseados em uma série de experimentos, esses pesquisadores relacionaram a ocorrência dessa doença à presença de uma nova classe de agentes infecciosos, que diferentemente de bactérias ou fungos, não eram retidos pelos conhecidos filtros de *Chamberland* (LECOQ, 2001; LUSTIG; LEVINE, 1992). A partir de então, o conceito de agentes filtráveis, não visíveis por microscopia óptica, mas capazes de causar doença em células e tecidos, teve origem. Mais tarde o termo "vírus" foi cunhado para designar esses agentes e rapidamente após o isolamento do vírus do mosaico do tabaco (1892), o primeiro vírus animal, vírus da febre aftosa (1898), e o primeiro vírus humano, vírus da febre amarela (1901), foram também isolados (LUSTIG; LEVINE, 1992).

A partir do século XX a virologia teve um desenvolvimento notável e os vírus passaram a ser comumente descritos como um grupo de parasitas ubíquos capazes de infectar organismos pertencentes aos três domínios da vida. Além disso, eles são tradicionalmente conhecidos pela dependência quase completa da maquinaria celular do hospedeiro para sua multiplicação e por apresentarem um genoma pequeno, codificador de poucas proteínas (IYER et al., 2006; LWOFF, 1957). Até recentemente a classificação desses micro-organismos era baseada em critérios negativos, como não serem visíveis em microscopia óptica e não serem retidos em filtros de 0,22 μm (LWOFF, 1957). Entretanto, essas características canonicamente relacionadas aos vírus e essa classificação por critérios negativos vêm sendo desconstruídas com a recente descoberta de novos vírus, que são incluídos no grupo dos "Vírus Grandes Núcleo-citoplasmáticos de DNA" (NCLDVs) (IYER; ARAVIND; KOONIN, 2001).

Os NCLDVs foram inicialmente descritos como um grupo de vírus hipoteticamente monofilético, apresentando genes conservados, denominados "core

genes", que estão envolvidos em boa parte das funções essenciais para a multiplicação viral, como transcrição, replicação e metabolismo do DNA, transcrição e processamento de RNA, e morfogênese viral (FILÉE; CHANDLER, 2010; IYER et al., 2006; IYER; ARAVIND; KOONIN, 2001; YUTIN et al., 2009). Além da relativa independência dos sistemas de replicação e transcrição dos seus hospedeiros conferida por esses genes, os NCLDVs compartilham outras características únicas da virosfera, como partículas virais de grande tamanho, sendo algumas visíveis em microscópio óptico, e genomas de dupla fita de DNA relativamente extensos, entre 100 Kb e 2,5 Mb, com capacidade de codificar centenas a milhares de proteínas (FILÉE; CHANDLER, 2010).

Atualmente o grupo dos NCLDVs é composto por sete famílias virais: *Poxviridae*, com representantes que infectam insetos e vertebrados, *Asfarviridae*, que infecta suínos, *Iridoviridae*, que infecta invertebrados e vertebrados pecilotérmicos, *Ascoviridae,* que infecta insetos, *Phycodnaviridae*, que infecta algas, *Mimiviridae* e *Marseilleviridae,* que infectam protistas. Além destes, outros vírus gigantes associados a protistas, recentemente descritos e ainda não agrupados em nenhuma família pelo Comitê Internacional de Taxonomia Viral (ICTV), também fazem parte deste grupo, sendo eles: extended *Mimiviridae*, pandoravírus, pithovírus, faustovírus, mollivírus, cedratvírus, kaumoebavírus, pacmanvírus, e orpheovírus (Tabela 1) (ANDREANI et al., 2016, 2017, 2018; BAJRAI et al., 2016; COLSON et al., 2013; LEGENDRE et al., 2014, 2015; RETENO et al., 2015; SCHULZ et al., 2017).

Tabela 1: Famílias e membros do grupo dos vírus grandes núcleo-citoplasmáticos de DNA e suas principais características.

Família	Hospedeiros	Tamanho do genoma (Kb)	Compartimento celular de multiplicação
Phycodnaviridae	Algas	150-400	Núcleo e citoplasma
Poxviridae	Insetos, reptéis, aves, mamíferos	130-380	Citoplasma
Asfarviridae	Mamíferos	170	Citoplasma
Ascoviridae	Insetos	150-190	Núcleo e citoplasma
Iridoviridae	Insetos, vertebrados pecilotérmicos	100-220	Núcleo e citoplasma

Mimiviridae	*Acanthamoeba* sp.	1.180-1.280	Citoplasma
Marseilleviridae	*Acanthamoeba* sp.	370	Núcleo e Citoplasma
Extended *Mimiviridae*	Algas	177-466	Citoplasma Núcleo (?)
Pandoravírus*	*Acanthamoeba* sp.	1900-2500	Núcleo e citoplasma
Pithovírus*	*Acanthamoeba* sp.	600	Citoplasma
Faustovírus*	*Vermamoeba vermiformis*	466	Citoplasma
Mollivírus*	*Acanthamoeba* sp.	651	Perinuclear Núcleo (?)
Cedratvírus*	*Acanthamoeba* sp.	589	Citoplasma
Kaumoebavírus*	*Vermamoeba vermiformis*	350	Citoplasma
Pacmanvírus*	*Acanthamoeba* sp.	395	Citoplasma
Orpheovírus*	*Vermamoeba vermiformis*	1400	Citoplasma

Fonte: Modificado de KOONIN; YUTIN, 2010.
*Vírus que compõe o NCLDV, mas ainda não possuem família reconhecida pelo comitê internacional de taxonomia de vírus – ICTV.

Acredita-se que os vírus gigantes só tenham sido recentemente descobertos devido às limitações técnicas dos procedimentos de isolamento viral clássicos que impregavam o uso de filtros microbiológicos de 0,22 μm, causando a retenção da maioria dos vírus gigantes (Figura 1) (COLSON et al., 2012). Como mencionado, esse critério de filtração era anteriormente utilizado como um dos fundamentos para a classificação virológica, entretanto, com a descoberta dos vírus gigantes, esse sistema se tornou arcaico. Diante disso, um novo critério dicotômico de classificação foi proposto por Raoult & Forterre que sugeriram a divisão dos organismos atuais em organismos celulares codificadores de ribossomos (REOs) em oposição aos organismos codificadores de capsídeo (CEOs). Segundo essa nova classificação, os REOs englobariam os três domínios da vida (archae, bacteria e eukarya) e os CEOs compreenderiam os vírus, uma vez que até então não havia relatos da presença de nenhuma sequência relacionada a ribossomos no genoma de nenhum agente viral (Figura 2) (RAOULT; FORTERRE, 2008).

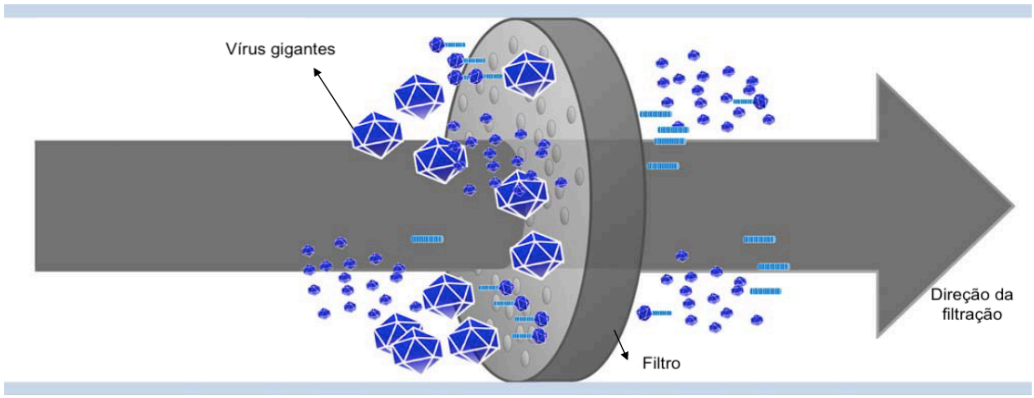

Figura 1: Ilustração esquemática evidenciando a retenção de vírus gigantes por filtros de 0,2 µm. A filtração faz parte dos procedimentos de isolamento viral clássicos e acredita-se que por esse motivo os vírus gigantes só tenham sido descobertos recentemente. **Fonte:** Modificado de COLSON et al., 2012.

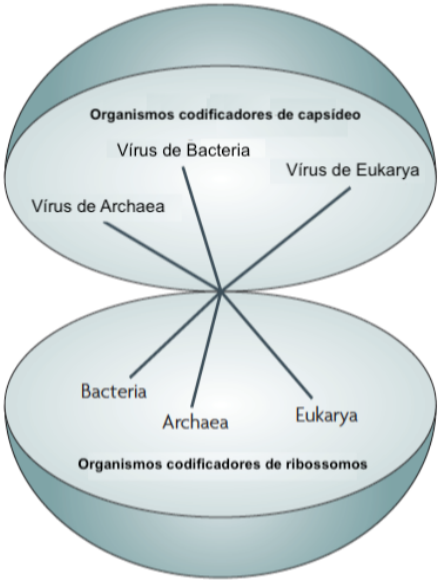

Figura 2: Redefinição da classificação dos vírus. Uma nova proposta de classificação sugere que os organismos sejam divididos em codificadores de ribossomos (REOs) em oposição aos organismos codificadores de capsídeo (CEOs), que englobariam os vírus. **Fonte:** Modificado de RAOULT; FORTERRE, 2008.

Apesar do conhecimento sobre os vírus gigantes representar apenas uma pequena fração em relação à até então conhecida virosfera, recentes estudos têm demonstrado que esses micro-organismos são habitantes ubíquos no planeta, e nessa nova era de descoberta estamos começando a apreciar uma enorme diversidade viral, muito além do que pensávamos originalmente. Sendo assim, a descoberta e a caracterização dos NCLDVs está em sua fase inicial e além de ser um campo aberto

para novas pesquisas, também representa um grande desafio para os virologistas (BOYER et al., 2010; COLSON et al., 2012; ETTEN; LANE; DUNIGAN, 2010; GALLOT-LAVALLÉE; BLANC, 2017).

1.2. Descoberta dos mimivírus e a família *Mimiviridae*

O isolamento do primeiro mimivírus ocorreu no ano de 1992, quando o Dr. Tim Rowbothan e seus colaboradores do Laboratório de Saúde Pública em Leeds na Inglaterra investigavam um surto de pneumonia de etiologia desconhecida em um hospital na cidade de Bradford (RAOULT; LA SCOLA; BIRTLES, 2007). Com o objetivo de isolar bactérias que pudessem estar relacionadas à ocorrência desse surto, Rowbothan inoculou amostras de água provenientes de torres de resfriamento de ar condicionado, que pensavam ser a provável origem da infecção, em uma cultura de *Acanthamoeba* spp. Esta técnica possibilitou a identificação e caracterização de novas espécies de *Legionella* e também o isolamento de um outro micro-organismo, semelhante a um pequeno coco Gram positivo, que foi inicialmente denominado de coco de Bradford (Figura 3) (ADENIKE et al., 2001; RAOULT, 2005). No entanto, após muitas tentativas frustradas de cultivo e identificação molecular usando iniciadores bacterianos universais para a região 16S do DNA ribossomal, os cocos de Bradford foram estocados (RAOULT; SCOLA; BIRTLES, 2007; LA SCOLA et al., 2003)

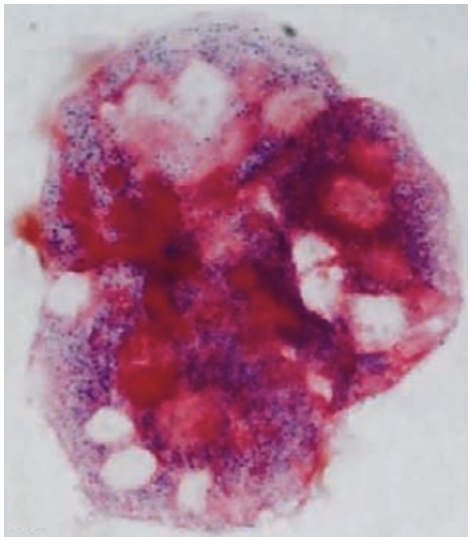

Figura 3: APMV, inicialmente chamado de Coco de Bradford, no interior de uma ameba de vida livre. O micro-organismo é corado de violeta através da coloração de Gram, e assim pode ser visualizado por microscopia óptica. **Fonte:** Modificado de RAOULT; LA SCOLA; BIRTLES, 2007.

Em 1995, a amostra contendo os cocos de Bradford foi levada para Marseille, França, onde um grupo de pesquisadores coordenados pelo pesquisador Didier Raoult deu continuidade aos estudos. A fim de tentar solucionar o que os pesquisadores acreditavam ser problemas técnicos da identificação molecular, os cocos de Bradford foram examinados por microscopia eletrônica. No entanto, o micro-organismo observado aparentemente apresentava um formato de simetria icosaédrica regular, muito semelhante ao dos iridovírus, com aproximadamente 600 nm de diâmetro, sugerindo que os cocos de Bradford na verdade se tratavam de vírus gigantes (Figura 4) (RAOULT, 2005; RAOULT; LA SCOLA; BIRTLES, 2007; LA SCOLA et al., 2003).

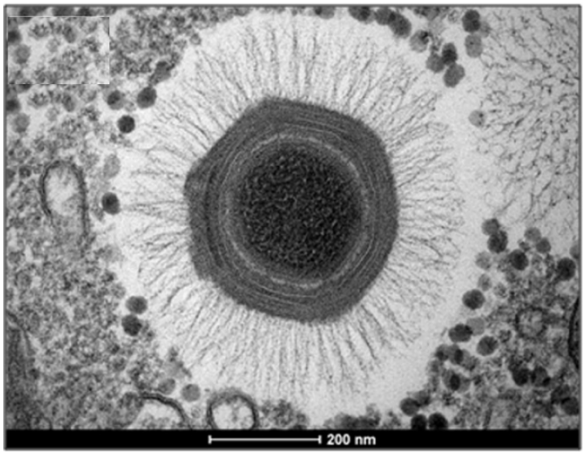

Figura 4: Imagem de microscopia eletrônica de transmissão do mimivírus. A estrutura da partícula do vírus gigante pode ser observada: capsídeo de simetria aparentemente icosaédrica circundado por fibrilas. **Fonte:** Modificado de ABRAHÃO et al., 2014.

Outras análises foram necessárias para comprovar a natureza viral do micro-organismo e demonstraram que ele era composto de um genoma extenso, de DNA dupla fita, e apresentava uma fase de eclipse, típica dos vírus, em sua multiplicação. Além disso, foi observado que a morfogênese das partículas virais ocorria no interior de estruturas intracelulares denominadas fábricas virais, semelhante ao observado também em outros vírus, como os poxvírus (RAOULT, 2005; RAOULT; LA SCOLA; BIRTLES, 2007; LA SCOLA et al., 2003).

Após a comprovação da natureza viral dos cocos de Bradford, o novo vírus foi denominado de Acanthamoeba polyphaga mimivirus (APMV), por infectar amebas do gênero *Acanthamoeba* e também por mimetizar micro-organismos, como bactérias, após coloração de Gram. Por apresentar características diferenciais que não permitiam sua classificação em nenhuma família viral já existente, a família *Mimiviridae* foi criada

para incluir o APMV e após outras análises filogenéticas também foi incluída no grupo dos NCLDVs (RAOULT, 2005; RAOULT; LA SCOLA; BIRTLES, 2007; LA SCOLA et al., 2003).

Atualmente *Mimiviridae* é a família com o maior número de vírus isolados entre os gigantes, aproximadamente 300, e é dividida em dois gêneros: o gênero *Mimivirus* (ou grupo I), que inclui os vírus semelhantes ao protótipo APMV, enquanto o gênero *Cafeteriavirus* (grupo II) é composto somente pelo *Cafeteria roenbergensis virus* (CroV). O grupo I é composto por vírus que infectam amebas do gênero *Acanthamoeba* e é subdivido, de acordo com análises filogenéticas baseadas na sequência da DNA polimerase B, em outras três linhagens: A, B e C. O APMV e o mamavírus estão incluídos na linhagem A, enquanto os moumovírus são classificados na linhagem B e o *Megavirus chilensis* na linhagem C (Figura 5) (ARSLAN et al., 2011; CLAVERIE, 2013; COLSON et al., 2011, 2012; GAIA et al., 2014).

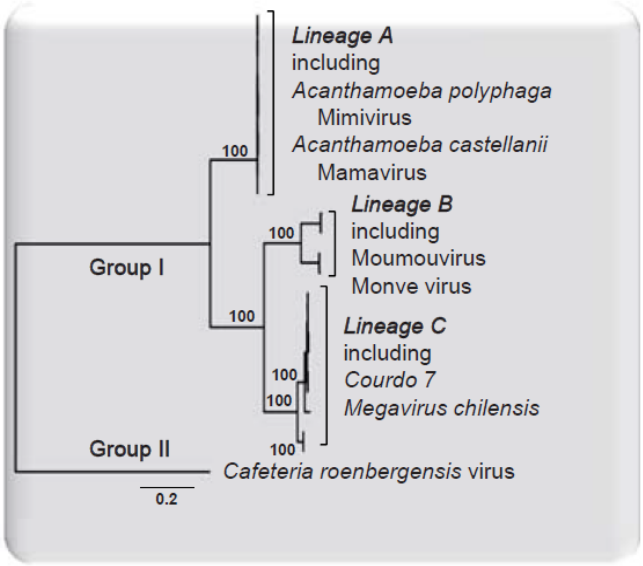

Figura 5: Gêneros e linhagens que compõem a família *Mimiviridae*. Reconstrução filogenética da família *Mimiviridae* evidencia a divisão dessa em dois gêneros, grupo I e grupo II, sendo o grupo I ainda subdividido em linhagens A, B e C. **Fonte:** Modificado de COLSON et al., 2012.

1.3. Acanthamoeba polyphaga mimivirus (APMV)

A descoberta do APMV levou ao desenvolvimento de diversos estudos que revelaram um vírus extremamente diferenciado com características morfológicas e genéticas bastante peculiares.

1.3.1. Estrutura

Análises de microscopia crio-eletrônica demonstraram que, estruturalmente, esse vírus apresenta um capsídeo de aproximadamente 500 nm de diâmetro, externamente recoberto por uma densa camada de longas fibrilas, de cerca de 125 nm, que fazem com que o diâmetro total das partículas virais sejam de aproximadamente 750 nm (XIAO et al., 2005, 2009). Acredita-se que o capsídeo viral seja formado por três camadas protéicas e que as fibrilas estejam associadas à camada protéica mais externa. Internamente ao capsídeo se encontra uma membrana lipídica, que é aparentemente derivada do retículo endoplasmático do hospedeiro. Essa membrana recobre a parede do cerne e essa, por sua vez, envolve o genoma viral que se encontra associado a uma matriz fibrosa (Figura 6) (ABRAHÃO et al., 2014; KLOSE et al., 2015; MUTSAFI et al., 2013).

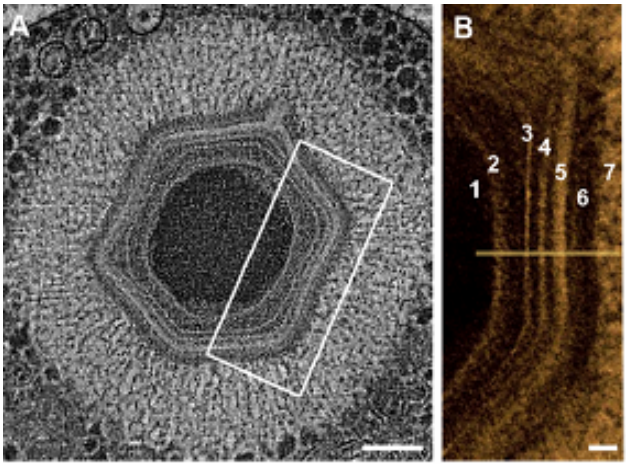

Figura 6: Organização das camadas da partícula viral de APMV. (A) Imagem de microscopia eletrônica de varredura e transmissão do corte de uma partícula madura de APMV evidenciando suas múltiplas camadas. (**B)** Ampliação da região delimitada em (A) evidenciando o cerne (1), parede do cerne (2), membrana interna (3), camadas protéicas do capsídeo (4), (5) e (6) e fibrilas (7). **Fonte:** Modificado de MUTSAFI et al., 2013.

A partícula viral ainda apresenta um único vértice modificado em formato de estrela do mar, denominado "star-gate", que confere ao vírus uma simetria pentagonal (pseudo-icosaédrica) (Figura 7) (ZAUBERMAN et al., 2008). Essa estrutura diferenciada possibilita a abertura do capsídeo e, consequentemente, a fusão da membrana viral interna com a membrana do fagossomo levando à formação de um canal de membranas por onde o DNA é liberado para o citoplasma da célula hospedeira (XIAO et al., 2009; XIAO; ROSSMANN, 2011).

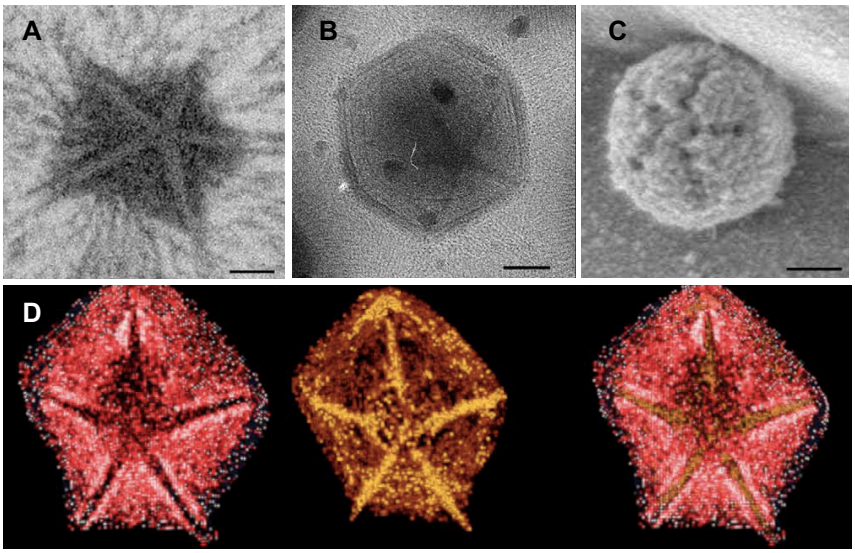

Figura 7: Estrutura do star-gate dos mimivírus. Star-gate observado por microscopia eletrônica de transmissão **(A)**, crio-microscopia **(B)** e microscopia eletrônica de varredura **(C)**. Em **(D)** reconstrução do star-gate revelando a presença de duas camadas do capsídeo em vermelho e laranja. Escala: 100 nm. **Fonte:** Modificado de ZAUBERMAN et al., 2008.

O star-gate é a única região do capsídeo dos mimivírus que não é recoberta por fibrilas. Essas estruturas apresentam uma composição protéica e são envoltas por uma matriz semelhante a peptideoglicanos, o que condiz com o fato do APMV ser corado pelo método de Gram e ter sido inicialmente identificado como uma bactéria (IYER et al., 2006; XIAO et al., 2009). Acredita-se que a função dessas fibrilas esteja diretamente relacionada à adesão viral à superfície celular e interação com bactérias, fungos e até mesmo artrópodes, sendo que a adesão a esses outros micro-organismos poderia facilitar a fagocitose dos mimivírus pelo seu hospedeiro natural (RODRIGUES et al., 2015).

1.3.2. Genoma

Além do seu grande tamanho e complexidade, APMV também apresenta um extenso genoma composto por uma molécula de dupla fita de DNA linear com aproximadamente 1,2 Mb. A partir desse genoma, cerca de 1000 proteínas são codificadas, sendo muitas delas sem função conhecida e outras nunca antes observadas na virosfera, na ocasião da descoberta desses vírus. Além disso, algumas das sequências do genoma dos mimivírus, denominadas de ORFans, também exibem pouca ou nenhuma homologia com quaisquer outras sequências nucleotídicas até então

conhecidas (ABRAHÃO et al., 2014; COLSON et al., 2017; LEGENDRE et al., 2010, 2011; RAOULT et al., 2004).

Os mimivírus também apresentam genes envolvidos na biossíntese de nucleotídeos (ribonucleotídeo redutases), na replicação e reparo de DNA (DNA polimerase da família B, chaperonas e topoisomerases do tipo I e II) e na transcrição (RNA polimerase DNA dependente). Além disso, também codificam fatores envolvidos na tradução, como tRNAs, aminoacil-tRNA sintetases, fatores de iniciação e elongação da tradução e fatores de liberação de peptídeos (COLSON et al., 2017; RAOULT et al., 2004; SUHRE; AUDIC; CLAVERIE, 2005; SUZAN-MONTI; LA SCOLA; RAOULT, 2006). Esse grande arsenal gênico pode ser importante por permitir que APMV utilize sua própria maquinaria em paralelo com os elementos análogos celulares para replicação de seu genoma e formação de progênie (COLSON et al., 2011; SUHRE; AUDIC; CLAVERIE, 2005). O estudo do repertório gênico dos mimivírus também evidenciou que o genoma desses vírus é uma quimera, sendo composto por ORFs que exibem sequências similares a homólogos encontrados nos três domínios da vida (Bacteria, Archea e Eukarya). Acredita-se que esses genes tenham sido adquiridos por transferência gênica horizontal (TGH) a partir dos seus hospedeiros, no caso as amebas, ou por transferência gênica lateral (TGL) a partir de outros micro-organismos que parasitam o mesmo hospedeiro de forma simpátrica. Além disso, a detecção de outros eventos de TGH envolvendo genes provenientes de diferentes eucariotos sugere que o espectro de hospedeiros de mimivírus pode ser bem maior do que o que se conhece atualmente. Logo, o processo de TGH e TGL parecem ser importantes no processo evolutivo do genoma dos mimivírus (CLAVERIE; ABERGEL, 2009; FILÉE; CHANDLER, 2010; MOREIRA; BROCHIER-ARMANET, 2008).

1.3.3. Ciclo de multiplicação

A multiplicação dos mimivírus ocorre no citoplasma das células hospedeiras, em zonas delimitadas denominadas de fábricas virais. Dessa maneira, até onde sabemos atualmente, o genoma de APMV não é direcionado até o núcleo da célula e não cruza a membrana nuclear. No entanto, esse processo não deve ser considerado um processo completamente independente do núcleo hospedeiro, uma vez que fatores nucleares

necessários à replicação podem participar do processo (ABRAHÃO et al., 2014; MUTSAFI et al., 2010; SUZAN-MONTI et al., 2007).

O ciclo de multiplicação se inicia com a penetração do vírus nas células hospedeiras através da fagocitose das partículas virais por amebas do gênero *Acanthamoeba* (Figura 8) (ANDRADE et al., 2017). Em seguida, partículas virais podem ser observadas dentro de fagossomos. Logo após, ocorre a abertura do star-gate e a extrusão da membrana interna da partícula viral que se funde com a membrana do fagossomo. Essa fusão leva à formação de um canal que permite que o cerne do APMV seja liberado no citoplasma da ameba (Figura 9A) (ABRAHÃO et al., 2014; MUTSAFI et al., 2010; SUZAN-MONTI et al., 2007).

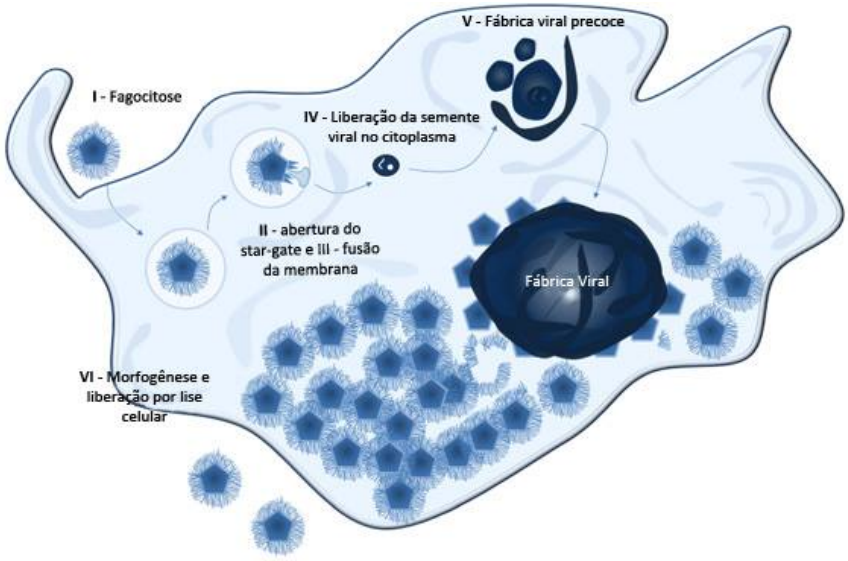

Figura 8: Ciclo de multiplicação do APMV em ameba. (**I**) Fagocitose. (**II**) Penetração viral por fagossomo, seguida por abertura do star-gate. (**III**) Fusão da membrana viral. (**IV**) Liberação do cerne viral. (**V**) Início da formação das fábricas virais. (**VI**) Crescimento das fábricas virais, seguida da morfogênese viral e liberação das novas partículas virais por lise celular. **Fonte:** Modificado de ABRAHÃO et al., 2014.

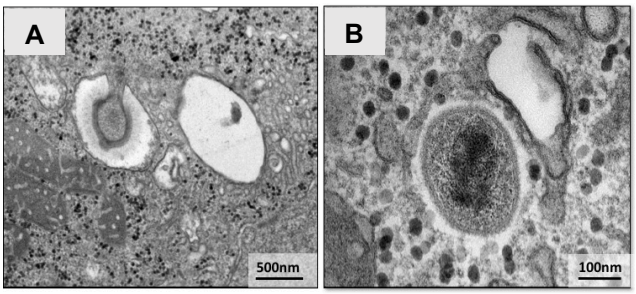

Figura 9: Imagens de microscopias eletrônica de transmissão evidenciando fusão da membrana interna viral com a membrana do fagossomo e a semente viral. (**A)** Partículas de APMV com membranas já fusionadas. (**B)** Semente viral formado após a extrusão do cerne viral. **Fonte:** Modificado de ANDRADE et al., 2017.

Após a liberação do cerne, o genoma viral é estabilizado sob a forma de núcleos esféricos livres, as chamadas sementes virais, ao redor das quais são formadas as fábricas virais, nas quais ocorre uma massiva replicação do DNA (Figura 9B). A transcrição dos genes ocorre de uma forma temporal: transcrição de genes precoces, intermediários e tardios (ANDRADE et al., 2017; LEGENDRE et al., 2010; MUTSAFI et al., 2010; SUHRE; AUDIC; CLAVERIE, 2005).

A fase tardia de multiplicação do APMV é caracterizada por um aumento da fábrica viral, devido à síntese de proteínas estruturais, e pelo início da morfogênese viral que se dá a partir de estruturas lamelares crescentes na periferia da fábrica viral (Figura 10A). Essas estruturas aumentam de tamanho pela incorporação de proteínas e, em seguida, as fibrilas são adquiridas em regiões denominadas de zonas de aquisição de fibrilas, concomitantemente à aquisição do genoma (Figura 10B). Posteriormente o ciclo de multiplicação é finalizado com a liberação das novas partículas virais pela lise celular (ANDRADE et al., 2017; CLAVERIE et al., 2009; KUZNETSOV et al., 2013; MUTSAFI et al., 2010).

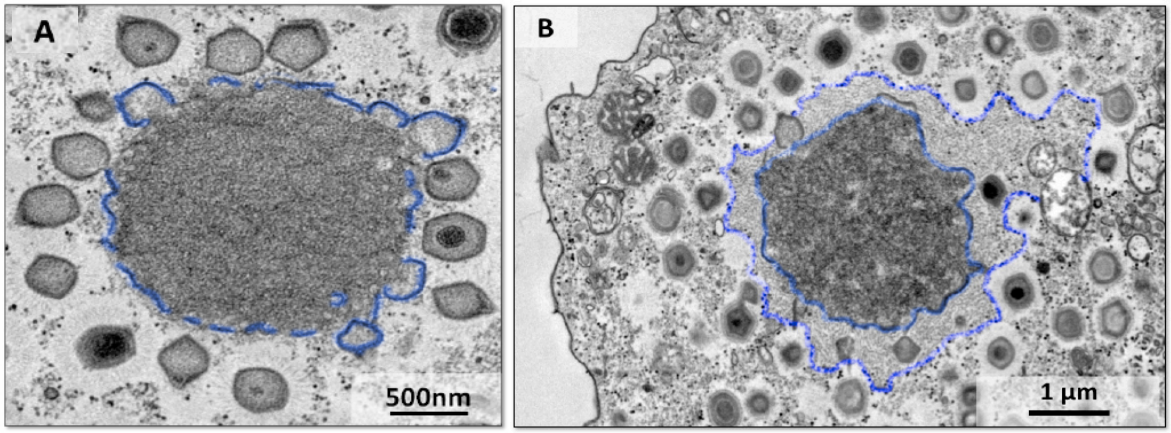

Figura 10: Imagens de microscopia eletrônica das fábricas virais dos mimivírus. **(A)** Estruturas lamelares crescentes na periferia da fábrica viral. **(B)** Zona de aquisição de fibrilas na periferia da fábrica viral. **Fonte:** Modificado de ANDRADE et al., 2017.

1.4. Diversidade de outros vírus gigantes

O isolamento dos mimivírus, além de ocasionar uma quebra de paradigmas na virologia, também levou ao crescimento do número de estudos de prospecção de vírus gigantes. Desde então, vários novos vírus, isolados a partir de amostras provenientes dos mais diferentes ambientes, têm sido descobertos e caracterizados (PAGNIER et al., 2013).

No ano de 2009, o mesmo grupo de pesquisadores franceses responsáveis pela descoberta do APMV, isolou um novo vírus gigante utilizando culturas de *Acanthamoeba polyphaga*. Denominado de Marseillevirus marseillevirus (MsV), esse novo micro-organismo, obtido a partir de amostras de água coletadas em uma torre de resfriamento de ar condicionado na cidade de Paris, apresenta partículas virais de simetria icosaédrica, com capsídeo de aproximadamente 250 nm circundado por curtas fibrilas de 12 nm, e genoma de aproximadamente 370 kb (Figura 11) (BOYER et al., 2009). Após o isolamento do primeiro marseillevírus, outros foram descobertos e, atualmente, todos esses isolados pertecem à família *Marseilleviridae*, que foi criada em 2013 pelo ICTV e representa a segunda maior família dentre os vírus gigantes de ameba (COLSON et al., 2013).

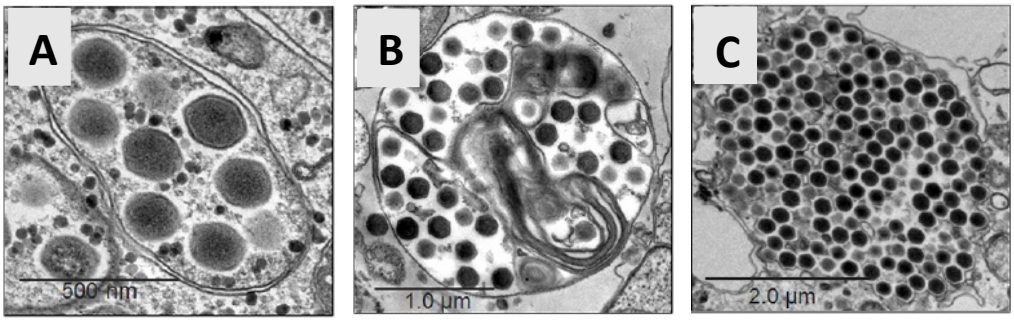

Figura 11: Imagens de microscopia eletrônica de partículas de Marseillevirus marseillevirus. **(A-C)** Grandes vesículas contendo várias partículas virais e apresentando uma ou duas membranas. **Fonte:** Modificado de ARANTES et al., 2016.

Assim como *Mimiviridae*, a família *Marseilleviridae* também é dividida em linhagens de acordo com diferenças genéticas e filogenéticas (AHERFI et al., 2014; DORNAS et al., 2016). A linhagem A é composta pelo vírus protótipo, Marseillevirus marseillevirus, e pelo Cannes 8 virus, Fointaine Saint-Charles virus, Senegalvirus, giant blood marseillevirus e Melbournevirus (AHERFI et al., 2013; COLSON et al., 2013; DOUTRE et al., 2014). A linhagem B possui dois isolados, Lausannevirus e Port-Miou virus, e a linhagem C é representada pelo Tunisvirus e pelo insectomine virus (AHERFI et al., 2014; BOUGHALMI et al., 2013; DOUTRE et al., 2014; THOMAS et al., 2011). Já a linhagem D foi proposta após a descoberta e caracterização do primeiro marseillevírus isolado no Brasil, denominado Brazilian marseillevirus (DORNAS et al., 2016).

Recentemente, nosso grupo de pesquisa demonstrou que, ao contrário do observado para os outros vírus gigantes, a penetração das partículas isoladas dos marseillevírus não ocorre por fagocitose, mas sim por meio de endocitose mediada por receptor. Além disso, foi demonstrado que os marseillevírus podem formar grandes vesículas, que contêm de dezenas a milhares de partículas virais, e que essas vesículas por sua vez poderiam estimular a fagocitose devido ao seu tamanho (Figura 11A-C) (ARANTES et al., 2016).

Em 2013, os primeiros pandoravírus, foram isolados por Philippe e colaboradores a partir de amostras de sedimentos marinhos no Chile (Pandoravirus salinus) (Figura 12A) e de lama de água doce em Melbourne (Pandoravirus dulcis). Esses vírus apresentam uma morfologia completamente diferente de qualquer outro vírus descrito, com uma partícula viral ovóide, em formato de ânfora e com um poro apical, de aproximadamente 1µm de comprimento e 0,5 µm de diâmetro. Além disso também apresentam genomas complexos e extensos, variando de 1,9 Mb, em Pandoravirus dulcis, a 2,5 Mb, em Pandoravirus salinus (PHILIPPE et al., 2013). Em 2015, dois novos pandoravírus foram isolados, Pandoravirus inopinatum, isolado a partir de amostras de um paciente com ceratite, e o primeiro pandoravírus brasileiro, isolado a partir da lagoa da Pampulha em Belo Horizonte (ANTWERPEN et al., 2015; DORNAS et al., 2015). De maneira semelhante aos outros vírus gigantes, o pandoravírus se multiplica no citoplasma das amebas, entretanto, durante esta fase ocorre uma desorganização nuclear, sugerindo que a multiplicação também possa envolver o núcleo das amebas, o que antes não havia sido observada para os demais gigantes.

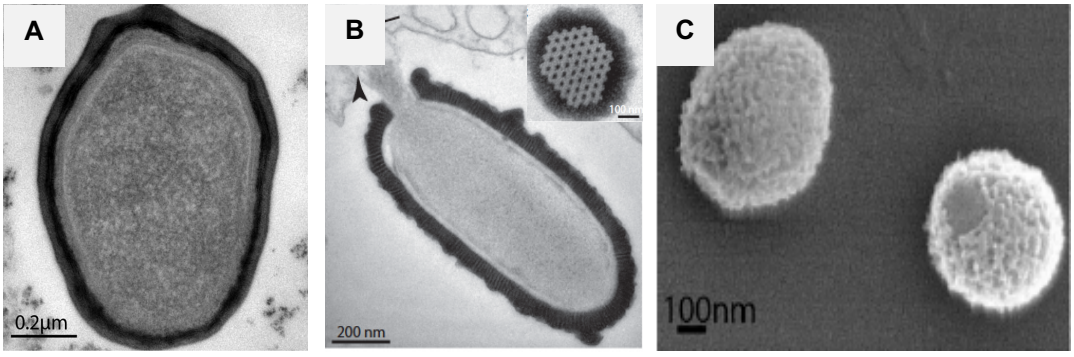

Figura 12: Partículas virais de pandoravírus, pithovírus e mollivírus. (A) Imagem de microscopia eletrônica de transmissão de Pandoravirus salinus e **(B)** pithovirus sibericum: evidenciando a estrututura do cork (detalhe). **(C)** Imagem de microscopia eletrônica de varredura de mollivirus sibericum. **Fonte:** Modificado de LEGENDRE et al., 2014, 2015; PHILIPPE et al., 2013.

Também no ano de 2013, os extended mimivírus, assim denominados por Yutin e colaboradores, foram inicialmente classificados como membros da família *Phycodnaviridae*. Entretanto, análises genômicas, particularmente do Organic Lake phycodnavirus e do Phaeocystis globosa virus, revelaram a presença de um grande número de genes homólogos em membros da família *Mimiviridae*. Estes resultados filogenéticos, levaram à proposição de um novo grupo de vírus, representando uma substancial expansão da família *Mimiviridae* e englobando vírus com genomas muito menores do que os dos membros originais dos mimivírus (YUTIN et al., 2013).

No ano de 2014, um vírus ainda maior do que os pandoravírus, foi descrito por Legendre e colaboradores. O pithovirus sibericum foi isolado a partir de amostras de *permafrost* siberiano datados de 30.000 anos, apresentando cerca de 1,5 μm de comprimento e um genoma surpreendentemente pequeno de aproximadamente 610 Kb (Figura 12B) (LEGENDRE et al., 2014). Pithovirus sibericum apresenta uma morfologia semelhante aos pandoravírus, no entanto o poro apical dos pithovírus é composto por uma estrutura denominada "cork" que é constituída por estrias verticais paralelas de 15 nm, semelhantes a favos de mel (LEGENDRE et al., 2014; OKAMOTO et al., 2017). Recentemente, Levasseur e colaboradores isolaram o segundo pithovírus denominado pithovirus massiliensis, isolado a partir de amostras coletadas em esgotos da cidade de La Ciotat, na França (LEVASSEUR et al., 2016).

A partir da mesma amostra de *permafrost* siberiano de 30.000 anos, outro vírus com morfologia bastante diferente à de pithovirus sibericum também foi isolado (LEGENDRE et al., 2015). Mollivirus sibericum apresenta uma partícula viral esférica não icosaédrica com diâmetro de 500-600 nm e um genoma de aproximadamente 652 Kb (Figura 12C). A análise dos genes de mollivirus demonstrou que cerca de 20% desses são homólogos aos genes de pandoravírus, sugerindo que esses vírus possam ser parentes distantes. Com relação ao ciclo de multiplicação, acredita-se que a replicação do DNA viral ocorra no núcleo das amebas, que apresenta deformação durante a infecção, e que a liberação da progênie ocorra por exocitose, uma vez que a lise viral não é observada (LEGENDRE et al., 2015).

Até 2015 o único protista utilizado no isolamento de vírus gigantes pertencia ao gênero *Acanthamoeba*, no entanto, Reteno e colaboradores descreveram o isolamento de oito novos vírus gigantes, denominados de faustovírus, utilizando amebas da espécie *Vermamoeba vermiformis* (RETENO et al., 2015). O protótipo, faustovirus E12, apresenta um capsídeo de simetria icosaédrica de aproximadamente 200 nm de

diâmetro, desprovido de fibrilas, que encapsida um genoma circular de cerca de 466 Kb. Além disso, análises filogenéticas demonstraram que esses vírus são relacionados ao African swine fever virus (ASFV), pertencente à família *Asfarviridae.*

Outros dois vírus posteriormente isolados, kaumoebavirus e pacmanvirus, também se mostraram filogeneticamente relacionados aos asfarvírus (ANDREANI et al., 2017; BAJRAI et al., 2016). O kaumoebavirus, também isolado em *V. vermiformis*, foi descoberto a partir de amostras de esgoto da cidade de Jeddah, Arábia Saudita, e apresenta um capsídeo de simetria icosaédrica de aproximadamente 250 nm e um genoma circular de DNA com 350 Kb (Figura 13A) (BAJRAI et al., 2016). O pacmanvirus, por sua vez, foi isolado em *A. castellanii* a partir de uma amostra ambiental coletada na Argélia apresentando uma partícula viral de 200 nm e um genoma linear de 395 Kb (Figura 13B) (ANDREANI et al., 2017).

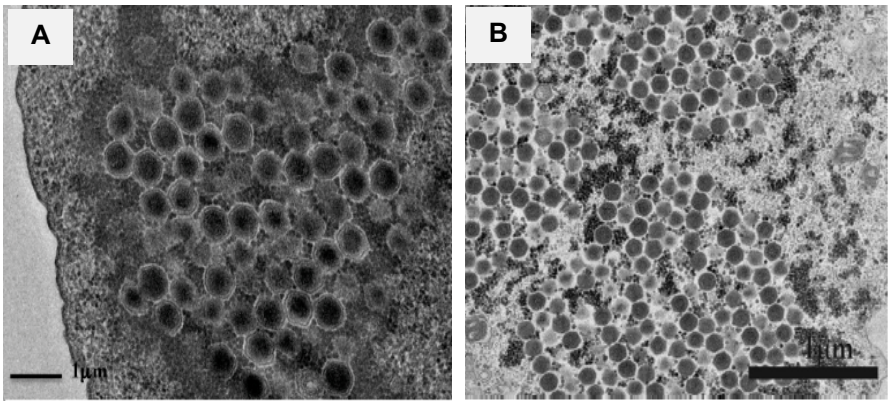

Figura 13: Imagens de microscopia eletrônica de transmissão de kaumoebavírus e pacmanvírus. (A) Diversas partículas de kaumoebavirus no interior de *V. vermiformis*. **(B)** Partículas de pacmanvirus no citoplasma de *A. castellanii*. **Fonte:** Modificado de ANDREANI et al., 2017; BAJRAI et al., 2016; RETENO et al., 2015.

Utilizando amostras também provenientes da Argélia, Andreani e colaboradores isolaram em *A. castellanii* outro gigante de morfologia similar aos phitovírus, porém com o diferencial de apresentar dois corks nos poros apicais da partícula, ao invés de somente um (ANDREANI et al., 2016). Denominado de cedratvirus A11, esse vírus apresenta vírions de aproximadamente 1 – 1,2 µm de comprimento e 0,5 µm de largura, contendo um genoma circular de DNA dupla fita de aproximadamente 589 Kb (Figura 14A). Análises gênicas não identificaram a presença de nenhum tRNA, mas levaram à predição de 574 genes, sendo 177 (30,8 %) desses considerados ORFans (ANDREANI et al., 2016).

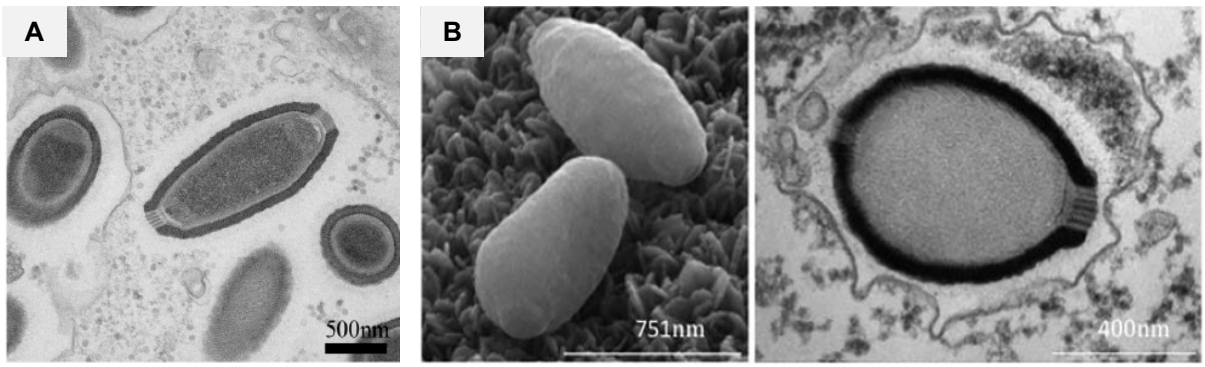

Figura 14: Partículas de cedratvírus. (A) Imagem de microscopia eletrônica de transmissão de cedratvirus A11 evidenciando os dois corks encontrados nos poros apicais da partícula. **(B)** Imagem de microscopia eletrônica de varredura (esquerda) e transmissão (direita) de cedratvirus laussanensis. Os corks podem ser observados em ambas as imagens. **Fonte:** Modificado de ANDREANI et al., 2016; BERTELLI et al., 2017.

Em 2017, um segundo cedratvírus, cedratvirus laussanensis, foi isolado a partir de amostras de água da comuna francesa de Morsang-sur-Seine. Com dimensões de 0,75 – 1 μm de comprimento e 0,4 – 0,6 de largura, cedratvirus laussanensis apresenta um genoma de 575 Kb, que apesar de menor do que o genoma de cedratvirus A11, é capaz de codificar 643 proteínas preditas (Figura 14B) (BERTELLI et al., 2017). Reconstruções filogenéticas utilizando grupos de proteínas ortólogas revelaram uma alta proximidade entre cedratvirus A11, cedratvirus laussanensis e os pithovírus, levantando a hipótese dos cedratvírus serem considerados novos membros da proposta família *Pithoviridae* (ANDREANI et al., 2016; BERTELLI et al., 2017).

Além dos dois peculiares corks, a partícula viral dos cedratvírus apresenta outras características marcantes, como a presença de um capsídeo estriado e de uma membrana interna que delimita um compartimento, aparentemente sem subestruturas, aonde se encontra o material genético viral (ANDREANI et al., 2016; BERTELLI et al., 2017). Apesar dessas diferenças, os cedratvírus apresentam similaridades com os demais gigantes, como um espectro de hospedeiros restrito, sendo capazes de estabelecer um ciclo viral produtivo somente em *A. castellanii*, e a capacidade de se multiplicarem em fabricas virais localizadas no citoplasma (Figura 15) (ANDREANI et al., 2016; BERTELLI et al., 2017).

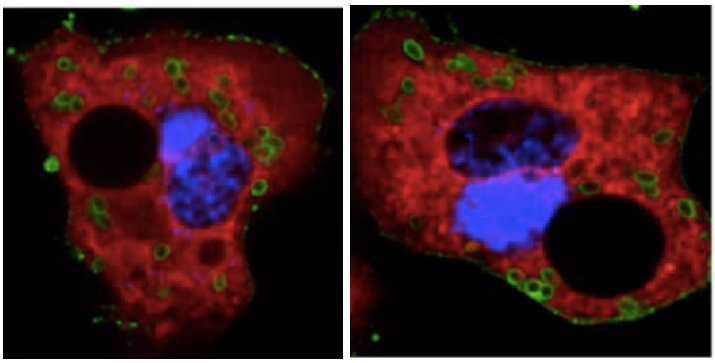

Figura 15: Imagens de microscopia confocal de *A. castellanii* infectadas com cedratvirus laussanensis evidenciando a presença da fábrica viral. Com o avançar da infecção, a fábrica viral aumenta de tamanho (DAPI – azul) e pode ser visualizada na região perinuclear. Vírus foram marcados com anticorpo anti-cedratvirus laussanensis (verde) e *A. castellanii* com concanavalina A (vermelho). **Fonte:** Modificado de BERTELLI et al., 2017.

Recentemente, estudos envolvendo análises de dados metagenômicos de amostras obtidas a partir de uma usina de tratamento de esgoto, localizada em Klosterneuburg, no leste da Áustria, levaram à identificação de novos micro-organismos. Denominados de klosneuvírus, esse grupo é composto por quatro vírus: o indivirus com genoma de 0,86 Mb; o hokovirus, com genoma de 1,33 Mb; o catovirus, com genoma de 1,53 Mb e o klosneuvirus, com genoma de 1,57 Mb. Embora não isolados, os novos vírus em questão chamaram a atenção devido ao seu conteúdo genético, que revelou a presença de um sistema de tradução complexo para um vírus, com a presença de 25 tRNAs, mais de 40 fatores de tradução e 19 aminoacil tRNA sintetases, dentre outros (SCHULZ et al., 2017).

Finalmente, no início desse ano, o mais novo vírus gigante foi publicado e isolado também por Andreani e colaboradores (ANDREANI et al., 2018). Denominado Orpheovirus IHUMI-LCC2, esse vírus foi descoberto a partir das fezes de um rato utilizando amebas *V. vermiformes* como plataforma de isolamento. Com relação à morfologia, a partícula viral apresenta um formato ovóide de 900-1300 nm com um poro apical semelhante ao apresentado pelos pandoravírus (Figura 16). Entretanto, apesar de se aparentar morfologicamente aos pandoravírus, análises filogenéticas indicam uma maior proximidade desses vírus com os pithovírus e os cedratvírus (ANDREANI et al., 2018).

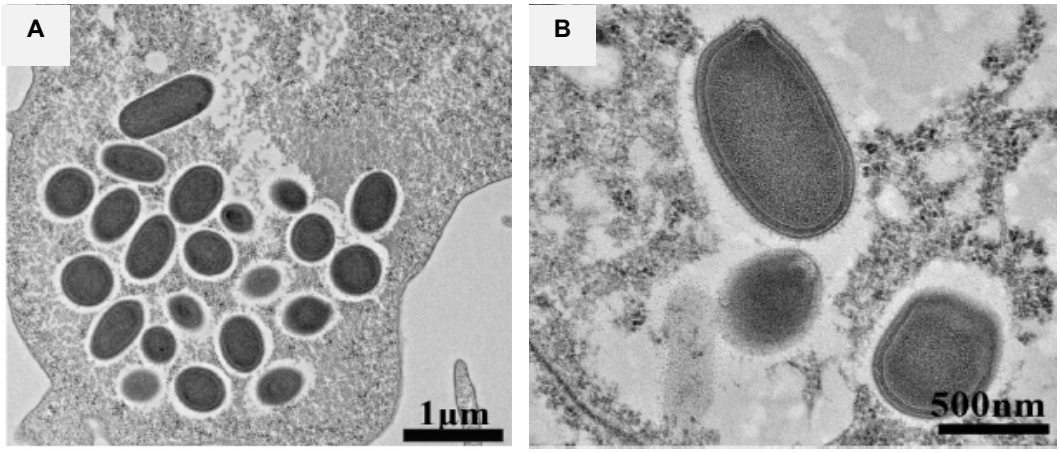

Figura 16: Imagens de microscopia eletrônica de transmissão do Orpheovirus IHUMI-LCC2. (A) Várias partículas no citoplasma da célula hospedeira. **(B)** Particula viral em maior aumento evidenciando o poro apical semelhante aos dos pandoravírus. **Fonte:** Modificado de ANDREANI et al., 2018.

Em conjunto, todos esses dados demonstram que vários estudos de prospecção já foram concluídos, e muitos outros ainda estão em andamento. Além disso, com o advento de projetos de metagenômica ambiental acredita-se que o número de novos vírus gigantes tenda a crescer ainda mais nos próximos anos.

1.5. Isolamento de vírus gigantes no Brasil

As pesquisas de vírus gigantes no Brasil tiveram início no ano de 2011 com a criação do Grupo de Estudo e Prospecção de Vírus Gigantes (GEPVIG), conduzido no Laboratório de Vírus da UFMG. Após sete anos de pesquisa, 39 artigos já foram publicados abordando vários aspectos relacionados ao estudo dos vírus gigantes, como prospecção, caracterização viral, interação vírus-hospedeiro, análises genômicas, dentre outros.

Os estudos de prospecção tiveram início após uma expedição à Amazônia, aonde foram coletadas amostras das águas do Rio Negro. A partir destas amostras o primeiro mimivírus brasileiro, nomeado de samba vírus (SMBV), foi isolado (Figura 17). Com uma partícula de aproximadamente 574 nm e um genoma de 1,2 kb, codificando 938 ORFs, o SMBV foi caracterizado como um novo vírus pertencente à linhagem A da família *Mimiviridae* (CAMPOS et al., 2014).

Além do SMBV, outros mimivírus foram descritos pelo GEPVIG, entre eles o Niemeyer vírus (NYMV) (Figura 17B), isolado de amostras de água coletadas na lagoa da Pampulha, Belo Horizonte, Minas Gerais (Figura 17B) (BORATTO et al., 2015), o Kroon vírus (KROV) (Figura 17C), isolado em 2012 de amostras de água de uma lagoa urbana na cidade de Lagoa Santa, Minas Gerais (BORATTO et al., 2017), Amazônia vírus (AMAV), isolado em 2011 de amostras de água do Rio Negro, (ASSIS et al., 2015), e oyster vírus (Figura 17D), isolado a partir de amostras de ostras de uma fazenda situada na costa sul de Florianópolis, Santa Catarina (ANDRADE et al., 2014). O isolamento de outros mimivírus também foi realizado a partir de amostras coletadas em diferentes ambientes do Hospital das Clínicas, em Belo Horizonte, Minas Gerais (DOS SANTOS SILVA et al., 2015). Todos os isolados acima citados foram caracterizados biologicamente e identificados filogeneticamente como mimivírus do grupo A, assim como o SMBV.

Entre outros vírus gigantes descobertos pelo grupo está o Brazilian marseillevírus (BrMsV) (Figura 17E), o primeiro marseillevírus brasileiro, isolado a partir de amostra de água coletada na lagoa da Pampulha, Belo Horizonte. O BrMsV é morfologicamente semelhante do MsV, medindo cerca de 250 nm de diâmetro. No entanto, este vírus é filogeneticamente distinto dos demais marseillevírus, o que levou à proposição da linhagem D para abrigar este novo isolado (DORNAS et al., 2016).

Em 2016, Andrade e colaboradores realizaram outro grande estudo de prospecção no qual foram avaliadas 976 amostras de solo, água doce, esgoto, água do mar, fezes de capivara, solo de lagoas salinas, aspirado de nasofaringe, água de bromélia e água de mangue. A partir deste estudo foram isolados 68 vírus gigantes, entre eles 26 mimivírus pertencentes à linhagem A, 13 da linhagem B, 2 da linhagem C e 23 sem classificação definida. Através deste estudo, também foi possível o isolamento de outros vírus gigantes, como 2 pandoravírus (Figura 17F), 1 marseillevírus e 1 cedratvírus, denominado cedratvirus getuliensis, que foi o primeiro isolado no Brasil (ANDRADE et al., 2018).

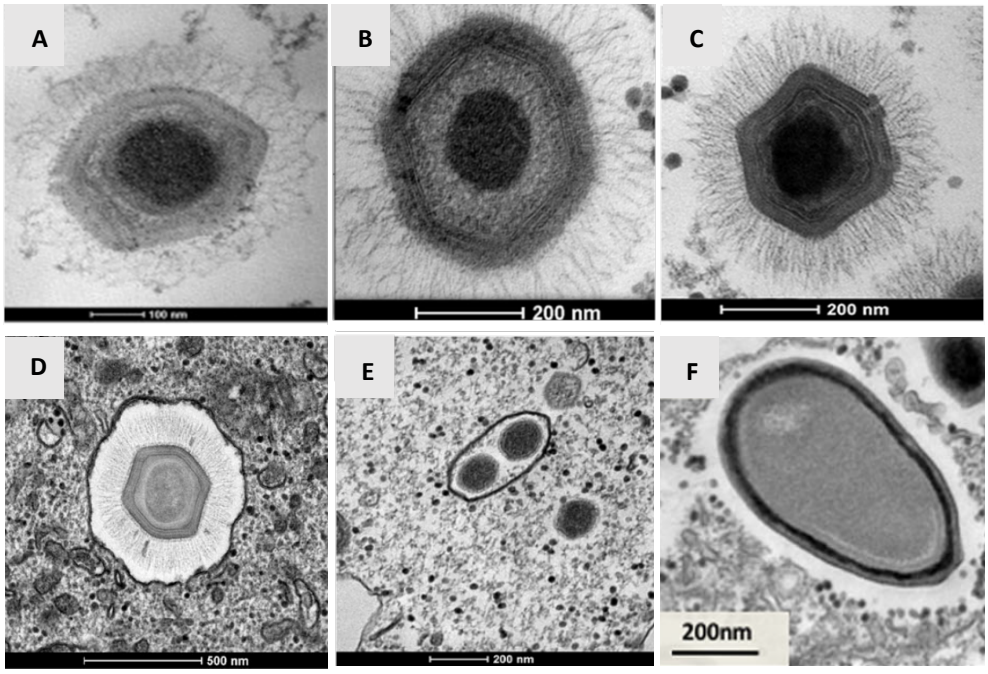

Figura 17: Vírus isolados pelo Grupo de Estudo e Prospecção de Vírus Gigantes. (A) Samba vírus, isolado a partir de amostra de água coletadas no Rio Negro, Amazônia. **(B)** Niemeyer vírus, isolado de água coletada na lagoa da Pampulha, Belo Horizonte. **(C)** Kroon vírus, isolado a partir de amostra de água da lagoa central, Lagoa Santa. **(D)** Oyster vírus, isolado a partir de água coletados de ostras, Santa Catarina. **(E)** Brazilian marseillevírus, isolado a partir de água coletada na lagoa da Pampulha, Belo Horizonte. **(F)** Pandoravirus isolado a partir de água coletada na lagoa da Pampulha, Belo Horizonte. **Fonte:** Modificado de ANDRADE et al., 2018, 2014, BORATTO et al., 2015, 2017; CAMPOS et al., 2014; DORNAS et al., 2016**.**

Recentemente, dois novos vírus gigantes, o tupanvirus soda lake e o tupanvirus deep ocean, foram isolados pelo nosso grupo de pesquisa e, diferentemente dos demais gigantes isolados até então, apresentam uma morfologia e um conteúdo gênico nunca antes observado em toda a virosfera.

1.6. Cedratvirus getuliensis

Como mencionado anteriormente, estudos de prospecção do GEPVIG levaram à descoberta do primeiro cedratvírus brasileiro. Cedratvirus getulienses foi isolado a partir de amostras de esgoto doméstico coletadas na cidade de Itaúna, Minas Gerais, em novembro de 2016. Em 2017, essas amostras foram submetidas ao protocolo de prospecção e isolamento viral sendo inoculadas em cultivos de amebas da espécie *A. castellanii* (ANDRADE et al., 2018). Após o isolamento, amostras de células infectadas

com o novo vírus foram enviadas para análise por microscopia eletrônica de transmissão (MET). A visualização por MET evidenciou a presença de um vírus com morfologia típica de outros cedratvírus, apresentando uma partícula ovóide, com dois corks localizados nos poros apicais e um capsídeo estriado (Figura 18). Além disso, o sequenciamento do genoma de cedratvirus getuliensis seguido da análise de sintenia revelou uma alta semelhança desse vírus com cedratvirus A11 e cedratvirus laussanensis, confirmando que o isolado em estudo realmente se tratava de um cedratvírus (estudo em andamento – dados não publicados).

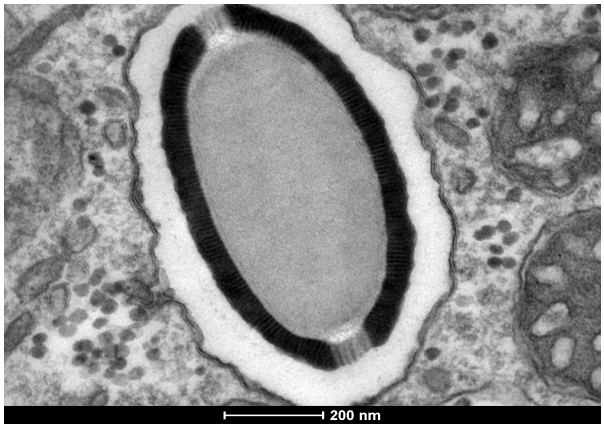

Figura 18: Imagem de microscopia eletrônica de transmissão de cedratvirus getuliensis. Partículas virais de cedratvirus getuliensis apresentam morfologia ovóide, corks nas regiões apicais e capsídeo estriado. **Fonte:** Banco de imagens do GEPVIG.

O isolamento de cedratvirus getuliensis representou a descoberta do terceiro cedratvírus no mundo. Entretanto, apesar de dois trabalhos terem sido anteriormente publicados, pouco ainda se sabe sobre as diferentes etapas que compõem o ciclo de multiplicação desses vírus, como penetração, morfogênese e liberação, sendo esse um campo aberto para novos estudos (ANDREANI et al., 2016; BERTELLI et al., 2017).

1.7. Tupanvírus

1.7.1. Descoberta

Desde o início dos estudos de prospecção, nosso grupo de pesquisa tenta buscar diferentes vírus gigantes a partir de coleções contendo amostras dos mais variados e extremos ambientes brasileiros. A história da descoberta do primeiro tupanvírus se iniciou justamente com o estudo de amostras provenientes de lagoas da região do

Pantanal – Mato Grosso do Sul (soda lakes), Nhecolândia, que representam um dos ambientes aquáticos mais extremos do planeta, com alta salinidade e pH. A partir da inoculação de algumas dessas amostras em cultivos de *A. castellanii,* um efeito citopático caracterizado por arredondamento e aglomeração amebiana, não antes visto para outros vírus gigantes, foi observado. A formação desses aglomerados, ou "cachos", levantou suspeitas sobre a possibilidade de um novo isolado viral e afim de confirmar esse resultado, amebas infectadas foram encaminhadas para microscopia eletrônica de varredura. A observação da amostra revelou a presença de um vírus com uma morfologia extremamente distinta, apresentando uma longa cauda, e em tributo às tribos indígenas Guarani, que tem como principal figura mitológica o Deus do trovão Tupã, esse novo micro-organismo foi denominado tupanvirus soda lake (Figura 19) (ABRAHÃO et al., 2018).

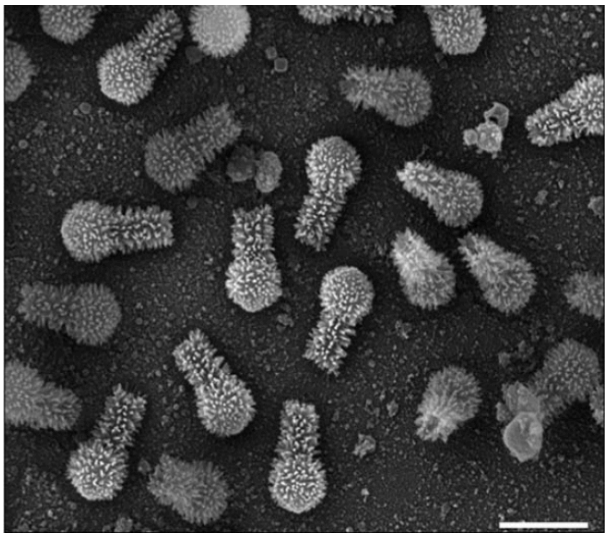

Figura 19: Partículas virais do tupanvírus observadas por microscopia eletrônica de varredura. Partículas virais de tupanvírus apresentam uma longa cauda. Barra de escala: 1 μm
Fonte: Modificado de ABRAHÃO et al., 2018.

Posteriormente um segundo tupanvírus, denominado tupanvírus deep ocean, foi isolado de amostras de sedimentos oceânicos coletados a 3.000 metros de profundidade na bacia de Campos dos Goytacases, Rio de Janeiro. Análises do genoma foram então conduzidas e evidenciaram a presença de diferenças consideráveis entre os dois isolados virais (ABRAHÃO et al., 2018).

1.7.2. Estrutura

Após a descoberta do tupanvírus, novas análises por microscopia eletrônica de transmissão e varredura foram feitas para melhor entender a morfologia desses vírus. Essas análises revelaram que a partícula viral é composta por um capsídeo de estrutura bastante similar ao dos mimivírus, com um tamanho aproximado de 450 nm, um vértice modificado em star-gate e fibrilas recobrindo a parte externa (Figura 20). Além disso, uma membrana lipídica foi observada na parte interna do capsídeo e, assim como em outros vírus gigantes, está associada ao início do ciclo de multiplicação dos tupanvírus (ABRAHÃO et al., 2018).

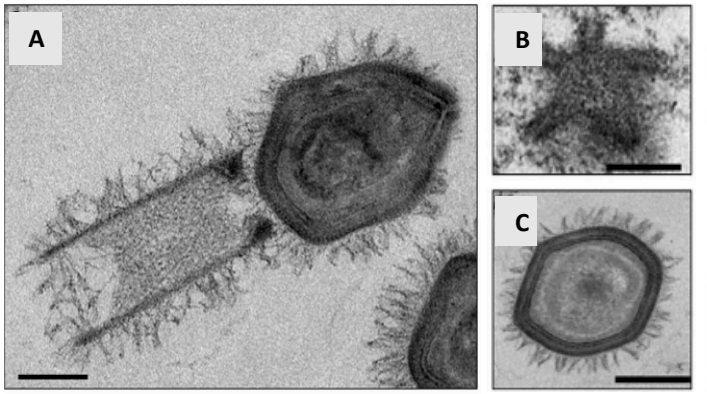

Figura 20: Estrutura da partícula viral do tupanvírus. (A) Imagem de microscopia eletrônica de transmissão evidenciando a estrutura de toda partícula viral. Barra de escala: 200 nm. **(B)** Star-gate em corte transversal. Barra de escala: 100 nm. **(C)** Capsídeo cortado transversalmente. Barra de escala: 200 nm. **Fonte:** Modificado de ABRAHÃO et al., 2018.

A despeito dessas similaridades, tupanvírus apresenta uma longa cauda cilíndrica ligada ao capsídeo, que nunca tinha sido observada em outros vírus (Figura 20A). Essa estrutura apresenta aproximadamente 550 nm de extensão e 450 nm de diâmetro, incluindo as fibrilas, e se encontra acoplada à base do capsídeo, na região oposta ao star-gate (Figura 21). Além disso, um conteúdo de natureza ainda não identificada pode ser observado no interior da cauda. Apesar de não aparentarem ser fortemente ligados, tentativas de separação por tratamentos mecânico e enzimáticos não foram capazes de separar a cauda e o capsídeo do tupanvírus (ABRAHÃO et al., 2018).

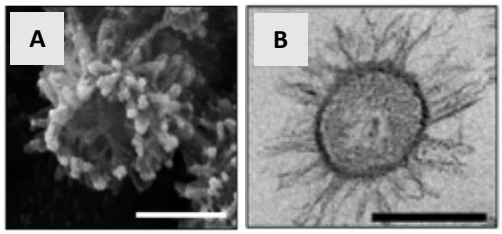

Figura 21: Estrutura da cauda do tupanvírus. (A) Imagem de microscopia eletrônica de varredura evidenciando base da cauda. Barra de escala: 250 nm. **(B)** Imagem de microscopia eletrônica de transmissão de corte transversal da cauda. Barra de escala: 200 nm. **Fonte:** Modificado de ABRAHÃO et al., 2018.

Juntamente, cauda e capsídeo fazem com que o tamanho total da partícula dos tupanvírus seja de ~1,2 μm de comprimento. Entretanto, devido a uma plasticidade no tamanho da cauda, partículas de até 2,3 μm podem ser observadas. A presença dessas partículas, denominadas de super-tupans, fazem dos tupanvírus os maiores vírus já descritos em toda a virosfera (ABRAHÃO et al., 2018).

1.7.3. Espectro de hospedeiros e ciclo de multiplicação

Em contraste aos demais vírus gigantes, os tupanvírus apresentam um amplo espectro de hospedeiros. Testes de permissividade foram conduzidos em um largo painel de protozoários e foi observado que tupanvírus é capaz de infectar e se multiplicar em diferentes espécies do gênero *Acanthamoeba (A. castellanii, A. sp E4, A. polyphaga e A. griffini)*, em *Vermamoeba vermiformis*, *Dyctiostelium discoideum* e também em *Willaertia magna.* Além de ocasionar uma infecção produtiva, com aumento do título viral nessas amebas, esse vírus também e capaz de causar outros três diferentes tipos de interação com outros protozoários: (I) um ciclo abortivo em *A. michelline* e *A. royreba*, (II) uma interação refratária em *Trichomonas tenax* e (III) uma interação citotóxica singular, sem multiplicação viral, em *Tetrahymena hyperangularis* (ABRAHÃO et al., 2018).

O ciclo de multiplicação do tupanvírus foi estudado por microscopia eletrônica de transmissão em *A. castellanii* e *V. vermiformis* e ocorre de maneira similar em ambas as células. Inicialmente as partículas virais se aderem à superfície celular e são internalizadas por fagocitose, sendo posteriormente observadas dentro de fagossomos no citoplasma (1-2 h.p.i) (Figura 22A e B). Em seguida, o genoma é liberado através da abertura do star-gate pela fusão da membrana interna do capsídeo com a membrana do

fagossomo. Curiosamente, a abertura do star-gate pode ser precedida, ou seguida, da invaginação da membrana do fagossomo para o interior da cauda, causando a liberação do conteúdo desta no citoplasma das amebas (Figura 22C e D). Após a fase típica de eclipse, fábricas virais são formadas no citoplasma e a morfogênese começa a ser observada (7-12 h.p.i) (Figura 22E). A análise da morfogênese viral revelou que a cauda é ligada ao capsídeo somente após a formação e fechamento do mesmo, sendo o processo associado à fábrica viral (Figura 22F). Em tempos tardios, (16-24 h.p.i), o citoplasma da ameba é preenchido com partículas virais maduras, seguido da lise celular e liberação dos vírus (ABRAHÃO et al., 2018).

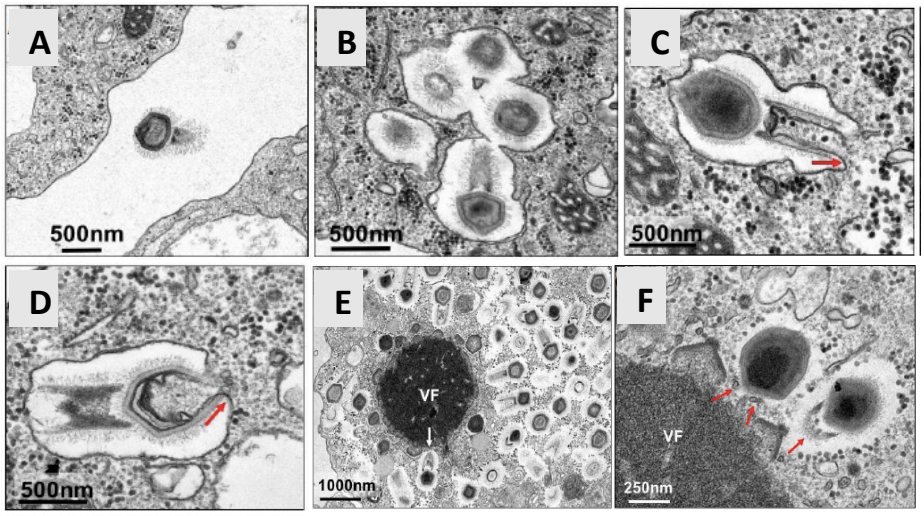

Figura 22: Ciclo de multiplicação de tupanvírus soda lake em *A. castellanii*. (A) As partículas são internalizadas através de fagocitose. **(B)** As partículas são observadas no interior de fagossomos. **(C)** Pode ocorrer fusão de membrana da cauda com o fagossomo (seta vermelha), causando a liberação do conteúdo da cauda no citoplasma. **(D)** O genoma é liberado através da abertura do star-gate e pela fusão da membrana interna do capsídeo com o fagossomo (seta vermelha). **(E)** Fábrica virail e morfogênese, evidenciando a presença de uma partícula viral completa (seta branca). **(F)** A cauda é ligada ao capsídeo (seta vermelha) após a formação e fechamento do mesmo, sendo o processo associado a fábrica viral. **Fonte:** Modificado de ABRAHÃO et al., 2018.

1.7.4. Genoma e aparato traducional

Tupanvirus soda lake e tupanvirus deep ocean apresentam um genoma composto por uma dupla fita de DNA linear, rico em conteúdo AT (28% GC), com aproximadamente 1,4 e 1,5 Mb, respectivamente. Além disso, 1276 e 1425 ORFs foram preditas, sendo 375 e 378 correspondentes a ORFans, respectivamente (ABRAHÃO et al., 2018).

A análise das ORFs dos dois tupanvírus revelou como principais *best hits* sequências das linhagens A, B e C de mimivírus e também dos klosneuvírus. Os demais *best hits* foram relacionados a Eukaria e Bacteria. A análise filogenética com base no gene da DNA polimerase B, comumente utilizado na filogenia de vírus gigantes, evidenciou o agrupamento dos tupanvírus com outros mimivírus, sugerindo que aqueles são parentes destes e possivelmente representam um novo gênero dentro de *Mimiviridae* (Figura 23) (ABRAHÃO et al., 2018).

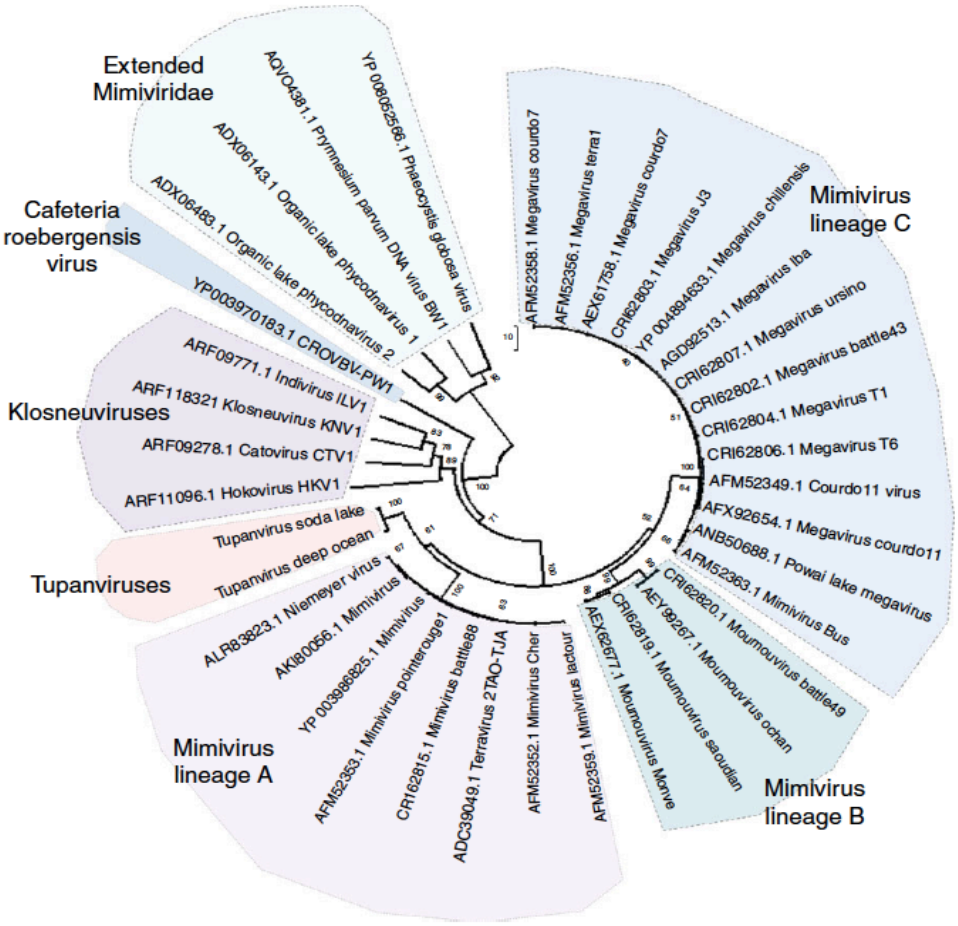

Figura 23: Árvore filogenética baseada no gene da DNA polimerase B. A análise filogenética demonstra que os tupanvírus se agrupam juntamente aos membros da família *Mimiviridae*, formando um novo gênero. **Fonte:** Modificado de ABRAHÃO et al., 2018.

Além de apresentarem o quarto maior genoma viral descrito até então, tupanvírus soda lake e tupanvírus deep ocean também apresentam o maior aparato traducional da virosfera, com 20 ORFs codificadoras de aminoacil-tRNA-sintetases (aaRS) e 67 e 70 tRNAs, associados a 46 e 47 códons, respectivamente. Tupanvírus deep ocean ainda apresenta um tRNA ambíguo relacionado ao raro aminoácido

pirrolisina. Dessa maneira, dentre os 22 aminoácidos existentes, tupanvírus deep ocean contém genes relacionados a 21 aminoácidos, com exceção somente para selenocisteína. A partir dessas informações, análises filogenéticas também foram desenvolvidas com o objetivo de investigar a possível origem dos genes de aaRS, no entanto não foi possível afirmar que a origem da maioria desses genes seja celular (ABRAHÃO et al., 2018).

Outros fatores envolvidos no processo de tradução foram identificados nos tupanvírus. Dentre eles, oito fatores de iniciação (F2 alfa, IF2 beta, IF2 gama, IF4e - duas cópias em tupanvirus soda lake, IF5a - 2 cópias em tupanvirus deep ocean, SUI1, IF4a), um fator de elongação/iniciação (GTP-binding elongation/initiation), um fator de elongação (Ef-aef-2) e um fator de terminação (ERF1). Além desses, outros fatores relacionados à maturação e estabilização de tRNAs, maturação de RNAm, *splicing* e modificação de proteínas ribossomais também foram relatados (ABRAHÃO et al., 2018).

Sendo assim, a caracterização genômica dos tupanvírus evidenciou um genoma complexo, com diversos fatores relacionados à síntese protéica sugerindo que esses vírus apresentam uma considerável independência da maquinaria celular do hospedeiro e levantando questionamentos sobre a presença de outras possíveis sequências, de natureza ribossomal, por exemplo, que pudessem complementar esse aparato de tradução.

1.8. Amebas de vida livre e outros protozoários

As amebas de vida livre (AVLs) são protozoários unicelulares ubíquos, sendo encontrados no solo, esgoto, poeira, ambientes aquáticos e ar atmosférico. Além disso, podem ser encontradas colonizando uma grande variedade de organismos, incluindo peixes, pássaros, mamíferos e seres humanos (KHAN et al., 2007; LIU et al., 2006). As AVLs têm sido amplamente utilizadas como plataforma de isolamento de vírus gigantes, principalmente amebas pertencentes ao gênero *Acanthamoeba* (LA SCOLA et al., 2003).

Apesar de *Acanthamoeba* ser composto por amebas consideradas de vida livre, algumas espécies desse gênero, principalmente *Acanthamoeba polyphaga* e *A. castellanii*, podem ser consideradas como patógenos oportunistas e causar doenças em humanos, como lesões cutâneas, ceratite e encefalite. Além das próprias amebas serem agentes causadores de doenças, elas também servem como plataformas de replicação

para outros micro-organismos patogênicos, incluindo bactérias causadoras de infecções respiratórias, como *Legionella pneumophila*, *Pseudomonas aeruginosa* e *Coxiella burnetii*, e leveduras, como *Cryptococcus neoformans* (CASTRILLÓN; OROZCO, 2013; SIDDIQUI; KHAN, 2012). Além disso, espécies de *Acanthamoeba* são hospedeiros de diversos vírus gigantes, como os mimivírus, marseillevírus, pandoravírus, cedratvírus, tupanvírus, entre outros. Desta forma estes protozoários são importantes reservatórios de diversos micro-organismos, sendo chamados de "cavalos de Tróia" do mundo microbiano (GREUB; RAOULT, 2004; PAGNIER et al., 2015; RAOULT; BOYER, 2010).

O ciclo de vida dessas amebas envolve dois estágios: uma forma vegetativa conhecida como trofozoíto (Figura 24A) e uma forma de resistência conhecida como cisto (Figura 24B). As amebas em estágio de trofozoíto se alimentam de bactérias, leveduras e algas por fagocitose, ou podem captar nutrientes dispersos no ambiente por pinocitose. Sob condições ótimas de crescimento, os trofozoítos se dividem por mitose. No entanto, sob condições adversas, como dessecação, privação de nutrientes, hiperosmolaridade e temperaturas extremas, eles sofrem diferenciação celular e dão origem aos cistos que desempenham um papel crucial na sobrevivência e propagação desses protozoários. Esse processo de diferenciação de trofozoíto para cisto é denominado encistamento e envolve um massivo *turnover* de componentes, assim como mudanças estruturais e funcionais em toda a célula (CASTRILLÓN; OROZCO, 2013; FOUQUE et al., 2012; MOON et al., 2008; SIDDIQUI; KHAN, 2012).

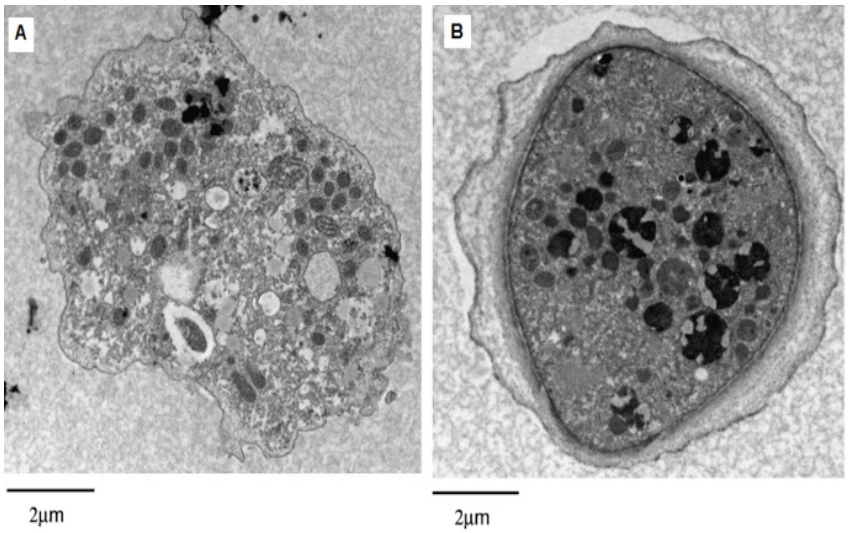

Figura 24: Estágios do ciclo de vida de amebas do gênero *Acanthamoeba*. (**A**) Estágio de trofozoíto. (**B**) Estágio de cisto. **Fonte:** Modificado de SIDDIQUI; KHAN, 2012.

Além das amebas, outro protista de vida livre, *Tetrahymena hiperangularis*, também foi recentemente associado ao estudo dos vírus gigantes (ABRAHÃO et al., 2018). *Tetrahymena* é um gênero constituído por protozoários ciliados, de formato ovóide/piriforme, que apresentam a superfície celular recoberta por fileiras de cílios uniformemente espaçadas (Figura 25). Assim como outros ciliados, esses protozoários apresentam uma "boca ciliar" (citóstomo) capaz de criar correntes de alimentação que direcionam os alimentos, na maioria das vezes bactérias, para a sua direção, sendo a partir daí ingeridos por fagocitose (GRONLIEN; BERG; LOVLIE, 2002; LYNN et al., 2000; WONG, 2017).

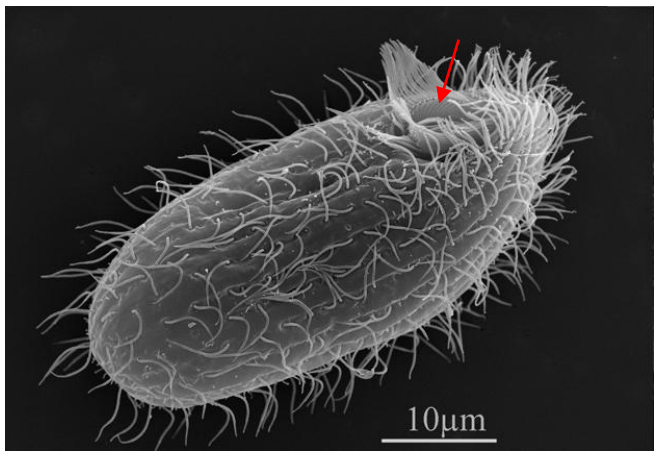

Figura 25: Imagem de microscopia óptica de *Tetrahymena* sp. É possível observar a presença do citóstomo (seta) e dos cílios distribuídos em fileiras espaçadas. Barra de escala: 10µm. **Disponível em:** <http://enfo.agt.bme.hu/drupal/node/12845>. Acesso em: 25 abr. 2018.

O processo de fagocitose em protozoários é amplamente utilizado para alimentação e é desencadeado pelo reconhecimento e adesão, seguido de internalização e degradação de partículas (ROWBOTHAM, 1980). Korn e Weisman demonstraram, através de experimentos utilizando esferas de látex de diferentes tamanhos, que a fagocitose em *Acanthamoeba*, por exemplo, é estimulada na presença de partículas acima de 500 nm (KORN; WEISMAN, 1967). O desencadeamento do processo de fagocitose é uma condição *sine qua non* para a maioria dos vírus gigantes iniciarem seu ciclo de multiplicação e formar sua progênie. A maioria desses vírus, a exemplo dos mimivírus, pandoravírus, pithovírus, cedratvírus e tupanvírus, cumprem o requisito primário para o estímulo da fagocitose, uma vez que apresentam partículas virais maiores que 500 nm (LEGENDRE et al., 2014, 2015; PHILIPPE et al., 2013; RETENO et al., 2015).

1.9. Interações entre vírus gigantes e protozoários

Os vírus apresentam uma especificidade notável quanto aos tipos de células que são capazes de infectar e multiplicar. Entender essa relação pode revelar uma gama de componentes do hospedeiro que são necessários para o estabelecimento da multiplicação viral e também os fatores de restrição impostos por esses organismos para limitar ou impedir o avanço de uma infecção viral. Por esse motivo, estudos envolvendo interações entre vírus-hospedeiros são indispensáveis no avanço da virologia.

Um interessante exemplo de interação vírus gigante-ameba foi recentemente observado pelo nosso grupo de pesquisa. Boratto e colaboradores descreveram que o APMV não é capaz de infectar cistos de *A. castellanii*, demonstrando que o encistamento pode prevenir a infecção por esses vírus. Por outro lado, quando trofozoítos são previamente infectados, o encistamento não é desencadeado, evidenciando que esses vírus são capazes de prevenir o processo de formação dos cistos (BORATTO et al., 2015).

Anteriormente, no ano de 2008, Frada e colaboradores descreveram um tipo de relação ecológica e evolutiva denominada de teoria do Gato Risonho. Essa teoria abrange uma interação previamente desconhecida entre um phycodnavírus, o *Emiliania huxleyi virus* (EhVs), também classificado como um NCLDV, e um eucarioto unicelular fotossintético, o cocolitoforídeo *Emiliania huxleyi*. Essa alga, apresenta dois estágios de vida: uma fase haplóide, não calcificada, e um fase diplóide, calcificada. Os autores observaram que o vírus é capaz de infectar e lisar somente as células em estágio diplóide, enquanto a fase haplóide é resistente à infecção pelo EhVs. Também foi demonstrado que a exposição das células diplóides ao vírus induz a transição das outras células vizinhas para o estágio haplóide resistente por meio de moléculas *quorum sensing* sinalizadoras (FRADA et al., 2008).

Com base nessas observações, nosso grupo propôs a expansão da Teoria do Gato Risonho para o mundo dos vírus gigantes e *Acanthamoeba*, uma vez que assim como *E. huxleyi*, essas amebas são capazes de evadir a infecção por mimivírus, e também marseillevírus, quando estão em um estágio de vida específico: o cisto (Figura 26). Embora não haja relatos de fatores *quorum sensing* envolvidos na comunicação amebiana e no desencadeamento do encistamento, análises experimentais demonstraram que durante uma infecção por APMV uma pequena porcentagem (1–4%) de amebas são capazes de encistar. Essa diferença de susceptibilidade viral entre os estágios de vida do

hospedeiro caracteriza um mecanismo de escape que garante a sobrevivência de *Acanthamoeba* e pode representar uma das razões do sucesso ecológico e evolutivo desse gênero (SILVA et al., 2016).

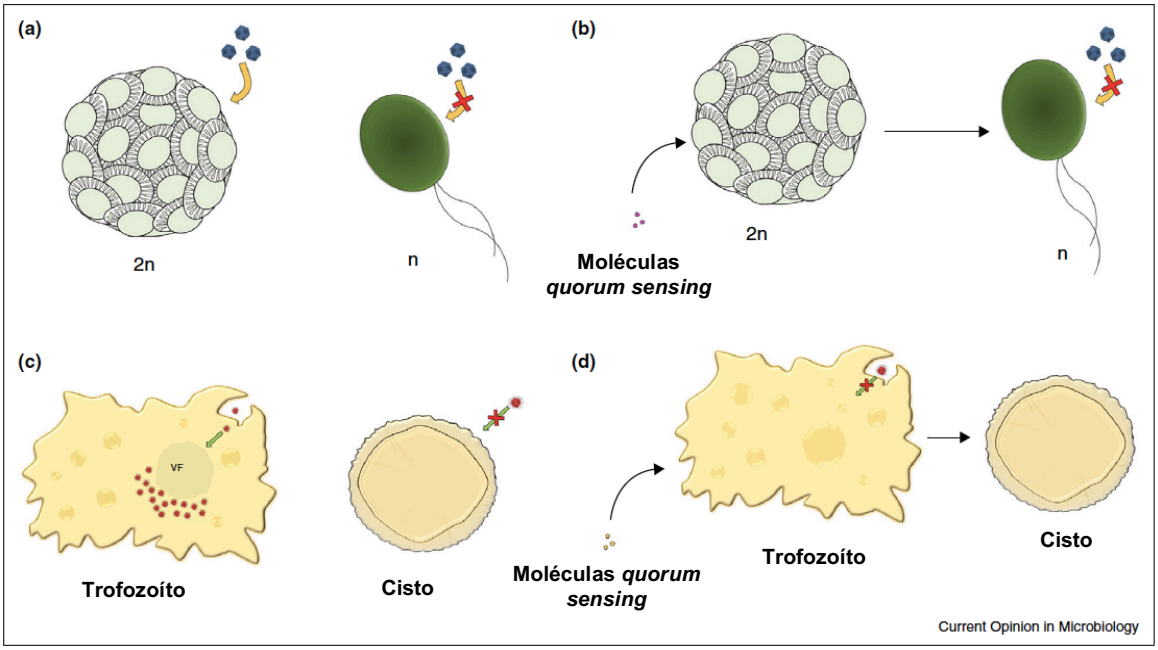

Figura 26: Teoria do Gato Risonho expandida para o universo dos vírus gigantes e amebas. (a) Emiliania huxleyi virus (EhV) infecta e causa a lise apenas de células na fase diploide do hospedeiro, enquanto a fase haplóide é resistente à infecção viral. **(b)** Moléculas quorum sensing secretadas por células diplóides infectadas com EhVs induzem a transição de células vizinhas para a fase haplóide, resistente à infecção. **(c)** Assim como EhVs, vírus gigantes infectam e causam a lise apenas de trofozoítos, enquanto os cistos são resistentes à infecção por APMV e marseillevírus. **(d)** Prováveis moléculas quorum sensing secretadas por trofozoítos infectados com vírus gigantes induzem a transição das células vizinhas para a fase de cisto. **Fonte:** Modificado de SILVA et al., 2016.

Além disso, a teoria do Gato Risonho pode ser considerada como uma relação complementar à teoria da Rainha Vermelha (VAN VALEN, 1973). Por um lado, a dinâmica da teoria do Gato Risonho demonstra a supressão da pressão viral por um curto prazo, permitindo que as amebas evoluam mecanismos de resistência a outros fatores de estresse. Contudo, pelo outro lado, a capacidade dos mimivírus impedirem o encistamento, uma vez que a infecção já tenha se iniciado, pode ser um exemplo da ocorrência da teoria da Rainha Vermelha. Dessa maneira, a ocorrência simultânea dessas duas teorias parece direcionar a evolução dos vírus gigantes e de seus hospedeiros (SILVA et al., 2016).

Outra interessante interação entre vírus gigantes e protozoários também foi observada logo após a descoberta do tupanvírus. Como mencionado anteriormente, o tupanvírus soda lake é capaz de ocasionar uma citotoxicidade que até então não tinha sido descrita para nenhum outro vírus conhecido. Esse perfil foi inicialmente observado após tentativas frustradas de realização do RNA-seq viral. Após a preparação de amostras para o sequenciamento, um controle de qualidade de dosagem do RNA total em espectrofotômetro demonstrou surpreendentemente a presença de uma ínfima quantidade de RNA. Para a confirmação de tal resultado, as amostras preparadas também foram submetidas a fracionamento eletroforético para análise da qualidade do RNA, entretanto nenhuma banda correspondente às subunidades ribossomais 18S e 28S do hospedeiro foram observadas, evidenciando a ocorrência de uma degradação ribossomal.

Esse perfil citotóxico, caracterizado pelo *shutting down* do RNA ribossomal da célula infectada, foi observado em *Tetrahymena hyperangularis*, um protozoário não permissivo ao tupanvírus, assim como em *A. castellanii e V. vermiformis* em alta multiplicidade de infecção viral. Além disso, a mesma citotoxicidade não foi observada nas mesmas condições para mimivírus, evidenciando que esse perfil é especificamente causado por tupanvirus soda lake. A observação desse fenômeno, em que uma partícula viral é responsável pela modulação de organismos independentemente da multiplicação, levou a questionamentos acerca do mecanismo pelo qual a degradação ribossomal ocorre, sugerindo a participação do canônico processo de ribofagia.

A descrição dessas relações demonstra que os estudos envolvendo interações entre os vírus gigantes e protozoários estão somente no início e que mais empenhos ainda são necessários para o melhor entendimento dessas singulares relações entre esses patógenos e seus hospedeiros.

1.10. Ribofagia: autofagia de ribossomos

Como mencionado, após a descoberta do fenótipo citotóxico causado por tupanvirus soda lake em células hospedeiras e não hospedeiras, novos questionamentos sobre qual mecanismo poderia estar relacionado a esse fenômeno foram levantados. Num primeiro momento, a hipótese inicial foi de que o *shutting down* do RNA ribossomal pudesse estar relacionado ao processo de ribofagia: um tipo seletivo de

autofagia, responsável pela degradação de ribossomos em períodos prolongados de privação de nutrientes (KRAFT et al., 2008).

A autofagia é um canônico mecanismo de degradação de macromoléculas e organelas celulares, que envolve a formação de vesículas especializadas, capazes de englobar porções citoplasmáticas, proteínas e organelas danificadas encaminhando-as para a degradação após fusão com lisossomos. A ocorrência desse processo apresenta alguns marcadores típicos como a formação de vesículas contendo dupla membrana, a acidificação de autofagossomos e a participação de um grupo de proteínas codificadas por genes denominados Atg (autophagy-related genes) (CHOI; BOWMAN; JUNG, 2018; KRAFT et al., 2008).

Em 2009, Moon e colaboradores descreveram um gene homólogo ao gene Atg-8 em amebas *A. castellanii*. Denominado de AcAtg-8, esse gene foi associado à biogênese e elongamento de membranas de fagóforos, precursores de autofagossomos maduros (MOON et al., 2009). Posteriormente, uma segunda isoforma de Atg8 (AcAtg-8b), foi descrita em *Acanthamoeba,* sendo também associada à ocorrência de autofagia (MOON et al., 2013). Nesses protozoários, o processo de autofagia é naturalmente requerido e responsável por mudanças na composição celular durante a diferenciação. Dessa maneira, durante o encistamento, por exemplo, em que um massivo turn-over de proteínas e outros componentes celulares pode ser observado, a autofagia é um dos mecanismos fundamentais (MOON et al., 2009, 2013).

2. JUSTIFICATIVA

Os vírus são as entidades biológicas em maior abundância e diversidade na natureza, sendo encontrados nos mais diferentes ambientes. Estima-se, por exemplo, que existam mais partículas virais na Terra do que estrelas no universo. Nos últimos anos, vários vírus foram descritos e isolados a partir de hospedeiros pertencentes aos três domínios da vida. No entanto, apesar dessa abundância e diversidade pouco ainda é conhecido sobre o papel dos vírus na natureza.

A descoberta dos vírus gigantes acarretou numa quebra de paradigmas no campo da virologia, uma vez que, anteriormente, acreditava-se que os vírus eram micro-organismos filtráveis através de membranas de 0,22 μm e não visíveis em microscopia ótica. Além disso, o estudo desses vírus revelou uma complexidade genética, proteica e estrutural nunca antes vista na virosfera e comparável ao apresentado por bactérias, arquéias e alguns eucariotos.

Na última década, os estudos de prospecção viral se intensificaram e outros vírus pertencentes à família *Mimiviridae*, como tupanvírus, assim como outros não pertencentes a essa família, como cedratvírus, também foram descritos. A análise do tupanvírus revelou a presença de um extenso aparato traducional e de uma interação caracterizada pelo *shutting down* do RNA ribossomal em células hospedeiras e não hospedeiras, desencadeando questionamentos relacionados à presença de outros fatores que pudessem complementar esse aparato de síntese proteica, assim como hipóteses acerca do mecanismo envolvido na degradação do RNA ribossomal. Já o isolamento do cedratvirus getuliensis representou a descoberta do terceiro cedratvírus descrito, no entanto, apesar de dois outros já terem sido caracterizados, ainda há poucas informações a respeito das etapas que envolvem a penetração, morfogênese e liberação desses vírus gigantes.

O isolamento desses novos vírus desencadeou debates e revelou um conhecimento ainda limitado da virosfera. Desta forma, o presente trabalho se faz necessário, uma vez que busca estudar características peculiares de dois vírus recentemente isolados, tupanvírus e cedratvírus, abordando aspectos relacionados ao ciclo de multiplicação, às sequências do genoma viral, assim como o aprofundamento de um perfil de interação entre vírus e hospedeiro nunca antes descrito na virosfera.

3. OBJETIVOS

3.1. Objetivo geral

Analisar interações entre vírus gigantes e protozoários a partir da investigação do mecanismo envolvido no *shutting down* do RNA ribossomal e da presença de sequências ribossomais em tupanvirus soda lake, assim como da caracterização do ciclo de multiplicação do Cedratvirus getuliensis.

3.2. Objetivos específicos

3.2.1. Investigação do *shutting down* do RNA ribossomal e da presença de sequências ribossomais em tupanvírus

- Investigar a ocorrência do perfil citotóxico relacionado ao *shutting down* do RNA ribossomal diante da infecção pelo tupanvirus soda lake;
- Avaliar a ação de inibidores farmacológicos na ocorrência do *shutting down*;
- Avaliar o papel do gene codificador de Atg8 no processo de *shutting down*;
- Avaliar a ocorrência de alterações nucleares durante o processo do *shutting down*;
- Investigar eventuais mudanças de pH ocasionadas pelo tupanvírus no citoplasma do hospedeiro;
- Investigar a formação de vesículas contendo ribossomos induzidas por tupanvírus por microscopia eletrônica de transmissão;
- Investigar a presença de sequências ribosomais no genoma do tupanvírus;
- Investigar a origem evolutiva dessas sequências ribossomais, assim como sua expressão durante a multiplicação viral.

3.2.2. Caracterização do ciclo de multiplicação do Cedratvirus getuliensis

- Elucidar o mecanismo de penetração do cedratvirus getuliensis em células de *A. castellanii* através do uso de diferentes inibidores farmacológicos;

- Avaliar o impacto do uso de inibidor de transporte de membrana no ciclo de multiplicação do cedratvirus getuliensis;
- Caracterizar a fábrica viral e investigar a ocorrência de alterações celulares durante a multiplicação viral;
- Investigar e descrever as etapas da morfogênese viral;
- Realizar a caracterização da partícula viral;
- Avaliar a ocorrência de partículas defectivas durante a multiplicação;
- Investigar os possíveis mecanismos de liberação das partículas virais ao final da multiplicação viral.

4. FLUXOGRAMA

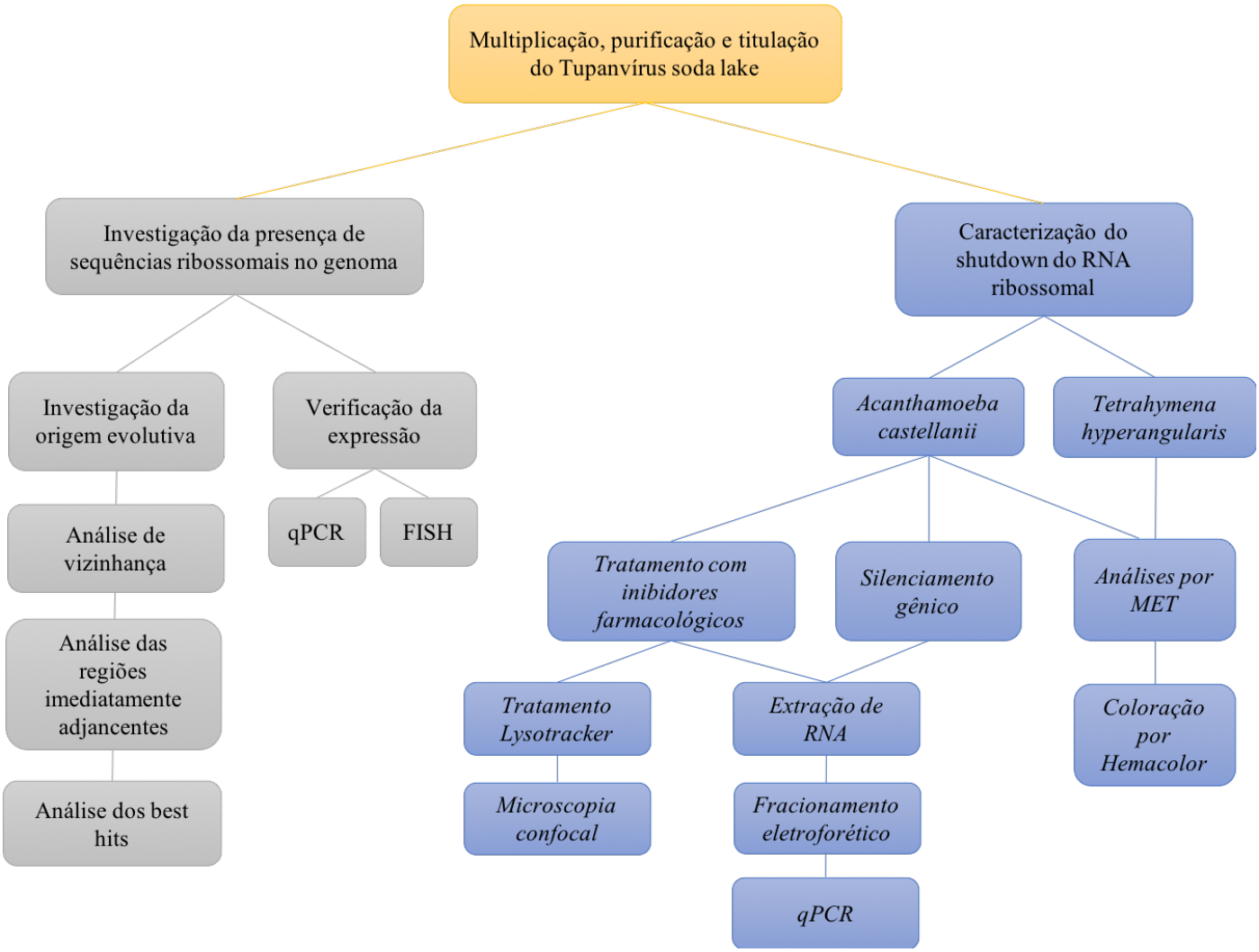

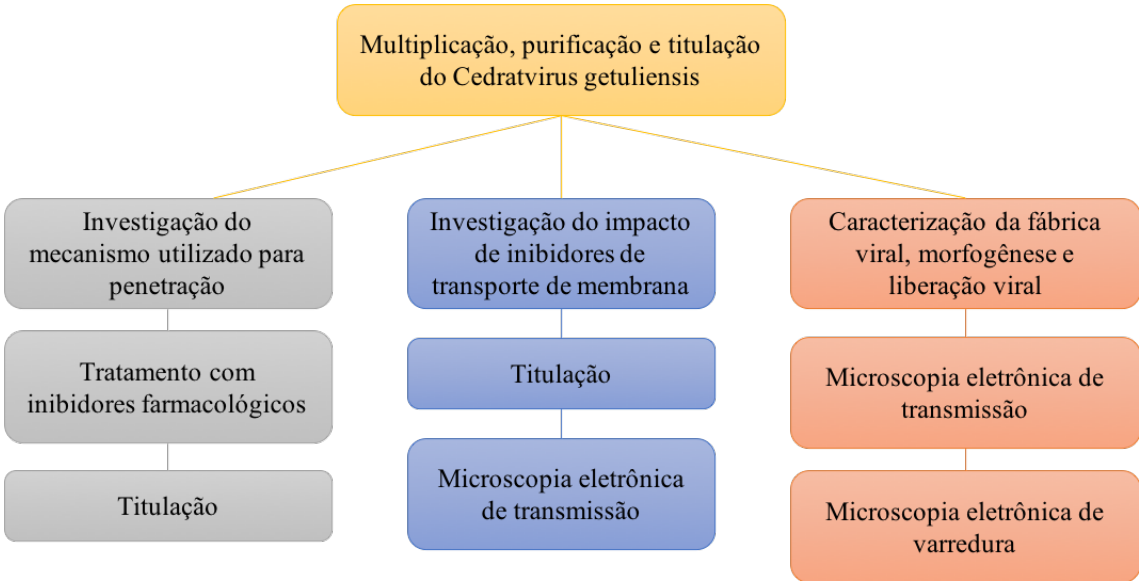

5. MATERIAIS E MÉTODOS

Com o objetivo de proporcionar uma melhor compreensão, os materiais e métodos realizados neste trabalho serão divididos em duas seções. A primeira (5.1) será referente à investigação do *shutting down* do RNA ribossomal e da presença de sequências ribossomais em tupanvírus. A segunda seção (5.2) abordará os experimentos conduzidos com o intuito de caracterizar o ciclo de multiplicação do cedratvirus getuliensis.

5.1. Investigação do *shutting down* do RNA ribossomal e da presença de sequências ribossomais em tupanvírus

Os experimentos descritos nessa seção foram desenvolvidos durante o período de doutorado sanduíche realizado na Aix Marseille Université – França, através do programa CAPES/COFECUB, sob supervisão do professor Bernard La Scola.

5.1.1. Investigação do *shutting down* do RNA ribossomal

Após a descoberta do fenótipo citotóxico causado por tupanvirus soda lake em células hospedeiras (*A. castellanii*) e não hospedeiras (*T. hyperangularis*), a hipótese inicial foi de que o shutting down do RNA ribossomal pudesse estar relacionado ao canônico processo de ribofagia/autofagia. Com o objetivo de corroborar ou não essa hipótese, uma gama de experimentos envolvendo o uso de inibidores de acidificação, a investigação da ocorrência de acidificação das células, o silenciamento gênico de Atg-8 e a observação da presença de vesículas com dupla membrana durante a infecção por tupanvirus soda lake foram realizados.

5.1.1.1. Sistema celular

Para a produção viral e experimentação foram utilizadas amebas *Acanthamoeba castellanii* (ATCC 30010) *e Tetrahymena hyperangularis* (ATCC 30273) originadas da *American Type Culture Collection* (Maryland, EUA). As amebas foram cultivadas em meio PYG comercial (Eurobio, França) suplementado com 500 U/mL de penicilina e 500 U/mL de estreptomicina (Gibco, EUA). As células *Acanthamoeba castellanii* foram

mantidas a 32 ºC e as células de *Tetrahymena hyperangularis* foram mantidas a 28 °C em estufa. Ambas as células foram cultivadas em garrafas (Corning Sigma-Aldrich, EUA) completamente vedadas, sendo os subcultivos realizados três vezes por semana ou de acordo com a necessidade.

5.1.1.2. Vírus

Para a realização dos experimentos descritos nesta seção foram utilizados tupanvirus isolados a partir do ambiente soda lake (previamente obtidos pelo nosso grupo de pesquisa, conforme descrito no item 1.7.1) e não submetidos ao processo de clonagem. Como vírus controle também foi utilizado o APMV, protótipo do grupo I, que foi gentilmente cedido pelo Dr. Didier Raoult (Aix-Marseille Université, França). Estoques virais de ambos os vírus foram produzidos e titulados, de acordo com a necessidade, em células de *A. castellanii*.

5.1.1.3. **Multiplicação e purificação viral** (ABRAHÃO et al., 2016)

Para a produção viral, $7x10^6$ amebas *A. castellanii,* cultivadas em garrafas de cultura T175 (Corning Sigma-Aldrich, EUA), foram infectadas com tupanvirus soda lake, em uma multiplicidade de infecção (MOI) de 0,1, ou com APMV, em uma MOI de 0,01. Após a infecção, as garrafas contendo os inóculos virais foram mantidas a 32 °C, completamente vedadas. A monocamada celular foi avaliada diariamente para acompanhamento da evolução do efeito citopático e após a lise celular, o sobrenadante e os fragmentos celulares foram coletados e submetidos a 3 ciclos de congelamento e descongelamento, visando a liberação de partículas virais eventualmente retidas em amebas não lisadas. Em seguida, o sobrenadante e o lisado foram filtrados em filtros de 0,8 μm (Millipore, E.U.A.) e submetidos à centrifugação a 11.000 x g, por 10 minutos, a 4°C em centrífuga *Jouan CR3i* (rotor AC100.10). O sobrenadante foi descartado e o *pellet* foi ressuspendido em solução salina para amebas (PAS) (Anexo I) para lavagem. Os tubos foram novamente centrifugados sob as mesmas condições e o *pellet* foi novamente ressuspendido em PAS e vagarosamente gotejado sobre 10 mL de uma solução de sacarose 24% (Sigma-Aldrich, EUA) em tubos para ultracentrifugação. Esses tubos foram então centrifugados a 36.000 x g, por 1 hora, a 4°C em ultra-centrífuga *Beckman Coulter – Optima XPN-80* (rotor SW 32 Ti) para que as partículas

virais fossem sedimentadas. Por fim, o sobrenadante foi descartado e o sedimento ressuspendido em 300 µL de PAS. Alíquotas das soluções virais foram feitas, identificadas e estocadas à -20 ºC.

5.1.1.4. **Titulação viral** (ABRAHÃO et al., 2016; REED; MUENCH, 1938)

Placas de 96 poços (BD-falcon, EUA) contendo 100 µL de meio PYG e $4x10^4$ amebas *A. castellanii*/poço foram utilizadas para titulação de vírus gigantes pelo método de diluição limitante (REED; MUENCH, 1938). As amostras virais a serem tituladas foram diluídas em PAS seriadamente, na razão de 10 (10^{-1} a 10^{-11}), e em seguida, um total de 100 µL de cada diluição foi adicionado a cada poço, em quadruplicata. Uma quadruplicata de poços foi reservada como controle de viabilidade de amebas. As placas foram vedadas completamente e incubadas a 32 ºC. Cada poço foi monitorado diariamente, para observação de efeitos citopáticos, e após 4 dias de incubação, o cálculo do título viral foi realizado e o valor foi expresso em $TCID_{50}$ por mililitro (mL) (REED; MUENCH, 1938).

5.1.1.5. Ensaios para reprodução e avaliação da ocorrência do *shutting down*

Para esses ensaios, $1x10^6$ amebas *A. castellanii* foram infectadas com tupanvírus ou APMV nas MOIs de 10 ou 100 e incubadas a 32 °C. Após 3 e 9 horas de infecção, células e sobrenadantes foram coletados e submetidos à centrifugação a 800 x g, por 10 minutos em centrífuga *Jouan CR3i* (rotor AC100.10). O sobrenadante foi descartado e o *pellet* foi congelado à -20 ºC para posterior extração de RNA. Em paralelo, para determinar se tupanvírus inativados também seriam capazes de induzir o *shutdown* do RNA ribossomal, partículas virais purificadas foram expostas à radiação UV, durante 1 hora a 60 W/m^2, ou aquecidas em termobloco (Eppendorf, Alemanha), durante 1 hora a 80 °C. Para confirmação da inativação, parte das partículas submetidas aos processos de aquecimento ou exposição à luz UV foram inoculadas em monocamadas de células *A. castellanii* para acompanhamento ou não de efeito citopático. Como controle viral, partículas de APMV também foram submetidas aos mesmos procedimentos. Em seguida, as partículas virais inativadas foram utilizadas para infectar $5x10^5$ amebas *A. castellanii*, na MOI de 100, e após 3 e 9 horas de infecção, células e sobrenadantes

também foram coletados, centrifugados e o *pellet* foi congelado à -20 ºC para extração de RNA.

Para investigação do *shutdown* em células não permissivas, $1x10^6$ células de *T. hyperangularis,* cultivadas em meio contendo 10% de PYG e 90% de PAS, foram infectadas com tupanvírus na MOI de 100. Após 1, 2, 3 e 4 dias de infecção, as células e o sobrenadante foram coletados e centrifugados a 800 x g, por 10 minutos em centrífuga *Jouan CR3i* (rotor AC100.10). O Sobrenadante foi então descartado e o *pellet* foi congelado à -20 ºC, também para posterior extração de RNA.

5.1.1.6. Extração de RNA e fracionamento eletroforético em gel de agarose

A extração de RNA total foi realizada a partir do *pellet* de células infectadas com tupanvírus e APMV utilizando-se o kit *Rneasy*® (Qiagen, Alemanha), de acordo com as recomendações do fabricante. Após a extração, o RNA resultante foi eluído em 30 μL de água livre de nuclease, acrescido de 1,5 μL de RNAseOUT (Invitrogen, EUA) e tratado com o kit Turbo DNA-Free (Invitrogen, EUA), também de acordo com as recomendações do fabricante para exclusão de DNA contaminante. Em seguida, o RNA foi dosado em nanodrop (Thermo Scientific, EUA).

Para visualização da possível degradação do RNA ribossomal, 10 μL do RNA total extraído e tratado com DNAse foi submetido a fracionamento eletroforético em gel de agarose 1,5%, contendo Sybr safe® (Invitrogen, EUA), em tampão TBE (Sigma-Aldrich, EUA) a 135 V por 40 minutos. O gel foi observado e imagens foram obtidas a partir de fotodocumentador de géis (Bio-rad, EUA). O restante do RNA extraído foi armazenado a -80 °C para posterior realização de RT-PCR.

5.1.1.7. Transcrição reversa e qPCR

A obtenção de cDNA foi realizada tendo como molde o RNA total extraído conforme o item anterior. As reações foram realizadas utilizando-se o kit SuperScript VILO cDNA Synthesis® (Invitrogen, EUA), contendo primers randômicos, conforme as recomendações do fabricante. O cDNA resultante foi utilizado como molde em reações de qPCR realizadas em placas de 48 poços, em duplicata, utilizando 5 μL de

QuantiTect SYBR Green Master Mix (Qiagen, Alemanha), 1 µL de amostra, 0,4 µM de iniciadores específicos para o 18S rRNA de *A. castellanii* (5′-TCCAATTTTCTGCCACCGAA-3′ e 5′-ATCATTACCCTAGTCCTCGCGC-3′) (MOON *et al*, 2008), e água q.s.p para 10 µL de reação. Controles negativos foram realizados nas mesmas condições, sendo a amostra substituída por 1 µL de água. As reações foram feitas no aparelho CFX96 Real-Time PCR Detection System (Bio-rad, EUA) seguindo as seguintes condições térmicas: 15 minutos a 95 °C, 40 ciclos de 95 °C por 30 segundos, 60 °C por 30 segundos e 72°C por 30 segundos, seguidos de curva de dissociação. Os gráficos foram elaborados utilizando o software GraphPad Prism versão 7.00 para Windows (GraphPad Software), sendo os valores expressos em unidades arbitrárias (Δ-Ct).

5.1.1.8. Ensaios com inibidores de acidificação

Para os ensaios com inibidores, $5x10^5$ células *A. castellanii*, cultivadas em garrafas T12,5 (BD-Falcon, EUA) contendo meio PYG, foram infectadas com tupanvírus, ou APMV, na MOI de 100 e incubadas a 32 °C. Uma hora após a infecção, cloroquina (Sigma-Aldrich, EUA), na concentração final de 100 µM, e bafilomicina A (Sigma-Aldrich, EUA), na concentração final de 10 nM, foram adicionadas ao sobrenadante da cultura infectada. Como controle, células não infectadas também foram tratadas com os mesmos inibidores sob as mesmas condições. Após 3 e 9 horas de infecção, as células e o sobrenadante foram coletados e centrifugados a 800 x g, por 10 minutos em centrífuga *Jouan CR3i* (rotor AC100.10). O Sobrenadante foi descartado e o *pellet* foi submetido à extração de RNA, seguido de fracionamento em gel de agarose, RT-PCR e qPCR, conforme descrito nos itens 5.1.1.6 e 5.1.1.7.

5.1.1.9. Silenciamento gênico do gene Atg8

Para o silenciamento gênico, duplex de pequenos RNAs de interferência (siRNA) para o gene Atg8, senso (5′GAACUCAUGUCGCACAUCUTT-3′) e anti-senso (5′AGAUGUGCGACAUGAGUUCTT-3′) previamente descritos por Moon e colaboradores (2009), foram sintetizados e marcados com FITC pela Eurogentec (Bélgica). Para a transfecção, 1 µg desses siRNAs foi diluído em meio PYG e incubado

por 20 minutos com 15 μL de lipofectamina RNAiMAX (Thermo Fisher Scientific, EUA). Em seguida, essa solução contendo meio, siRNA e lipofectamina foi adicionada a tubos de microcentrífuga contendo $1x10^6$ amebas *A. castellanii* e imediatamente infectadas com tupanvírus ou APMV, na MOI de 100. Após 1 hora em homogeneização em agitador rotativo (Stuart, Reino Unido), as células e o sobredante foram transferidos para placas de 6 poços (BD-Falcon, EUA) contendo meio PYG e incubados a 32 °C em estufa por 9 horas. Posteriormente a esse tempo, as células e o sobrenadante foram coletados, centrifugados e o *pellet* foi submetido à extração de RNA, seguido de fracionamento em gel de agarose, RT-PCR e qPCR, conforme descrito nos itens 5.1.1.6 e 5.1.1.7.

Como controle de transfecção, $2x10^5$ células infectadas foram paralelamente coletadas e processadas em centrífuga para citocentrifugação do tipo Shandon Cytospin 4 (Thermo Electron Corporation) a 800 rpm por 10 min. As lâminas foram fixadas com metanol (Merck Millipore, EUA) e após secagem, foram montadas com ProLong Gold Antifade Mountant with DAPI (Thermo Fisher Scientific, EUA) e lamínulas. Em seguida foram analisadas em microscópio de fluorescência DMI6000B (Leica, Alemanha). Como controle biológico, o efeito do siRNA foi avaliado a partir da inibição do processo de encistamento que também requer a partipação do gene Atg8 (MOON *et al*, 2009). Para tanto as células foram submetidas ao mesmo processo de transfecção descritos no parágrafo anterior, no entanto após esse processo, as células e o sobrenadante foram coletados, centrifugados e o *pellet* foi ressuspendido em meio Neff (Anexo II), para indução do encistamento, e transferido para placas de 6 poços (BD-Falcon, EUA), que foram incubados a 32 °C por 3 dias. Após esses dias, cistos e sobrenadantes foram novamente centrifugados e os cistos foram ressuspendidos em SDS 0,5% (Sigma-Aldrich, EUA). Em seguida o numero de cistos maduros foi contado em Kova slides (Kova, EUA).

5.1.1.10. Análise da acidificação celular

Com o intuito de investigar a ocorrência da acidificação das células infectadas por tupanvírus ou APMV, amebas *A. castellanii* foram submetidas ao mesmo padrão de infecção e tratamento com bafilomicina A, conforme descrito no item anterior. No entanto, 1 hora antes do tempo de coleta, as células foram incubadas com LysoTracker Red DND-99 (Thermo Fisher Scientific, EUA) na concentração final de 75 nM. Após 9

horas de infecção, células e sobrenadante foram coletados e centrifugados a 800 x g, por 10 minutos em centrífuga *Jouan CR3i* (rotor AC100.10). O sobrenadante foi então descartado e o *pellet* foi ressuspendido em 1 mL de PAS contendo somente bafilomicina A, também na concentração de 10 nM. Em seguida, 20 µL dessa suspensão foram adicionados a lâminas de vidro, sendo essas recobertas com lamínulas e imediatamente analisadas em microscópio confocal (Zeiss, Alemanha) para avaliação da fluorescência.

5.1.1.11. Análise das mudanças celulares ocorridas durante o *shutdown*

Para a avaliação de possíveis mudanças nucleares e citoplasmáticas durante a ocorrência do *shutdown*, células *A. castellanii* e *T. hyperangularis* foram infectadas conforme descrito no item 5.1.1.5. Após 9 horas e 1, 2, 3 e 4 dias de infecção, respectivamente, as células foram submetidas à citocentrifugação, conforme item 5.1.1.9. Em seguida, as lâminas foram fixadas com metanol (Merck Millipore, EUA) e após secagem, foram coradas conforme recomendações do fabricante em Hemacolor (Merck Millipore, EUA), montadas com lamínulas e observadas em microscópio óptico Olympus BX40 (EUA).

Em paralelo, $2x10^6$ células *A. castellanii* e *T. hyperangularis,* também preparadas conforme descrito no item 5.1.1.5. e, após diferentes tempos, foram fixadas com solução de glutaraldeído 2.5% para análise por microscopia eletrônica de transmissão. A inclusão das amostras e as secções ultrafinas foram realizadas no Centro de Microscopia da Aix-Marseille Université, assim como a aquisição de eletromicrografias a partir do microscópio eletrônico Tecnai G20.

5.1.2. Investigação da presença e caracterização de sequências ribossomais em tupanvírus

Para a investigação da presença de sequências ribossomais no genoma viral, dados referentes ao RNAseq do tupanvirus soda lake, previamente realizado pelo nosso grupo de pesquisa, foram avaliados e alinhados a outras sequências disponíveis no GenBank com a utilização da ferramenta blastn do *National Center for Biotechnology Information* (NCBI). Além disso, todas as demais caracterizações foram baseadas na anotação do genoma desse vírus, que se encontra disponível no GenBank sob o número de acesso KY523104.

5.1.2.1. Avaliação dos Best hits

Para a caracterização das possíveis sequências ribossomais, uma análise de similaridade de nucleotídeos também com base em outras sequências disponíveis no GenBank foi realizada com a utilização da ferramenta blastn NCBI. A partir dessa análise, os 100 primeiros *best-hits* resultantes foram tabulados e usados para a construção de diagramas com o intuito de investigar a origem evolutiva dessas sequências. Em seguida, esses *hits* também foram alinhados, utilizando a ferramenta Clustal W do programa Mega 7.0, e usados para a construção de árvores filogenéticas através do método de máxima verossimilhança com 1000 replicatas.

5.1.2.2. Análise de vizinhança e de regiões imediatamente adjacentes

Para a investigação da localização genômica, as sequências identificadas foram alinhadas ao genoma completo do tupanvirus soda lake utilizando-se novamente a ferramenta blastn (NCBI). Após o alinhamento, e com base na anotação do genoma, a análise dos genes localizados em regiões imediatamente adjacentes às sequências, assim como em regiões vizinhas, também foi realizada e esquematizada. De maneira semelhante, essas análises também foram conduzidas para investigar a presença dessas sequências nos genomas de tupanvirus deep ocean (MF405918) e de outros representantes das três linhagens da família *Mimiviridae*: APMV (HQ336222.2), Acanthamoeba polyphaga moumouvirus (JX962719.1) e megavirus LBA (JX885207.1).

5.1.2.3. Avaliação da expressão

Para averiguar a expressão das sequências identificadas foram utilizadas duas diferentes técnicas: FISH (*fluorescence in situ hybridization)* e qPCR. Para tanto, $1x10^6$ amebas *A. castellanii* foram infectadas com tupanvírus na MOI de 5 e incubadas a 32 °C. Como controle, células não infectadas foram mantidas sob as mesmas condições. Após 30 minutos, 6 horas e 12 horas de infecção, células e sobrenadantes foram coletados e submetidos à centrifugação a 800 x g, por 10 minutos em centrífuga *Jouan CR3i* (rotor AC100.10). O sobrenadante foi descartado e o *pellet* foi ressuspendido em PAS. $2x10^5$ células foram então submetidas à citocentrifugação para confecção de lâminas, conforme descrito no item 5.1.1.9, e o restante das células foi novamente

centrifugado. O *pellet* resultante foi submetido à extração de RNA e produção de cDNA, conforme os itens 5.1.1.6 e 5.1.1.7.

Para a técnica de FISH, sondas específicas para o 18S rRNA de *A. castellanii* (5′-TTCACGGTAAACGATCTGGGCC-3′-fluorophore Alexa 488), assim como para as sequências identificadas nesse estudo, cópia 1 RNA (5′-AGTGGAACTCGGGTATGGTAAAA-3′-fluorophore Alexa 555) e cópia 2 RNA (5′-GGCCAAGCTAATCACTTGGG-3′-fluorophore Alexa 555), foram desenhadas, utilizando-se as ferramentas online primer3 e Mathfish, e posteriormente sintetizados pela Eurogentec (Bélgica). Essas sondas foram reconstituídas e diluídas na concentração final de 2 μM em tampão de hibridização (900mM NaCl, 20mM Tris/HCL, 5mM EDTA, 0.01% SDS, 10–25% formamida em água destilada) (Sigma-Aldrich, EUA). Em seguida, o tampão de hibridização contendo as sondas foi adicionado sobre as lâminas previamente preparadas. As lâminas foram então recobertas com lamínulas, seladas com silicone líquido e submetidas ao processo de hibridização a 46 °C, por 16 horas, em hibridizador com controle de temperatura (ThermoBrite StatSpin, EUA). Após o processo de hibridização, o silicone e as lamínulas foram retirados e as lâminas foram submetidas à lavagem com tampão de lavagem (0.45–0.15M NaCl, 20mM Tris/HCL, 5 mM EDTA, e 0.01% SDS) (Sigma-Aldrich, EUA) a 48 °C por 10 minutos. Em seguida, as lâminas foram analisadas em microscópio invertido de fluorescência DMI6000B (Leica, Alemanha).

As reações de qPCR foram realizadas de acordo com o item 5.1.1.7 utilizando-se iniciadores específicos para as sequências identificadas, cópia 1 (5′-GCATCAAGTGCCAACCCATC-3′ e 5′-CTGAAATGGGCAATCCGCAG-3′) e cópia 2 (5′-CCAAGTGATTAGCTTGGCCATAA-3′ e 5′-CGGGAAGTCCCTAAAGCTCC-3′), assim como para o gene constitucional amebiano GAPDH (5′-GTCTCCGTCGTCGATCTCAC-3′ and 5′-GCGGCCTTAATCTCGTCGTA-3′). Os iniciadores foram desenhados com o auxilio da ferramenta online primer designing tool (NCBI). Os gráficos foram elaborados utilizando o software GraphPad Prism versão 7.00 para Windows (GraphPad Software) e os resultados foram analisados pelo método de quantificação relativa $2^{(-\Delta\Delta Ct)}$, sendo os valores expressos em unidades arbitrárias.

5.2. Caracterização do ciclo de multiplicação do cedratvirus getuliensis

Os experimentos expostos nessa seção foram conduzidos durante o período do doutorado realizado no Laboratório de Vírus, no departamento de Microbiologia dessa universidade.

5.2.1. Sistema celular

Para a produção viral e experimentação foram utilizadas amebas *Acanthamoeba castellanii* originadas da *American Type Culture Collection* (ATCC 30010) (Maryland, E.U.A.) e gentilmente cedidas pelo Laboratório de Culturas especiais, Aix Marseille Université, França. As amebas foram cultivadas em meio PYG (Anexo III) suplementado com 25 mg/mL fungizone (anfotericina B, Cristália, São Paulo, Brasil), 500 U/mL de penicilina (Schering-Plough, Brasil) e 50 mg/mL de gentamicina (Schering-Plough, Brasil). As células foram mantidas em estufa a 32 ºC, sendo as garrafas (Kasvi, Brasil) completamente vedadas. Os subcultivos foram realizados três vezes por semana ou de acordo com a necessidade.

5.2.2. Vírus

Os experimentos descritos neste trabalho foram realizados utilizando o cedratvirus getuliensis, descrito no item 1.6, previamente isolado pelo nosso grupo de pesquisa (ANDRADE *et al*, 2018).

5.2.3. Multiplicação e purificação viral (ABRAHÃO et al., 2014, 2016)

Para a produção viral, $7x10^6$ amebas *A. castellanii,* cultivadas em garrafas de cultura T175 (Kasvi, Brasil), foram infectadas com uma multiplicidade de infecção (MOI) de 0,01, com o estoque viral do cedratvirus getuliensis. Após a infecção, as garrafas contendo os inóculos virais foram mantidas em estufa a 32 °C, completamente vedadas. A monocamada celular foi avaliada diariamente para acompanhamento da evolução do efeito citopático e após a lise celular (cerca de 3-4 dias pós infecção) o sobrenadante e os fragmentos celulares foram coletados em tubos cônicos de 50 mL (BD-Falcon, EUA) e submetidos a 3 ciclos de congelamento e descongelamento,

visando a liberação de partículas virais eventualmente retidas em amebas não lisadas. Em seguida, os tubos foram centrifugados a 800 x g, por 10 minutos, a 4°C em centrífuga *Sorvall RI 6000B* (rotor H1000B). O *pellet* resultante foi descartado e o sobrenadante foi centrifugado novamente a 36.000 x g, por 20 minutos, a 4°C em ultra-centrífuga *Combi Sorvall* (rotor AH-62va). Logo após a centrifugação, o sobrenadante foi descartado, o *pellet* resultante foi ressuspendido em PAS para lavagem e os tubos foram novamente centrifugados sob as mesmas condições em ultra-centrífuga. Em seguida, o *pellet* foi novamente ressuspendido em PAS e vagarosamente gotejado sobre 10 mL de uma solução de sacarose 40% (Sigma-Aldrich, EUA) em tubos para ultracentrifugação. Esses tubos foram então centrifugados a 36.000 x g, por 1 hora, a 4°C para que as partículas virais fossem sedimentadas. Por fim, o sobrenadante foi descartado e o sedimento ressuspendido em 300 µL de PAS. Alíquotas da solução viral foram feitas, identificadas, estocadas à -20 ºC e posteriormente tituladas conforme item 5.1.1.4.

5.2.4. Infecção para análise do ciclo de multiplicação

Para avaliar as diferentes etapas do ciclo de multiplicação do cedratvirus getuliensis, $7x10^6$ células de *A. castellanii* cultivadas em garrafas T175 (Kasvi, Brasil) foram submetidas a uma infecção viral assincrônica usando uma baixa MOI de 0,01. Após a infecção, as células foram incubadas a 32 °C por 24 horas e em seguida todo o conteúdo da garrafa foi coletado e submetido à centrifugação a 800 x g, por 10 minutos, a 4°C em centrífuga *Sorvall RI 6000B* (rotor H1000B). Após a centrifugação o sobrenadante foi descartado e o *pellet* foi processado para análise por microscopia eletrônica de transmissão.

5.2.5. Microscopia eletrônica de transmissão

O *pellet* resultante do item anterior foi lavado com tampão fosfato de sódio 0,1 M por duas vezes. Após a lavagem, o sobrenadante foi descartado e o *pellet* foi fixado em solução glutaraldeído a 2,5% em tampão fosfato de sódio 0,1 M (Sigma-Aldrich, EUA), durante 1h à temperatura ambiente. Após este período a suspensão foi centrifugada e o sobrenadante descartado. Em seguida o *pellet* foi ressuspendido em 1mL de tampão fosfato de sódio 0,1M e novamente centrifugado a 900 x g durante 10

minutos para obtenção do *pellet*. O material foi enviado ao Centro de Microscopia da Universidade Federal de Minas Gerais, onde foi fixado com 2% de tetróxido de ósmio e incorporado em resina EPON. As secções ultrafinas foram analisadas através de microscópio eletrônico de transmissão (Spirit Biotwin FEI - 120 kV).

5.2.6. Microscopia eletrônica de varredura

Para a realização da microscopia eletrônica de varredura, 10 µL de cedratvirus getulienses purificado, ou células *A. castellanii* infectadas na MOI de 0,01 em tempo precoce (1 hora) ou tardio (24 horas) foram espalhados sobre lamínulas circulares tratadas com Poly-L-Lisina. Após a secagem do material, as lamínulas foram adicionadas a placas de 24 poços (Kasvi, Brasil) e o material foi fixado com glutaraldeído 2,5%, em tampão cacodilato 0,1M por 1 hora. Decorrido esse tempo, o fixador foi removido e as amostras foram lavadas três vezes com tampão cacodilato 0,1M. As etapas seguintes da preparação: fixação secundária com tetróxido de ósmio 1%, imersão em Ácido Tânico 1%, desidratação em solução crescente de álcool etílico, secagem das amostras em ponto crítico de CO_2 e metalização com ouro/5nm de espessura foram realizadas pelo próprio Centro de Microscopia da UFMG. Após todo o processamento, as amostras foram analisadas em microscópio eletrônico de varredura FEG Quanta 200 FEI.

5.2.7. Ensaios de penetração viral

Os ensaios de penetração viral foram realizados com objetivo de investigar a principal via de penetração utilizada pelo cedratvirus getuliensis para infectar *A. castellanii*. Para tanto, foram utilizados diferentes inibidores farmacológicos para avaliar distintas vias endocíticas comumente utilizadas pelos vírus: (I) a cloroquina, que inibe a endocitose mediada por clatrina e caveolina ao prevenir a acidificação do endossomo; (II) a citocalasina D, que promove desestabilização do citoesqueleto celular e consequentemente a ocorrência da fagocitose; (III) o 5-(*N*-ethyl-*N*-isopropyl) amiloride (EIPA), um inibidor de macropinocitose.

Para estes testes, $5x10^5$ células de *A. castellanii* foram pré-tratadas com 2 µM de citocalasina D (Sigma-Aldrich, EUA), 100 µM de cloroquina (Sigma-Aldrich, EUA),

ou 1 μM de EIPA (Sigma-Aldrich, EUA). Após 1 hora, as células foram infectadas com cedratvirus getuliensis na MOI de 5. Grupos controle não pré-tratados e infectados também foram preparados. Depois de 30 minutos de infecção, células e sobrenadantes foram coletados e conjuntamente centrifugados a 800 x g em centrífuga *Sorvall RI 6000B* (rotor H1000B) por 10 minutos. O *pellet* resultante foi lavado três vezes com PAS e posteriormente submetido a três ciclos de congelamento e descongelamento para lise celular e liberação de partículas virais. Em seguida as amostras foram submetidas à titulação viral de acordo com o item 5.1.1.4. Todos os ensaios foram feitos em triplicata e os gráficos foram elaborados utilizando o software GraphPad Prism versão 7.00 para Windows (GraphPad Software). Análises estatísticas também foram realizadas no mesmo programa, sendo os valores analisados por teste One-way ANOVA, seguido de pós-teste de Bonferroni.

5.2.8. Ensaio de tráfego de membrana

Com o intuito de avaliar o papel de membranas do hospedeiro na multiplicação viral, $5x10^5$ amebas *A. castellanii* foram infectadas com cedratvirus getuliensis na MOI de 5. Após 30 minutos de infecção, as amebas foram lavadas com PAS, transferidas para placas de 6 poços (Kasvi, Brasil) contendo 1 mL de PYG e incubadas à 32 °C. Depois de 1 hora, brefeldina A (Sigma-Aldrich, EUA), um inibidor de tráfego de membranas, foi adicionado aos poços com células infectadas na concentração final de 10 μM. Após 8 e 24 horas de infecção, as amebas foram coletadas para titulação viral, conforme item 5.1.1.4, e análise por microscopia eletrônica de transmissão, conforme item 5.2.5. Todos os ensaios também foram feitos em triplicata e os gráficos foram gerados a partir do software GraphPad Prism, assim como as estatísticas.

6. RESULTADOS

Assim como no tópico de materiais e métodos, os resultados também foram divididos em duas seções para melhor compreensão. Os dados apresentados na seção 6.1, correspondem aos resultados obtidos na investigação do *shutting down* e da presença de sequências ribossomais em tupanvírus. Já os dados apresentados na seção 6.2 correspondem aos resultados referentes aos estudos com cedratvirus getuliensis.

6.1. Investigação do *shutting down* do RNA ribossomal e da presença de sequências ribossomais em tupanvírus

6.1.1. Investigação do *shutting down* do RNA ribossomal

6.1.1.1. Avaliação da reprodução e ocorrência do *shutdown*

A observação incial do *shutdown* de RNA ribossomal em células infectadas por tupanvírus levantou questionamentos sobre sua ocorrência e reprodutibilidade, evidenciando a necessidade de uma caracterização mais aprofundada. Com esse intuito novos experimentos foram conduzidos inicialmente em *A. castellanii*, em diferentes tempos e MOIs. Os dados revelaram a reprodutibilidade do fenômeno do *shutting down* do RNA ribossomal de amebas *A. castellanii* em altas MOIs (10 e 100), corroborado através do fracionamento do RNA total em géis de agarose, assim como por qPCR utilizando-se iniciadores específicos para o 18S rRNA (Figura 27A e C). O *shutdown* ribossomal se mostrou diretamente proporcional à multiplicidade de infecção, sendo observada uma degradação mais intensa em amebas infectadas com tupanvírus na MOI de 100 (50-80% de redução), do que nas células infectadas com MOI de 10 (30% de redução) (Figura 27A). Além disso, também foi possível observar diferenças temporais na ocorrência do *shutdown* na MOI de 100, sendo notável uma maior degradação em tempo tardio (80% de redução – 9 horas), do que em tempo inicial de infecção (50% de redução – 3 horas) (Figura 27A). Como esperado, nenhuma alteração no padrão de abundância ribossomal foi observada para as amebas infectadas com APMV, sugerindo que a ocorrência do *shutdown* está relacionada especificificamente à infecção por tupanvírus (Figura 27B e D).

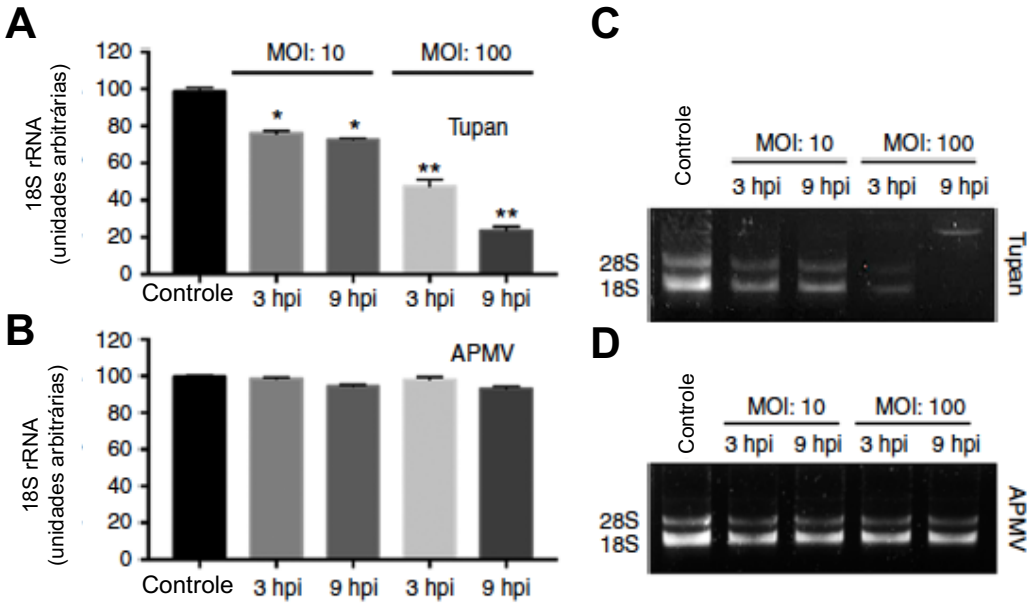

Figura 27: *Shutdown* ribossomal em amebas *A. castellanii*. (A) e **(B)** Quantificação relativa do 18S rRNA por qPCR de amebas *A. castellanii* infectadas por tupanvírus (A) ou APMV (B) nas MOIs de 10 e 100, nos tempos de 3 e 9 horas. **(C)** e **(D)** Fracionamento em gel de agarose do RNA total de amebas infectadas nas mesmas condições descritas em (A) e (B). Os controles de todos os ensaios foram submetidos às mesmas condições experimentais e coletados no tempo de 9 horas. APMV: Acanthamoeba polyphaga mimivirus. *:$p < 0.05$; **:$p < 0.01$. As barras de erro representam o desvio padrão.

Os ensaios conduzidos com partículas inativadas de tupanvírus demonstraram que a ocorrência do *shutdown* não parece ser dependente da multiplicação viral, uma vez que a infecção com partículas expostas à radiação UV também levou à degradação ribossomal de maneira semelhante ao observado para infecções com partículas virais viáveis (Figura 28). Entretanto, a infecção com partículas virais inativadas por calor (80 °C) não foi capaz de causar o *shutdown*, sugerindo que esse fenômeno citotóxico possa estar relacionado a presença de algum fator viral termosensível.

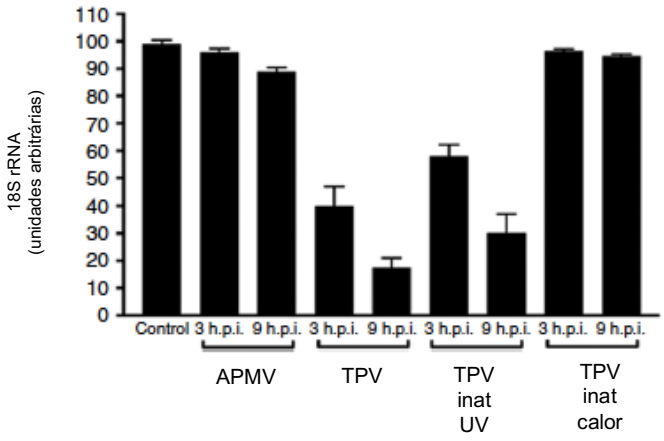

Figura 28: Ocorrência do *shutdown* em amebas infectadas por tupanvírus inativado. Quantificação relativa do 18S rRNA por qPCR de amebas *A. castellanii* infectadas com APMV ou com tupanvírus inativados por radiação UV ou calor, nas MOIs de 10 e 100, nos tempos de 3 e 9 horas. O controle foi submetido às mesmas condições experimentais e coletado no tempo de 9 horas. APMV: Acanthamoeba polyphaga mimivirus. TPV: tupanvirus. As barras de erro representam o desvio padrão.

Após a realização desses experimentos, ensaios abordando a ocorrência do *shutdown* em *T. hyperangularis* também foram desenvolvidos. No entanto, a reprodução da degradação ribossomal nesses protozoários revelou um perfil distinto, uma vez que o *shutdown* foi observado somente após dias de infecção e não em horas de infecção, como observado para *A. castellani.* O fracionamento do RNA total revelou uma alteração inicial entre o 2° e o 3° dia, entretanto, somente no 4° dia uma degração ribossomal mais intensa foi observada (Figura 29).

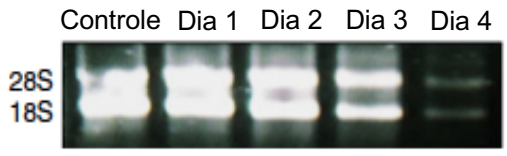

Figura 29: *Shutdown* em *T. hyperangularis*. Fracionamento em gel de agarose do RNA total de *T. hyperangularis* infectadas por tupanvírus após 1, 2, 3 e 4 dias, na MOI de 100. O controle foi submetido às mesmas condições experimentais e coletado no 4° dia após a infecção.

6.1.1.2. Avaliação da ação de inibidores na ocorrência do *shutdown*

Após a observação da reprodutibilidade e a melhor caracterização do *shutdown*, o próximo passo foi investigar qual mecanismo poderia estar relacionado com a degradação ribossomal. Como mencionado anteriormente, a hipótese inicial foi de que esse fenômeno pudesse estar relacionado ao canônico processo de ribofagia e com o intuito de corroborar ou não essa hipótese, alguns experimentos envolvendo os principais marcadores de autofagia foram desenvolvidos. O primeiro deles foi realizado com o intuito de avaliar o papel de dois inibidores farmacológicos de acidificação de autofagossomos, cloroquina e bafilomicina A, na ocorrência do *shutdown*.

Os ensaios conduzidos revelaram, surpreendentemente, que o tratamento com cloroquina não foi capaz de evitar a ocorrência do *shutdown*, sendo observada uma redução de aproximadamente 50% do 18S rRNA das amebas (3 horas de infecção) tratadas ou não com esse inibidor (Figura 30A). Um perfil semelhante também foi observado após 9 horas de infecção, uma vez que a mesma degradação ribossomal (~ 70%) foi observada na presença ou ausência da cloroquina (Figura 30B).

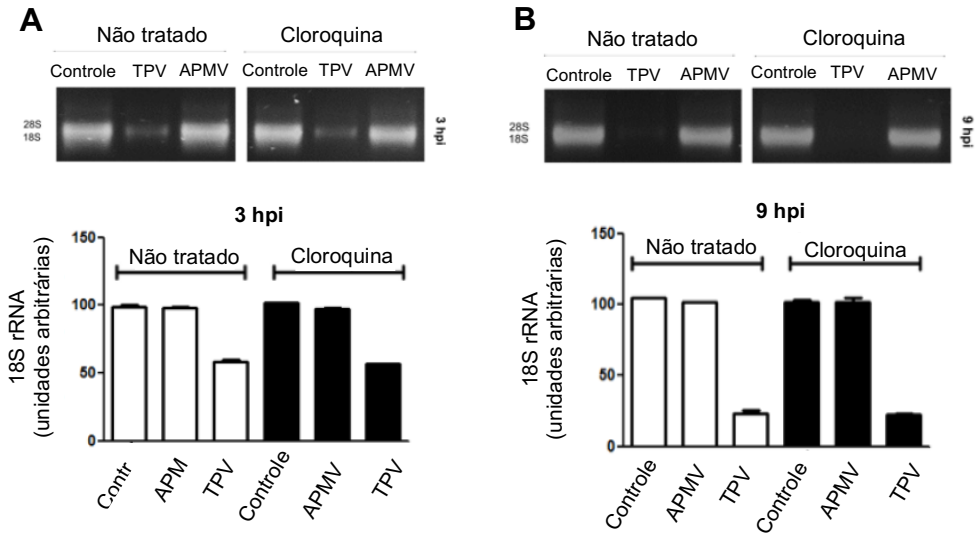

Figura 30: O tratamento com cloroquina não altera a ocorrência do *shutdown* em *A. castellanii*. O fracionamento em gel de agarose, assim como a quantificação relativa do 18S rRNA de amebas infectadas por tupanvírus ou APMV na MOI de 100, nos tempos de 3 **(A)** e 9 horas **(B)**, revelaram que a ocorrência de degradação ribossomal não é alterada com o tratamento com cloroquina. APMV: Acanthamoeba polyphaga mimivirus; TPV: tupanvirus. As barras de erro representam o desvio padrão.

De maneira similar, o tratamento com bafilomicina A também não impediu o *shutdown*. Uma degradação ribossomal de proporções similares entre o grupo tratado e não tratado foi observado tanto no tempo de 3 horas pós infecção (Figura 31A), como no tempo de 9 horas pós infecção (Figura 31B).

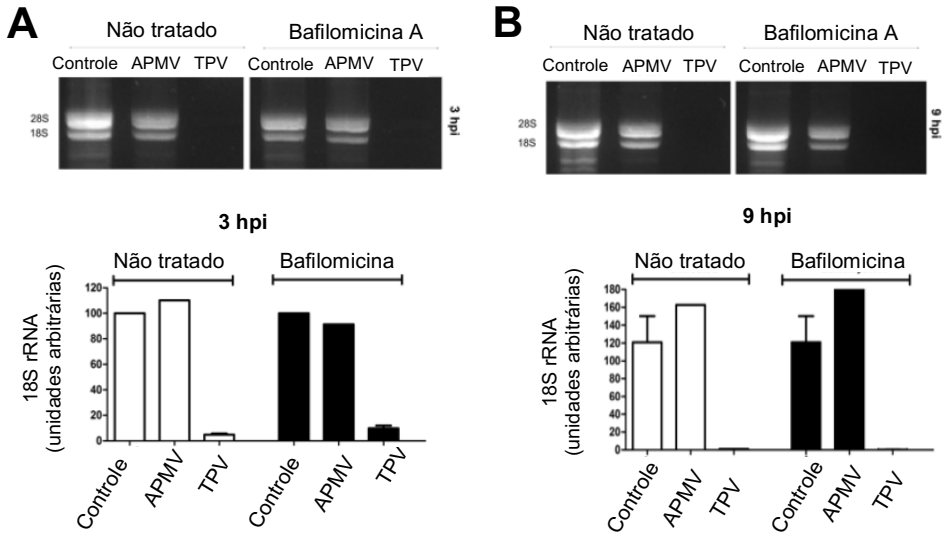

Figura 31: O tratamento com bafilomicina A não altera a ocorrência do *shutdown* em *A. castellanii*. A quantificação relativa do 18S rRNA, assim como o fracionamento em gel de agarose do RNA total de amebas infectadas por tupanvírus ou APMV na MOI de 100, nos tempos de 3 **(A)** e 9 horas **(B)**, revelaram a ocorrência do *shutdown* também na presença do inibidor bafilomicina A. APMV: Acanthamoeba polyphaga mimivirus; TPV: tupanvirus. As barras de erro representam o desvio padrão.

Em conjunto, o tratamento com ambos os inibidores sugere que a acidificação de autofagossomos, pelas vias inibidas por essas drogas, aparentemente, não é um fator necessário para a ocorrência do *shutting down* do RNA ribossomal de amebas *A. castellanii*.

6.1.1.3. Análise do papel do gene Atg8 no *shutdown*

O segundo experimento desenvolvido, ainda na tentativa de confirmar ou não se o mecanismo de autofagia estava envolvido no processo do *shutdown,* foi relacionado à análise do papel do gene Atg8, que, como já citado, faz parte de uma família de genes envolvidos no processo de autofagia, mais especificamente na formação da membrana

do autofagossomo. Com esse objetivo, pequenos RNAs de interferência foram sintetizados e utilizados no silenciamento desse gene.

Após o silenciamento, não foi possível observar a presença de bandas referentes às subunidades ribossomais 18S e 28S através do fracionamento do RNA total de amebas infectadas com tupanvírus, indicando que o *shutdown* ainda ocorre diante do silenciamento do gene Atg8 (Figura 32A). Da mesma maneira, a comparação das médias da quantificação relativa do 18S rRNA por qPCR entre o grupo controle e o grupo infectado por tupanvírus, também evidenciou uma redução ribossomal similar entre as amebas transfectadas com o siRNA (~ 80% de redução) e as amebas não transfectadas (~ 85% de redução) (Figura 32B). Sendo assim, ambos os resultados sugerem que o gene Atg8 não tem um papel crucial na ocorrência do *shutdown*, uma vez que seu silenciamento não afetou a degradação ribossomal.

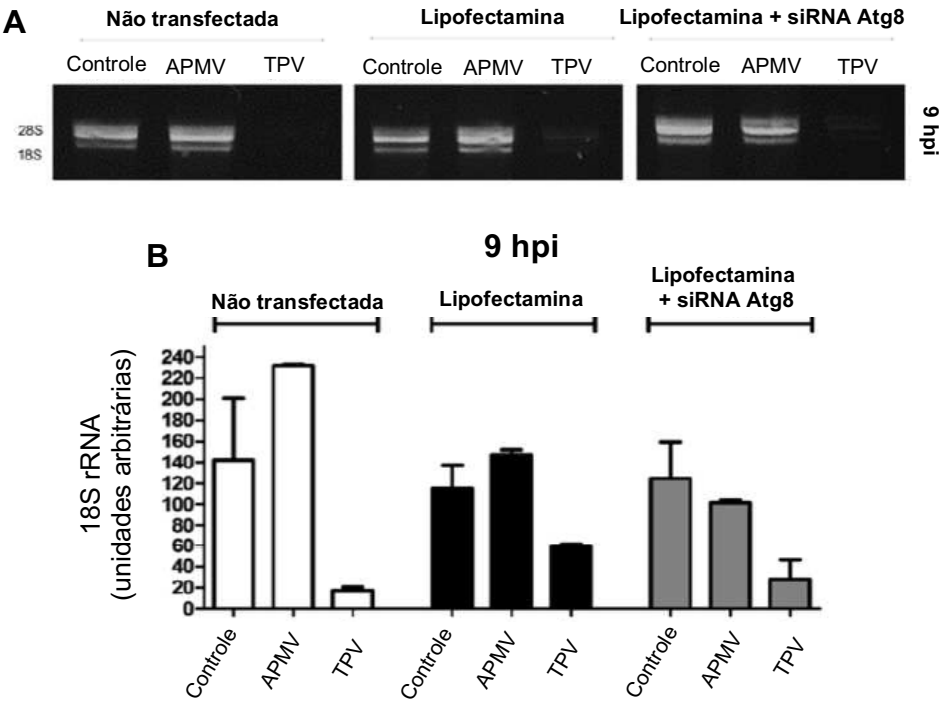

Figura 32: O *shutdown* ocorre mesmo após o silenciamento do gene Atg8. O fracionamento em gel de agarose **(A)**, assim como a quantificação relativa do 18S rRNA **(B)** de amebas infectadas por tupanvírus na MOI de 100, no tempo de 9 horas, revelaram que a ocorrência de degradação ribossomal não é alterada pelo silenciamento do gene Atg8. APMV: Acanthamoeba polyphaga mimivirus; TPV: tupanvirus. As barras de erro representam o desvio padrão.

Para comprovação do silenciamento, dois diferentes controles foram realizados. O controle de transfecção evidenciou a ocorrência bem-sucedida da transfecção dos siRNAs marcados com FITC a partir da observação de fluorescência somente nas amebas que foram submetidas a esse processo (Figura 33). Já o controle biológico de silenciamento foi avaliado a partir da inibição do processo de encistamento que também requer a partipação do gene Atg8. Dessa maneira, trofozoítos de *A. castellanii* submetidos ao mesmo protocolo de silenciamento e posteriormente induzidos ao encistamento, deram origem a um menor número de cistos maduros do que os trofozoítos não transfectados, evidenciando a ocorrência do silenciamento (Figura 34).

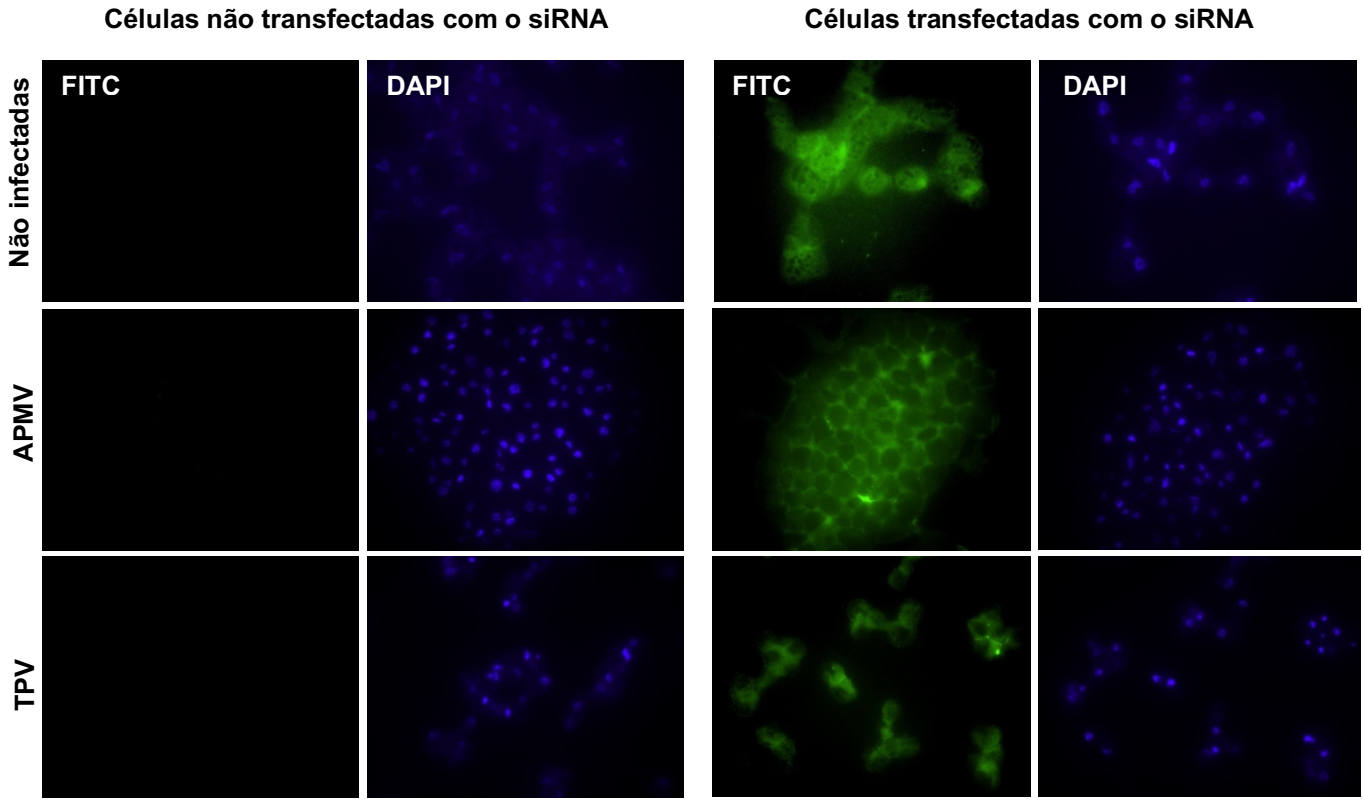

Figura 33: Controle de transfecção dos siRNAs marcados com FITC em amebas *A. castellanii.* Uma intensa fluorescência é observada nas células que foram submetidas à transfecção, enquanto para as células não transfectas não foi possível a mesma observação. Aumento de 640x. APMV: Acanthamoeba polyphaga mimivirus; TPV: tupanvirus.

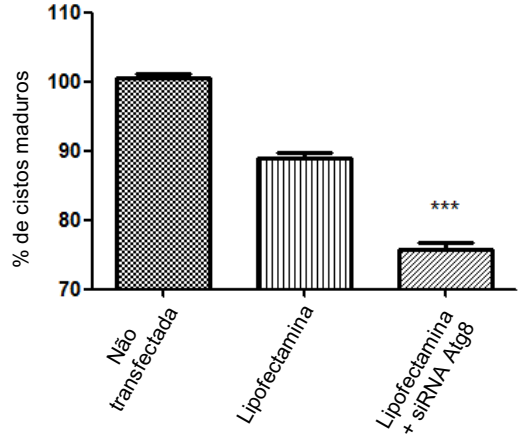

Figura 34: Controle biológico da ocorrência do silenciamento. Após 3 dias de encistamento, um menor número de cistos maduros foi observado para as amebas transfectadas com siRNAs para o gene Atg8, evidenciando a ocorrência do silenciamento gênico. ***:$p < 0.001$. As barras de erro representam o desvio padrão.

6.1.1.4. Investigação de alterações no pH amebiano durante a infecção por tupanvírus

Uma vez que inibidores farmacológicos de acidificação de autofagossomos, assim como o silenciamento do gene Atg8, não foram capazas de alterar o perfil de ocorrência do *shutdown* ribossomal, o próximo passo foi verificar se durante a infecção por tupanvírus alguma alteração no pH amebiano era observada. Para tanto utilizamos o lysotracker, uma sonda vital constituída por bases fracas conjugadas a um fluoróforo, que tem afinidade por compartimentos ácidos. Em paralelo, amebas também foram tratadas com bafilomicina A, um inibidor de bombas de H^+ V-ATPase que impedem a acidificação de compartimentos celulares, como vacúolos.

Como esperado, amebas controle, não infectadas, apresentaram compartimentos ácidos, visualizados como pontos vermelhos dispersos pelo citoplasma da célula (Figura 35A). Também como previsto, diante do tratamento com bafilomicina A, as células apresentaram uma fluorescência menos intensa, como demonstrado na Figura 36. Por sua vez, amebas infectadas com APMV também apresentaram compartimentos ácidos no citoplasma, de maneira semelhante ao observado para o controle de célula (Figura 35B). Entretanto, o tratamento com bafilomicina A não foi capaz de alterar esse perfil, sendo a mesma intensidade de fluorescência observada na presença ou ausência dessa droga (Figura 36).

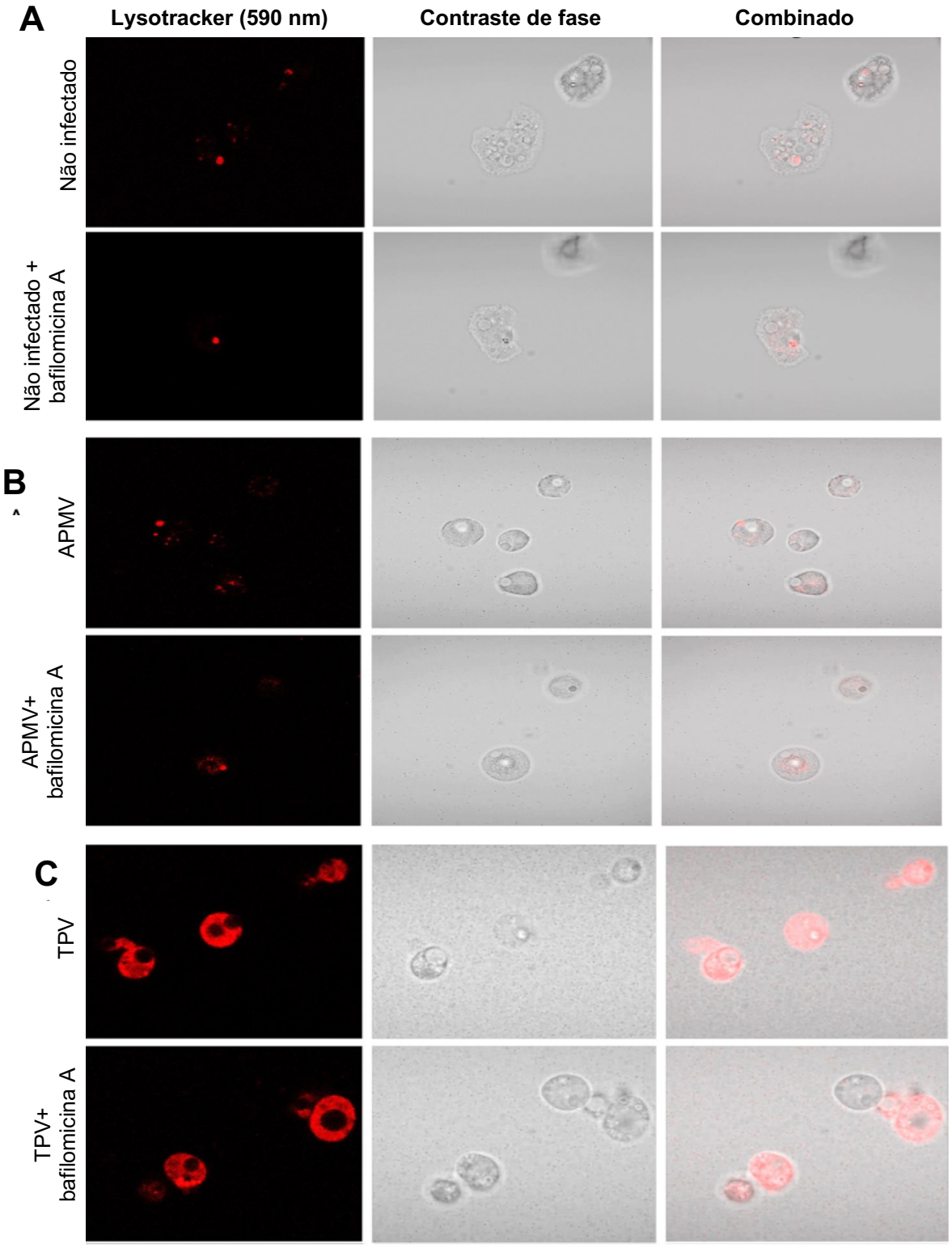

Figura 35: Tupanvírus induz uma intensa acidificação do citoplasma de amebas *A. castellanii*. (A) Amebas não infectadas apresentam compartimentos ácidos, que na presença de bafilomicina A apresentam uma fluorescência menos intensa. **(B)** *A. castellanii* infectadas por APMV (MOI de 100, 9 hpi) apresentam compartimentos menos ácidos do que o controle que não são alterados pelo tratamento com bafilomicina A. **(C)** Amebas infectadas por tupanvírus (MOI de 100, 9 hpi) apresentam uma intensa acidificação de todo o citoplasma, que também não é alterada pela presença de bafilomicina A. Aumento de 640x. APMV: Acanthamoeba polyphaga mimivirus; TPV: tupanvirus.

Surpreendentemente, um perfil bastante diferencial foi notado para amebas infectadas por tupanvírus, uma vez que uma intensa acidificação não compartimentalizada e abrangendo todo o citoplasma amebiano foi observada (Figura 35C). Entretanto, assim como observado para APMV, a presença da droga bafilomicina A não alterou esse perfil, sendo notável uma intensidade de fluorescência similar nas células tratadas ou não com esse inibidor (Figura 36). Sendo assim, foi verificado que concomitante, temporalmente, ao processo de *shutdown* ocorre uma alteraçao de pH em todo o citoplasma da célula hospedeira, tornando-o extremamente ácido quando comparado ao controle.

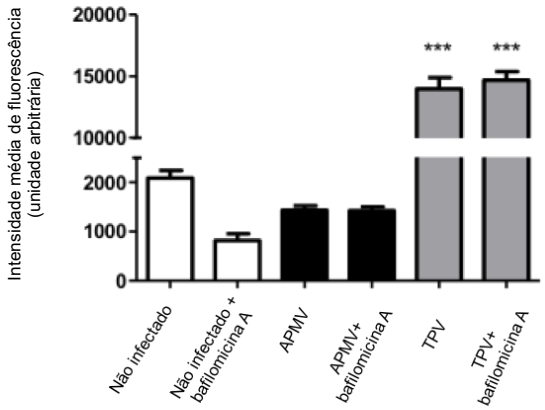

Figura 36: Medida da intensidade de fluorescência de amebas tratadas com lysotracker e infectas por tupanvírus. Amebas não infectadas na presença de bafilomicina A apresentam uma fluorescência menos intensa do que amebas não infectadas e não tratadas. Já *A. castellanii* infectadas por APMV na MOI de 100 no tempo de 9 horas, tratadas ou não com bafilomicina A, apresentam menor intensidade de fluorescência do que células não infectadas. Curiosamente, amebas infectadas por tupanvírus, também na MOI de 100 no tempo de 9 horas, apresentam uma intensa fluorescência, que também não é alterada pela presença de bafilomicina A. APMV: Acanthamoeba polyphaga mimivirus; TPV: tupanvirus. ***:$p < 0.001$. As barras de erro representam o desvio padrão.

6.1.1.5. Investigação de alterações citoplasmáticas e nucleares durante o *shutdown*

Ainda na investigação do mecanismo associado à degradação ribossomal, alguns experimentos foram conduzidos para a avaliação de possíveis mudanças citoplasmáticas e nucleares durante a ocorrência do *shutdown* em células *A. castellanii* e *T. hyperangularis*.

Análises por microscopia eletrônica de transmissão de amebas *A. castellanii* infectadas por tupanvírus revelaram a presença de vesículas contendo ribossomos. Além disso, também foi possível observar que essas vesículas são formadas próximo à periferia do núcleo, a partir da invaginação de membranas, que por sua vez englobam ribossomos (Figura 37A). Posteriormente essas vesículas parecem se agregar formando vesículas maiores contendo uma grande quantidade de ribossomos (Figura 37B). Curiosamente, essas vesículas, em sua maioria, apresentam somente uma membrana, sendo que vesículas com dupla membrana, são raramente observadas. Com o avançar da infecção, e temporalmente ao *shutdown* (9 hpi), essas vesículas não são mais observadas no citoplasma das amebas, sugerindo a ocorrência de depleção.

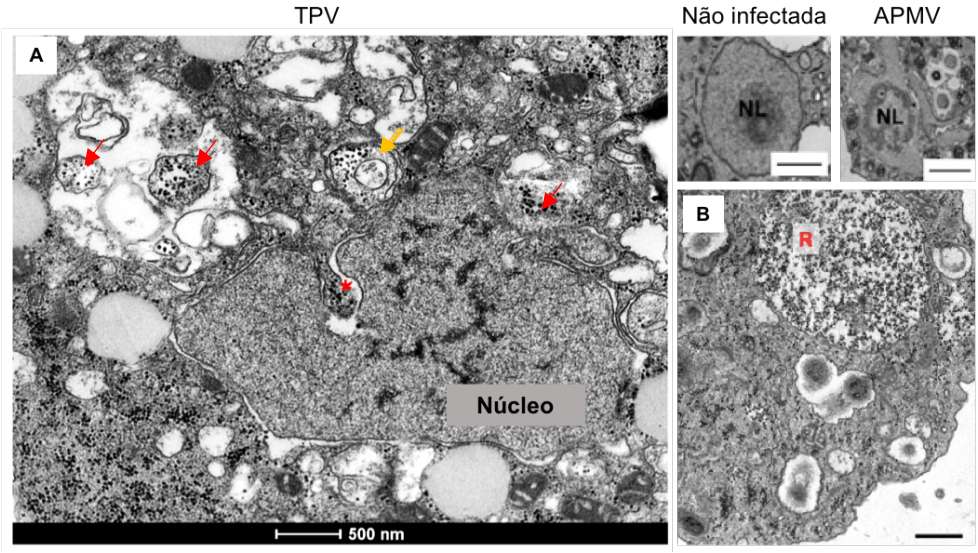

Figura 37: Formação de vesículas contendo ribossomos em amebas *A. castellanii* infectadas por tupanvírus. (A) Vesículas com uma membrana (setas vermelhas) e raramente com duas membranas (seta amarela) são formadas na periferia nuclear (*) de amebas infectadas por tupanvírus (MOI de 100, 2 hpi). O mesmo perfil não é observado em amebas não infectadas ou infectadas com APMV. Barra de escala APMV e não infectada: 1µm. **(B)** Vesículas maiores contendo uma grande quantidade de ribossomos (MOI de 100, 6 hpi). Barra de escala: 1µm. R: ribossomos; NL: nucléolo. APMV: Acanthamoeba polyphaga mimivirus; TPV: tupanvirus.

O acompanhamento do *shutdown* em *T. hyperangularis*, por sua vez, demonstrou a ocorrência de um aumento do número de vacúolos no citosol com o passar dos dias, sendo que uma maior vacuolização foi observada no 4° dia (Figura 38A), quando uma maior degradação ribossomal também ocorre. Além dessas alterações citoplasmáticas, a presença de vesículas contendo ribossomos também foi

notável nesse protozoário, sendo essas bastante similares às observadas em *A.castellanii* (Figura 38B).

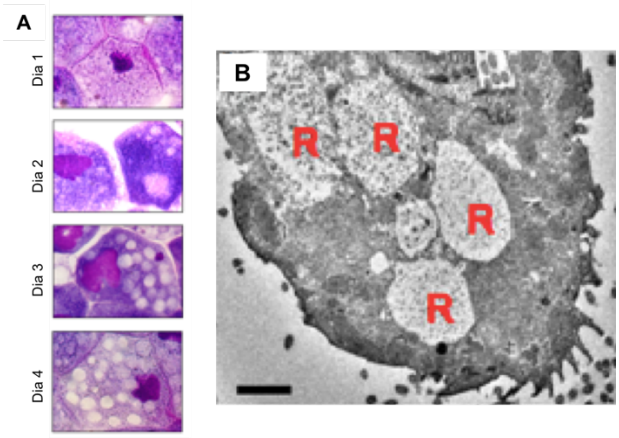

Figura 38: Alterações citoplasmáticas observadas em *T. hyperangularis* infectadas por tupanvírus. (A) Uma intensa vacuolização do citoplasma do protozoário é observada com o avançar dos dias de infecção por tupanvírus (MOI de 100). Aumento de 1000x. **(B)** Grandes vesículas contendo uma grande quantidade de ribossomos também são observadas. (MOI de 100, 6 hpi). Barra de escala: 3,5 µm. R: ribossomos.

Além dessas diferenças citoplasmáticas, alterações nucleares temporalmente associadas à ocorrência do *shutdown* também foram observadas em *A. castellanii* (Figura 39A) e *T. hyperangularis* (Figura 39B). Essas alterações, caracterizadas por uma desorganização e degradação do núcleo e do nucléolo, foram claramente observadas após a coloração por hemacolor e também por microscopia eletrônica de transmissão (Figura 37A).

Em *A. castellanii* não infectadas, o nucléolo é claramente visível no interior do núcleo, que se mantem organizado. Diante da infecção por APMV uma branda desorganização nuclear é observada. Entretanto, essa desorganização é incomparável à degradação nuclear sofrida por amebas infectadas por tupanvírus na MOI de 100. Nessa situação, após coloração por hemacolor, o núcleo e o nucléolo não são evidentes, sendo possível somente a visualização da fabrica viral do tupanvírus (Figura 39A).

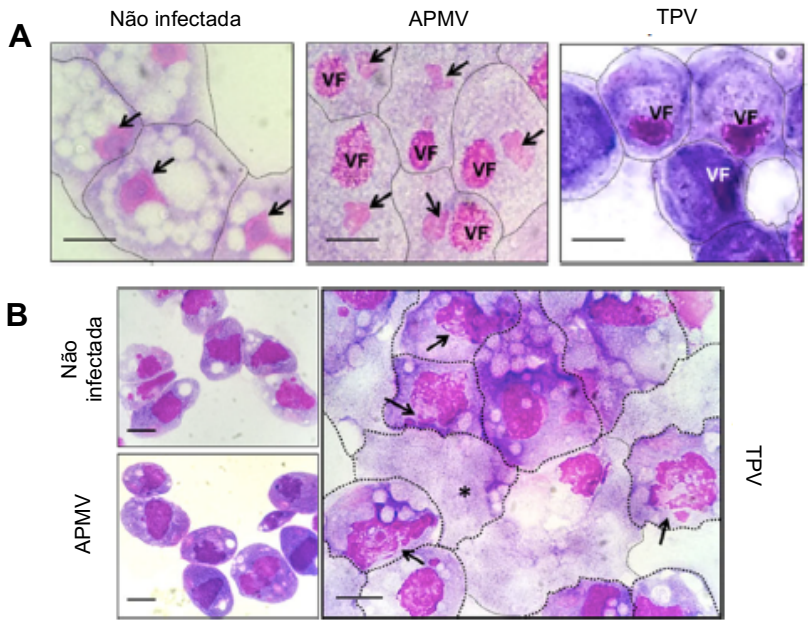

Figura 39: Alterações nucleares observadas em *A. castellanii* e *T. hyperangularis* infectadas por tupanvírus. (A) Amebas *A. castellanii* infectadas por tupanvírus (MOI de 100, 9 hpi) apresentam uma intensa degradação do núcleo e do nucléolo. Amebas infectadas por APMV apresentam uma desorganização nuclear (setas) não comparável à degradação ocasionada por tupanvírus. Controles de células apresentam nucléolos bem definidos no interior do núcleo (setas). **(B)** *T. hyperangularis* infectadas por tupanvírus (MOI de 100, 4 dias pós infecção) também apresentam desorganização nuclear (setas), sendo que em algumas células os núcleos não são evidentes (*). Tanto as células não infectadas, quanto as células incubadas com APMV não apresenta mudança na morfologia nuclear. Aumento de 1000x.VF: Fábrica viral. APMV: Acanthamoeba polyphaga mimivirus; TPV: tupanvirus.

Um padrão semelhante de desorganização nuclear também foi observado em *T. hyperangularis*, sendo que em algumas células, como demonstrado na Figura 39B, o núcleo também não é evidente. Entretanto, diferentemente de *A. castelanii*, nenhuma desorganização foi observada nas células incubadas com APMV, sendo essas comparáveis ao controle de células (Figura 39B).

Em conjunto esses dados revelaram a ocorrência de mudanças celulares, tanto em *A. castellanii*, como *T. hyperangularis*, temporalmente associadas à ocorrência do *shutdown*, como a formação de vesículas contendo ribossomos e a degração do núcleo e do nucléolo, que é diretamente associado à biogênese de ribossomos.

6.1.2. Investigação da presença e caracterização de sequências ribossomais em tupanvírus

6.1.2.1. Presença de sequências 18S-like em tupanvírus

Em paralelo aos experimentos desenvolvidos na caracterização do *shutdown* do RNA ribossomal, investigações sobre a presença de sequências ribossomais também foram conduzidas. Essas investigações tiveram início com a análise de dados provenientes do RNAseq do tupanvírus, que havia sido realizado previamente pelo nosso grupo de pesquisa. Apesar do sequenciamento não ter sido capaz de alcançar uma ampla cobertura do genoma, algumas *reads* virais foram geradas e avaliadas. No entanto, a análise de algumas dessas *reads virais* demonstrou uma alta similaridade com sequências de *Vermamoeba vermiformis* (antigamente denominada *Hartmannella vermiformis*), mais especificamente com sequências parciais do gene da subunidade 18S do rRNA.

Após essa observação, o alinhamento do genoma completo do tupanvirus soda lake com a família *Hartmannellidae* foi realizado, levando à identificação de uma sequência viral apresentando 74% de similaridade com o gene da subunidade 18S de *H. vermiformis*. Essa sequência de 101 pares de bases foi então denominada de cópia 1 e localiza-se na região intergênica 798.441-798.541 do genoma viral. Em seguida, o alinhamento da cópia 1 com o genoma completo do tupanvírus foi realizado e uma segunda sequência, com 80% de similaridade, também foi observada. Essa sequência de 88 pares de bases foi denominada de cópia 2 e, assim como a cópia 1, se localiza na região intergênica 692.605-692.692.

6.1.2.2. Avaliação dos *best hits*

Após a identificação dessas duas sequências 18S-*like* em tupanvírus, o próximo passo foi realizar uma análise evolutiva a partir da tabulação e avaliação dos 100 primeiros *hits* para essas sequências (Anexo IV). Essas análises revelaram que os *best hits*, para ambas as cópias, correspondem, principalmente, a regiões intrônicas, mais especificamente a fragmentos de íntrons self-splicing do grupo I, de sequências de 18S rRNA de diversos organismos, como fungos, amebas e algas (Figura 40A e B). A identificação dessa similaridade com íntrons foi possível somente para depósitos

completos no *GenBank*, em que a informação relativa a íntrons e éxons estavam disponíveis. Dessa maneira, na ausência desse tipo de informação os hits foram tabulados como genes de 18S e não como íntrons, conforme pode ser observado nos gráficos da Figura 40.

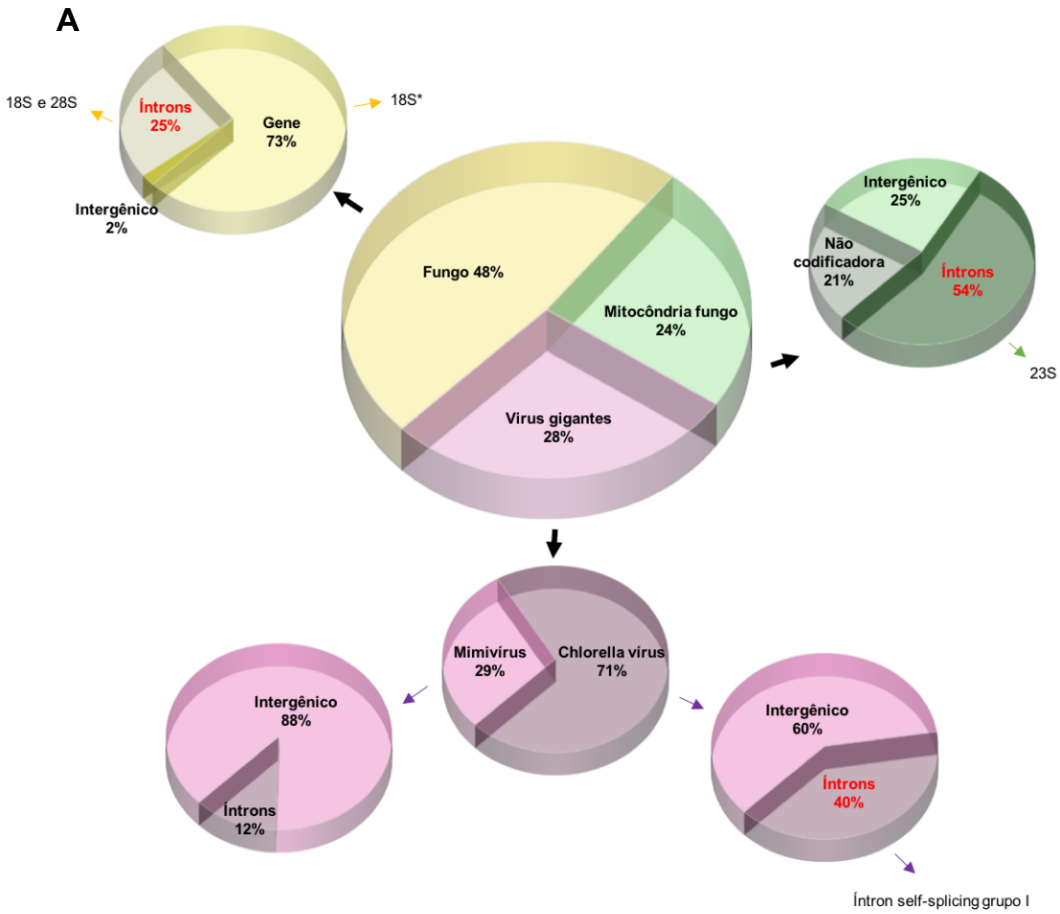

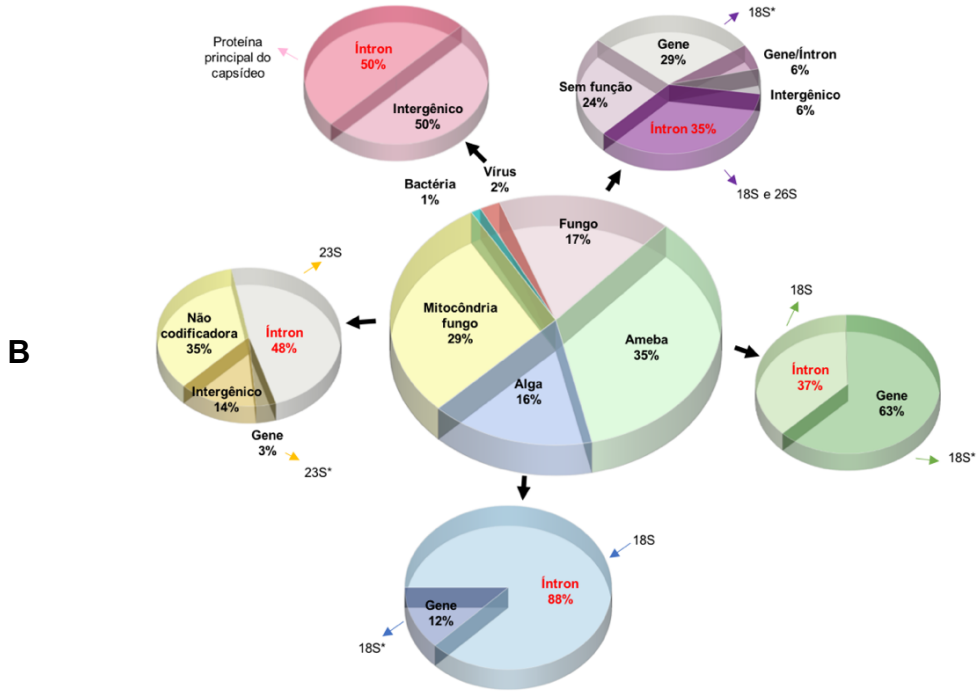

Figura 40: Análise dos best hits das cópias de regiões intrônicas de 18S em tupanvírus soda lake. Os 100 best hits para as cópias 1 **(A)** e 2 **(B)** foram tabulados e graficamente representados evidenciando a similaridade, principalmente, com regiões intrônicas de sequências de 18S de diversos organismos. * Na ausência de depósitos detalhados contendo informações de íntrons e éxons os dados foram identificados como genes.

A avaliação dos *best hits* também evidenciou a presença de sequências similares às copias 1 e 2 de tupanvirus soda lake em outros vírus do grupo dos NCLDVs, como phycodnavírus e mimivírus. Em alguns Chlorella vírus foi possível a identificação de 3 a 4 cópias. Já em membros da família *Mimiviridae* foram identificadas uma única cópia em vírus pertencentes às linhagens A e B, e duas em vírus da linhagem C. Como esperado, duas cópias também foram encontradas no genoma do tupanvirus deep ocean.

Análises filogenéticas das sequências identificadas em vírus gigantes, assim como de sequências dos *best hits* também foram realizadas e sugeriram que as cópias 1 e 2 de tupanvirus soda lake e tupanvirus deep ocean tiveram origens separadas e parecem ser filogeneticamente relacionadas às cópias únicas das linhagens A e B, assim como da cópia 1 da linhagem C e das sequências intrônicas de 18S rRNA de mitocôndrias de fungos. Além disso, também foi observado que as diversas cópias dos phycodnavírus aparentam ser filogeneticamente relacionadas entre si, assim como à cópia 2 da linhagem C e sequências de 18S de fungos. Dessa maneira, as cópias da linhagem C parecem ter tido origens distintas (Figura 41).

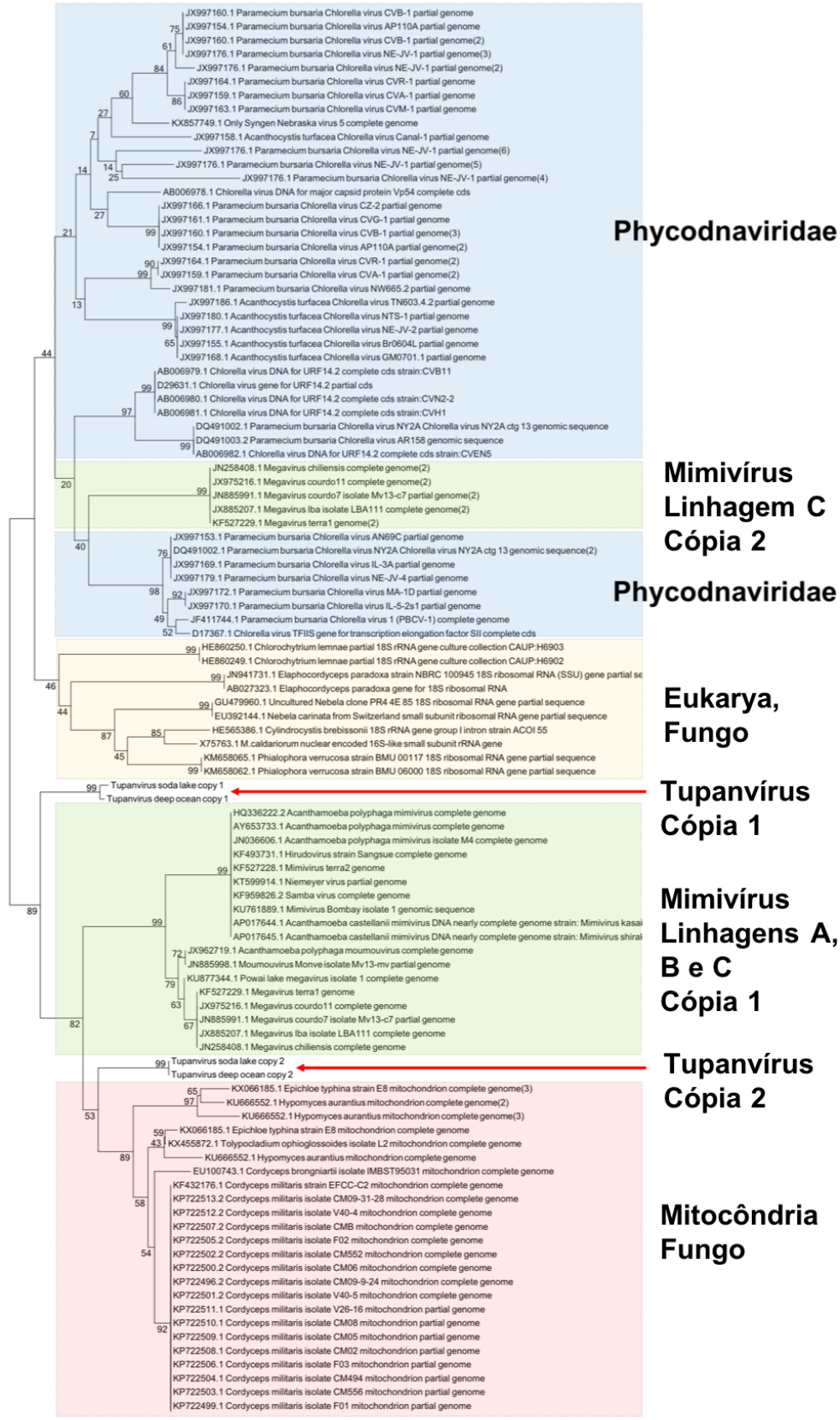

Figura 41: Árvore filogenética das sequências intrônicas de 18S presentes em mimivírus, phycodnavírus, fungos e mitocôndrias de fungos. As sequências intrônicas foram alinhadas, utilizando-se a ferramenta Clustal W do programa Mega 7.0, e usadas na construção da árvore filogenética através do método de máxima verossimilhança com 1000 replicatas.

6.1.2.3. Análise de vizinhança e de regiões imediatamente adjacentes

Com o objetivo de avaliar quais genes estariam próximos às cópias 1 e 2 de tupanvirus soda lake, análises da vizinhança de ambas as sequências intrônicas de 18S foram realizadas. Essas análises revelaram a presença de genes codificadores de proteínas hipotéticas e ORFans próximas a ambas as cópias. Além disso, uma ilha de tRNAs, composta por sequências relativas a seis tRNAs, também foi observada a 15 kpb de distância da cópia 1. No entanto nenhum outro gene relacionado ao processo de tradução foi identificado nas proximidades das duas cópias (Figura 42).

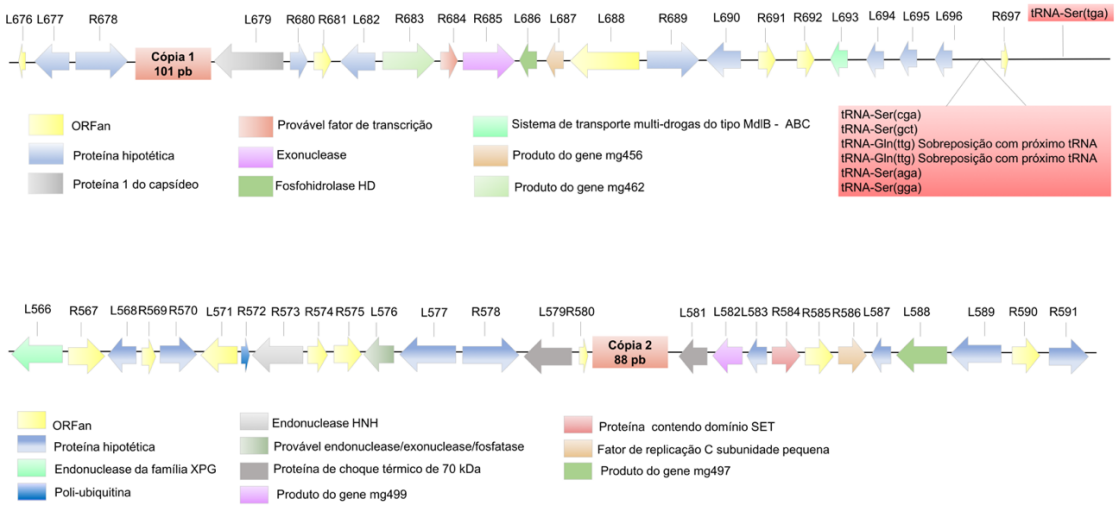

Figura 42: Análise da vizinhança das cópias 1 e 2 de tupanvirus soda lake. Genes codificadores de proteínas hipotéticas e ORFans são observados nas proximidades de ambas as cópias. Uma ilha de tRNAs também pode ser observada a 15 kpb de distância da cópia 1.

Além das análises de vizinhança, as regiões imediatamente adjacentes às sequências intrônicas de 18S presentes na família *Mimiviridae* também foram estudadas. Para tanto, além de tupanvirus soda lake e tupanvirus deep ocean, um membro de cada linhagem foi selecionado para avaliação. As análises demonstraram que as cópias únicas das linhagens A e B, assim como a cópia 1 da linhagem C, similarmente se localizam em uma região intrônica do gene da RNA polimerase subunidade 1 (Figura 43A, B e C). Curiosamente, próximo a essas cópias está presente uma endonuclease também codificada por íntrons self-splicing. Já a cópia 2 da linhagem C se localiza entre o gene codificador da proteína 1 do capsídeo e íntron codificador de nuclease (Figura 43C). Por sua vez, ambas as cópias de tupanvirus soda lake e

tupanvirus deep ocean se localizam em regiões intergênicas: as cópias 1 entre proteínas hipotéticas e proteínas 1 do capsídeo, e as cópias 2 entre ORFans e proteínas de choque térmico de 70 kDa (Figura 43D e E).

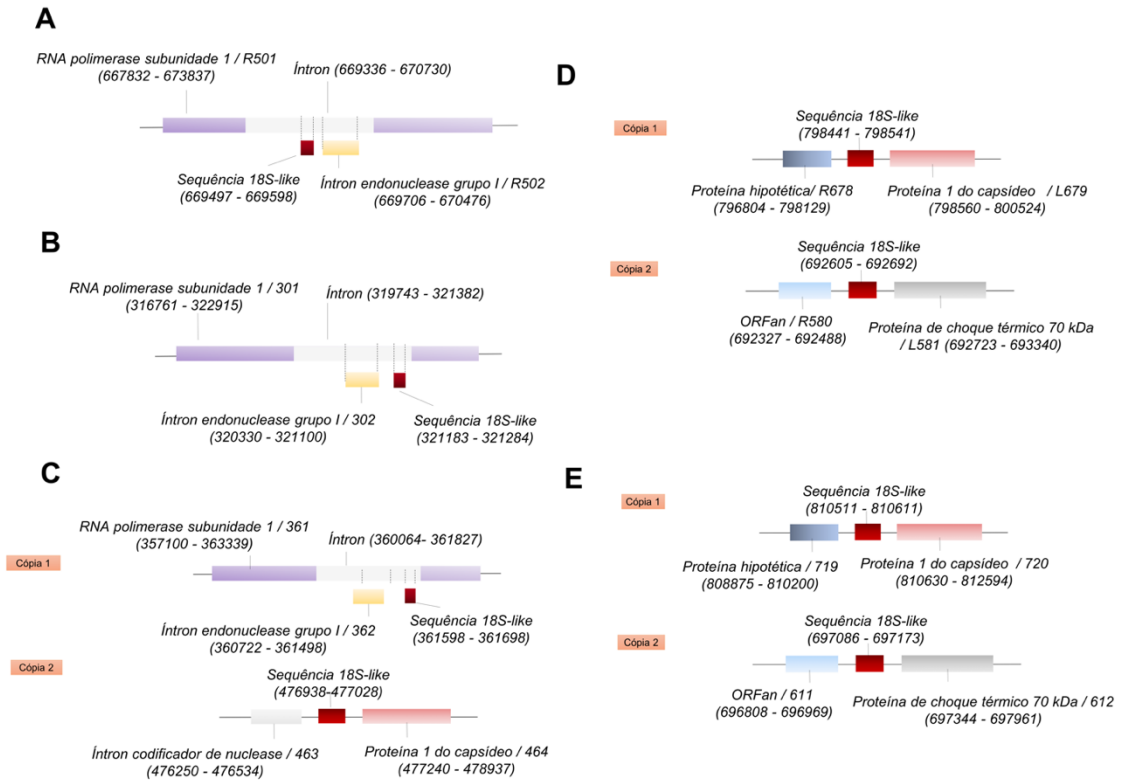

Figura 43: Análise das regiões imediatamente adjacentes às cópias de 18S-like em mimivírus. (A) Acanthamoeba polyphaga mimivirus; **(B)** Acanthamoeba polyphaga moumouvirus; **(C)** megavirus LBA; **(D)** tupanvirus soda lake; **(E)** tupanvirus deep ocean.

6.1.2.4. Análise da expressão das cópias 1 e 2

O próximo passo no estudo das cópias de íntrons de 18S foi avaliar a expressão dessas duas sequências durante a infecção por tupanvirus soda lake. Inicialmente a expressão foi averiguada através da técnica de FISH utilizando-se sondas para o 18S rRNA de *A. castellanii,* assim como para ambas as cópias de tupanvírus. Após a hibridização e avaliação microscópica, foi possível observar uma considerável fluorescência, relativa às sondas para as duas cópias de íntrons de 18S, nas células infectadas por tupanvírus (Figura 44). Além disso, essa fluorescência, indicativa de expressão gênica, foi observada de maneira similar para ambas as cópias e ao longo de

toda a infecção viral, especialmente nos tempos intermediários (6 hpi) e tardios (12 hpi) (Figura 44).

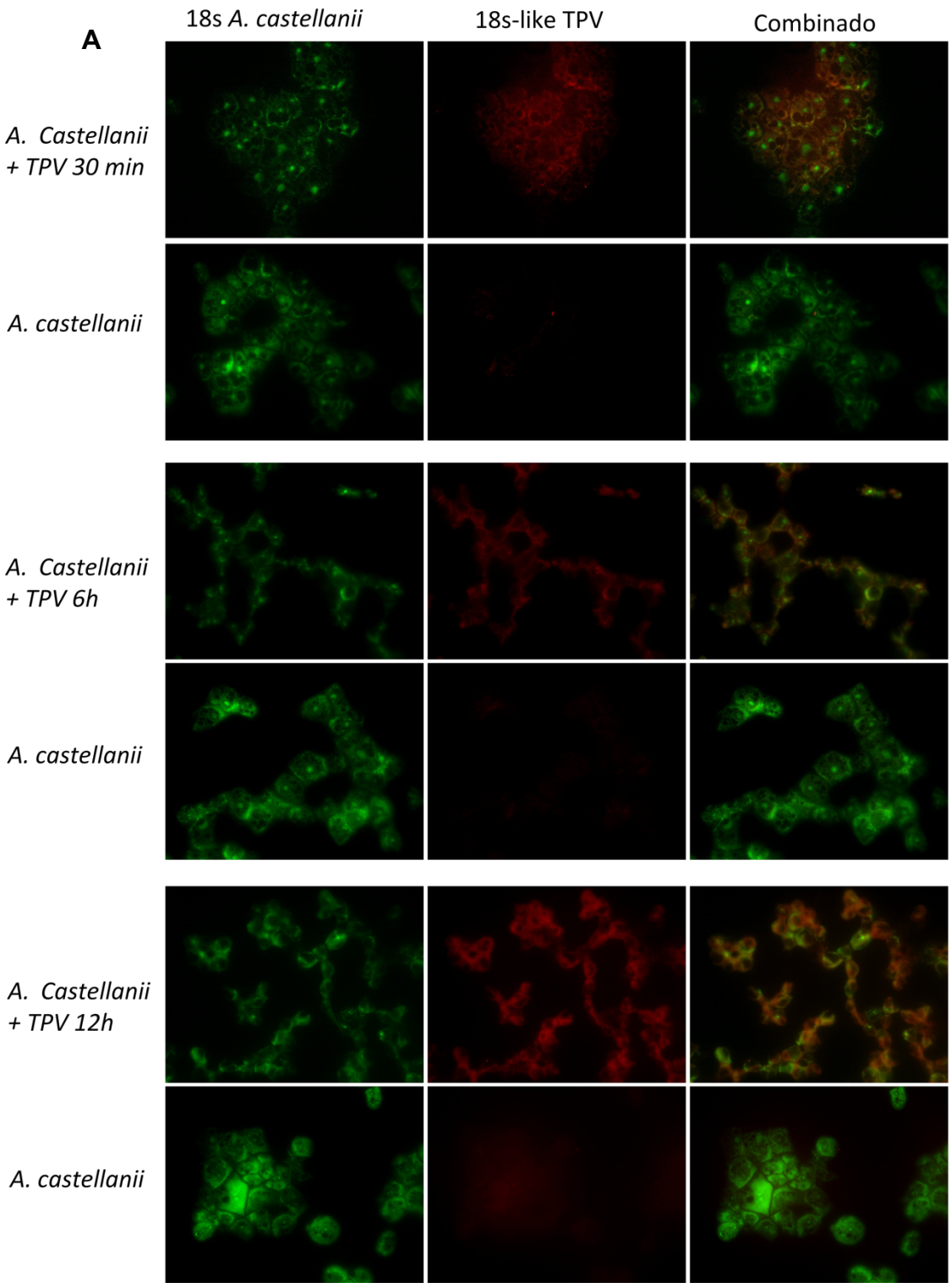

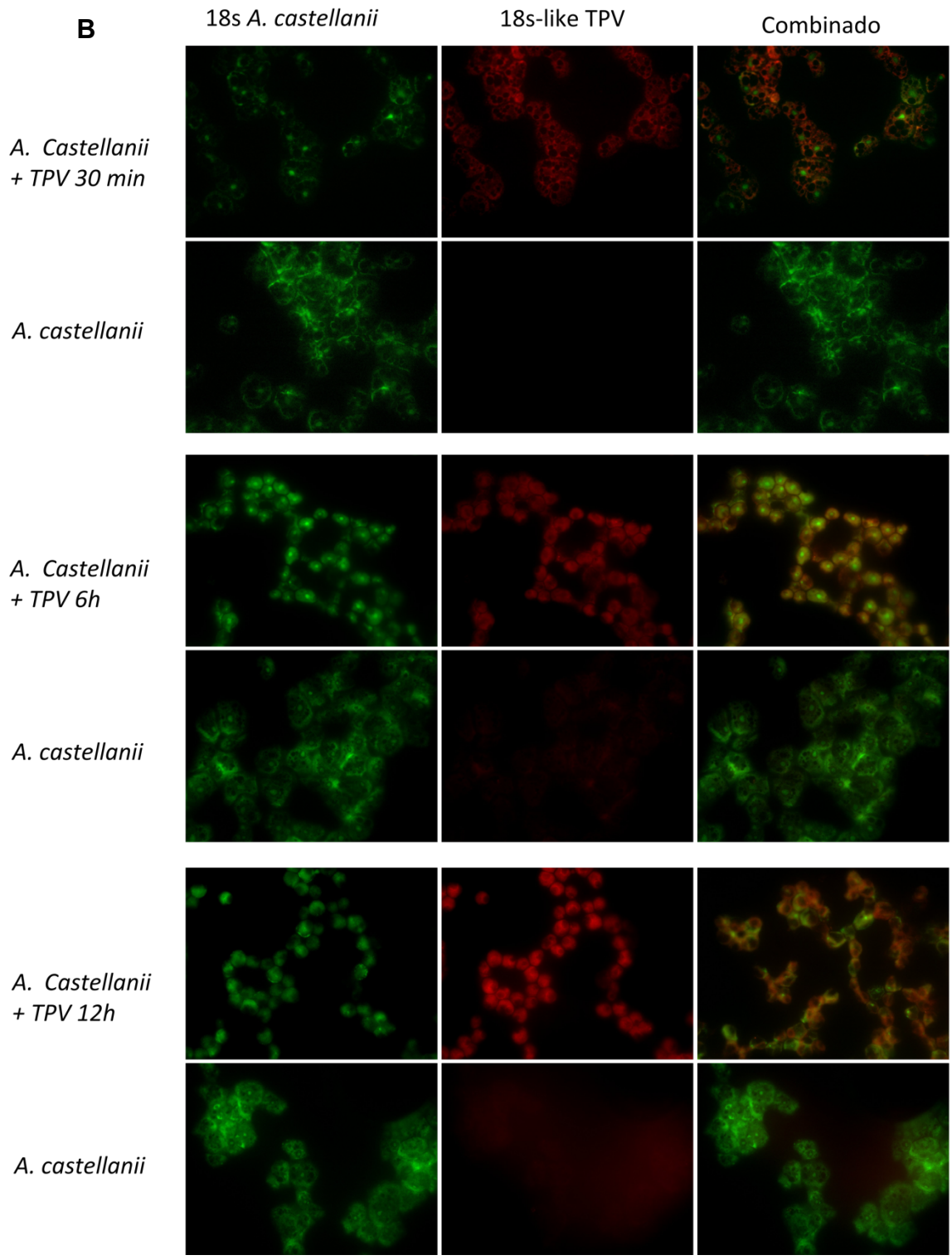

Figura 44: Análise da expressão das cópias de 18S-like de tupanvirus soda lake por FISH. Fluorescência indicativa de hibridização entre sondas e alvos pode ser observada tanta para a cópia 1 **(A)**, quanto para a cópia 2 **(B)** durante diferentes tempos de infecção, sendo mais intensa nos tempos intermediários (6 hpi) e tardios (12 hpi).

Em seguida, a avaliação da expressão das cópias 1 e 2 presentes em tupanvírus também foi checada por qPCR a partir da utilização de iniciadores específicos. Similarmente ao anteriormente observado para os experimentos com FISH, também foi possível observar a expressão de ambas as cópias durante a infecção viral, sendo que uma maior expressão, quando comparada ao tempo precoce de 30 minutos, foi notada nos tempos de 6 e 9 horas pós infecção (Figura 45).

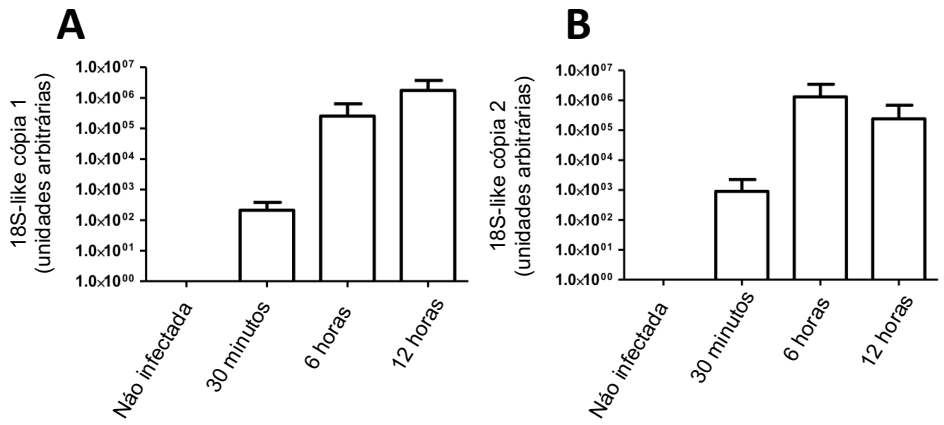

Figura 45: Análise da expressão das cópias de 18S-like de tupanvírus soda lake por qPCR. Células *A. castellanii* infectadas por 30 minutos, 6 horas ou 12 horas foram infectadas com tupanvirus soda lake na MOI de 5, submetidas à extração de RNA total, transcrição reversa e o cDNA resultante foi utilizado como molde para PCR em tempo real. É possível observar a expressão das cópias 1 **(A)** e 2 **(B)** em difentes tempos de infecção, principal nos tempos de 6 e 9 horas. As barras de erro representam o desvio padrão.

Em conjunto, os dados relativos aos experimentos envolvendo FISH e qPCR sugeriram que, embora as duas cópias de 18S-like sejam localizadas em regiões intergênicas, elas são altamente expressas ao longo da infecção por tupanvirus soda lake.

6.2. Caracterização do ciclo de multiplicação do cedratvirus getuliensis

Os estudos de prospecção de vírus gigantes vêm avançando consideravelmente nos últimos anos, possibilitando o isolamento de diferentes vírus. Entretanto apesar dessas novas descobertas, pouco ainda é conhecido sobre a biologia da maioria desses vírus. Esse também é o caso dos cedratvírus, que anteriormente ao isolamento do cedratvirus getuliensis, eram representados somente por dois outros isolados. Com o intuito de fornecer mais informações acerca desses vírus, uma caracterização

aprofundada do ciclo de multiplicação do cedratvirus getuliensis foi desenvolvida durante a realização dessa tese.

6.2.1. Ação de diferentes inibidores na penetração de cedratvirus getuliensis

Para investigar o principal mecanismo de penetração utilizado por cedratvirus getuliensis, ensaios com diferentes inibidores farmacológicos foram realizados. Os dados revelaram que o pré-tratamento de células *A. castellanii* com citocalasina D levou a uma diminuição considerável do título viral, quando comparado a amebas não tratadas, indicando que esses vírus podem penetrar nas células hospedeiras por fagocitose, após adesão (Figura 46A e B). Imagens de microscopia eletrônica de transmissão (MET) também corroboraram essa hipótese, uma vez que partículas virais puderam ser observadas dentro de vesículas semelhantes a fagossomos, apresentando mais do que 500 nm (Figura 46 C e D).

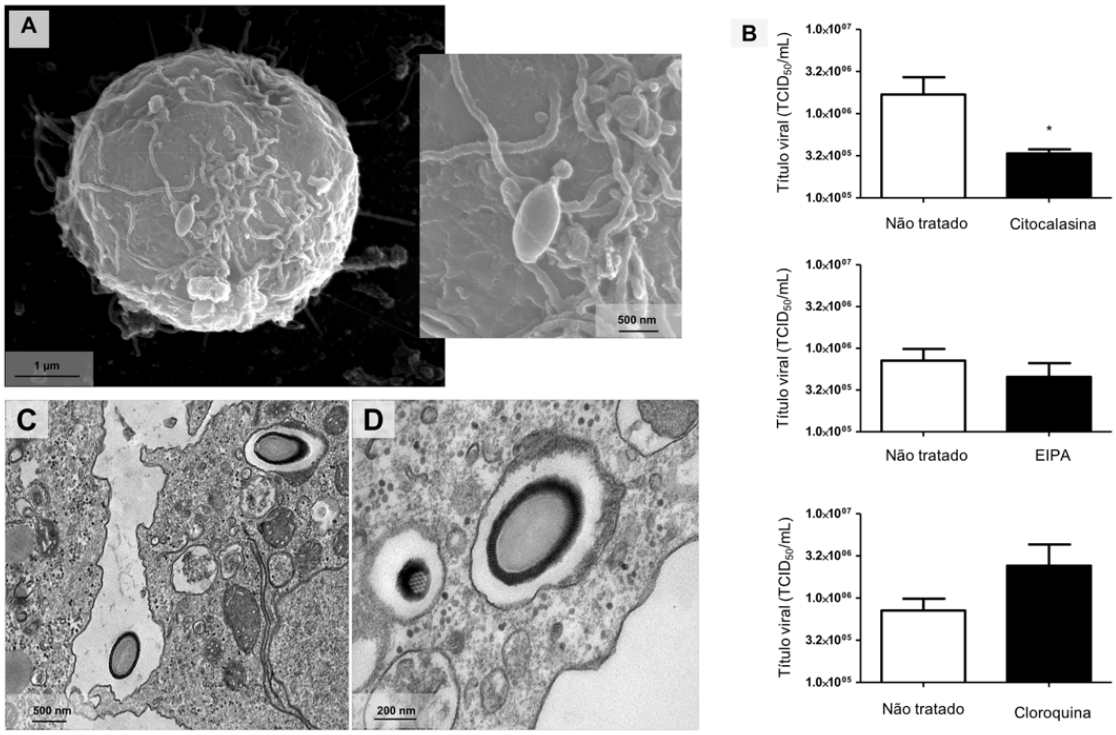

Figura 46: Penetração do cedratvirus getuliensis em amebas *A. castellanii*. (A) Imagens de microscopia eletrônica de varredura evidenciando uma partícula viral aderida à ameba. **(B)** Impacto de diferentes inibidores na penetração viral. O tratamento com citocalasina reduzia o título viral de maneira significativa. **(C)** e **(D)** Imagens de microscopia eletrônica de transmissão de partículas virais no interior de vesículas similares a fagossomos. *:$p < 0.05$. As barras de erro representam o desvio padrão.

Ao contrário do observado para citocalasina D, o pré-tratamento com cloroquina curiosamente revelou uma tendência biológica de aumento do título viral. Já o tratamento com EIPA não foi capaz de induzir uma redução significativa do título viral, sugerindo que a macropinocitose aparentemente não é um mecanismo essencial para a penetração (Figura 46 B).

6.2.2. Caracterização da fábrica viral de cedratvirus getuliensis e observação de outras mudanças celulares

Após o estudo da penetração, o próximo passo na investigação do ciclo de cedratvirus getuliensis foi a caracterização das fábricas virais observadas durante a multiplicação viral no citoplasma da célula hospedeira. Imagens de microscopia eletrônica de transmissão revelaram que as fábricas virais de cedratvirus getuliensis possuem tamanho semelhante ao do núcleo e são elétron-lucentes, sendo, por esse motivo, de difícil distinção do restante do citoplasma da célula. Além disso, essas fábricas virais, aparentemente, se localizam na região perinuclear, entretanto apesar da proximidade, nenhuma alteração nuclear foi observada, sugerindo que essa estrutura não é afetada pela multiplicação viral (Figura 47A).

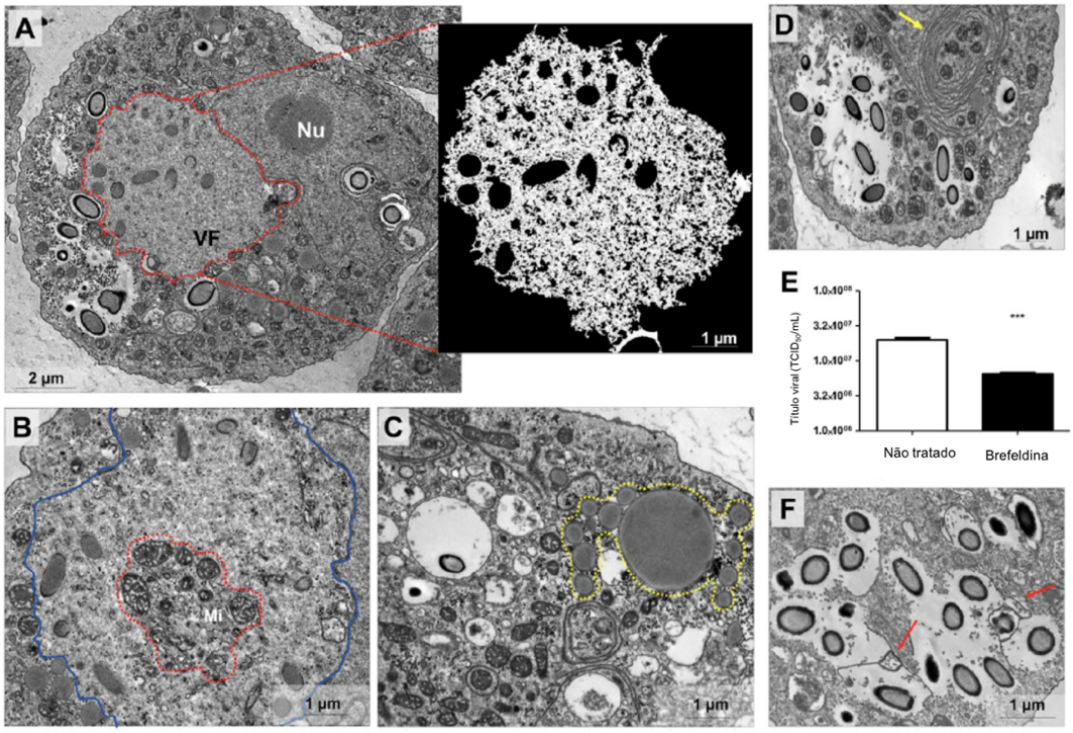

Figura 47: Fábrica viral de cedratvirus getuliensis e outras alterações celulares observadas durante a multiplicação viral. (A) Fábrica viral de cedratvirus getuliensis contornada em

vermelho e em destaque. **(B)** Mitocôndrias ao redor e no interior (destacadas em vermelho) da fábrica viral (contornada em azul). **(C)** Acumulação e polarização de lisossomos no citoplasma (contornado em amarelo). **(D)** Tráfego de membranas no citoplasma celular (seta amarela). **(E)** O tratamento com brefeldina A reduz o título viral de maneira significativa. **(F)** Células tratadas com brefeldina apresentando degradação de membranas. VF: fábrica viral; Nu: núcleo; Mi: mitocôndria. ***:$p < 0.001$. As barras de erro representam o desvio padrão.

Além da formação da fábrica viral, outras alterações celulares foram observadas durante a multiplicação do cedratvirus getuliensis, como a concentração de mitocôndrias ao redor e no interior da fábrica viral e a acumulação e polarização de estruturas semelhantes a lisossomos no citoplasma do hospedeiro (Figura 47B e C). Outra alteração observada foi um exacerbado tráfego de membranas que aparentemente são importantes para a morfogênese e exocitose das partículas virais. Para corroborar essa hipótese, tratamentos com brefeldina A foram realizados e foi observado que a ação dessa droga é capaz de impactar de maneira significativa o título viral. Além disso, imagens de microscopia eletrônica de transmissão evidenciaram um decréscimo do tráfego e uma degradação de membranas em células também tratadas com esse inibidor (Figura 47D, E e F).

6.2.3. Morfogênese das partículas virais de cedratvirus getuliensis

O estudo da progressão da infecção viral por MET evidenciou que a morfogênese do cedratvirus getuliensis envolve a formação de estruturas elétron-densas subsequentes visualizadas no interior e na periferia da fábrica viral. As imagens obtidas sugerem que a morfogênese se inicia a partir de crescentes apresentando aproximadamente 100 nm (Figura 48A). Em seguida, secções longitudinais demonstraram a ocorrência de um alongamento longitudinal dessas estruturas, que assumem uma conformação de "grampo" (Figura 48B). Secções transversais, por sua vez, revelaram a presença de capsídeos ainda não preenchidos, apresentando uma morfologia similar a "ferraduras" e uma típica parede estriada (Figura 48C). Além disso, secções longitudinais também possibilitaram a observação de somente um cork, localizado em um dos polos da partícula viral (Figura 48D). Nessa etapa da morfogênese as partículas parecem ser cilindros lateralmente abertos, uma vez que em cortes longitudinais as mesmas aparecem como retângulos e em cortes transversais como "ferraduras" (Figura 48E e F). Em seguida, um preenchimento progressivo da

partícula viral, seguido do fechamento lateral do capsídeo e emergência/incorporação do segundo cork também foi observado (Figura 48G a J).

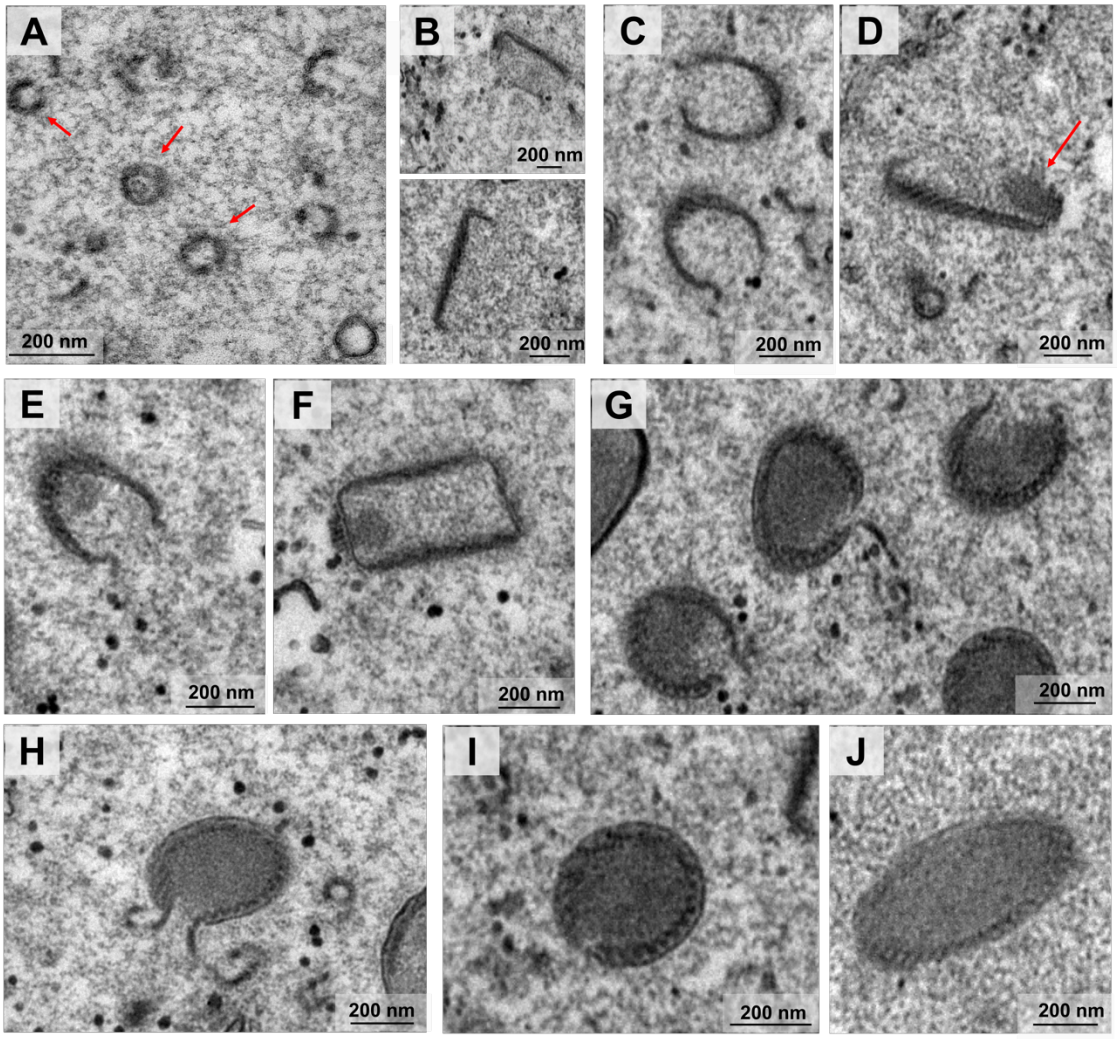

Figura 48: A morfogênese de cedratvirus getuliensis envolve a ocorrência de estruturas complexas subsequentes. (A) Primeiras estruturas observadas apresentam um formato de crescentes. **(B)** Cortes longitudinais evidenciam o alongamento longitudinal da partícula fazendo com que o capsídeo assuma uma conformação similar a "grampos". **(C)** Cortes transversais possibilitam a observação de capsídeos vazios com uma conformação de "ferradura". **(D)** Secções longitudinais demonstram capsídeos em forma de grampo com somente um cork evidente (seta vermelha) em um dos polos. Nesse estágio da morfogênese a partícula aparenta ser um cilindro aberto, uma vez que cortes longitudinais revelam as mesmas como retângulos **(F)** e cortes transversais com morfologia de "ferradura" **(E)**. **(G-I)** Preenchimento progressivo do capsídeo. **(J)** Fechamento completo do capsídeo.

Após o completo fechamento da partícula viral, também foi observado que o capsídeo sofre mudanças relacionadas à sua espessura. Esse espessamento se apresentou de maneira progressiva e em regiões localizadas ao redor da fábrica viral (Figura 49A e

B). MET evidenciaram que inicialmente essa estrutura apresenta uma parede fina, que não é capaz de recobrir lateramente ambos os corks, no entanto, com o avançar da maturação, a parede se torna mais grossa e passa a adquirir a mesma espessura de ambos os corks (Figura 49C a H).

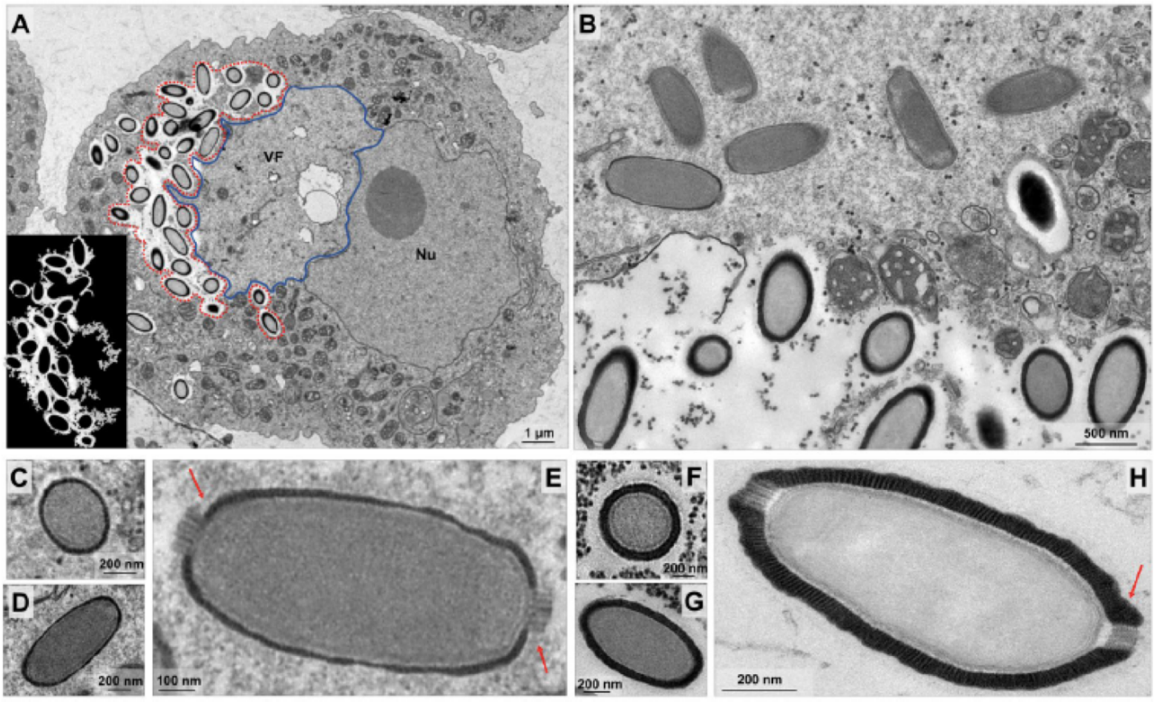

Figura 49: Espessamento do capsídeo viral de cedratvirus getuliensis. (A) Partículas virais sofrem diferenciação em regiões específicas na periferia da fábrica viral (contornada em vermelho e em detalhe). **(B)** Periferia da fábrica viral evidenciando o espessamento do capsídeo viral. Secções transversais **(C)** e longitudinais **(D)** de capsídeos apresentando uma fina parede que não recobre lateralmente ambos os corks **(E)** (setas vermelhas). **(F)** e **(G)** O capsídeo sofre espessamento com o avançar da maturação e adquire a mesma espessura de ambos os corks **(H)** (seta vermelha). VF: fábrica viral; Nu: núcleo.

6.2.4. Caracterização da progênie viral

Após a avaliação da morfogênese viral, a caracterização da progênie viral também foi realizada. A observação de partículas virais maduras revelou que essas apresentam um formato ovóide e medem ~1 µm de comprimento e 0,5 µm de diâmetro. Além disso, MET também demonstraram a presença de um capsídeo apresentando típicas listras paralelas, que aparecem como pontos organizados, em secções superficiais de partículas maduras (Figura 50A e B). No interior do capsídeo também foi possível observar a presença de uma membrana, que por sua vez delimita um compartimento

interno sem subestruturas evidentes (Figura 50B). Além disso, as partículas também apresentaram dois corks, característicos dos cedratvirus, em ambos os polos da partícula viral. Entretanto, apesar desses corks serem encontrados nas extremidades, eles não se localizam em pontos antipodais, apresentando um desalinhamento entre seus centros (Figura 50A e C).

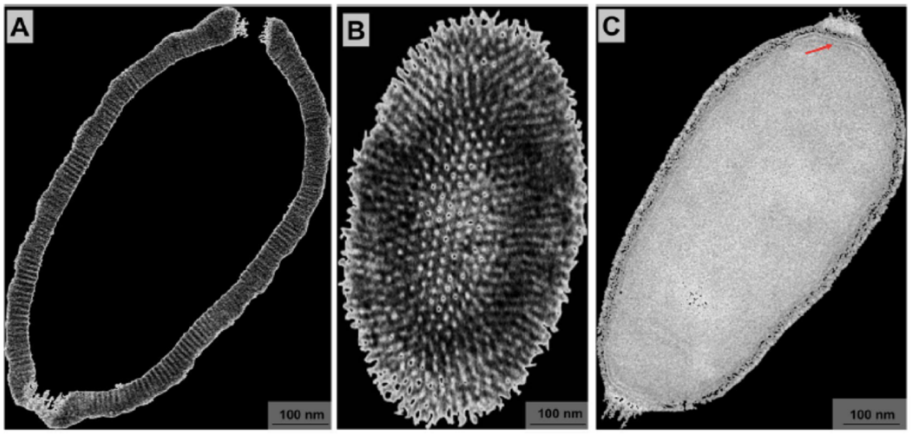

Figura 50: Partículas de cedratvirus getuliensis apresentam um formato ovóide e um capsídeo estriado. (A) Típico capsídeo viral apresentando listras paralelas e cork em pontos não antipodais. **(B)** Corte superficial de uma partícula madura evidenciando que as listras paralelas do capsídeo se apresentam como pontos organizados. **(C)** Interior do capsídeo é composto por uma membrana (seta vermelha) que delimita um compartimento interno homogêneo e sem subestruturas.

Apesar da maioria das partículas virais de cedratvirus getuliensis apresentarem morfologia semelhante (Figura 51A), algumas partículas de tamanho diferente também foram observas por microscopia eletrônica de varredura e apresentaram 2,04 μm, quase o dobro do tamanho da maioria das partículas (Figura 51B).

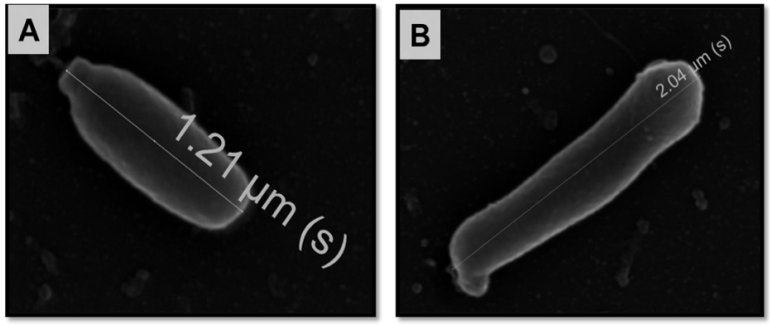

Figura 51: Imagens de microscopia eletrônica de varredura de partículas de cedratvirus getuliensis evidenciando a plasticidade dessas estruturas. A maioria das partículas virais apresentam ~1 μm de comprimento **(A)**, entretanto, partículas com quase o dobro de tamanho **(B)** também podem ser observadas.

Além disso, algumas estruturas de morfologia incomum compostas por porções de corks, capsídeos, membrana e material elétron-denso também foram notadas, sugerindo que essas pudessem representar partículas defectivas ou prematuras. A quantificação da ocorrência dessas estruturas também foi realizada e observou-se que aproximadamente 7% das células apresentam pelo menos uma dessas formações, sendo essas detectadas em paralelo a partículas comuns, em diferentes regiões do citoplasma e não restritas à região da fábrica viral (Figura 52).

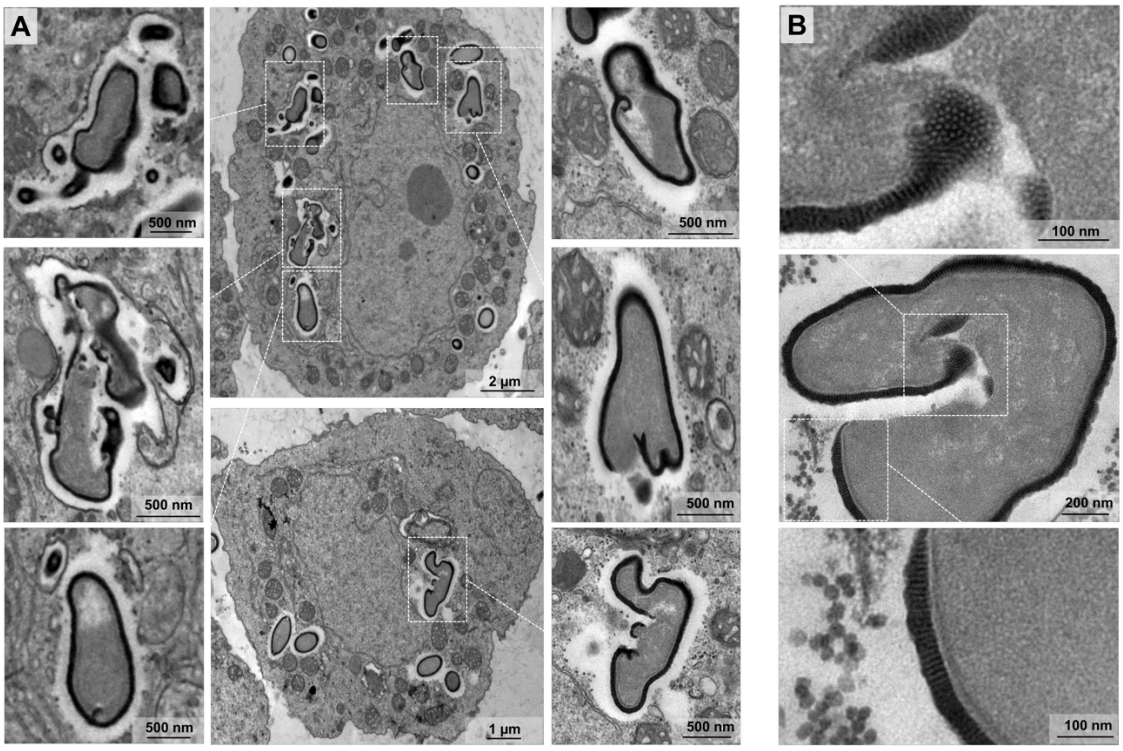

Figura 52: Estruturas de morfologia incomum observadas em meio à progênie viral. (A) e **(B)** Estruturas amorfas semelhante a partículas virais defectivas e compostas por porções de corks, capsídeo estriado, membranas e materiais elétron-densos, que podem ser visualizados no citoplasma da célula hospedeira em paralelo a partículas de morfologia comum.

6.2.5. Liberação das partículas virais ao final do ciclo de multiplicação

O próximo passo após a caracterização da progênie viral foi a análise da liberação das partículas virais formadas durante a multiplicação viral. Através de MET foi possível observar que em seguida ao processo de aumento de espessura da parede do capsídeo viral, as partículas maduras podem ser observadas imersas no citoplasma da célula viral ou também envoltas por membranas (Figura 53A). Além disso, mais de uma partícula viral foi observada dentro da mesma vesícula, que por sua vez também

apresentou uma ou mais camadas de membranas em sua composição (Figura 53B a E). Ademais, algumas partículas também foram observadas no interior de vesículas e no exterior da membrana celular (Figura 53F).

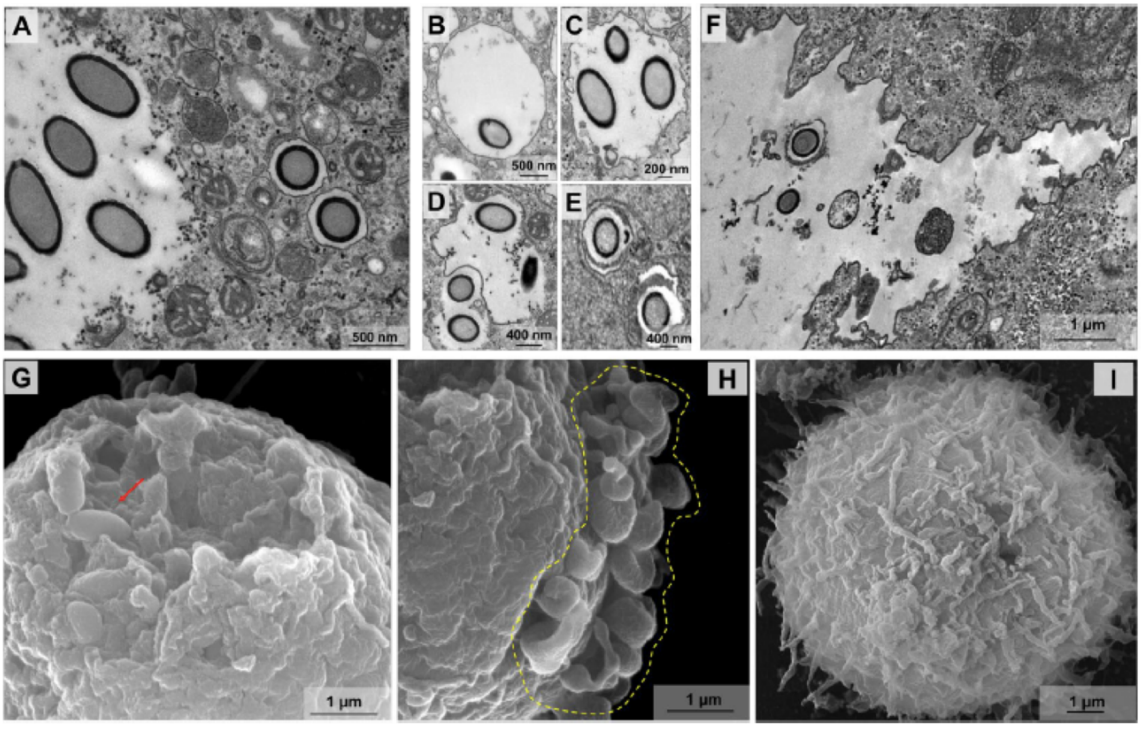

Figura 53: Partículas de cedratvirus getuliensis podem ser liberadas por lise celular ou exocitose. (A) Novas partículas virais são encontradas imersas no citoplasma ou no interior de vesículas. **(B)** e **(C)** Vesículas apresentando uma ou mais partículas virais. **(D)** Partículas sendo englobadas por membranas. **(E)** Vesícula com mais de uma membrana. **(F)** Partícula no interior de uma vesícula e aparentemente no exterior na membrana celular. **(G)** Imagens de microscopia eletrônica de varredura evidenciando dano na membrana celular e a emergência de partículas virais (seta vermelha). **(H)** Blebs (contornados de amarelo) na membrana celular podem ser observados ao final da infecção viral. **(I)** Célula controle, não infectada, apresentando membrana citoplasmática íntegra e sem protrusões.

Além desses dados, que sugerem a ocorrência de exocitose das partículas virais, também foi observardo por microscopia eletrônica de varredura a presença de uma grande quantidade de amebas apresentando danos substanciais na membrana celular a partir dos quais novas partículas virais parecem emergir (Figura 53G). Em paralelo a essa lise celular, a formação de protrusões membranosas denominadas de *blebs* também foi observada (Figura G e H).

7. DISCUSSÃO

A compreensão atual da virosfera mudou drasticamente após a descoberta dos mimivírus, que abriu o caminho para o isolamento de outros vírus tão ou mais complexos capazes de infectar amebas. Embora muitos estudos já tenham sido desenvolvidos destacando que os vírus gigantes podem ser filogeneticamente relacionados, formando o grupo monofilétido dos NCLDVs juntamente com outros grandes vírus de DNA (IYER et al., 2006; IYER; ARAVIND; KOONIN, 2001), estes vírus apresentam diferenças notáveis em relação à estrutura, genoma, ciclos de multiplicação e, consequentemente, interação com seus hospedeiros.

Recentemente, dois novos vírus, tupanvirus soda lake e cedratvirus getuliensis, foram descobertos pelo nosso grupo de pesquisa, a partir de um extenso trabalho de prospecção viral utilizando diferentes amostras dos mais diversos ambientes. A caracterização inicial do tupanvírus evidenciou, além da presença de um extenso aparato traducional, uma curiosa interação caracterizada pelo *shutdown* do RNA ribossomal em células hospedeiras e não hospedeiras. Por sua vez, a descoberta do cedratvirus getuliensis representou o isolamento do terceiro cedratvírus no mundo, revelando a acensão de um novo grupo viral e evidenciando o nosso ainda limitado conhecimento acerca da biologia desses vírus. Nesse contexto, o presente estudo apresenta características peculiares de ambos os isolados virais, abordando aspectos relacionados ao ciclo de multiplicação de cedratvirus getuliensis, à presença e caracterização de sequências 18S-*like* no genoma de tupanvirus soda lake, assim como o aprofundamento de um perfil de interação entre vírus e protozoário nunca antes descrito na virosfera.

A reprodução e caracterização aprofundada do *shutdown* em células *A. castellanii* revelou que a degradação do RNA ribossomal ocorre somente em células infectadas por tupanvírus, mas não por APMV, sob determinadas condições de infecção, sendo diretamente dependente da quantidade de partículas virais presentes, suportado pela necessidade de uma alta multiplicidade de infecção (MOI=100), assim como pelo tempo de interação entre vírus-hospedeiro, evidenciado por uma maior degradação em tempos mais tardios de infecção (9 hpi) (Figura 27). Além disso, o fato do *shutdown* ocorrer mesmo na presença de partículas inativadas por UV, mas não por calor, sugere que esse fenômeno possa ser induzido pela presença de algum fator viral, provavelmente, de natureza protéica, uma vez que proteínas são termo-sensíveis, sofrendo desnaturação, e consequente perda de função nessas condições (Figura 28)

(WU, 1925). Ademais, uma vez que o *shutdown* ocorre independentemente da multiplicação, como observado para *T. hyperangularis,* acredita-se que esse fator possa ser carreado pela partícula viral e liberado no citoplasma do hospedeiro. De fato, algumas imagens prévias de MET já evidenciaram, por exemplo, a liberação do conteúdo presente na cauda do tupanvírus no citosol de *A. castellanii* e também *T. hyperangularis* (ABRAHÃO et al., 2018). No entanto, mais estudos para corroborar essa hipótese são necessários, uma vez que os estudos de proteômica da partícula evidenciaram que mais da metade das proteínas virais presentes são desconhecidas, sendo algumas dessas codificados por ORFans. Além disso, as análises conduzidas também não foram capazes de identificar quais proteínas estariam associadas à composição exclusiva da cauda de tupanvírus (ABRAHÃO et al., 2018).

Apesar do *shutdown* também ser observado em *T. hyperangularis*, um diferente perfil temporal de ocorrência foi notado. Somente no 4° dia pós infecção uma degração ribossomal mais intensa foi detectada nesse protozoário, sugerindo que as diferenças biológicas existentes entre *A. castellanii* e *T. hyperangularis* possam acarretar em respostas diferentes à presença do patógeno (Figura 29). De fato, outras alterações além da degradação ribossomal foram observadas em *T. hyperangularis*, como diminuição da motilidade desses protozoários, aumento da vacualização e presença de uma grande quantidade de vesículas extracelulares provavelmente correspondentes a egestão de rejeitos não digeridos pelo citopígio (ABRAHÃO et al., 2018; DÜRICHEN et al., 2016; THURMAN; DRINKALL; PARRY, 2010)

Como mencionado anteriormente, após a caracterização do processo do *shutdown*, alguns outros experimentos foram conduzidos para corroborar, ou refutar, a hipótese inicial de que a degradação ribossomal ocorria pelo canônico processo de ribofagia. O primeiro experimento realizado com esse intuito foi a avaliação da inibição do processo de autofagia pelo uso de inibidores farmacológicos. O tratamento com as drogas cloroquina e bafilomicina A para inibição desse mecanismo já havia sido empregado anteriormente em diversos estudos e em diferentes células, inclusive em *A. castellanii* (JHA et al., 2014; MOON et al., 2015; REDMANN et al., 2017; SOLITRO; MACKEIGAN, 2016). No entanto, o tratamento com ambas as drogas não foi capaz de impedir o processo de *shutdown*, sugerindo que a acidicação de lisossomos, assim como a fusão de autofagossomos com essas organelas, não são processos inerentes para a ocorrência da degradação ribossomal ocasionada pelo tupanvírus (Figuras 31 e 32).

O próximo experimento conduzido na investigação do *shutdown* foi baseado no silenciamento do gene Atg-8 a partir do uso de siRNAs, previamente utilizados (MOON et al., 2009). Os resultados obtidos revelaram que alterações na biogênese da membrana de fagóforos, precursores dos autofagossomos, ocasionados pelo silenciamento não são capazes de evitar a degradação do RNA ribossomal de amebas *A. castellanii* diante da infecção por tupanvírus (Figura 32) (MOON et al., 2009; XIE; NAIR; KLIONSKY, 2008). É sabido que a família de genes codificadores de proteínas associadas à autofagia (Atg) contém mais de 35 genes em leveduras, no entanto, poucos homólogos foram descritos em *A. castellanii*, como Atg16, Atg3 e curiosamente uma segunda cópia de Atg8, denominada Atg8b (MIZUSHIMA; YOSHIMORI; OHSUMI, 2011; MOON et al., 2013). Entretanto, apesar de somente um dos genes Atg8 ter sido silenciado nesse trabalho, estudos prévios já demonstraram que a inibição da expressão de uma das cópias é capaz de afetar consideravelmente a ocorrência da autofagia (MOON et al., 2013). Além disso, os dados obtidos através do silenciamento gênico corroboram os dados anteriores envolvendo o uso de inibidores farmacológicos, sugerindo que o processo de autofagia não está diretamente relacionado ao *shutdown*.

Além do silenciamento gênico e do uso de inibidores de autofagia, experimentos para avaliar a ocorrência de acidificação de compartimentos celulares também foram realizados. Os dados obtidos revelaram uma intensa acidificação do citoplasma de amebas *A. castellanii* infectadas por tupanvírus que coincide temporalmente com a observação do *shutdown*. Diversos trabalhos previamente publicados já demonstraram que diferentes vírus utilizam da acidificação de endossomos ou fagossomos como estratégia para desnudamento e liberação do material genético viral no citoplasma (ANDRADE et al., 2017; BRINDLEY; MAURY, 2005; GROVE; MARSH, 2011; TOWNSLEY et al., 2006). Entretanto, a acificação causada por tupanvírus não foi restrita a compartimentos celulares, como aqui observado durante a infecção por APMV, ou como comumente observado no processo de autofagia, mas abrangeu todo o citoplasma celular de uma maneira que, até onde se sabe, não foi observada em outras infecções virais (Figura 35) (CHOI; BOWMAN; JUNG, 2018). Além disso, essa alteração no pH do citosol não foi afetada pelo tratamento com bafilomicina A, sugerindo que a acidificação ocorre de maneira independente de V-ATPases (Figura 36).

Concomitante à ocorrência do *shutdown* e à acidificação do citoplasma amebiano, outras alterações celulares foram observadas, como a formação de vesículas,

em sua maiora apresentando membrana única, contendo ribossomos em *A. castellanii* e *T. hyperangularis* (Figura 37 e 39). De fato, uma típica característica dos autofagossomos envolvidos no processo de ribofagia é a presença de duplas membranas, entretanto, raramente vesículas com duas membranas foram observadas durante o *shutdown* (KRAFT et al., 2008). Além disso, MET revelaram que a formação dessas vesículas ocorre principalmente na periferia da membrana nuclear, após invaginação e englobamento de ribossomos (Figura 37). Em seguida, essas vesículas se fundem com outras, formando grandes estruturas que não são mais observadas nos tempos do *shutdown*, sugerindo a ocorrência de depleção das mesmas por um mecanismo ainda desconhecido. Ademais, a infecção por tupanvírus também induziu uma extrema degradação do núcleo e do nucléolo em ambos os protozoários, sendo que em amebas *A. castellanii* o completo desaparecimento do núcleo/nucléolo foi observado em células coradas por hemacolor durante o *shutdown* (Figura 39). Nesse contexto, somente as fábricas virais são visualizadas no interior das células hospedeiras, fortalecendo o conceito de *virocell*, previamente proposto por Forterre (FORTERRE, 2013).

Vários estudos já foram conduzidos demonstrando que a multiplicação de diferentes vírus envolve a interação com o nucléolo do hospedeiro (Salvetti & Greco, 2014). Além disso, desorganizações nucleares já foram observadas em outros vírus gigantes, como pandoravírus, mollivírus e também aqui demonstrado para APMV em alta MOI (LEGENDRE et al., 2015; PHILIPPE et al., 2013). Entretanto, nenhuma alteração previamente reportada foi tão intensa, ou ocorreu de maneira concomitante com uma considerável degradação ribossomal como observado diante da infecção por tupanvírus.

Em conjunto, os dados aqui apresentados sugerem que o *shutdown* do RNA ribossomal não é diretamente relacionado ao canônico processo de ribofagia/autofagia. Embora a formação de vesículas contendo ribossomos e a degradação do nucléolo possam estar relacionadas a ocorrência desse fenômeno durante a infecção por tupanvírus, os mecanismos envolvidos na degradação ribossomal, após a formação de grandes vesículas contendo ribossomos, ainda precisam ser mais investigados. Como perspectiva, uma hipótese que poderia ser explorada é a possibilidade do tupanvírus ocasionar modificações ribossomais que favorecessem a tradução de suas proteínas, em oposição às proteínas celulares, como já descrito anteriormente para poxvírus (JHA et al., 2017).

Em paralelo aos experimentos desenvolvidos na caracterização do *shutdown* do RNA ribossomal, investigações sobre a presença de sequências ribossomais em tupanvírus também foram conduzidas. Nossas análises revelaram a presença de duas cópias (Cópia 1 e 2) no genoma desses vírus apresentando uma alta similaridade com partes de sequências intrônicas de 18S rDNA, mais especificamente com íntrons self-splicing do grupo I, presentes em diferentes organismos, como fungos, amebas e algas. De fato, os íntrons self-splicing do grupo I são amplamente distribuídos na natureza e são presentes no genoma de vários organismos, como bactérias, plantas, mitocôndrias, cloroplastos e eucariotos, sendo que no genoma desses últimos esses íntrons interrompem exclusivamente sequências de genes ribossomais (EDGELL; CHALAMCHARLA; BELFORT, 2011; HAUGEN; SIMON; BHATTACHARYA, 2005; MACHOUART et al., 2004).

Curiosamente, a presença de outras cópias de partes de íntrons de 18S também foi identificada em outros vírus do grupo dos NCLDVs, como mimivírus e phycodnavírus. Entre os representantes da família *Mimiviridae* foram identificadas uma única cópia em vírus pertencentes às linhagens A e B, e duas em vírus da linhagem C e em tupanvirus deep ocean. Apesar da descrição da presença dessas sequências já terem sido relatadas previamente para Chlorella virus e também para bacteriofágos, essa foi a primeira vez que essas cópias foram descritas em vírus gigantes (BONOCORA; SHUB, 2004; NISHIDA et al., 1998).

As análises filogenéticas realizadas com o intuito de avaliar a origem evolutiva dessas sequências, demonstraram que as cópias de tupanvirus soda lake e tupanvirus deep ocean tiveram origens separadas e parecem ser filogeneticamente relacionadas às cópias únicas das linhagens A e B, assim como da cópia 1 da linhagem C e das sequências intrônicas de 18S rRNA de mitocôndrias de fungos. Já as diversas cópias dos phycodnavírus aparentam ser filogeneticamente relacionadas entre si, assim como à cópia 2 da linhagem C e sequências de 18S de fungos (Figura 41). Um resultado semelhante também foi observado previamente para Chlorella virus, sugerindo um parentesco das sequências presentes nesses vírus com a presente no rRNA de uma variedade de organismos, como fungos e protozoários (NISHIDA et al., 1998).

A avaliação das regiões imediatamente adjacentes às sequências intrônicas de 18S presentes na família *Mimiviridae*, demonstraram que as cópias únicas das linhagens A e B, assim como a cópia 1 da linhagem C, se localizam em uma região intrônica do gene da RNA polimerase subunidade 1 (Figura 43A, B e C). A localização intrônica

dessas sequências em genes não ribossomais não foi relatada para eucariotos, entretanto, íntrons do grupo I já foram encontrados inseridos em uma ampla variedade de genes, como DNA polimerase e proteína principal do capsídeo em bacteriófagos e phycodnavírus (BONOCORA; SHUB, 2004; NISHIDA et al., 1998). Curiosamente, próximo a todas as cópias presentes nas três linhagens de mimivírus, uma endonuclease codificada por íntrons self-splicing foi observada. Alguns grupos de íntrons self-splicing possuem ORFs que codificam endonucleases que promovem a mobilidade desses íntrons de um local para outro no genoma e também de um organismo para outro (EDGELL; CHALAMCHARLA; BELFORT, 2011; HAUGEN; SIMON; BHATTACHARYA, 2005; MACHOUART et al., 2004). Dessa maneira, a presença dessas enzimas pode sugerir a ocorrência da mobilidade dessas sequências o que representaria um possível cenário da origem dessas cópias em genomas virais.

Entretanto, para tupanvirus soda lake e deep ocean, a análise das regiões imediatamente adjacentes evidenciou que ambas as cópias, surpreendentemente, se localizam em regiões intergênicas, conforme predição gênica, o que até então não havia sido descrito para esse grupo de íntrons self-splicing (Figura 43D e E). Além disso, nenhuma endonuclease foi identificada nas proximidades das duas cópias em ambos os tupanvírus, sugerindo a ocorrência de um cenário evolutivo diferente dos outros mimivírus. A fim de checar a expressão de ambas as cópias, análises envolvendo FISH e qPCR foram conduzidas e revelaram que, apesar das sequências se localizarem em regiões intergênicas elas são altamente expressas durante todo o ciclo de multiplicação, mas principalmente nos tempos intermediários (6 hpi) e tardios (12 hpi) (Figura 44 e 46). Apesar dos resultados observados, o motivo pelo qual essas sequências são expressas e como elas seriam expressas ainda não foi completamente elucidado, entretanto, uma aparente colocalização entre as sondas específicas para as cópias virais e para o 18S amebiano foi observada, sugerindo uma possível interação entre essas sequências intrônicas e os ribossomos de *A. castellanii*. No entanto, para corroborar essa evidência, novos experimentos ainda precisam ser conduzidos com sondas marcadas com um maior número de fluoróforos afim de possibilitar o aumento da captação do sinal de fluorescência por microscópio confocal.

Após a caracterização dos aspectos descritos em tupanvirus soda lake, a presente tese também teve como objetivo a condução do primeiro estudo aprofundado do ciclo

de multiplicação dos cedratvírus, fornecendo informações relevantes para o melhor entendimento da biologia do cedratvirus getuliensis.

Inicialmente, devido ao tamanho da partícula viral dos cedratvírus, havia sido proposto que esses vírus poderiam iniciar seu ciclo de multiplicação a partir da penetração por fagocitose, entretanto, nenhum dado experimental havia sido fornecido para sustentar essa hipótese, exceto por algumas imagens de microscopia eletrônica de transmissão. Diante disso, novos experimentos foram conduzidos utilizando-se diferentes inibidores de endocitose. Os dados obtidos demostraram que a inibição da fagocitose por citocalasina D, um inibidor previamente utilizado em amebas *A. castellanii*, capaz de inibir a polimerização de actina resulta em uma redução significativa da incorporação de partículas virais de cedratvirus getuliensis, sugerindo que o principal mecanismo de penetração utilizado por esse vírus é a fagocitose (Figura 46B, C e D; Figura 54 – 1) (ALSAM et al., 2005; CHRISMAN; ALVAREZ; CASADEVALL, 2010; SOTO-ARREDONDO et al., 2014; TAYLOR et al., 1995). Em contrapartida, o tratamento com EIPA, um inibidor de macropinocitose capaz de bloquear as trocas celulares de Na^+ e H^+, não afetou a penetração de partículas virais (Figura 46B). Entretanto, como o efeito desse inibidor em *Acanthamoeba* ainda não foi profundamente estudado, a penetração de cedratvirus getuliensis por macropinocitose não pode ser completamente descartada. Além disso, alguns trabalhos prévios desmonstraram que o inibidor citocalasina também é capaz de interferir na ocorrência de macropinocitose, reforçando assim a necessidade de estudos mais aprofundados do mecanismo de ação do EIPA em *Acanthamoeba* (KUHN et al., 2014; MICHAEL et al., 2013; SOLDATI; SCHLIWA, 2006). Já o tratamento com cloroquina, interessantemente, demonstrou uma tendência biológica de aumento do título viral, sugerindo que esse inibidor pode se acumular no interior de fagossomos, impedindo a acidificação e culminando em um aumento do pH, prevenindo assim a ocorrência do processo de desnudamento e preservando um maior número de partículas não desnudadas e infecciosas no interior de fagossomos (Figura 46B) (DUTTA; DONALDSON, 2012; JHA et al., 2014; MOON et al., 2015).

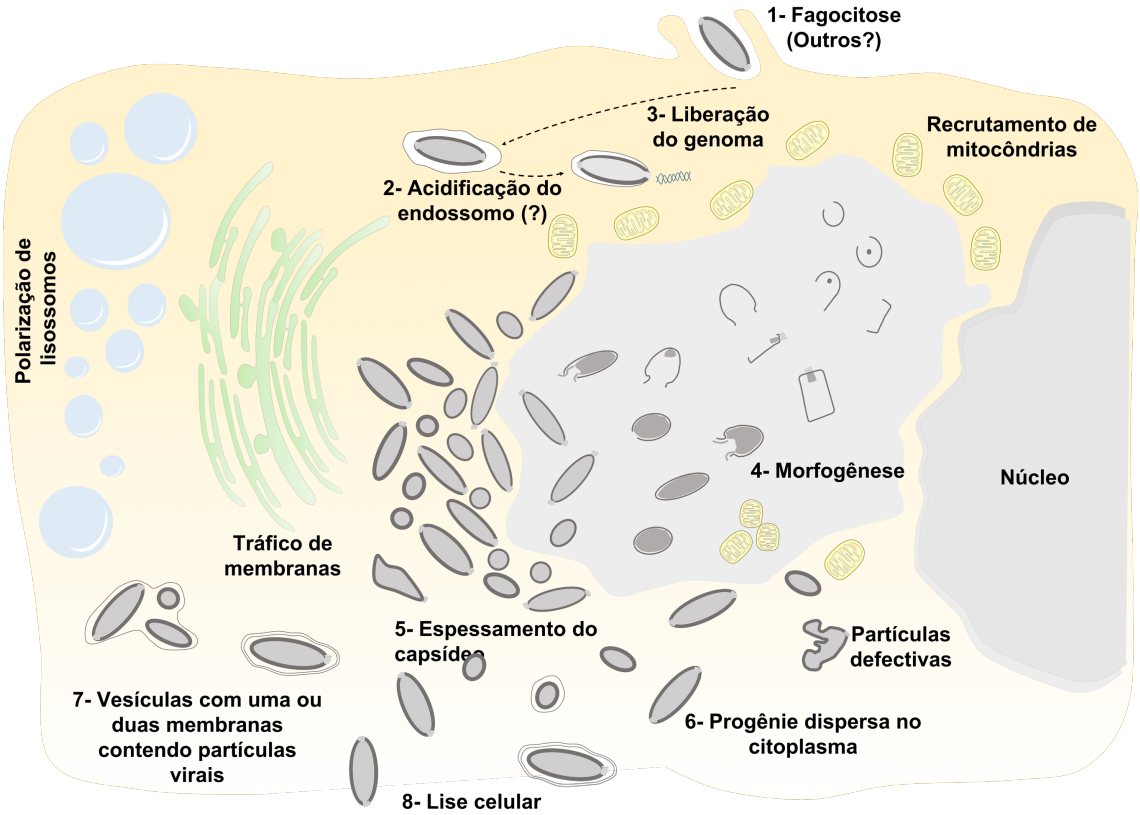

Figura 54: Representação esquemática do ciclo de multiplicação do cedratvirus getuliensis. (1) Partículas virais penetram na célula hospedeira por fagocitose. **(2-3)** Após a penetração, um cork é expelido e ocorre a fusão da membrana interna com a membrana do fagossomo possibilitando a liberação do genoma no citoplasma. **(4)** Após uma fase de eclipse típica, ocorre a formação de uma fábrica viral elétron-lucente no interior da qual ocorre a morfogênese viral. **(5)** O espessamento do capsídeo também ocorre na periferia da fábrica viral e novas partículas virais podem ser observadas dispersas no citoplasma **(6)** ou no interior de vesículas **(7)**. **(8)** A progênie viral é liberada principalmente por lise celular, entretanto a exocitose também parece ocorrer.

Com relação ao processo de desnudamento, já foi demonstrado por outros estudos que esse parece ocorrer após a extrusão de somente um dos corks, possibilitando assim a fusão da membrana interna, também observada nos dados aqui apresentados, com a membrana do fagossomo e a liberação do material genético no citoplasma da célula hospedeira (Figura Figura 54 - 2 e 3) (ANDREANI et al., 2016; BERTELLI et al., 2017). O mecanismo preciso envolvido no desencadeamento do desnudamento, ainda não é completamente elucidado, mas acredita-se que ele possa estar relacionado à acidificação do fagossomo, de maneira similar ao observado para os mimivírus (ANDRADE et al., 2017). Além disso, outro ponto que ainda permanece obscuro nessa etapa do ciclo de multiplicação é qual dos corks estaria envolvido no processo de

liberação do material genético, no entanto, nenhuma outra diferença, além de não se localizarem em pontos antipodais, já foi descrita para ambos os corks.

Após o desnudamento e uma típica fase de eclipse, MET evidenciaram a formação de uma grande fábrica viral nas proximidades do núcleo celular, que aparentemente não é envolvido no processo de multiplicação, uma vez que permaneceu inalterado durante todo o ciclo de multiplicação, diferentemente do observado para outros vírus gigantes, como pandoravírus e mollivírus (LEGENDRE et al., 2015; PHILIPPE et al., 2013). Ao contrário do observado também para os mimivírus, que apresentam uma fábrica viral elétron-densa dividida em partes (uma basicamente relacionada à replicação do genoma e morfogênese e outra relacionada a aquisição de fibrilas), a fábrica viral do cedratvirus getuliensis se mostrou elétron-lucente e sem subdivisões (Figura 47A; Figura 54 – 4) (ANDRADE et al., 2017; KUZNETSOV et al., 2013; SUZAN-MONTI et al., 2007). Além disso, similarmente aos pithovírus, nenhuma delimitação foi observada ao redor da fábrica viral do cedratvirus getuliensis sendo essa de difícil diferenciação do restante do citoplasma.

No interior e na periferia dessas fábricas virais também foi observada uma complexa morfogênese de partículas virais do cedratvirus getuliensis, envolvendo a formação de estruturas elétron-densas subsequentes (Figura 54 – 4) . As imagens obtidas sugerem que a morfogênese se inicia a partir de crescentes de origem ainda desconhecidas de ~100 nm. Estruturas similares já foram observadas durante a multiplicação de vaccinia vírus, mimivírus e asfarvírus, sugerindo a ocorrência de etapas comuns na multiplicação dos NCLDVs (Figura 48A) (MUTSAFI et al., 2010, 2013; SUAREZ et al., 2013; SUAREZ et al., 2015).

A morfogênese completa do cedratvirus getulienses se mostrou relativamente semelhante à de pithovírus, com partículas apresentando uma morfologia ligeiramente retangular no início, seguido por um espessamento do capsídeo e subsequente aquisição de um formato oval (Figura 49; Figura 50; Figura 54 – 5) (LEGENDRE et al., 2014). Mas diferentemente dos pithovírus, cedratvirus getuliensis adquire um segundo cork no final da morfogênese. Além disso, nenhuma estrutura em formato de ferradura, indicativa da presença de uma partícula lateralmente aberta, foi descrita para os pithovírus. As imagens obtidas também demonstraram que é através dessa abertura lateral que essas partículas são preenchidas por um material elétron-denso, sugerindo a ocorrência da aquisição do genoma e de proteínas virais nessa etapa da morfogênese (Figura 48G, H e I).

A caracterização da progênie viral revelou a presença de partículas apresentando em sua maioria 1 μm, entretanto, vírus de mais de 2 μm também foram observados, evidenciando uma plasticidade no tamanho do cedratvirus getuliensis, que também já havia sido relatada para os pithovírus (Figura 51) (LEGENDRE et al., 2014; OKAMOTO et al., 2017). Além disso, a presença de partículas virais amorfas, observadas durante o ciclo de multiplicação dos cedratvirus getuliensis, também já tinham sido descritas por Legendre e colaboradores (2014), entretanto esses pesquisadores descreveram essas estruturas como possíveis reservatórios de componentes necessários à morfogênese viral. No entanto, a hipótese dessas estruturas serem, na realidade, partículas defectivas não pode ser descartada, uma vez que a ocorrência de partículas anormais já foi previamente relatada para outros vírus gigantes (Figura 52) (ABRAHÃO et al., 2014; ANDRADE et al., 2017).

O fim do ciclo de multiplicação do cedratvirus getulienses foi caracterizado pela liberação das novas partículas virais principalmente por lise celular (Figura 54 – 8). Entretanto, a liberação por exocitose também parece ocorrer, uma vez que partículas virais foram observadas no interior de membranas no citoplasma da célula hospedeira (Figura 54 – 7). A origem dessas membranas, assim como da membrana observada no interior dos vírions, ainda não é clara, no entanto, os experimentos envolvendo o tratamento com brefeldina A revelaram um impacto significativo do título viral, demonstrando que o tráfego de membranas é importante para o processo de morfogênese e/ou exocitose das partículas virais.

Durante o ciclo de multiplicação do cedratvirus getuliensis outras alterações celulares também foram observadas. Uma delas foi o recrutamento de mitocôndrias para a região da fábrica viral, o que pode estar relacionado com a otimização de aquisição de energia que é requerida para a multiplicação viral (Figura 47B). Além dessa alteração, a polarização de estruturas que remetem a lisossomos também foi notada, sugerindo a possibilidade de ocorrência de autofagia de vírions ou de componentes virais, uma vez que essas organelas atuam como estruturas degradativas. Entretanto, o real impacto dessas organelas na multiplicação viral ainda precisa ser melhor estudado.

Ainda há algumas perguntas a serem respondidas sobre o ciclo de multiplicação deste novo grupo de vírus, especialmente no nível molecular. Investigações adicionais usando diferentes técnicas de microscopia, combinadas com transcriptômica e dados proteômicos, certamente fornecerão informações valiosas sobre a dinâmica de interação

vírus-hospedeiro e preencherão algumas lacunas remanescentes relativas ao ciclo de multiplicação dos cedratvírus.

8. CONCLUSÕES

- O *shutdown* do RNA ribossomal é causa ou consequência de um padrão citotóxico que ocorre em células não permissivas, como *T. hyperangularis*, e também em células permissivas, como *A. castellanii* e *V. vermiformis*, em alta multiplicidade de infecção e dependente do tempo de interação entre vírus e hospedeiro;

- A degradação ribossomal também é observada diante da infecção com partículas de tupanvírus inativadas por UV, mas não por calor;

- O shutdown aparentemente não está associado ao processo de ribofagina, uma vez que o tratamento de amebas *A. castellanii* com inibidores de autofagia, assim como o silenciamento do gene Atg8 não impedem a ocorrência da degradação ribossomal induzido pelo tupanvírus;

- Durante a infecção pelo tupanvírus, uma notável acidificação do citoplasma de células *A. castellanii* é observada;

- A infecção pelo tupanvirus soda lake induz uma progressiva degradação do núcleo/nucléolo temporariamente associada ao *shutdown*. O APMV também é capaz de ocasionar mudanças no nucléolo da célula hospedeira, entretanto essas alterações não apresentam a mesma proporção das observadas diante da infecção pelo tupanvírus;

- Pequenas vesículas, compostas em sua maioria por uma única membrana, contendo ribossomos próximo à membrana nuclear foram observadas. Essas vesículas, posteriormente, se agregam formando grandes estruturas que são depletadas do citoplasma no mesmo tempo que o *shutdown* pode ser detectado;

- Duas cópias de sequências similares a partes de regiões intrônicas de 18S, mais especificamente a íntrons self-splicing do grupo I, foram encontradas no genoma de tupanvírus;

- Cópias similares também foram encontradas nos genomas de mimivírus das linhagens A, B e C e também em tupanvirus deep ocean;

- A análise filogenética das duas cópias presentes em tupanvírus evidenciou que elas apresentam origens separadas, e apesar de estarem localizadas em regiões intergênicas do genoma, são altamente expressas durante o ciclo de multiplicação, mais especificamente durante as fases intermediárias e tardias.

- O estudo aprofundado do ciclo de multiplicação do cedratvirus getuliensis revelou através do uso de diferentes inibidores de endocitose que a penetração desses vírus em amebas *A. castellanii* ocorre principalmente por fagocitose;

- Foi possível observar a presença de uma fábrica viral elétron-lucente localizada na periferia do núcleo;

- A morfogênese de cedratvirus getuliensis é complexa e envolve estruturas elétron-densas subsequentes que podem ser observadas no interior e na periferia da fábrica viral;

- Alterações celulares como recrutamento de mitocôndrias, polarização de lisossomos e intenso tráfego de membranas foram observadas ao longo da multiplicação de cedratvirus getuliensis;

- A análise da progênie viral envidenciou a presença de partículas com uma plasticidade de tamanho, assim como partículas defectivas;

- A liberação das novas partículas virais ocorre principalmente por lise celular, entretanto a liberação por exocitose também parece ocorrer.

9. REFERÊNCIAS BIBLIOGRÁFICAS

ABRAHÃO, J. et al. Tailed giant Tupanvirus possesses the most complete translational apparatus of the known virosphere. **Nature Communications**, v. 9, n. 1, 2018.

ABRAHÃO, J. S. et al. Acanthamoeba polyphaga mimivirus and other giant viruses: An open field to outstanding discoveries. **Virology Journal**, v. 11, n. 1, p. 1–12, 2014.

ABRAHÃO, J. S. et al. Mimiviruses: Replication, purification, and quantification. **Current Protocols in Microbiology**, v. 2016, p. 14G.1.1-14G.1.13, 2016.

ADENIKE, A. A. et al. Legionella drozanskii sp. nov., Legionella rowbothamii sp. nov. and Legionella fallonii sp. nov.: Three unusual new Legionella species. **International Journal of Systematic and Evolutionary Microbiology**, v. 51, n. 3, p. 1151–1160, 2001.

AHERFI, S. et al. Complete genome sequence of Cannes 8 virus, a new member of the proposed family “marseilleviridae”. **Virus Genes**, v. 47, n. 3, p. 550–555, 2013.

AHERFI, S. et al. The expanding family Marseilleviridae. **Virology**, v. 466–467, p. 27–37, 2014.

ALSAM, S. et al. Mechanisms associated with Acanthamoeba castellanii (T4) phagocytosis. **Parasitology Research**, v. 96, n. 6, p. 402–409, 2005.

ANDRADE, A. C. D. S. P. et al. Ubiquitous giants: A plethora of giant viruses found in Brazil and Antarctica. **Virology Journal**, v. 15, n. 1, p. 1–10, 2018.

ANDRADE, A. C. DOS S. P. et al. Filling gaps about mimivirus entry, uncoating and morphogenesis. **Journal of Virology**, p. JVI.01335-17, 2017.

ANDRADE, K. R. et al. Oysters as hot spots for mimivirus isolation. **Archives of Virology**, v. 160, n. 2, p. 477–482, 2014.

ANDREANI, J. et al. Cedratvirus, a double-cork structured giant virus, is a distant relative of pithoviruses. **Viruses**, v. 8, n. 11, p. 1–11, 2016.

ANDREANI, J. et al. Pacmanvirus, a New Giant Icosahedral Virus at the Crossroads between Asfarviridae and Faustoviruses. **Journal of Virology**, v. 91, n. 14, p. e00212-17, 2017.

ANDREANI, J. et al. Orpheovirus IHUMI-LCC2: A new virus among the giant viruses. **Frontiers in Microbiology**, v. 8, n. JAN, p. 1–11, 2018.

ANTWERPEN, M. H. et al. Whole-genome sequencing of a pandoravirus isolated from keratitis-inducing acanthamoeba. **Genome announcements**, v. 3, n. 2, p. e00136-15, 2015.

ARANTES, T. S. et al. The Large Marseillevirus Explores Different Entry Pathways by Forming Giant Infectious Vesicles. **Journal of Virology**, v. 90, n. 11, p. 5246–5255, 2016.

ARSLAN, D. et al. Distant Mimivirus relative with a larger genome highlights the fundamental features of Megaviridae. **Proceedings of the National Academy of Sciences**, v. 108, n. 42, p. 17486–17491, 2011.

ARTENSTEIN, A. W. The discovery of viruses: Advancing science and medicine by challenging dogma. **International Journal of Infectious Diseases**, v. 16, n. 7, p. e470–e473, 2012.

ASSIS, F. L. et al. Pan-genome analysis of Brazilian lineage a amoebal mimiviruses. **Viruses**, v. 7, n. 7, p. 3483–3499, 2015.

BAJRAI, L. H. et al. Kaumoebavirus, a new virus that clusters with Faustoviruses and Asfarviridae. **Viruses**, v. 8, n. 11, 2016.

BERTELLI, C. et al. Cedratvirus lausannensis – digging into Pithoviridae diversity. **Environmental Microbiology**, v. 19, n. 10, p. 4022–4034, 2017.

BONOCORA, R. P.; SHUB, D. A. A self-splicing group I intron in DNA polymerase genes of T7-like bacteriophages. **Journal of Bacteriology**, v. 186, n. 23, p. 8153–8155, 2004.

BORATTO, P. et al. Acanthamoeba polyphaga Mimivirus Prevents Amoebal Encystment-Mediating Serine Proteinase Expression and Circumvents Cell Encystment. **Journal of Virology**, v. 89, n. 5, p. 2962–2965, 2015.

BORATTO, P. V. M. et al. The analysis of KV mimivirus major capsid gene and its transcript highlights a distinct pattern of gene evolution and splicing among mimiviruses. **Journal of Virology**, n. November, p. JVI.01782-17, 2017.

BOUGHALMI, M. et al. First isolation of a giant virus from wild Hirudo medicinalis leech: Mimiviridae isolation in Hirudo medicinalis. **Viruses**, v. 5, n. 12, p. 2920–2930, 2013.

BOYER, M. et al. Giant Marseillevirus highlights the role of amoebae as a melting pot in emergence of chimeric microorganisms. **Proceedings of the National Academy of Sciences**, v. 106, n. 51, p. 21848–21853, 2009.

BOYER, M. et al. Phylogenetic and phyletic studies of informational genes in genomes highlight existence of a 4th domain of life including giant viruses. **Plos one**, v. 5, n. 12, 2010.

BRINDLEY, M. A.; MAURY, W. Endocytosis and a low-pH step are required for productive entry of equine infectious anemia virus. **Journal of virology**, v. 79, n. 23, p. 14482–8, 2005.

CAMPOS, R. K. et al. Samba virus: A novel mimivirus from a giant rain forest, the Brazilian Amazon. **Virology Journal**, v. 11, n. 1, p. 1–11, 2014.

CASTRILLÓN, J.; OROZCO, L. Acanthamoeba spp. como parásitos patógenos y oportunistas. **Revista chilena Infectol**, v. 30, n. 2, p. 147–155, 2013.

CHOI, Y.; BOWMAN, J. W.; JUNG, J. U. Autophagy during viral infection — a double-edged sword. **Nature Reviews Microbiology 2018**, p. 1, 2018.

CHRISMAN, C. J.; ALVAREZ, M.; CASADEVALL, A. Phagocytosis of cryptococcus neoformans by, and nonlytic exocytosis from, Acanthamoeba castellanii. **Applied and Environmental Microbiology**, v. 76, n. 18, p. 6056–6062, 2010.

CLAVERIE, J.-M.; ABERGEL, C. Mimivirus and its Virophage. **Annual Review of Genetics**, v. 43, n. 1, p. 49–66, 2009.

CLAVERIE, J. Giant virus in the sea. **Proc Natl Acad Sci USA**, n. December, p. 1–4, 2013.

CLAVERIE, J. M. et al. Mimivirus and Mimiviridae: Giant viruses with an increasing number of potential hosts, including corals and sponges. **Journal of Invertebrate Pathology**, v. 101, n. 3, p. 172–180, 2009.

COLSON, P. et al. The giant Cafeteria roenbergensis virus that infects a widespread marine phagocytic protist is a new member of the fourth domain of life. **PLoS ONE**, v. 6, n. 4, p. 13–17, 2011.

COLSON, P. et al. Reclassification of giant viruses composing a fourth domain of life in the new order Megavirales. **Intervirology**, v. 55, n. 5, p. 321–332, 2012.

COLSON, P. et al. “Marseilleviridae”, a new family of giant viruses infecting amoebae. **Archives of Virology**, v. 158, n. 4, p. 915–920, 2013.

COLSON, P. et al. Mimivirus: Leading the way in the discovery of giant viruses of amoebae. **Nature Reviews Microbiology**, 2017.

COLSON, P. et al. Viruses with more than 1,000 genes: Mamavirus, a new Acanthamoeba polyphaga mimivirus strain, and reannotation of mimivirus genes. **Genome Biology and Evolution**, v. 3, n. 1, p. 737–742, 2011.

DORNAS, F. P. et al. Isolation of new Brazilian giant viruses from environmental samples using a panel of protozoa. **Frontiers in microbiology**, v. 6, p. 1086, 2015.

DORNAS, F. P. et al. A Brazilian marseillevirus is the founding member of a lineage in family marseilleviridae. **Viruses**, v. 8, n. 3, 2016.

DOS SANTOS SILVA, L. K. et al. High positivity of mimivirus in inanimate surfaces of a hospital respiratory-isolation facility, Brazil. **Journal of Clinical Virology**, v. 66, p. 62–65, 2015.

DOUTRE, G. et al. Genome Analysis of the First Marseilleviridae Representative from Australia Indicates that Most of Its Genes Contribute to Virus Fitness. **Journal of Virology**, v. 88, n. 24, p. 14340–14349, 2014.

DÜRICHEN, H. et al. Ingestion and digestion studies in Tetrahymena pyriformis based on chemically modified microparticles. **European Journal of Protistology**, v. 52, p. 45–57, 2016.

DUTTA, D.; DONALDSON, J. G. Search for inhibitors of endocytosis. **Cellular Logistics**, v. 2, n. 4, p. 203–208, 2012.

EDGELL, D. R.; CHALAMCHARLA, V. R.; BELFORT, M. Learning to live together : mutualism between self - splicing introns and their hosts. **BMC Biology**, v. 9, n. 22, 2011.

ETTEN, J. L. VAN; LANE, L. C.; DUNIGAN, D. D. NIH Public Access. **October**, p. 83–99, 2010.

FILÉE, J.; CHANDLER, M. Gene exchange and the origin of giant viruses. **Intervirology**, v. 53, n. 5, p. 354–361, 2010.

FORTERRE, P. The virocell concept and environmental microbiology. **ISME Journal**, v. 7, n. 2, p. 233–236, 2013.

FOUQUE, E. et al. Cellular, biochemical, and molecular changes during encystment of free-living amoebae. **Eukaryotic Cell**, v. 11, n. 4, p. 382–387, 2012.

FRADA, M. et al. The “Cheshire Cat” escape strategy of the coccolithophore Emiliania huxleyi in response to viral infection. **Proceedings of the National Academy of Sciences of the United States of America**, v. 105, n. 41, p. 15944–9, 2008.

GAIA, M. et al. Zamilon, a novel virophage with Mimiviridae host specificity. **PLoS ONE**, v. 9, n. 4, p. 1–8, 2014.

GALLOT-LAVALLÉE, L.; BLANC, G. A glimpse of nucleo-cytoplasmic large DNA virus biodiversity through the eukaryotic genomicswindow. **Viruses**, v. 9, n. 1, 2017.

GREUB, G.; RAOULT, D. Microorganisms Resistant to Free-Living Amoebae**. Clinical Microbiology Reviews**, 2004.

GRONLIEN, H. K.; BERG, T.; LOVLIE, A. M. In the polymorphic ciliate Tetrahymena vorax, the non-selective phagocytosis seen in microstomes changes to a highly selective process in macrostomes. **The Journal of experimental biology**, v. 205, n. Pt 14, p. 2089–2097, 2002.

GROVE, J.; MARSH, M. The cell biology of receptor-mediated virus entry. **Journal of Cell Biology**, 2011.

HAUGEN, P.; SIMON, D. M.; BHATTACHARYA, D. The natural history of group I introns. **Trends in Genetics**, v. 21, n. 2, p. 111–119, 2005.

IYER, L. M. et al. Evolutionary genomics of nucleo-cytoplasmic large DNA viruses. **Virus Research**, v. 117, n. 1, p. 156–184, 2006.

IYER, L. M.; ARAVIND, L.; KOONIN, E. V. Common Origin of Four Diverse Families of Large Eukaryotic DNA Viruses. **Journal of Virology**. v. 75, n. 23, p. 11720–11734, 2001.

JHA, B. K. et al. Chloroquine has a cytotoxic effect on acanthamoeba encystation through modulation of autophagy. **Antimicrobial Agents and Chemotherapy**, v. 58, n. 10, p. 6235–6241, 2014.

JHA, S. et al. Trans-kingdom mimicry underlies ribosome customization by a poxvirus kinase. **Nature**, v. 546, n. 7660, p. 651–655, 2017.

KHAN, M. et al. Pneumonia in mice inoculated experimentally with Acanthamoeba polyphaga mimivirus. **Microbial Pathogenesis**, v. 42, n. 2–3, p. 56–61, 2007.

KLOSE, T. et al. A Mimivirus Enzyme that Participates in Viral Entry. **Structure**, v. 23, n. 6, p. 1058–1065, 2015.

KOONIN, E. V.; YUTIN, N. Origin and evolution of eukaryotic large nucleo-cytoplasmic DNA viruses. **Intervirology**, v. 53, n. 5, p. 284–292, 2010.

KORN, E. D.; WEISMAN, R. A. Phagocytosis of latex beads by Acanthamoeba. II. Electron microscopic study of the initial events. **Journal of Cell Biology**, v. 34, n. 1, p. 219–227, 1967.

KRAFT, C. et al. Mature ribosomes are selectively degraded upon starvation by an autophagy pathway requiring the Ubp3p/Bre5p ubiquitin protease. **Nature Cell Biology**, v. 10, n. 5, p. 602–610, 2008.

KUHN, D. A. et al. Different endocytotic uptake mechanisms for nanoparticles in epithelial cells and macrophages. **Beilstein Journal of Nanotechnology**, v. 5, n. 1, p. 1625–1636, 2014.

KUZNETSOV, Y. G. et al. Morphogenesis of Mimivirus and Its Viral Factories: an Atomic Force Microscopy Study of Infected Cells. **Journal of Virology**, v. 87, n. 20, p. 11200–11213, 2013.

LA SCOLA, B. et al. A Giant Virus in Amoebae. **Science.** (New York, N.Y.), v. 299, n. March, p. 2033, 2003.

LECOQ, H. Découverte du premier virus, le virus de la mosaïque du tabac : 1892 ou 1898 ? **Comptes Rendus de l'Académie des Sciences - Series III - Sciences de la Vie**, v. 324, n. 10, p. 929–933, 2001.

LEGENDRE, M. et al. mRNA deep sequencing reveals 75 new genes and a complex transcriptional landscape in Mimivirus. **Genome Research**, v. 20, n. 5, p. 664–674, 2010.

LEGENDRE, M. et al. Breaking the 1000-gene barrier for Mimivirus using ultra-deep genome and transcriptome sequencing. **Virology Journal**, v. 8, n. 1, p. 99, 2011.

LEGENDRE, M. et al. Thirty-thousand-year-old distant relative of giant icosahedral DNA viruses with a pandoravirus morphology. **Proceedings of the National Academy of Sciences**, v. 111, n. 11, p. 4274–4279, 2014.

LEGENDRE, M. et al. In-depth study of *Mollivirus sibericum* , a new 30,000-y-old giant virus infecting *Acanthamoeba*. **Proceedings of the National Academy of Sciences**, v. 112, n. 38, p. E5327–E5335, 2015.

LEVASSEUR, A. et al. Comparison of a Modern and Fossil Pithovirus Reveals Its Genetic Conservation and Evolution. **Genome biology and evolution**, v. 8, n. 8, p. 2333–2339, 2016.

LIU, H. et al. Genetic diversity of Acanthamoeba isolates from ocean sediments. **The Korean journal of parasitology**, v. 44, n. 2, p. 117–125, 2006.

LUSTIG, A; LEVINE, A J. One hundred years of virology. **Journal of virology**, v. 66, n. 8, p. 4629–4631, 1992.

LWOFF, A. The Concept of Virus. **Journal of General Microbiology**, v. 17, n. 23 August, p. 239–253, 1957.

LYNN, D. H. et al. Characterization of a new species of the ciliate Tetrahymena (Ciliophora: Oligohymenophorea) isolated from the urine of a dog: First report of Tetrahymena from a mammal. **Acta Protozoologica**, v. 39, n. 4, p. 289–294, 2000.

MACHOUART, M. et al. Polymorphisms and intronic structures in the 18S subunit ribosomal RNA gene of the fungi Scytalidium dimidiatum and Scytalidium hyalinum: Evidence of an IC1 intron with an His-Cys endonuclease gene. **FEMS Microbiology Letters**, v. 238, n. 2, p. 455–467, 2004.

MICHAEL, D. R. et al. Differential regulation of macropinocytosis in macrophages by cytokines: Implications for foam cell formation and atherosclerosis. **Cytokine**, v. 64, n. 1, p. 357–361, 2013.

MIZUSHIMA, N.; YOSHIMORI, T.; OHSUMI, Y. The Role of Atg Proteins in Autophagosome Formation. **Annual Review of Cell and Developmental Biology**, v. 27, n. 1, p. 107–132, 2011.

MOON, E. K. et al. Characterization of a serine proteinase mediating encystation of Acanthamoeba. **Eukaryotic Cell**, v. 7, n. 9, p. 1513–1517, 2008.

MOON, E. K. et al. Autophagy protein 8 mediating autophagosome in encysting Acanthamoeba. **Molecular and Biochemical Parasitology**, v. 168, n. 1, p. 43–48, 2009.

MOON, E. K. et al. Identification of Atg8 isoform in encysting Acanthamoeba. **Korean Journal of Parasitology**, v. 51, n. 5, p. 497–502, 2013.

MOON, E. K. et al. Autophagy inhibitors as a potential antiamoebic treatment for Acanthamoeba keratitis. **Antimicrobial Agents and Chemotherapy**, v. 59, n. 7, p. 4020–4025, 2015.

MOREIRA, D.; BROCHIER-ARMANET, C. Giant viruses, giant chimeras: The multiple evolutionary histories of Mimivirus genes. **BMC Evolutionary Biology**, v. 8, n. 1, 2008.

MUTSAFI, Y. et al. Vaccinia-like cytoplasmic replication of the giant Mimivirus. **Proceedings of the National Academy of Sciences**, v. 107, n. 13, p. 5978–5982, 2010.

MUTSAFI, Y. et al. Membrane Assembly during the Infection Cycle of the Giant Mimivirus. **PLoS Pathogens**, v. 9, n. 5, 2013.

NISHIDA, K. et al. Group I introns found in Chlorella viruses: Biological implications. **Virology**, v. 242, n. 2, p. 319–326, 1998.

OKAMOTO, K. et al. Structural variability and complexity of the giant Pithovirus sibericum particle revealed by high-voltage electron cryo-Tomography and energy-filtered electron cryo-microscopy. **Scientific Reports**, v. 7, n. 1, 2017.

PAGNIER, I. et al. A decade of improvements in mimiviridae and marseilleviridae isolation from amoeba. **Intervirology**, v. 56, n. 6, p. 354–363, 2013.

PAGNIER, I. et al. Isolation of Vermamoeba vermiformis and associated bacteria in hospital water. **Microbial Pathogenesis**, v. 80, p. 14–20, 2015.

PHILIPPE, N. et al. Pandoraviruses: Amoeba viruses with genomes up to 2.5 Mb reaching that of parasitic eukaryotes. **Science**, v. 341, n. 6143, p. 281–286, 2013.

RAOULT, D. et al. The 1.2-megabase genome sequence of Mimivirus. **Science**, v. 306, n. 5700, p. 1344–1350, 2004.

RAOULT, D. The journey from Rickettsia to mimivirus. **ASM News**, v. 71, n. 6, p. 278–284, 2005.

RAOULT, D.; BOYER, M. Amoebae as genitors and reservoirs of giant viruses. **Intervirology**, 2010.

RAOULT, D.; FORTERRE, P. Redefining viruses: Lessons from Mimivirus. **Nature Reviews Microbiology**, v. 6, n. 4, p. 315–319, 2008.

RAOULT, D.; SCOLA, B. L.; BIRTLES, R. The Discovery and Characterization of Mimivirus, the Largest Known Virus and Putative Pneumonia Agent. **Clinical Infectious Diseases**, v. 45, n. 1, p. 95–102, 2007.

REDMANN, M. et al. Inhibition of autophagy with bafilomycin and chloroquine decreases mitochondrial quality and bioenergetic function in primary neurons. **Redox Biology**, v. 11, n. November 2016, p. 73–81, 2017.

REED, L. J.; MUENCH, H. A simple method of estimating fifty per cent endpoints. **The American Jounal of Hygiene**, v. 27, n. 3, p. 493–497, 1938.

RETENO, D. G. et al. Faustovirus, an Asfarvirus-Related New Lineage of Giant Viruses Infecting Amoebae. **Journal of Virology**, v. 89, n. 13, p. 6585–6594, 2015.

RODRIGUES, R. A. L. et al. Mimivirus Fibrils Are Important for Viral Attachment to the Microbial World by a Diverse Glycoside Interaction Repertoire. **Journal of Virology**, v. 89, n. 23, p. 11812–11819, 2015.

ROWBOTHAM, T. J. Preliminary report on the pathogenicity of Legionella pneumophila for freshwater and soil amoebae. **Journal of Clinical Pathology**, v. 33, n. 12, p. 1179–1183, 1980.

SCHULZ, F. et al. Giant viruses with an expanded complement of translation system components. **Science**. v. 85, n. April, p. 82–85, 2017.

SIDDIQUI, R.; KHAN, N. A. **Biology and pathogenesis of AcanthamoebaParasites and Vectors**, 2012.

SILVA, L. K. DOS S. et al. Acanthamoeba and mimivirus interactions: The role of amoebal encystment and the expansion of the “Cheshire Cat” theory**. Current Opinion in Microbiology**, 2016.

SOLDATI, T.; SCHLIWA, M. Powering membrane traffic in endocytosis and recycling. **Nature Reviews Molecular Cell Biology**, 2006.

SOLITRO, A. R.; MACKEIGAN, J. P. Leaving the lysosome behind: novel developments in autophagy inhibition. **Future Medicinal Chemistry**, v. 8, n. 1, p. 73–86, 2016.

SOTO-ARREDONDO, K. J. et al. Biochemical and cellular mechanisms regulating Acanthamoeba castellanii adherence to host cells. **Parasitology**, v. 141, n. 4, p. 531–541, 2014.

SUA;REZ, C. et al. Open membranes are the precursors for assembly of large DNA viruses. **Cellular Microbiology**, v. 15, n. 11, p. 1883–1895, 2013.

SUAREZ, C. et al. African swine fever virus assembles a single membrane derived from rupture of the endoplasmic reticulum. **Cellular Microbiology**, v. 17, n. 11, p. 1683–1698, 2015.

SUHRE, K.; AUDIC, S.; CLAVERIE, J.-M. Mimivirus gene promoters exhibit an unprecedented conservation among all eukaryotes. **Proceedings of the National Academy of Sciences of the United States of America**, v. 102, n. 41, p. 14689–93, 2005.

SUZAN-MONTI, M. et al. Ultrastructural characterization of the giant volcano-like virus factory of Acanthamoeba polyphaga Mimivirus. **PLoS ONE**, v. 2, n. 3, 2007.

SUZAN-MONTI, M.; LA SCOLA, B.; RAOULT, D. **Genomic and evolutionary aspects of MimivirusVirus Research**, 2006.

TAYLOR, W. M. et al. In vitro characterization of Acanthamoeba castellanii cytopathic effect. **The Journal of parasitology**, v. 81, n. 4, p. 603–609, 1995.

THOMAS, V. et al. Lausannevirus, a giant amoebal virus encoding histone doublets. **Environmental Microbiology**, v. 13, n. 6, p. 1454–1466, 2011.

THURMAN, J.; DRINKALL, J.; PARRY, J. D. Digestion of bacteria by the freshwater ciliate Tetrahymena pyriformis. **Aquatic Microbial Ecology**, v. 60, n. 2, p. 163–174, 2010.

TOWNSLEY, A. C. et al. Vaccinia Virus Entry into Cells via a Low-pH-Dependent Endosomal Pathway. **Journal of Virology**, v. 80, n. 18, p. 8899–8908, 2006.

VAN VALEN, L. A new evolutionary theory. **Evolutionary Theory**, v. 1, p. 1–30, 1973.

WONG, O. G. T. Investigation of prey ingestion and digestion in the ciliate predator Tetrahymena pyriformis and the impact on growth. **A thesis submitted to Lancaster University in fulfilment of**. [s.l: s.n.].

WU, H. NATURE OF HEAT DENATURATION OF PROTEINS. Heat Denaturation of Proteins. **Journal of Biological Chemistry**, v. 64, p. 369, 1925.

XIAO, C. et al. Cryo-electron microscopy of the giant mimivirus. **Journal of Molecular Biology**, v. 353, n. 3, p. 493–496, 2005.

XIAO, C. et al. Structural studies of the giant Mimivirus. **PLoS Biology**, v. 7, n. 4, p. 0958–0966, 2009.

XIAO, C.; ROSSMANN, M. G. Structures of giant icosahedral eukaryotic dsDNA viruses. **Current Opinion in Virology**, v. 1, n. 2, p. 101–109, 2011.

XIE, Z.; NAIR, U.; KLIONSKY, D. J. Atg8 Controls Phagophore Expansion during Autophagosome Formation. **Molecular Biology of the Cell**, v. 19, n. 8, p. 3290–3298, 2008.

YUTIN, N. et al. Eukaryotic large nucleo-cytoplasmic DNA viruses: Clusters of orthologous genes and reconstruction of viral genome evolution. **Virology Journal**, v. 6, p. 1–13, 2009.

YUTIN, N. et al. Mimiviridae: Clusters of orthologous genes, reconstruction of gene repertoire evolution and proposed expansion of the giant virus family. **Virology Journal**, v. 10, n. 1, p. 1, 2013.

ZAUBERMAN, N. et al. Distinct DNA exit and packaging portals in the virus Acanthamoeba polyphaga mimivirus. **PLoS Biology**, v. 6, n. 5, p. 1104–1114, 2008.

10. ANEXOS

10.1. Anexo I – Preparação de solução PAS

A solução salina para amebas é a solução utilizada para o cultivo das amebas de vida livre, além de ser usada em experimentos para que não haja intensa multiplicação das amebas, visto que é um mais meio pobre. Para preparar 1000 ml desta solução, inicialmente, prepara-se duas soluções chamadas de solução A e solução B. Para a solução A, adiciona-se as seguintes substâncias em 10 ml de água estéril: 0,16µM sulfato de magnésio heptahidratado (MgSO4.7H2O) (Merck, Alemanha); 0,1mM de fosfato dibásico de sódio (Na2HPO4) (Merck, Alemanha); 0,1mM de fosfato monobásico de potássio (KH2PO4) (Merck, Alemanha); NaCl (2mM) ; Na2HPO4 (0,0001mM). Para o preparo da solução B, adiciona-se 0,272 µM de cloreto de cálcio (CaCl2.2H2O) (Merck, Alemanha). As soluções A e B são filtradas em filtro de 0,22µm a fim de deixar a solução final estéril e também eliminar possíveis cristais formados durante o preparo e posteriormente adicionadas a um volume final de 1 litro de água. Esta solução é mantida em câmara fria até o momento de uso. Como controle, uma alíquota da solução preparada deve ser incubada a 37ºC para verificar se a mesma está contaminada; além disso, outra alíquota é incubada em meio tioglicolato para verificação de crescimento de microorganismos.

10.2. Anexo II – Preparação de meio NEFF

A indução do encistamento foi feita por choque hiperosmótico através da utilização de uma solução salina de Neff que possui uma grande quantidade de magnésio em sua composição. Para o preparo dessa solução foram utilizados 20 mM de Tris-HCl (Merck, Alemanha), 100 mM de cloreto de potássio (KCl) (Merck, Alemanha), 8 mM de sulfato de magnésio heptahidratado (MgSO4.7H2O) (Merck, Alemanha), 0,4 mM de cloreto de cálcio (CaCl2) (Merck, Alemanha), 1 mM de bicarbonato de sódio (NaHCO3) (Merck, Alemanha) e H2O destilada em q.s.p. 1 litro. Após a homogeneização da solução o pH foi ajustado para 9,0. Em seguida o meio foi autoclavado a 121°C por 15 minutos. Após o resfriamento o meio foi armazenado em câmara fria (temperatura de 4 a 8°C) até o momento de uso.

10.3. Anexo III – Preparação do meio PYG

O meio de cultura PYG (meio protease peptona extrato de levedura e glicose) foi o meio utilizado para o cultivo de amebas de vida livre. Três soluções diferentes foram preparadas separadamente, em seguida foram misturadas e o volume foi completado para 1 litro. Em um recipiente foi preparada a primeira solução contendo 300 mL de água destilada, 8 µM de sulfato de magnésio heptahidratado ($MgSO_4.7H_2O$) (Merck, Alemanha), 0,5 µM de cloreto de cálcio ($CaCl_2$) (Merck, Alemanha), 5 nM de sulfato de ferro amoniacal hexahidratado ($Fe(NH_4)_2(SO_4).6H_2O$) (Merck, Alemanha), 1,4 mM de fosfato dibásico de sódio heptahidratado ($Na_2HPO_4.7H_2O$) (Merck, Alemanha), 2,5 mM de fosfato monobásico de potássio (KH_2PO_4) (Merck, Alemanha), 3,4 mM de citrato de sódio dihidratado ($C_6H_5Na_3O_7.2H_2O$) (Merck, Alemanha), que em seguida foi homogeneizada até a completa dissolução. A segunda solução foi preparada em outro recipiente, adicionando, à 200 mL de água destilada, 20g de protease peptona (extrato bactopeptona) (Merck, Alemanha). A terceira solução foi preparada adicionando 0,05 M de glicose (Merck, Alemanha) à 200 mL de água destilada. As três soluções foram adicionadas a um mesmo recipiente e homogeneizadas. Em seguida o volume foi completado para 1L e o pH ajustado a 6,5 (Anexo I). O meio foi autoclavado a 121°C por 15 minutos, e após o resfriamento foi filtrado em filtros de 0,22 µm para retirada de eventuais cristais. O meio foi armazenado em câmara fria (temperatura de 4 a 8°C) até o momento do uso. Foi feito também o teste de esterilidade em que 1 mL do meio foi adicionado a 9 mL de meio tioglicolato, por 7 dias a 37°C. Para uso, o meio foi suplementado com 200 U/mL de Penicilina (Cristália, Brasil), 50 µg /mL de Gentamicina (Sigma-Aldrich, EUA) e 2,5 µg/mL de Anfotericina B (Sigma-Aldrich, EUA).

10.4. Anexo IV – Tabela best hits das cópias 1 e 2

10.4.1. Cópia 1

Description	Description	Total Score	Query cove	E valeu	Ident	Acession	Strand	Localization	Function	Environmental genes / Intron information	
Paramecium bursaria Chlorella virus KS1B, partial genome	84.2	84.2	90%	4,00E-13	82%	JX997171.1	Plus	135479 - 13556	Intergenic	gene="KS1B_328L (135009..135143) hypothetical protein	gene="KS1B_329L" (135482..135664) hypothetical protein
Chlorella virus DNA for URF14.2, complete cds, strain:CVH1	84.2	84.2	90%	4,00E-13	82%	AB006981.1	Minus	267 - 178	Intron	group I self-splicing intron = large self-splicing ribozymes	no protein indentification
Chlorella virus DNA for URF14.2, complete cds, strain:CVN2-2	84.2	84.2	90%	4,00E-13	82%	AB006980.1	Minus	267 - 178	Intron	group I self-splicing intron = large self-splicing ribozymes	no protein indentification
Chlorella virus DNA for URF14.2, complete cds, strain:CVB11	80.6	80.6	90%	5,00E-12	82%	AB006979.1	Minus	266 - 178	Intron	group I self-splicing intron = large self-splicing ribozymes	no protein indentification
Chlorella virus gene for URF14.2, partial cds	80.6	80.6	90%	5,00E-12	82%	D29631.1	Minus	358-270	Intron	group I self-splicing intron = large self-splicing ribozymes	no protein indentification
Paramecium bursaria Chlorella virus NE-JV-4, partial genome	77.0	77.0	99%	6,00E-11	79%	JX997179.1	Plus	74248 - 74346	Intergenic	NE-JV-4_140L (72740..73987)hypothetical protein"	NE-JV-4_144L" (74389..74967) "transcription elongation factor S-II"
Paramecium bursaria Chlorella virus IL-3A, partial genome	77.0	77.0	99%	6,00E-11	79%	JX997169.1	Plus	68183 - 68281	Intergenic	IL-3A_134L (66675..67922) hypothetical protein	IL-3A_138L (68324..68902) transcription elongation factor S-II
Paramecium bursaria Chlorella virus AN69C, partial genome	77.0	77.0	99%	6,00E-11	79%	JX997153.1	Plus	69555 - 69653	Intergenic	AN69C_137L (68047..69294) hypothetical protein	AN69C_141L (69696..70274) transcription elongation factor S-II
Paramecium bursaria Chlorella virus NY2A Chlorella virus NY2A ctg_1	77.0	146	99%	6,00E-11	79%	DQ491002.1	Plus	80555 - 80653	Intergenic	B173L (79050..80294) hypothetical protein	b174L (80671..80976) hypothetical protein
Paramecium bursaria Chlorella virus MA-1D, partial genome	75.2	75.2	99%	2,00E-10	78%	JX997172.1	Plus	36982 - 37081	Intergenic	MA-1D_076R (34578..36773) Chlorovirus glycoprotein repeat domain-containing protein"	MA-1D_081L (37124..37699) transcription elongation factor S-II
Paramecium bursaria Chlorella virus IL-5-2s1, partial genome	75.2	75.2	99%	2,00E-10	78%	JX997170.1	Plus	27419 - 27518	Intergenic	IL-5-2s1_057R (24890..27210) Chlorovirus glycoprotein repeat domain-containing protein	IL-5-2s1_062L (27561..28136) transcription elongation factor S-II

Tolypocladium ophioglossoides isolate L2 mitochondrion, complete	73.4	73.4	89%	7,00E-10	81%	KX455872.1	Minus	1024 - 934	Intron	group IC1 - Intron of the large subunit ribosomal RNA gene	
Cordyceps militaris isolate CM09-31-28 mitochondrion, complete ge	73.4	73.4	89%	7,00E-10	81%	KP722513.2	Minus	991 - 901	Intron	group IC1 - Intron of the large subunit ribosomal RNA gene	
Cordyceps militaris isolate V40-4 mitochondrion, complete genome	73.4	73.4	89%	7,00E-10	81%	KP722512.2	Minus	991 - 901	Intron	group IC1 - Intron of the large subunit ribosomal RNA gene	
Cordyceps militaris isolate CMB mitochondrion, complete genome	73.4	73.4	89%	7,00E-10	81%	KP722507.2	Minus	2183 - 2093	Intron	product="large subunit ribosomal RNA"	
Cordyceps militaris isolate F02 mitochondrion, complete genome	73.4	73.4	89%	7,00E-10	81%	KP722505.2	Minus	2183 - 2093	Intron	group IC1 - Intron of the large subunit ribosomal RNA gene	
Cordyceps militaris isolate CM552 mitochondrion, complete genom	73.4	73.4	89%	7,00E-10	81%	KP722502.2	Minus	991 - 901	Intron	group IC1 - Intron of the large subunit ribosomal RNA gene	
Cordyceps militaris isolate CM06 mitochondrion, complete genome	73.4	73.4	89%	7,00E-10	81%	KP722500.2	Minus	991 - 901	Intron	group IC1 - Intron of the large subunit ribosomal RNA gene	
Cordyceps militaris isolate CM09-9-24 mitochondrion, complete gen	73.4	73.4	89%	7,00E-10	81%	KP722496.2	Minus	991 - 901	Intron	group IC1 - Intron of the large subunit ribosomal RNA gene	
Cordyceps militaris isolate V40-5 mitochondrion, complete genome	73.4	73.4	89%	7,00E-10	81%	KP722501.2	Minus	2182 - 2092	Intron	group IC1 - Intron of the large subunit ribosomal RNA gene	
Cordyceps militaris isolate V26-16 mitochondrion, partial genome	73.4	73.4	89%	7,00E-10	81%	KP722511.1	Minus	1637 - 1547	Intergenic	orf245 441..1178 hypothetical protein"	orf253 1841..2602 hypothetical protein
Cordyceps militaris isolate CM08 mitochondrion, partial genome	73.4	73.4	89%	7,00E-10	81%	KP722510.1	Minus	1637 - 1547	Intergenic	orf245 441..1178 hypothetical protein"	orf253 1841..2602 hypothetical protein
Cordyceps militaris isolate CM05 mitochondrion, partial genome	73.4	73.4	89%	7,00E-10	81%	KP722509.1	Minus	1637 - 1547	Intergenic	orf245 441..1178 hypothetical protein"	orf253 1841..2602 hypothetical protein
Cordyceps militaris isolate CM02 mitochondrion, partial genome	73.4	73.4	89%	7,00E-10	81%	KP722508.1	Minus	1637 - 1547	Intergenic	orf245 441..1178 hypothetical protein"	orf253 1841..2602 hypothetical protein
Cordyceps militaris isolate F03 mitochondrion, partial genome	73.4	73.4	89%	7,00E-10	81%	KP722506.1		1637 - 1547	Intergenic	orf245 441..1178 hypothetical protein"	orf253 1841..2602 hypothetical protein
Cordyceps militaris isolate CM494 mitochondrion, partial genome						KP722504.1	Minus	445 - 355	beginning of genome	before orf253 (5649..1410) hypothetical protein	no coding region ?
Cordyceps militaris isolate CM556 mitochondrion, partial genome	73.4	73.4	89%	7,00E-10	81%	KP722503.1	Minus	445 - 355	beginning of genome	before orf253 (5649..1410) hypothetical protein	
										before orf253	

Cordyceps militaris isolate F01 mitochondrion, partial genome	73.4	73.4	89%	7,00E-10	81%	KP722499.1	Minus	445 - 355	beginning of genome	(5649..1410) hypothetical protein		
Cordyceps militaris isolate CM07 mitochondrion, partial genome	73.4	73.4	89%	7,00E-10	81%	KP722498.1	Minus	445 - 355	beginning of genome	before orf253 (5649..1410) hypothetical protein		
Cordyceps militaris isolate CMA mitochondrion, partial genome	73.4	73.4	89%	7,00E-10	81%	KP722497.1	Minus	445 - 355	beginning of genome	before orf253 (5649..1410) hypothetical protein		
Cordyceps militaris isolate V26-17 mitochondrion, complete genom	73.4	73.4	89%	7,00E-10	81%	KP719097.1	Minus	2183 - 2093	Intron	group IC1 - Intron of the large subunit ribosomal RNA gene		
Cordyceps militaris isolate CM01 mitochondrion, complete genome	73.4	73.4	89%	7,00E-10	81%	KP719096.1	Minus	2183 - 2093	Intron	group IC1 - Intron of the large subunit ribosomal RNA gene		
Megavirus terra1 genome	73.4	141	100%	7,00E-10	79%	KF527229.1	Plus Minus	291328 - 291418 406780 - 406679				
Cordyceps militaris strain EFCC-C2 mitochondrion, complete genom	73.4	73.4	89%	7,00E-10	81%	KF432176.1	Minus	2096 - 2006	Intron	Intron of the large subunit ribosomal RNA gene		
Paramecium bursaria Chlorella virus CVR-1, partial genome	73.4	128	99%	7,00E-10	78%	JX997164.1	Minus	126029 - 12593	Intergenic	CVR-1_335R (124800..125822) hypothetical protein	CVR-1_340L" (126251..127294)GIY-YIG catalytic domain-containing endonuclease	
							Plus	292511 - 29259	Intergenic	CVR-1_889R (291909..292334) hypothetical protein	CVR-1_892L (292677..294242)major capsid protein VP54	
Paramecium bursaria Chlorella virus CVA-1, partial genome	73.4	128	99%	7,00E-10	78%	JX997159.1	Minus	123016 - 12291	Intergenic	CVA-1_327R (121787..122809) hypothetical protein	CVA-1_332L" (123238..124281) GIY-YIG catalytic domain-containing endonuclease"	
							Plus	289510 - 28959	Intergenic	CVA-1_883R (288362..289333) hypothetical protein	CVA-1_886L (289676..291241)major capsid protein VP54	
Acanthocystis turfacea Chlorella virus Canal-1, partial genome	73.4	73.4	98%	7,00E-10	77%	JX997158.1	Minus	239885 - 23978	Intergenic	Canal-1_767R (239174..239770) transcription elongation factor S-II	Canal-1_770R (240146..241345) hypothetical protein	
Megavirus lba isolate LBA111, complete genome	73.4	139	99%	7,00E-10	79%	JX885207.1	Minus	477028 - 47693	Intergenic	LBA_00463 (476250..476534) putative intron encoded nuclease	LBA_00464 (477240..478937) capsid protein 1	
							Plus	361598 - 36169	Intergenic	LBA_00362 (360722..361498)putative intron encoded endonuclease	LBA_00364 (363489..363716) hypothetical protein	
							Minus	496950 - 49686	Intergenic	CE11_00491 (496172..496456) putative intron encoded nuclease	CE11_00493 (498942..500453)hypothetical protein	

Megavirus courdo11, complete genome	73.4	141	100%	7,00E-10	79%	JX975216.1	Plus	381666 - 38176	Intergenic	CE11_00388 (380789..381565) putative intron encoded endonuclease	CE11_00390 (383557..383784) hypothetical protein"
							Minus	215338 - 21524	Intergenic	c7_R542 (214560..214844) putative nuclease	c7_R543 (215550..217247) capsid protein 1
Megavirus courdo7 isolate Mv13-c7, partial genome	73.4	141	100%	7,00E-10	79%	JN885991.1	Plus	103060 - 10316	Intergenic	c7_L432 (102183..102959) putative intron-encoded endonuclease	c7_R434 (104951..105178) hypothetical protein
							Minus	510425 - 51033	Intergenic	mg465(509287..509931) putative intron encoded nuclease	mg466 (512417..513928)hypothetical protein
Megavirus chiliensis, complete genome	73.4	139	99%	7,00E-10	79%	JN258408.1	Plus	393422 - 39352	Intergenic	mg374 (392546..393322)putative intron encoded endonuclease	mg375 (395313..395540)hypothetical protein
Paramecium bursaria Chlorella virus 1 (PBCV-1), complete genome	73.4	73.4	99%	7,00E-10	78%	JF411744.1	Plus	66401 - 66499	Intron	hypothetical protein	
Neofabraea malicorticis isolate AFTOL-ID 149 18S ribosomal RNA gen	73.4	73.4	47%	7,00E-10	94%	AY544706.1	Minus	1275 - 1228	18s gene	18S ribosomal RNA	
Powai lake megavirus isolate 1, complete genome	71.6	71.6	100%	2,00E-09	78%	KU877344.1	Plus	381531 - 38163	Intergenic	(380653..381429) hypothetical protein	(381737..383272)DNA-directed RNA polymerase subunit 1
Uncultured fungus clone whitespruce.2_81817 18S ribosomal RNA g	69.8	69.8	47%	8,00E-09	92%	KU305957.1	Minus	285 - 238	18s gene	18S ribosomal RNA	
Paramecium bursaria Chlorella virus AR158 genomic sequence	69.8	69.8	99%	8,00E-09	76%	DQ491003.2	Plus	183677 - 18377	Intergenic	C437L (183215..183514)hypothetical protein	C438L (183987..184739)GIY-YIG endonuclease
Uncultured soil fungus clone B_Canopy_300_02_10 18S ribosomal R	69.8	69.8	47%	8,00E-09	92%	AY382408.1	Minus	508 - 461	18s gene	18S ribosomal RNA	
Uncultured soil fungus clone B_Canopy_300_01_16 18S ribosomal R	69.8	69.8	47%	8,00E-09	92%	AY382403.1	Minus	473 - 426	18s gene	18S ribosomal RNA	
Chlorella virus DNA for URF14.2, complete cds, strain:CVEN5	69.8	69.8	99%	8,00E-09	76%	AB006982.1	Minus	267 - 169	Intron	group I self-splicing intro	Não havia identificação da proteína
Uncultured fungus clone P004.2_153340 18S ribosomal RNA gene, p	68.0	68.0	47%	3,00E-08	92%	KU305998.1	Minus	289 - 241	18s gene	18S ribosomal RNA	
Uncultured fungus clone P020.1_91453 18S ribosomal RNA gene, pa	68.0	68.0	47%	3,00E-08	92%	KU305969.1	Minus	290 - 242	18s gene	18S ribosomal RNA	
Uncultured fungus clone P014.3_84465 18S ribosomal RNA gene, pa	68.0	68.0	47%	3,00E-08	92%	KU305954.1	minus	301 - 253	18s gene	18S ribosomal RNA	
Byssochlamys spectabilis gene for 18S rRNA, strain:IAM 13426	68.0	68.0	47%	3,00E-08	92%	AB023946.1	Minus	1281 - 1233	Intron	18S ribosomal RNA	
Dimargaris bacillispora strain NRRL 2808 28S ribosomal RNA, partial s	68.0	68.0	46%	3,00E-08	91%	NG_027650.	Minus	2318 - 2272	Intron	28S ribosomal RNA	
Paecilomyces variotii small subunit 18S rRNA gene	68.0	68.0	47%	3,00E-08	92%	Z69593.1	Minus	150 - 102	Intron	18S ribosomal RNA	
Uncultured fungus clone P021.3_89428 18S ribosomal RNA gene, pa	66.2	66.2	46%	1,00E-07	92%	KU305984.1	minus	295 - 248	18s gene	18S ribosomal RNA	
Hypomyces aurantius mitochondrion, complete genome	66.2	169	93%	1,00E-07	77%	KU666552.1	minus	14324 - 14234	Intron	hypothetical protein orf105 (38301..38618) hypothetical protein group IC1 - Intron of the large subunit ribosomal RNA gene	trnR(acg)(40841..40911) tRNA-Arg
							minus	39725 - 39631	Intergenic		
							minus	12362 - 12268	Intron		
Cordyceps brongniartii isolate IMBST95031 mitochondrion, complet	66.2	66.2	91%	1,00E-07	79%	EU100743.1	Minus	939 - 846	Intron	large subunit ribosomal RNA	

Chlorella virus DNA for major capsid protein Vp54, complete cds	66.2	66.2	99%	1,00E-07	75%	AB006978.1	Minus	1475 - 1375	Intron	group I self-splicing intron	Protein= major capsid protein Vp54	
Uncultured fungus clone whitespruce.2_639620 18S ribosomal RNA	64.4	64.4	47%	3,00E-07	90%	KU306041.1	Minus	255 - 208	18s gene	18S ribosomal RNA		
Chaenotheca trichialis voucher Prieto 3028 (S) 18S ribosomal RNA ge	64.4	64.4	47%	3,00E-07	90%	JX000069.1	Minus	1206 - 1159	18s gene	18S ribosomal RNA		
Piloderma fallax CFMR:S-12 18S small subunit ribosomal RNA gene, p	64.4	64.4	47%	3,00E-07	90%	GU187644.1	Minus	1235 - 1188	18s gene	18S ribosomal RNA		
Fusarium solani f. piperis strain MAFF236572 small subunit ribosoma	64.4	64.4	47%	3,00E-07	92%	AF150487.1	Minus	186 - 139	intron-like sequence	18S ribosomal RNA		
Coniochaeta malacotricha partial 18S rRNA gene, strain MA3371	64.4	64.4	47%	3,00E-07	90%	AJ496243.1	Minus	1292 - 1245	intron	18S ribosomal RNA		
Lichenomphalia umbellifera voucher J. Geml-2 (CFMR) 18S small sub	62.6	62.6	47%	1,00E-06	90%	KF381538.1	Minus	1310 - 1262	18s gene	18S ribosomal RNA		
							Plus	102987 - 10308	Intergenic	NE-JV-1_323R (101544..102782) PBCV-specific basic adaptor domain-containing protein	NE-JV-1_327L (103111..103695)transcription elongation factor S-II	
							Plus	153232 - 15333	Intergenic	NE-JV-1_471R (152204..153010) GIY-YIG catalytic domain-containing endonuclease	NE-JV-1_472L (153440..154273)hypothetical protein	
Paramecium bursaria Chlorella virus NE-JV-1, partial genome	62.6	289	99%	1,00E-06	75%	JX997176.1						
							Plus	199927 - 20002	Intergenic	NE-JV-1_608L (199415..199597)hypothetical protein	NE-JV-1_609R (200181..200588) protein of unknown function	
							Plus	282510 - 28259	Intergenic	NE-JV-1_839L (280833..282194) hypothetical protein	NE-JV-1_843L (282676..284241)major capsid protein VP54	
							Minus	158879 - 15879	Intergenic	NE-JV-1_481R (157053..158039) hypothetical protein	NE-JV-1_483L (159152..160096)GIY-YIG catalytic domain-containing endonuclease	
Acanthamoeba polyphaga moumouvirus, complete genome	62.6	62.6	100%	1,00E-06	76%	JX962719.1	Plus	321183 - 32128	Intergenic	Moumou_00302	Moumou_00303	
Moumouvirus Monve isolate Mv13-mv, partial genome	62.6	62.6	100%	1,00E-06	76%	JN885998.1	Minus	311621 - 31152	intron	DNA-directed RNA polymerase subunit 1		
Rasamsonia argillacea gene for 18S rRNA, partial sequence, strain: IF(	62.6	62.6	47%	1,00E-06	90%	AB033533.1	Minus	1704 - 1656	18s gene	18S ribosomal RNA		
Rasamsonia argillacea gene for 18S rRNA, partial sequence, strain: IF(	62.6	62.6	47%	1,00E-06	90%	AB033532.1	Minus	1704 - 1656	18s gene	18S ribosomal RNA		
Rasamsonia argillacea gene for 18S rRNA, partial sequence, strain: IF(	62.6	62.6	47%	1,00E-06	90%	AB033531.1	Minus	1706 - 1658	18s gene	18S ribosomal RNA		
Geosmithia argillacea gene for 16S-like rRNA, group I intron	62.6	62.6	47%	1,00E-06	90%	AB013734.1	Minus	147 - 99	Intron	Group I intron inserted at position 1512 of 16S-like rRNA gene		
Chlorella virus TFIIS gene for transcription elongation factor SII, com	62.6	62.6	94%	1,00E-06	77%	D17367.1	minus	845 - 751	Intron	gene transcription elongation factor SII		
Uncultured fungus clone whitespruce.6_260654 18S ribosomal RNA	60.8	60.8	47%	4,00E-06	88%	KU305992.1	Minus	256 - 209	18s gene	18S ribosomal RNA		
Uncultured fungus clone P015.2_96454 18S ribosomal RNA gene, par	60.8	60.8	47%	4,00E-06	88%	KU305986.1	Minus	278 - 231	18s gene	18S ribosomal RNA		
Uncultured fungus clone whitespruce.6_268621 18S ribosomal RNA	60.8	60.8	47%	4,00E-06	88%	KU305975.1	Minus	257 - 210	18s gene	18S ribosomal RNA		
Monoraphidium sp. NS16 18S ribosomal RNA gene, partial sequence	60.8	60.8	45%	4,00E-06	89%	KP162147.1	Minus	1524 - 1479	Intron	18S ribosomal RNA		
Uncultured fungus clone 68_NA3_P31_L13 18S ribosomal RNA gene,	60.8	60.8	47%	4,00E-06	88%	KC965543.1	Minus	167 - 120	18s gene	contains 18S ribosomal RNA, internal transcribed spacer 1, 5.8S ribosomal RNA, internal transcribed spacer 2, and 28S ribosomal RNA		
Scolecobasidium excentricum strain CBS 469.95 small subunit riboso	60.8	60.8	47%	4,00E-06	88%	KF282683.1	Minus	1521 - 1474	Intron	18S ribosomal RNA		

Paramecium bursaria Chlorella virus NW665.2, partial genome	60.8	60.8	99%	4,00E-06	74%	JX997181.1	Minus 112379 - 11228	Intergenic	NW665.2_315R (111146..112180) hypothetical protein	NW665.2_320R (112334..112462) hypothetical protein
Elaphocordyceps paradoxa strain NBRC 100945 18S ribosomal RNA (S	60.8	60.8	99%	4,00E-06	75%	JN941731.1	Minus 1343 - 1242	18s gene	18S ribosomal RNA	
Ceratocystiopsis minima strain WIN(M)61 18S ribosomal RNA gene, p	60.8	60.8	35%	4,00E-06	97%	HQ634852.1	Minus 1272 - 1237	intron	group I class C1	18S ribosomal RNA
Cylindrocystis brebissonii 18S rRNA gene group I intron, strain ACOI !	60.8	60.8	99%	4,00E-06	76%	HE565386.1	Minus 217 - 117	intron	group I intron	18S ribosomal RNA
Acremonium psammosporum strain CBS 590.63 18S ribosomal RNA g	60.8	60.8	47%	4,00E-06	88%	HQ232204.1	Minus 1267 - 1220	18s gene	18S ribosomal RNA	
Akanthomyces arachnophilus strain BCC01860 small subunit riboson	60.8	60.8	47%	4,00E-06	88%	GQ249950.1	Minus 1237 - 1190	18s gene	18S ribosomal RNA	
Olpidiopsis porphyrae gene for 18S rRNA, partial sequence	60.8	108	100%	4,00E-06	77%	AB287418.1	Minus 2345 - 2244 Minus 747 - 712	intron intron	18S ribosomal RNA 18S ribosomal RNA	
Uncultured fungal contaminant 18S small subunit ribosomal RNA ge	60.8	60.8	47%	4,00E-06	88%	EF053568.1	Minus 1468 - 1421	18s gene	18S ribosomal RNA	
Isaria tenuipes genes for 18S rRNA, ITS1, 5.8S rRNA, ITS2, 28S rRNA, p	60.8	60.8	47%	4,00E-06	88%	AB086204.2	Minus 1302 - 1255	18s gene	18S ribosomal RNA	
Isaria tenuipes genes for 18S rRNA, ITS1, 5.8S rRNA, ITS2, 28S rRNA, p	60.8	60.8	47%	4,00E-06	88%	AB086222.1	Minus 1279 - 1232	18s gene	18S ribosomal RNA	
Isaria tenuipes genes for 18S rRNA, ITS1, 5.8S rRNA, ITS2, 28S rRNA, p	60.8	60.8	47%	4,00E-06	88%	AB086223.1	Minus 1280 - 1233	18s gene	18S ribosomal RNA	
Isaria tenuipes genes for 18S rRNA, ITS1, 5.8S rRNA, ITS2, 28S rRNA, p	60.8	60.8	47%	4,00E-06	88%	AB086220.1	Minus 1288 - 1241	18s gene	18S ribosomal RNA	
Isaria tenuipes genes for 18S rRNA, ITS1, 5.8S rRNA, ITS2, 28S rRNA, p	60.8	60.8	47%	4,00E-06	88%	AB086217.1	Minus 1288 - 1241	18s gene	18S ribosomal RNA	
Isaria tenuipes genes for 18S rRNA, ITS1, 5.8S rRNA, ITS2, 28S rRNA, p	60.8	60.8	47%	4,00E-06	88%	AB086215.1	Minus 1288 - 1241	18s gene	18S ribosomal RNA	
Isaria tenuipes genes for 18S rRNA, ITS1, 5.8S rRNA, ITS2, 28S rRNA, p	60.8	60.8	47%	4,00E-06	88%	AB086210.1	Minus 1279 - 1232	18s gene	18S ribosomal RNA	
Isaria tenuipes genes for 18S rRNA, ITS1, 5.8S rRNA, ITS2, 28S rRNA, p	60.8	60.8	47%	4,00E-06	88%	AB086209.1	Minus 1270 - 1223	18s gene	18S ribosomal RNA	
Isaria tenuipes genes for 18S rRNA, ITS1, 5.8S rRNA, ITS2, 28S rRNA, p	60.8	60.8	47%	4,00E-06	88%	AB086205.1	Minus 1302 - 1255	18s gene	18S ribosomal RNA	
Isaria tenuipes genes for 18S rRNA, ITS1, 5.8S rRNA, ITS2, 28S rRNA, p	60.8	60.8	47%	4,00E-06	88%	AB086206.1	Minus 1302 - 1255	18s gene	18S ribosomal RNA	
Isaria tenuipes genes for 18S rRNA, ITS1, 5.8S rRNA, ITS2, 28S rRNA, p	60.8	60.8	47%	4,00E-06	88%	AB086203.1	Minus 1302 - 1255	18s gene	18S ribosomal RNA	
M.caldariorum nuclear encoded 16S-like small subunit rRNA gene	60.8	60.8	99%	4,00E-06	76%	X75763.1	Minus 2009 - 1909	Intron	Group I	nuclear encoded 16s like small subunit ribosomal
Gibellula formosana genes for 18S rRNA, ITS1, 5.8S rRNA, ITS2, 28S rF	60.8	60.8	47%	4,00E-06	88%	AB100360.1	Minus 1290 - 1243	18s gene	18S ribosomal RNA	

10.4.2. Cópia 2

Description	Max score	Total Score	Query cover	E valeu	Ident	Acession	Strand	Localization	Function	Environmental genes / Intron information	
Albugo laibachii Nc14, genomic contig CONTIG_1223_NC14_v4_2941_98	87.8	87.8	96%	2,00E-14	84%	FR824925.1	plus	291 - 377	DNA genomic	CONTIG_1223_NC14_v4_2941_98	
Leptosphaeria biglobosa THlaspii 1Bcn65_scaffold00057 complete sequer	86.0	86.0	98%	9,00E-14	83%	FO905844.1	plus	76317 - 76405	DNA genomic		
Cordyceps militaris isolate CM09-31-28 mitochondrion, complete genom	73.4	73.4	0,98	5E-10	0,81	KP722513.2	minus	904 - 991	intron	group IC1	gene: large subunit ribosomal RNA
Cordyceps militaris isolate V40-4 mitochondrion, complete genome	73.4	73.4	0,98	5E-10	0,81	KP722512.2	minus	904 - 991	intron	group IC1	gene: large subunit ribosomal RNA
								2096 - 2183		group IC1	
							minus		intron		gene: large subunit ribosomal RNA
							minus	749 - 836	intron	group IC1	gene: large subunit ribosomal RNA
Cordyceps militaris isolate CM8 mitochondrion, complete genome	73.4	128	98%	5,00E-10	81%	KP722507.2					
							minus	2096 - 2183	intron	group IC1	gene: large subunit ribosomal RNA
							minus	749 - 836	intron	group IC1	gene: large subunit ribosomal RNA
Cordyceps militaris isolate F02 mitochondrion, complete genome	73.4	128	98%	5,00E-10	81%	KP722505.2					
Cordyceps militaris isolate CM552 mitochondrion, complete genome	73.4	73.4	0,98	5E-10	0,81	KP722502.2	minus	904 - 991	intron	group IC1	gene: large subunit ribosomal RNA
Cordyceps militaris isolate CM06 mitochondrion, complete genome	73.4	73.4	0,98	5E-10	0,81	KP722500.2	minus	904 - 991	intron	group IC1	gene: large subunit ribosomal RNA
Cordyceps militaris isolate CM09-9-24 mitochondrion, complete genome	73.4	73.4	0,98	5E-10	0,81	KP722496.2	minus	904 - 991	intron	group IC1	gene: large subunit ribosomal RNA
							minus	2095 - 2182	intron	group IC1	gene: large subunit ribosomal RNA
	73.4	128	98%	5,00E-10	81%			749 - 836		group IC1	
Cordyceps militaris isolate V40-5 mitochondrion, complete genome						KP722501.2	minus	1550 - 1637	intron	hypothetical protein (441..1178)	gene: large subunit ribosomal RNA
									intergenic		hypothetical protein (1841..2602)
	73.4	128	98%	5,00E-10	81%			155 - 242	beginning of genome	before the first gene: hypothetical protein (1841..2602)	
Cordyceps militaris isolate V26-16 mitochondrion, partial genome						KP722511.1	minus	1550 - 1637	intergenic	hypothetical protein (441..1178)	hypothetical protein (1841..2602)
	73.4	128	98%	5,00E-10	81%			155 - 242	beginning of genome	before the first gene: hypothetical protein (1841..2602)	
Cordyceps militaris isolate CM08 mitochondrion, partial genome						KP722510.1	minus	1550 - 1637	intergenic	hypothetical protein (441..1178)	hypothetical protein (1841..2602)
	73.4	128	98%	5,00E-10	81%			155 - 242	beginning of genome	before the first gene: hypothetical protein (1841..2602)	
Cordyceps militaris isolate CM05 mitochondrion, partial genome						KP722509.1	minus	1550 - 1637	intergenic	hypothetical protein (441..1178)	hypothetical protein (1841..2602)
	73.4	128	98%	5,00E-10	81%			155 - 242	beginning of genome	before the first gene: hypothetical protein (1841..2602)	
Cordyceps militaris isolate CM02 mitochondrion, partial genome						KP722508.1	minus	1550 - 1637	intergenic	hypothetical protein (441..1178)	hypothetical protein (1841..2602)
	73.4	128	98%	5,00E-10	81%			155 - 242	beginning of genome	before the first gene: hypothetical protein (1841..2602)	
Cordyceps militaris isolate F03 mitochondrion, partial genome						KP722506.1	minus				

Cordyceps militaris isolate CM494 mitochondrion, partial genome	73.4	73.4	98%	5,00E-10	81%	KP722504.1	minus	358 - 445	beginning of genome	before the first gene: hypothetical protein (649..1410)		
Cordyceps militaris isolate CM556 mitochondrion, partial genome	73.4	73.4	98%	5,00E-10	81%	KP722503.1	minus	358 - 445	beginning of genome	before the first gene: hypothetical protein (649..1410)		
Cordyceps militaris isolate F01 mitochondrion, partial genome	73.4	73.4	98%	5,00E-10	81%	KP722499.1	minus	358 - 445	beginning of genome	before the first gene: hypothetical protein (649..1410)		
Cordyceps militaris isolate CM07 mitochondrion, partial genome	73.4	73.4	98%	5,00E-10	81%	KP722498.1	minus	358 - 445	beginning of genome	before the first gene: hypothetical protein (649..1410)		
Cordyceps militaris isolate CMA mitochondrion, partial genome	73.4	73.4	98%	5,00E-10	81%	KP722497.1	minus	358 - 445	beginning of genome	before the first gene: hypothetical protein (649..1410)		
								2095 - 2182	intron	group IC1	gene: large subunit ribosomal RNA	
Cordyceps militaris isolate V26-17 mitochondrion, complete genome	73.4	128	98%	5,00E-10	81%	KP719097.1	minus	749 - 836	intron	group IC1	gene: large subunit ribosomal RNA	
								2095 - 2182	intron	group IC1	gene: large subunit ribosomal RNA	
Cordyceps militaris isolate CM01 mitochondrion, complete genome	73.4	128	98%	5,00E-10	81%	KP719096.1	minus	749 - 836	intron	group IC1	gene: large subunit ribosomal RNA	
								2009 - 2096	intron	large subunit ribosomal RNA	Overlapping the orfs, however the	
Cordyceps militaris strain EFCC-C2 mitochondrion, complete genome	73.4	132	98%	5,00E-10	81%	KF432176.1	minus	662 -749	intron	large subunit ribosomal RNA	next gene code a ribosomal protein	
Cordyceps brongniartii isolate IMBST95031 mitochondrion, complete ge	73.4	73.4	98%	5,00E-10	80%	EU100743.1	minus	851 - 939	intron	group IC1	gene: large subunit ribosomal RNA	
Tolypocladium ophioglossoides isolate L2 mitochondrion, complete genc	69.8	69.8	98%	7,00E-09	80%	KX455872.1	minus	937 - 1024	intron	group IC1	gene: large subunit ribosomal RNA	
Monoraphidium sp. KMMCC 1531 18S ribosomal RNA gene, partial seque	68.0	68.0	100%	2,00E-08	79%	JQ315550.1	minus	1060 - 1147	gene	18s gene		
Symbiochloris symbiontica strain SAG 2099 18S ribosomal RNA gene, part	68.0	68.0	98%	2,00E-08	78%	GU017646.1	minus	1711 - 1796	intron	group I	18s gene	
Uncultured Nebela clone PR4_4E_85 18S ribosomal RNA gene, partial seq	68.0	68.0	100%	2,00E-08	79%	GU479960.1	minus	1215 - 1302	gene	18s gene		
Nebela carinata from Switzerland small subunit ribosomal RNA gene, part	68.0	68.0	100%	2,00E-08	79%	EU392144.1	minus	678 - 765	intron	18s gene		
Nebela carinata from Sweden small subunit ribosomal RNA gene, partial s	68.0	68.0	100%	2,00E-08	79%	EU392143.1	minus	725 - 812	intron	18s gene		

Leptosphaeria maculans lepidii ibcn84_scaffold00004 complete sequenc	66.2	155	98%	8,00E-08	78%	FO906020.1	plus minus plus plus	64857 - 64945 26932 - 127018 66594 - 66680 60412 - 60500		**Not open!**		
Leptosphaeria maculans brassicae wa74_scaffold00107 complete sequen	66.2	271	100%	8,00E-08	78%	FO906979.1	plus plus minus plus minus minus	65799 - 65887 62582 - 62670 25225 - 125311 29060 - 29120 44559 - 14447 39474 - 139562	 intergenic intergenic	Just complete sequence, without annotation! predicted protein (142190..142791) predicted protein (122789..123004)	 "predicted protein (148013..148213) "predicted protein (142190..142791)
Leptosphaeria maculans JN3 SuperContig_30_v2	66.2	271	100%	8,00E-08	78%	NW_0035338	minus plus minus	42694 - 142782 78573 - 78659 23523 - 23583	gene/intron intergenic intergenic	Part of the sequence are in coding sequence for a gene and the other part is a intron predicted protein(65064..65285) predicted protein(22626..>22910)	predicted protein (142190..142791) predicted protein(81215..81417) predicted protein(25158..>25457)
Spizellomyces sp. NBRC 105423 gene for 18S ribosomal RNA, partial sequ	66.2	66.2	100%	8,00E-08	79%	AB586075.1	minus	1696 - 1784	gene	18s gene		
Hypomyces aurantius mitochondrion, complete genome	64.4	64.4	98%	3,00E-07	79%	KU666552.1	minus	14237 - 14324	intron	group=IC1		
Nebela carinata isolate DL3_122 small subunit ribosomal RNA gene, partia	64.4	64.4	100%	3,00E-07	78%	JF694283.1	minus	392 - 479	gene	18s gene		
Nebela tubulosa from France small subunit ribosomal RNA gene, partial s	64.4	64.4	100%	3,00E-07	78%	EU392148.1	minus	710 - 797	intron	18s gene		
Naegleria sp. NG236 LSU rRNA gene group I intron, 389bp	64.4	64.4	98%	3,00E-07	79%	AJ001314.1	minus	89 - 176	intron	group I intron	Large subunit ribossomal	
Olpidiopsis porphyrae gene for 18S rRNA, partial sequence	62.6	167	100%	1,00E-06	78%	AB287418.1	minus minus	2257 - 2345 725 - 813 1767 - 1767		Just complete sequence, without annotation!		
Leptosphaeria biglobosa brassicae b35_scaffold00056 complete sequenc	60.8	60.8	96%	3,00E-06	77%	FO905608.1	plus	42919 - 43005		Just complete sequence, without annotation!		
Uncultured fungus isolate RFLP-145 18S ribosomal RNA gene, partial sequ	60.8	60.8	93%	3,00E-06	77%	DQ309135.1	minus	96 - 178	gene	18s gene		
Botryotinia fuckeliana B05.10 mitochondrion, complete genome	60.8	60.8	98%	3,00E-06	77%	KC832409.1	minus	60288 - 60376	intergenic	ATP synthase subunit (959988..60194)	GIY-YIG endonuclease (60824..62437)	
Physarum album voucher AMFD168 small subunit ribosomal RNA gene, p	60.8	60.8	100%	3,00E-06	76%	DQ903681.2	minus	698 - 784	intron	group I intron S529	18s gene	
Nebela tincta isolate 2.65.6Ntincta small subunit ribosomal RNA gene, pa	59.0	59.0	100%	1,00E-05	76%	KF476129.1	minus	252 -339	gene	18s gene		
Nebela tincta isolate 2.21.6_3Ntincta small subunit ribosomal RNA gene,	59.0	59.0	100%	1,00E-05	76%	KF476115.1	minus	368 - 445	gene	18s gene		
Nebela flabellulum isolate 2.21.2Nflabellulum small subunit ribosomal RI	59.0	59.0	100%	1,00E-05	76%	KF476113.1	minus	13 - 100	gene	18s gene		
Nebela flabellulum isolate 2.21.1_Nflabellulum small subunit ribosomal F	59.0	59.0	100%	1,00E-05	76%	KF476112.1	minus	232 - 319	gene	18s gene		
Monoraphidium terrestre 18S rRNA gene	59.0	59.0	36%	1,00E-05	100%	Y17817.1	minus	714 - 745	intron	group I intron	18s gene	
Monoraphidium sp. ABC-02 18S ribosomal RNA gene, partial sequence	57.2	57.2	100%	4,00E-05	77%	KP688585.1	minus	311 - 399	gene	18s gene		
Myxozyma melibiosi strain NRRL Y-11781 26S ribosomal RNA gene, partia	57.2	57.2	100%	4,00E-05	77%	DQ518988.1	minus	2269 - 2357	intron	26s gene		
Spizellomyces punctatus DAOM BR117 18S ribosomal RNA rRNA	55.4	55.4	100%	1,00E-04	75%	XR_00167715	minus	2149 - 2236	gene	18s gene		
Monoraphidium sp. NS16 18S ribosomal RNA gene, partial sequence	55.4	55.4	100%	1,00E-04	75%	KP162147.1	minus	1489 - 1576	intron	18s gene		
Gonapodya sp. JEL612 18S ribosomal RNA gene and internal transcribed s	55.4	55.4	100%	1,00E-04	77%	KJ668070.1	minus	1270 - 1359	intron	18s gene		
Rhynchosporium secalis mitochondrion, complete genome	55.4	55.4	98%	1,00E-04	75%	KF650575.1	minus	52546 - 52634	intergenic	GIYYIG - endonuclease family (50903..52351)	tRNA-Lys (53750..53821)	
Rhynchosporium commune mitochondrion, complete genome	55.4	55.4	98%	1,00E-04	75%	KF650573.1	minus	53149 - 53237	intergenic	GIYYIG - endonuclease family (51506..52954)	tRNA-Lys (54353..54424)	
Rhynchosporium agropyri mitochondrion, complete genome	55.4	55.4	98%	1,00E-04	75%	KF650572.1	minus	52442 - 52530	intergenic	GIYYIG - endonuclease family (50682..52247)	tRNA-Lys (53649..53720)	
Heterolobosea sp. AGBS-2011 strain SD1A 18S ribosomal RNA gene, partia	55.4	55.4	100%	1,00E-04	75%	HQ898858.1	minus	2215 - 2302	intron	18s gene		

Rhombocystis complanata strain KR 1998/2 18S ribosomal RNA gene, part	55.4	55.4	37%	1,00E-04	97%	HM483518.1	minus	1221-1253	intron	group I intron	18s gene
Spizellomyces sp. NBRC 106283 gene for 18S ribosomal RNA, partial sequ	55.4	55.4	100%	1,00E-04	75%	AB586079.1	minus	2137 - 2224	gene	18s gene	
Spizellomyces punctatus strain ATCC 48900 18S ribosomal RNA, partial se	55.4	55.4	100%	1,00E-04	75%	NG_017173.1	minus	2123 - 2210	intron	18s gene	
Ankistrodesmus sp. NDem 9/21 T-6w 18S ribosomal RNA gene, partial sec	55.4	55.4	100%	1,00E-04	75%	AY846374.1	minus	1196 - 1283	intron	18s gene	
Nebela tincta isolate 2.119.5Ntincta small subunit ribosomal RNA gene, p	53.6	53.6	40%	5,00E-04	94%	KF476127.1	minus	246 - 280	gene	18s gene	
Nebela tincta isolate 2.119.4Ntincta small subunit ribosomal RNA gene, p	53.6	53.6	100%	5,00E-04	76%	KF476126.1	minus	251 - 341	gene	18s gene	
Nebela tincta isolate 2.119.3Ntincta small subunit ribosomal RNA gene, p	53.6	53.6	40%	5,00E-04	94%	KF476125.1	minus	246 - 280	gene	18s gene	
Nebela tincta isolate 2.93.2Ntincta small subunit ribosomal RNA gene, pa	53.6	53.6	40%	5,00E-04	94%	KF476124.1	minus	246 - 280	gene	18s gene	
Nebela flabellulum isolate 2.21.5Nflabellulum small subunit ribosomal RI	53.6	53.6	40%	5,00E-04	94%	KF476114.1	minus	251 - 285	gene	18s gene	
Nebela tincta isolate Nt_AO2.04_6 small subunit ribosomal RNA gene, pa	53.6	53.6	40%	5,00E-04	94%	KF476099.1	minus	363 - 397	gene	18s gene	
Nebela flabellulum from United Kingdom small subunit ribosomal RNA ge	53.6	53.6	40%	5,00E-04	94%	EU392152.1	minus	758 - 792	intron	18s gene	
Nebela tincta var. tincta from Sweden small subunit ribosomal RNA gene,	53.6	53.6	40%	5,00E-04	94%	EU392151.1	minus	746 - 780	intron	18s gene	
Nebela tincta var. major from Sweden small subunit ribosomal RNA gene,	53.6	53.6	40%	5,00E-04	94%	EU392150.1	minus	725 - 759	intron	18s gene	
Porosia bigibbosa from Switzerland small subunit ribosomal RNA gene, pa	53.6	53.6	40%	5,00E-04	94%	EU392147.1	minus	698 - 732	intron	18s gene	
Myxozyma sirexii 26S ribosomal RNA gene, partial sequence	53.6	53.6	100%	5,00E-04	76%	DQ518994.1	minus	2345 - 2433	intron	26s gene	
Monoraphidium saxatile strain Mary 9/21 T-5w 18S ribosomal RNA gene,	53.6	53.6	100%	5,00E-04	76%	AY846384.1	minus	1201 - 1289	intron	18s gene	
Chlorella virus DNA for major capsid protein Vp54, complete cds	53.6	53.6	100%	5,00E-04	76%	AB006978.1	minus	1387 - 1475	intron	group I self-splicing intron	major capsid protein Vp54
Bacillus endophyticus strain Hbe603, complete genome	51.8	51.8	98%	0.002	77%	CP011974.1	minus	74508 - 237459	intergenic	hypothetical protein	hypothetical protein
Nephrochlamys subsolitaria genes for 18S rRNA, ITS1, 5.8S rRNA, ITS2, 28	51.8	51.8	37%	0.002	94%	AB917131.1	minus	1603 - 1635	intron	group I intron S943	18s gene
Raphidocelis rotunda strain SAG 31.88 18S ribosomal RNA gene, complet	51.8	51.8	37%	0.002	94%	KF673390.1	minus	1605 - 1637	intron	18s gene	
Raphidocelis contorta strain SAG 11.81 18S ribosomal RNA gene, complet	51.8	51.8	37%	0.002	94%	KF673377.1	minus	1215 - 1247	intron	18s gene	
Chlamydomyzium sp. TYJ-2012 voucher SL38 18S ribosomal RNA gene, pa	51.8	99	100%	0.002	75%	JQ031283.1	minus	1859 - 1946	gene	18s gene	
Ankistrodesmus gracilis strain Itas 9/21 S-2w 18S ribosomal RNA gene, pa	51.8	51.8	37%	0.002	94%	AY846371.1	minus	1251 - 1283	intron	18s gene	
Pyxidiophora arvernensis 18S rRNA gene, partial sequence, and type I intr	51.8	51.8	98%	0.002	75%	U43339.1	minus	132 - 221	intron	type I intron	18s gene
Hirsutella rhossiliensis isolate USA-87-5 mitochondrion, complete genom	50.0	50.0	98%	0.006	74%	KU203675.1	minus	3422 - 3509	gene	large subunit ribosomal RNA	
Difflugia acuminata small subunit ribosomal RNA gene, partial sequence	50.0	50.0	100%	0.006	74%	JQ366064.1	minus	747 - 834	intron	18s gene	
Heterolobosea sp. AGBS-2011 strain AS12B 18S ribosomal RNA gene, part	50.0	50.0	100%	0.006	74%	HQ898857.1	minus	2597 - 2684	intron	18s gene	
Brachyalara straminea strain CBS 622.82 18S ribosomal RNA gene, partial	50.0	50.0	87%	0.006	74%	HQ609482.1	minus	1219 - 1295	intron	18s gene	
Brachyalara straminea strain CBS 114633 18S ribosomal RNA gene, partial	50.0	50.0	87%	0.006	74%	HQ609481.1	minus	1174 - 1250	intron	18s gene	
Dunaliella sp. GSL020 18S ribosomal RNA gene, partial sequence	50.0	50.0	100%	0.006	73%	GQ243427.1	minus	937 - 1025	intron	18s gene	
Desmodesmus insignis strain JNU24 18S ribosomal RNA gene, partial sequ	48.2	48.2	100%	0.022	76%	KU175228.1	minus	1240 - 1328	intron	group I intron S943	18s gene
Bacillus phage Moonbeam, complete genome	48.2	48.2	98%	0.022	73%	KM236246.1	minus	41546 - 41633	intergenic	tail protein (41120..41537)	DNA-binding protein (41967..43232)
Zygnema circumcarinatum strain SAG 698-1a 18S ribosomal RNA gene, pa	48.2	48.2	100%	0.022	74%	KM020155.1	minus	1899 - 1987	intron	group I	18s gene
Hyalosphenia papilio isolate HP_TN3.109.2.10 small subunit ribosomal RI	48.2	48.2	40%	0.022	92%	KF476096.1	minus	360 - 394	gene	18s gene	
Hyalosphenia elegans isolate HE_DL3_63_11.4 small subunit ribosomal R	48.2	48.2	40%	0.022	92%	KF476092.1	minus	360 - 394	gene	18s gene	
Hyalosphenia elegans isolate HE_DL3_63_13 small subunit ribosomal RN	48.2	48.2	40%	0.022	92%	KF476091.1	minus	360 - 394	gene	18s gene	
Hyalosphenia papilio isolate HP_TN3.86 small subunit ribosomal RNA ger	48.2	48.2	40%	0.022	92%	KF476090.1	minus	360 - 394	gene	18s gene	
Hyalosphenia elegans isolate HE_AO122_20.1 small subunit ribosomal RN	48.2	48.2	40%	0.022	92%	KF476089.1	minus	360 - 394	gene	18s gene	
Hyalosphenia papilio isolate HP_DL3_62_1 small subunit ribosomal RNA g	48.2	48.2	40%	0.022	92%	KF476088.1	minus	360 - 394	gene	18s gene	
Hyalosphenia papilio isolate HP_DL62.2 small subunit ribosomal RNA gen	48.2	48.2	40%	0.022	92%	KF476087.1	minus	345 - 379	gene	18s gene	
Hyalosphenia elegans isolate HE_AO122_20l small subunit ribosomal RN	48.2	48.2	40%	0.022	92%	KF476082.1	minus	355 - 389	gene	18s gene	
Hyalosphenia papilio isolate HP_TN2_137_1.6 small subunit ribosomal RI	48.2	48.2	40%	0.022	92%	KF476079.1	minus	360 - 394	gene	18s gene	
Hyalosphenia elegans isolate HE_AO122_24.7 small subunit ribosomal RN	48.2	48.2	40%	0.022	92%	KF476078.1	minus	360 - 394	gene	18s gene	

11. DISCIPLINAS E PRODUÇÃO CIENTÍFICA

11.1. Disciplinas cursadas durante o doutorado

Período	Turma	Disciplina
2015/2	DIP MIC836 B	TOP. ESP. EM MICROBIOLOGIA
2016/1	DIP MOF888 A	TOP. ESPECIAIS DE BIOLOGIA CELULAR III
2017/2	DIP MIC857 1	TREINAMENTO DIDATICO EM MICROBIOLOGIA II

11.2. Trabalhos apresentados em eventos científicos

SILVA, L. K. S.; ANDRADE, A. C. S. P.; HIROYUKI, H.; Andreani, J.; LEVASSEUR, A.; ABRAHAO, J. S.; LA SCOLA, B. **Genomic and microscopical characterization of Borelyvirus: a new giant virus isolated from Serra do Cipó national park, Minas Gerais**. In: XXVIII Congresso Brasileiro de Virologia, 2017, Belo Horizonte. XXVIII Congresso Brasileiro de Virologia, 2017.

SILVA, L. K. S.; ANDRADE, A. C. S. P.; HIROYUKI, H.; Andreani, J.; LEVASSEUR, A.; ABRAHAO, J. S.; LA SCOLA, B. **Genomic and microscopical characterization of Borelyvirus: a new giant virus isolated from Serra do Cipó**. In: IV Simpósio de Microbiologia da UFMG, 2017, Belo Horizonte. IV Simpósio de Microbiologia da UFMG, 2017.

SILVA, L. K. S.; RODRIGUES, R.A.L.; ARANTES, T. S.; SILVA, L. C. F.; BORATTO, P. V. M.; KROON, E. G.; CLEMENTE, W. T.; ABRAHAO, J. S. **Mimivirus in hospital environment: assessment of distribution and biological, molecular and structural diversity of viral isolated.** In: XXVI Brazilian Congress of Virology, 2015, Florianópolis. Virus reviews and research - Journal of the Brazilian Society for Virology, 2015. v. 20. p. 21-22.

SILVA, L. K. S.; RODRIGUES, R.A.L.; ARANTES, T. S.; BORATTO, P. V. M.; SILVA, L. C. F.; ANDRADE, K. R.; KROON, E. G.; CLEMENTE, W. T.; ABRAHAO, J. S. **Mimivírus em ambiente hospitalar: avaliação da distribuição e da diversidade biológica, molecular e estrutural de isolados virais.** In: II Simpósio de Microbiologia da UFMG, 2015, Belo Horizonte. Microbiologia Translacional do ambiente natural às aplicações biotecnológicas, 2015. v. 1. p. 46-47.

11.3. Artigos publicados relacionados a tese de doutorado

SILVA, LUDMILA KAREN DOS SANTOS; BORATTO, PAULO VICTOR MIRANDA; LA SCOLA, BERNARD; BONJARDIM, CLÁUDIO ANTÔNIO; ABRAHÃO, JÔNATAS SANTOS. **Acanthamoeba and mimivirus interactions: the role of amoebal encystment and the expansion of the -Cheshire Cat theory**. Current Opinion in Microbiology, v. 31, p. 9-15, 2016.

ABRAHÃO, JÔNATAS; SILVA, LORENA; SILVA, LUDMILA SANTOS; KHALIL, JACQUES YAACOUB BOU; RODRIGUES, RODRIGO; ARANTES, THALITA; ASSIS, FELIPE; BORATTO, PAULO; ANDRADE, MIGUEL; KROON, ERNA GEESSIEN; RIBEIRO, BERGMANN; BERGIER, IVAN; SELIGMANN, HERVE; GHIGO, ERIC; COLSON, PHILIPPE; LEVASSEUR, ANTHONY; KROEMER, GUIDO; RAOULT, DIDIER; LA SCOLA, BERNARD. **Tailed giant Tupanvirus possesses the most complete translational apparatus of the known virosphere**. Nature Communications, v. 9, p. 1-12, 2018.

SILVA, LUDMILA KAREN DOS SANTOS; ANDRADE, ANA CLÁUDIA DOS SANTOS PEREIRA; DORNAS, FÁBIO PIO; RODRIGUES, RODRIGO ARAÚJO LIMA; ARANTES, THALITA; KROON, ERNA GEESSIEN; BONJARDIM, CLÁUDIO ANTÔNIO; ABRAHÃO, JÔNATAS SANTOS. **Cedratvirus getuliensis replication cycle: an in-depth morphological analysis**. Scientific Reports, v. 8, p. 1-11, 2018.

Available online at www.sciencedirect.com

ScienceDirect

Current Opinion in Microbiology

Acanthamoeba and mimivirus interactions: the role of amoebal encystment and the expansion of the 'Cheshire Cat' theory

Ludmila Karen dos Santos Silva[1], Paulo Victor Miranda Boratto[1], Bernard La Scola[2], Cláudio Antônio Bonjardim[1] and Jônatas Santos Abrahão[1]

Acanthamoeba are natural hosts for giant viruses and their life cycle comprises two stages: a trophozoite and a cryptobiotic cyst. Encystment involves a massive turnover of cellular components under molecular regulation. Giant viruses are able to infect only the trophozoite, while cysts are resistant to infection. Otherwise, upon infection, mimiviruses are able to prevent encystment. This review highlights the important points of Acanthamoeba and giant virus interactions regarding the encystment process. The existence of an acanthamoebal non-permissive cell for Acanthamoeba polyphaga mimivirus, the prototype member of the Mimivirus genus, is analyzed at the molecular and ecological levels, and compared to a similar phenomenon previously described for Emiliana huxleyi and its associated phycodnaviruses: the 'Cheshire Cat' escape strategy.

Addresses
[1] Laboratório de Vírus, Departamento de Microbiologia, Instituto de Ciências Biológicas (ICB), Universidade Federal de Minas Gerais, Brasil (UFMG), Postal code 486, Belo Horizonte, Minas Gerais, Brazil
[2] URMITE CNRS UMR 6236–IRD 3R198, Aix Marseille Universite, Marseille, France

Corresponding author: Abrahão, Jônatas Santos (jonatas.abrahao@gmail.com)

Current Opinion in Microbiology 2016, **31**:9–15

This review comes from a themed issue on **Environmental microbiology**

Edited by **Didier Raoult** and **Jonatas Abrahao**

http://dx.doi.org/10.1016/j.mib.2016.01.003

1369-5274/Published by Elsevier Ltd.

Introduction

The genus *Acanthamoeba* comprises free-living amoebas widely distributed in nature that are capable of causing disease in humans [1,2]. The life cycle of these amoebas consists of two cellular forms — one vegetative and the other resistant — known as the trophozoite and cyst, respectively [3•,4••]. These amoebas also serve as platforms of replication for a large number of microorganisms, including bacteria and yeasts [4••,5]. More recently, it was demonstrated that some *Acanthamoeba* species are also natural hosts for giant viruses belonging to the *Mimiviridae* family [6,7,8••].

Acanthamoeba polyphaga mimivirus (APMV) was the first mimivirus isolated and it is the prototype species of the *Mimivirus* genus, *Mimiviridae* family [8••,9–11]. This family is phylogenetically grouped into the proposed *Megavirales* order which includes, among others, *Phycodnaviridae and Marseilleviridae* members [9–13].

Due to increasing interest in giant viruses and acanthamoebas, new studies are being developed in order to clarify this host–pathogen interaction. Recently, we demonstrated that APMV is able to infect *Acanthamoeba* in the trophozoite stage, but is unable to infect cysts. Moreover, when trophozoites are infected with APMV immediately before suffering an encystment stimulus, encystment is not triggered [4••]. The existence of a non-permissive cell stage may represent an interesting way for the host to escape its parasite, as a stratagem in the context of the host–virus fight for supremacy.

In this brief review, we discuss some aspects of the interaction between mimivirus and *Acanthamoeba*, emphasizing the mechanisms involved in the process of encystment and the ability of these viruses to interfere in this process to ensure viral infection. We will also mention new studies that are being developed in order to clarify the virus–host relationship and discuss this interaction based on the 'Cheshire Cat' theory [14••,15].

Factors involved in the encystment process

Acanthamoeba and other free-living amoebas developed, throughout their evolution, a strategy in response to adverse conditions and stress: they differentiate from trophozoites, the vegetative form, to cysts, the resistant form, in order to produce a cryptobiotic cell that is spherical and composed by a double wall [16•,17]. This process, named encystment, involves massive turnover of cellular components and remodeling of organelle structure and function [17].

There are several signals responsible for inducing encystment, such as starvation, osmotic stress, temperature, and the presence of bacteria or their toxins [18–25]. Encystment is also efficiently induced by glucose, magnesium ions and taurine as well as catecholamine, which induces the synthesis of cyclic AMP (cAMP), a second messenger that is capable of inducing the formation of cysts (Figure 1) [26,27].

Encystment induces various morphological changes involving, among other things, cytoskeletal rearrangements. Some studies have shown that the transcription of genes involved in actin synthesis is slightly suppressed during encystment, while protein synthesis is dramatically reduced, indicating a modulation of the process of translation [28]. In addition, another research has described partial actin degradation during the early stages of encystment, thus demonstrating that the cytoskeleton plays a crucial role in cyst formation [29].

Different proteases are likely involved in encystment. Some of these are the serine proteases that are induced during encystment and specifically detected in cysts [30]. Studies using small interfering RNAs (siRNA) and pharmacological inhibitors have shown that these proteases are essential for the formation of cysts; moreover, it has been suggested that these proteases may also mediate autophagic processes that allow the occurrence of protein turnover during cell differentiation of trophozoites into cysts [19,31,32]. Another class of proteases involved is the cysteine proteases [33,34]. Studies have shown a dramatic increase in the levels of these proteases during encystment, more specifically during the early stage of encystment. Moreover, these proteins are required for the complete morphogenesis of cysts and seem to be correlated with autophagosomal degradation of cell constituents, particularly mitochondria, during encystment of *Acanthamoeba* (Figure 1) [33,34].

Beyond these factors, an amoebal molecule called encystment-enhancing activity (EEA), is also able to induce the encystment process. The nature of this factor has not yet been described, however, it is known that EEA is produced in high concentrations in amoebal cultures, suggesting that this factor could act as a *quorum-sensing* molecule (Figure 1) [35].

Few signaling pathways have been proposed to be involved in encystment. In *Acanthamoeba*, pharmacological inhibition of Ras, a small GTPase that can activate the

Figure 1

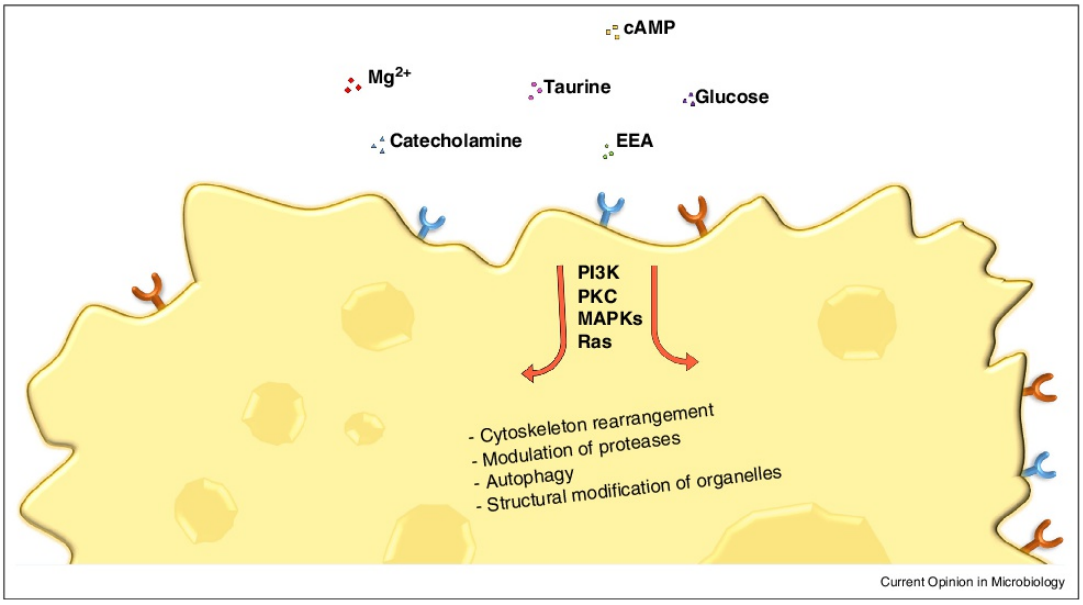

Molecules, signaling pathways and responses involved with the encystment of Acanthamoeba. Encystment is efficiently stimulated by glucose, magnesium ions, taurine, catecholamine, cyclic AMP (cAMP) and also the supposed quorum-sensing molecule EEA. Proteins involved with some signaling pathways, such as Ras, PI3K, PKC and mitogen-activated protein kinases (MAPKs) that are associated with the formation of cysts are also shown. Furthermore, the presence of these molecules and activation of these pathways are associated with autophagy, modulation of proteases and morphological changes as cytoskeleton rearrangement and structural modification of organelles.

Mitogen-Activated Protein Kinases (MAPK) pathway, is associated with a reduced rate of encystment. In addition, other studies have indicated the involvement of PI3K in this process, since inhibition of this enzyme also decreases the formation of cysts [17]. Other results suggest that type C protein kinases (PKC) play an important role in the formation of mature cysts (Figure 1) [36].

Recently, we have concentrated on the study of MAPK pathways to verify whether these signaling pathways are associated with the encystment of *Acanthamoeba*. Preliminary results demonstrated that the MEK/ERK pathway appears to be directly involved in this process, since robust ERK activation was observed at early times during encystment, which strongly suggests that MEK/ERK might be associated with the encystment process. However, more studies are being carried out in order to confirm and clarify the role played by this pathway during the encystment of *Acanthamoeba* (unpublished data).

Although the encystment process is related to a response to adverse conditions and to the presence of some pathogens, it is important to highlight that some bacterias can survive within cysts [17]. *Mycobacterium*, for example, is able to live in the space between their cyst walls for long periods probably due to the presence of some functional cellulases [37,38]. Similarly, *Legionella pneumophila* can be not only protected inside amoebas during harsh conditions, but also can be eventually transmitted to other susceptible hosts [39].

Host–pathogen interaction between *Acanthamoeba* and giant virus

As previously mentioned, Boratto *et al.*, 2015, described an intriguing host–pathogen interaction between *Acanthamoeba* and mimivirus. It was demonstrated that APMV is able to infect *Acanthamoeba* trophozoites, resulting in an increased viral titers and an evident cytopathic effect (Figure 2a). Of note, this virus was unable to infect cysts of *A. castellanii*, suggesting that encystment might prevent infection by APMV (Figure 2b). Moreover, APMV infection is also hampered once the process of encystment has been triggered, when the stimulus to encyst is given immediately before amoebal infection with the giant virus (Figure 2c). The authors also demonstrated in this study that when trophozoites are infected by APMV,

Figure 2

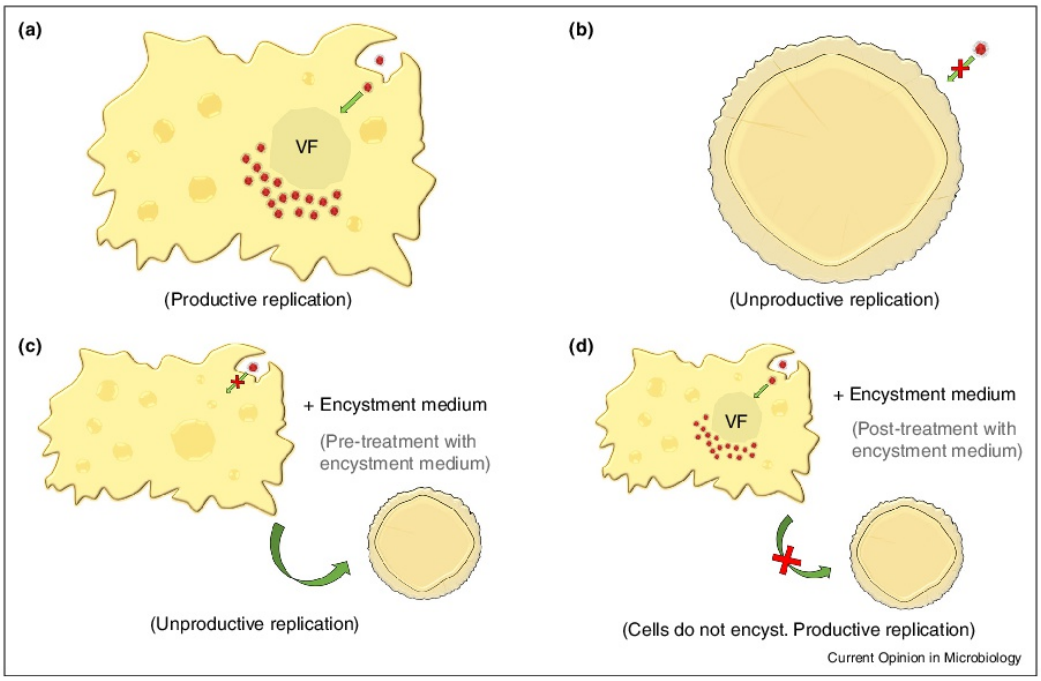

Interaction between Acanthamoeba and APMV. **(a)** APMV is able to infect *A. castellanii* trophozoites, resulting in a productive replication with increased number of viral particles. **(b)** APMV is unable to infect cysts of *A. castellanii*, suggesting that encystment might prevent infection by giant viruses, characterizing an unproductive replication. **(c)** Once the process of encystment has been triggered by pre-treatment with encystment medium, the infection by APMV is hampered and the encystment normally occurs. **(d)** When trophozoites are primarily infected with APMV and then exposed to the encystment stimulus, infection results in productive APMV replication and the encystment is not triggered. VF: viral factory.

directly before suffering the encystment stimulus, encystment is not triggered, indicating that stimulation does not interfere with an ongoing APMV infection and showing that the virus is able to evade the process of cyst formation (Figure 2d) [4••]. In our laboratory, a similar pattern of infection has also been observed for another giant virus, known as marseillevirus (Figure 3) [40]. These viruses, as well as mimivirus, are able to infect only one stage of the *Acanthamoeba* life cycle, the trophozoite stage, while cysts are still non-permissive (Figure 2) (unpublished data). Cysts are likely more resistant to infection because of their cryptobiotic nature; in this state, most of the metabolic processes are stopped, including the ability to phagocytose, which is the mechanism used for the entry of giant viruses [41].

With the purpose of verifying how mimivirus could avoid the *Acanthamoeba* encystment, gene expression analyses were also performed and it was demonstrated that these viruses are able to block the expression of serine proteases, which, as mentioned above, are essential during the encystment process [4••,19]. However, more studies are required in order to clarify how exactly the virus is able to reduce the expression of these proteases. It is already known that APMV contains a gene named R700 that encodes a serpin-like protein, a family of serine protease inhibitors that might be involved in this down regulation [42,43].

Despite the great importance of the host–pathogen interactions between amoebas and giant viruses, it is important to point out that *Acanthamoeba* cells are not exposed solely to those parasites in nature. *Acanthamoeba* harbors a number of endosymbionts [7,44,45]. The exact nature of these symbiotic relationships and the benefit they represent for amoebas is not fully understood [3•]. Besides the existence of endosymbionts, the discovery of virophages (giant viruses-infecting viruses) added one more piece in this remarkable and complex ecological puzzle [46].

The 'Cheshire Cat' applied to *Acanthamoeba* and the giant virus world

The 'Cheshire Cat' strategy described a previously unknown kind of ecological and evolutionary interaction that held critical significance for the life cycle and survival of the host and also a way to escape from the constraints imposed by pathogens in their evolution. The strategy described the relationship between a large virus, the phycodnavirus known as *Emiliania huxleyi virus* (EhVs), and a photosynthetic unicellular eukaryote, the coccolithophore known as *Emiliania huxleyi*, which, like the acanthamoebas, also presents two stages in its life cycle: a non-calcified, haploid phase and a calcified, diploid form. The authors observed that the virus infects and lysis only diploid-phase cells, whereas the haploid phase is unrecognizable and therefore resistant to EhVs infection. The authors also demonstrated that exposure

Figure 3

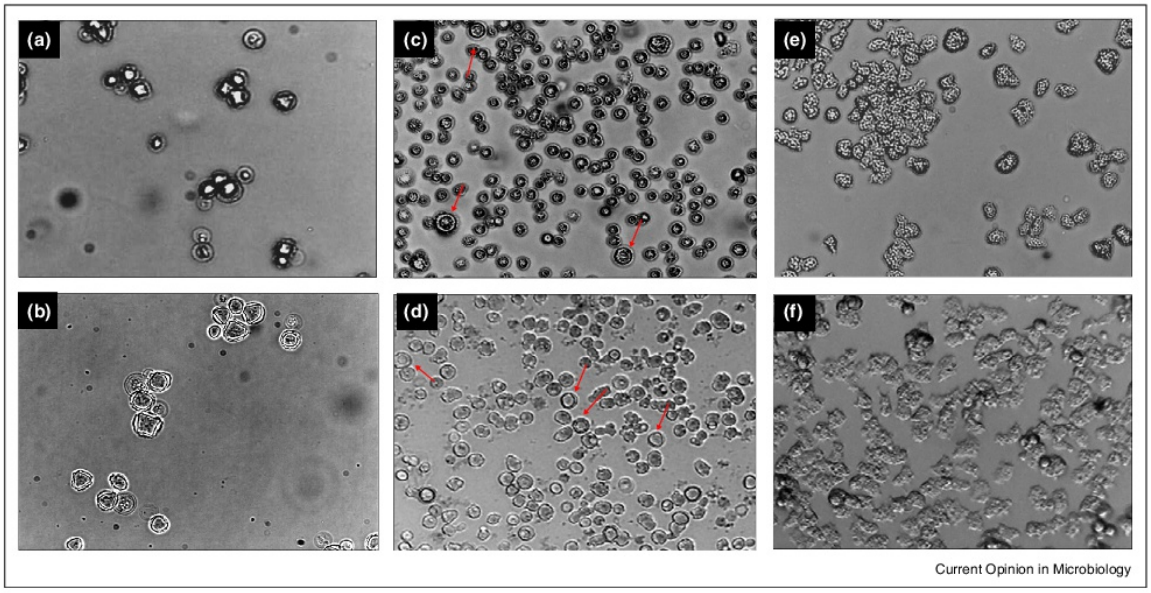

Marseillevirus, as APMV, is able to infect *Acanthamoeba* trophozoites, but is unable to infect cysts. *A. castellanii* cysts showing no evidence of cytopathic effect after exposure to marseillevirus **(a)** and APMV **(b)**. *A. castellanii* trophozoites after infection with marseillevirus **(c)** and APMV **(d)** showing evident cytopathic effect, as observed by cell rounding and lysis. Note that a small percentage of acanthamoeba cells (1–4%) are able to encyst (red arrows). **(e,f)** Controls, non-infected *A. castellanii* trophozoites. VF: viral factories.

Figure 4

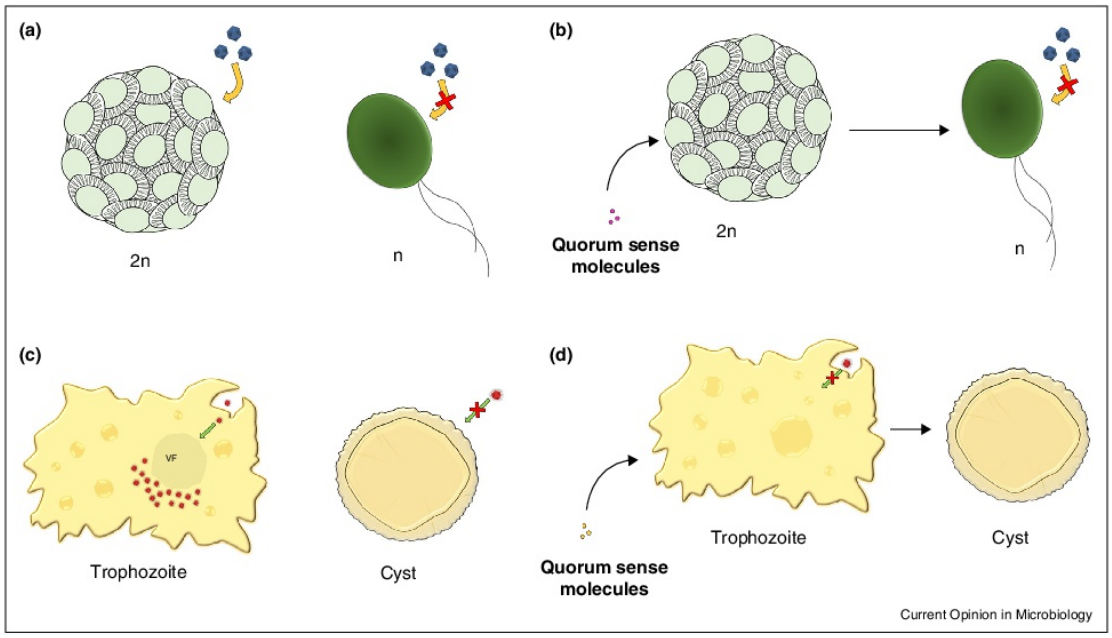

The 'Cheshire Cat' theory expanded to the giant virus and Acanthamoeba world. **(a)** The *Emiliania huxleyi* virus (EhVs) infects and lysis only diploid-phase cells, whereas the haploid phase is unrecognizable and therefore resistant to EhVs infection. **(b)** Quorum-sensing molecules secreted by diploid *E. huxleyi* infected with EhVs induce the transition of neighboring cells to the haploid infection-resistant phase. **(c)** Like EhVs, giant virus infects and lysis only thophozoite cells, whereas the cysts are resistant to APMV and marseillevirus infection. **(d)** Putative quorum-sensing molecules secreted by trophozoites infected with giant viruses induce the transition of neighboring cells to the cyst-resistant phase.

of diploid *E. huxleyi* to EhVs induces the transition of neighboring cells to the haploid infection-resistant phase [14••]. In light of these observations, we propose that this theory could be expanded to the giant virus and *Acanthamoeba* world. Like *E. huxleyi*, these amoebas are able to escape the infection by giant viruses, such as mimivirus and also marseillevirus, when they are in a specific stage of their life cycle: the cyst (Figure 4) [4••]. Although there is a lack of information regarding soluble factors involved in amoebal communication that would be related to the triggering of encystment, previous data have shown that during APMV infection a small percentage of acanthamoeba cells are able to encyst (1–4%) (Figure 3) [4••,35]. Although it seems to be a catastrophe for an amoebal population, this may represent the survival of host species in a natural spot and/or circumstance. This drastic difference in viral susceptibility between life cycle stages provides an escape mechanism that ensures the survival of the *Acanthamoeba* and could be one of the reasons for the ecological and evolutionary success of this genus (Figure 3) [47,48].

The 'Cheshire Cat' strategy may be considered an opposite force to the classic 'Red Queen' co-evolutionary arms race theory, however they can be seen as complementary forces [14••,15]. The 'Cheshire Cat' dynamics liberate the amoebas from short-term viral pressure, thus allowing the host to evolve resistance to other stress factors. However, over a much longer time than classically inferred, a counteractive evolution of new arms by the virus may occur. The capacity of mimivirus to prevent the encystment process when the infection has already been initiated could be an example of the occurrence of 'Red Queen' theory. In light of this, the simultaneous occurrence of both theories seems to drive the evolution of giant viruses and their hosts.

Conclusions

Encystment is a complex process that could be triggered by several different stimuli and induces morphological changes that are regulated at the molecular level. Cysts are essential for the persistence and spreading of amoebas, and also protect *Acanthamoeba* populations against giant virus infections, in a similar pattern to the one observed in the described 'Cheshire Cat' strategy, representing an important barrier to giant virus dissemination. On the other hand, by the classic 'Red Queen' coevolutionary arms race, we discussed the capacity of mimivirus to prevent the encystment process, when the infection

has already been initiated, thus maintaining the susceptibility of amoebas to infection by viruses and other endosymbionts.

Studies focusing on the interactions between *Acanthamoeba* spp. and the infecting giant viruses are still at the beginning and more efforts are necessary to understand this unique and ancient host–pathogen interaction.

Acknowledgements

Scholarships were provided by the Conselho Nacional de Desenvolvimento Científico e Tecnológico, the Fundação de Amparo à Pesquisa do Estado de Minas Gerais and Coordenação de Aperfeiçoamento de Pessoal de Nível Superior.

References and recommended reading

Papers of particular interest, published within the period of review, have been highlighted as:

- • of special interest
- •• of outstanding interest

1. Dendana F, Sellami A, Sellami H, Cheikhrouhou F, Neji S, Makni F, Ayadi A: **Pathogenic free-living amoebae: epidemiology and clinical review**. *Pathologie Biologie* 2012, **60**:399-405.

2. Abedkhojasteh H, Niyyati M, Rezaei S, Mohebali M, Farnia S, Kazemi-Rad E, Roozafzoon R, Sianati H, Rezaeian M, Heidari M: **Identifying differentially expressed genes in trophozoites and cysts of *Acanthamoeba* T4 genotype: implications for developing new treatments for *Acanthamoeba* keratitis**. *Eur J Protistol* 2015, **51**:34-41.

3. • Siddiqui R, Khan NA: **Biology and pathogenesis of *Acanthamoeba***. *Parasit Vectors* 2012, **5**:6.
A comprehensive review describing the biology, classification, ecology and also the clinical role of *Acanthamoeba*.

4. •• Boratto P, Albarnaz JD, Almeida GM, Botelho L, Fontes AC, Costa AO, Santos Dde A, Bonjardim CA, La Scola B, Kroon EG *et al.*: **Acanthamoeba polyphaga mimivirus prevents amoebal encystment-mediating serine proteinase expression and circumvents cell encystment**. *J Virol* 2015, **89**:2962-2965.
One of the first studies to describe the host–pathogen interaction concerning mimivirus and *Acanthamoeba*, showing a drastic difference in viral susceptibility between life cycle stages of *Acanthamoeba* and the ability of APMV prevent the encystment process.

5. La Scola B, Raoult D: **Survival of *Coxiella burnetii* within free living amoeba *Acanthamoeba castellanii***. *Clin Microbiol Infect* 2001, **7**:75-79.

6. Boratto PV, Dornas FP, Andrade KR, Rodrigues R, Peixoto F, Silva LC, La Scola B, Costa AO, de Almeida GM, Kroon EG *et al.*: **Amoebas as mimivirus bunkers: increased resistance to UV light, heat and chemical biocides when viruses are carried by amoeba hosts**. *Arch Virol* 2014, **159**:1039-1043.

7. Raoult D, Boyer M: **Amoebae as genitors and reservoirs of giant viruses**. *Intervirology* 2010, **53**:321-329.

8. •• La Scola B, Audic S, Robert C, Jungang L, de Lamballerie X, Drancourt M, Birtles R, Claverie JM, Raoult D: **A giant virus in amoebae**. *Science* 2003, **299**:2033.
A study describing the discovery of APMV and also the genomic and biological characterization of this first member of the *Mimiviridae* family.

9. Claverie JM, Ogata H, Audic S, Abergel C, Suhre K, Fournier PE: **Mimivirus and the emerging concept of giant virus**. *Virus Res* 2006, **117**:133-144.

10. Raoult D: **The journey from Rickettsia to Mimivirus**. *ASM News* 2005, **71**:278-284.

11. Raoult D, La Scola B, Birtles R: **The discovery and characterization of Mimivirus the largest known virus and putative pneumonia agent**. *Clin Infect Dis* 2007, **45**:95-102.

12. Arslan D, Legendre M, Seltzer V, Abergel C, Claverie JM: **Distant Mimivirus relative with a larger genome highlights the fundamental features of Megaviridae**. *Proc Natl Acad Sci U S A* 2011, **108**:17486-17491.

13. Rodrigues RA, Silva LK, Dornas FP, de Oliveira DB, Magalhães TF, Santos DA, Costa AO, de Macêdo Farias L, Magalhães PP, Bonjardim CA *et al.*: **Mimivirus fibrils are important for viral attachment to microbial world by a diverse glycoside interaction repertoire**. *J Virol* 2015. pii: JVI. 01976-15.

14. •• Frada M, Probert I, Allen MJ, Wilson WH, de Vargas C: **The "Cheshire Cat" escape strategy of the coccolithophore *Emiliania huxleyi* in response to viral infection**. *Proc Natl Acad Sci U S A* 2008, **105**:15944-15949.
An important study describing a curious relationship between the phycodnavirus *Emiliania huxleyi* virus (EhVs) and the photosynthetic unicellular eukaryote *Emiliania huxleyi*, that is named by the authors as 'Cheshire Cat' strategy.

15. Van Valen L: **A new evolutionary law**. *Evol Theory* 1973, **1**:1-30.

16. • Fouque E, Trouilhé MC, Thomas V, Hartemann P, Rodier MH, Héchard Y: **Cellular, biochemical, and molecular changes during encystment of free-living amoebae**. *Eukaryot Cell* 2012, **11**:382-387.
A comprehensive review describing the main factors involved in the encystment process of free-living amoebas, including *Acanthamoeba*.

17. Lloyd D: **Encystment in *Acanthamoeba castellanii*: a review**. *Exp Parasitol* 2014, **145**:S20-S27.

18. Castrillón JC, Orozco LP: ***Acanthamoeba* spp. como parásitos patógenos y oportunistas**. *Rev Chilena Infectol* 2013, **30**:147-155.

19. Moon EK, Chung DI, Hong YC, Kong HH: **Characterization of a serine proteinase mediating encystation of *Acanthamoeba***. *Eukaryot Cell* 2008, **7**:1513-1517.

20. Aksozek A, McClellan K, Howard K, Niederkorn JY, Alizadeh H: **Resistance of *Acanthamoeba castellanii* cysts to physical, chemical and radiological conditions**. *J Parasitol* 2002, **88**:621-623.

21. Byers TJ: **Growth, reproduction, and differentiation in *Acanthamoeba***. *Int Rev Cytol* 1979, **61**:283-338.

22. Cordingley JS, Wills RA, Villemez CL: **Osmolarity is an independent trigger of *Acanthamoeba castellanii* differentiation**. *J Cell Biochem* 1996, **61**:167-171.

23. de Moraes J, Alfieri SC: **Growth, encystment, and survival, of *Acanthamoeba castellanii* grazing on different bacteria**. *FEMS Microbiol Ecol* 2008, **66**:221-229.

24. El-Etr SH, Margolis JJ, Monack D, Robison RA, Cohen M, Moore E, Rasley A: ***Francisella tularensis* type A strains cause the rapid encystment of *Acanthamoeba castellanii* and survive in amoebal cysts for three weeks postinfection**. *Appl Environ Microbiol* 2009, **75**:7488-7500.

25. Lee X, Reimmann C, Greub G, Sufrin J, Croxatto A: **The *Pseudomonas aeruginosa* toxin L-2-amino-4-methoxy-trans-3-butenoic acid inhibits growth and induces encystment in *Acanthamoeba castellanii***. *Microbes Infect* 2012, **14**:268-272.

26. Neff RJ, Ray SA, Benton WF, Wilborn M: **Induction of synchronous encystement (differentiation) in *Acanthamoeba* sp.** *Methods Cell* 1964, **1**:55-83.

27. Raizada MK, Murti CR: **Changes in the activity of certain enzymes of *Hartmannella* (Culbertson strain A-1) during encystment**. *J Protozool* 1971, **18**:115-119.

28. Jantzen H: **Control of actin synthesis during the development of *Acanthamoeba castellanii***. *Dev Biol* 1981, **82**:113-126.

29. Bouyer S, Rodier MH, Guillot A, Héchard Y: ***Acanthamoeba castellanii*: proteins involved in actin dynamics, glycolysis, and proteolysis are regulated during encystation**. *Exp Parasitol* 2009, **123**:90-94.

30. Moon EK, Chung DI, Hong YC, Kong HH: **Differentially expressed genes of *Acanthamoeba castellanii* during encystation**. *Korean J Parasitol* 2007, **45**:283-285.

31. Dudley R, Alsam S, Khan NA: **The role of proteases in the differentiation of *Acanthamoeba castellanii***. *FEMS Microbiol Lett* 2008, **286**:9-15.

32. Moon EK, Chung DI, Hong YC, Kong HH: **Autophagy protein 8 mediating autophagosome in encysting *Acanthamoeba***. *Mol Biochem Parasitol* 2009, **168**:43-48.

33. Leitsch D, Köhsler M, Marchetti-Deschmann M, Deutsch A, Allmaier G, Duchêne M, Walochnik J: **Major role for cysteine proteases during the early phase of *Acanthamoeba castellanii* encystment**. *Eukaryot Cell* 2010, **9**:611-618.

34. Moon EK, Hong Y, Chung DI, Kong HH: **Cysteine protease involving in autophagosomal degradation of mitochondria during encystation of Acanthamoeba**. *Mol Biochem Parasitol* 2012, **185**:121-126.

35. Akins RA, Byers TJ: **Differentiation promoting factors induced in acanthamoeba by inhibitors of mitochondrial macromolecule synthesis**. *Dev Biol* 1980, **78**:126-140.

36. Moon EK, Chung DI, Hong Y, Kong HH: **Protein kinase C signaling molecules regulate encystation of *Acanthamoeba***. *Exp Parasitol* 2012, **132**:524-549.

37. Steinert M, Birkness K, White E, Fields B, Quinn F: ***Mycobacterium avium* bacilli grow saprozoically in coculture with *Acanthamoeba polyphaga* and survive within cyst walls**. *Appl Environ Microbiol* 1998, **64**:2256-2261.

38. Varrot A, Leydier S, Pell G, Macdonald JM, Stick RV, Henrissat B, Gilbert HJ, Davies GJ: ***Mycobacterium tuberculosis* strains possess functional cellulases**. *J Biol Chem* 2005, **280**:20181-20184.

39. Kilvington S, Price J: **Survival of *Legionella pneumophila* within cysts of *Acanthamoeba polyphaga* following chlorine exposure**. *J Appl Bacteriol* 1990, **68**:519-525.

40. Boyer M, Yutin N, Pagnier I, Barrassi L, Fournous G, Espinosa L, Robert C, Azza S, Sun S, Rossmann MG *et al.*: **Giant Marseillevirus highlights the role of amoebae as a melting pot in emergence of chimeric microorganisms**. *Proc Natl Acad Sci U S A* 2009, **106**:21848-21853.

41. Ghigo E, Kartenbeck J, Lien P, Pelkmans L, Capo C, Mege JL, Raoult D: **Ameobal pathogen mimivirus infects macrophages through phagocytosis**. *PLoS Pathog* 2008, **4**:e1000087.

42. Legendre M, Santini S, Rico A, Abergel C, Claverie JM: **Breaking the 1000-gene barrier for Mimivirus using ultra-deep genome and transcriptome sequencing**. *Virol J* 2011, **8**:99.

43. Assis FL, Bajrai L, Abrahao JS, Kroon EG, Dornas FP, Andrade KR, Boratto PV, Pilotto MR, Robert C, Benamar S *et al.*: **Pan-genome analysis of Brazilian lineage A amoebal mimiviruses**. *Viruses* 2015, **7**:3483-3499.

44. Fritsche TR, Gautom RK, Seyedirashti S, Bergeron DL, Lindquist TD: **Occurrence of bacterial endosymbionts in *Acanthamoeba* spp. isolated from corneal and environmental specimens and contact lenses**. *J Clin Microbiol* 1993, **31**:1122-1126.

45. Greub G, Raoult D: **Microorganisms resistant to free-living amoebae**. *Clin Microbiol Rev* 2004, **17**:413-433.

46. Slimani M, Pagnier I, Raoult D, La Scola B: **Amoebae as battlefields for bacteria, giant viruses, and virophages**. *J Virol* 2013, **87**:4783-4785.

47. De Jonckheere JF: **Ecology of Acanthamoeba**. *Rev Infect Dis* 1991, **5**:S385-S387.

48. Geisen S, Fiore-Donno AM, Walochnik J, Bonkowski M: **Acanthamoeba everywhere: high diversity of Acanthamoeba in soils**. *Parasitol Res* 2014, **113**:3151-3158.

nature COMMUNICATIONS

ARTICLE

DOI: 10.1038/s41467-018-03168-1 OPEN

Tailed giant Tupanvirus possesses the most complete translational apparatus of the known virosphere

Jônatas Abrahão[1,2], Lorena Silva[1,2], Ludmila Santos Silva[1,2], Jacques Yaacoub Bou Khalil[3], Rodrigo Rodrigues[2], Thalita Arantes[2], Felipe Assis[2], Paulo Boratto[2], Miguel Andrade[4], Erna Geessien Kroon[2], Bergmann Ribeiro[4], Ivan Bergier[5], Herve Seligmann[1], Eric Ghigo[1], Philippe Colson[1], Anthony Levasseur[1], Guido Kroemer[6,7,8,9,10,11,12], Didier Raoult[1] & Bernard La Scola[1]

Here we report the discovery of two Tupanvirus strains, the longest tailed *Mimiviridae* members isolated in amoebae. Their genomes are 1.44–1.51 Mb linear double-strand DNA coding for 1276–1425 predicted proteins. Tupanviruses share the same ancestors with mimivirus lineages and these giant viruses present the largest translational apparatus within the known virosphere, with up to 70 tRNA, 20 aaRS, 11 factors for all translation steps, and factors related to tRNA/mRNA maturation and ribosome protein modification. Moreover, two sequences with significant similarity to intronic regions of 18 S rRNA genes are encoded by the tupanviruses and highly expressed. In this translation-associated gene set, only the ribosome is lacking. At high multiplicity of infections, tupanvirus is also cytotoxic and causes a severe shutdown of ribosomal RNA and a progressive degradation of the nucleus in host and non-host cells. The analysis of tupanviruses constitutes a new step toward understanding the evolution of giant viruses.

[1] MEPHI, APHM, IRD 198, Aix Marseille Univ, IHU-Méditerranee Infection, 19-21 Bd Jean Moulin, 13005 Marseille, France. [2] Laboratório de Vírus, Instituto de Ciências Biológicas, Departamento de Microbiologia, Universidade Federal de Minas Gerais, Belo Horizonte 31270-901, Brazil. [3] CNRS, 13005 Marseille, France. [4] Laboratório de Microscopia Eletrônica e Virologia, Departamento de Biologia Celular, Instituto de Ciências Biológicas, Universidade de Brasília, Asa Norte, Brasília 70910-900, Brazil. [5] Lab. Biomass Conversion, Embrapa Pantanal, R. 21 de Setembro 1880, 79320-900 Corumbá/MS, Brazil. [6] Cell Biology and Metabolomics Platforms, Gustave Roussy Cancer Campus, Villejuif 94805, France. [7] Equipe 11 labellisée Ligue Nationale contre le Cancer, Centre de Recherche des Cordeliers, Paris 75006, France. [8] Institut National de la Santé et de la Recherche Médicale (INSERM), Paris 75654, France. [9] Université Paris Descartes, Sorbonne Paris Cité, Paris 75015, France. [10] Université Pierre et Marie Curie, Paris 75005, France. [11] Pôle de Biologie, Hôpital Européen Georges Pompidou, AP-HP, Paris 75015, France. [12] Department of Women's and Children's Health, Karolinska University Hospital, Stockholm SE-171 76, Sweden. Jônatas Abrahão, Lorena Silva and Ludmila Santos Silva contributed equally to this work. Correspondence and requests for materials should be addressed to D.R. (email: didier.raoult@gmail.com) or to B.S. (email: bernard.la-scola@univ-amu.fr)

Translation is one of the canonical frontiers between the cell world and the virosphere. Even the simplest non-viral obligatory intracellular parasites present a wealthy set of translation apparatus, including aminoacyl tRNA synthetases, tRNAs, peptide synthesis factors and ribosomal proteins[1–3]. The nature of the parasitism of the most of non-viral obligatory intracellular parasites relies on partial or severe deficiency of genes related to energy production. Although sharing a similar lifestyle with those organisms, the most of the virus lack not only energy production genes, but also translation-related genes[1–3].

In this context, the discovery of mimiviruses and other amoeba-infecting giant viruses surprised the scientific community due their unusual sizes and long genomes, able to encode from hundreds to thousands of genes, including tRNAs, peptide synthesis factors and, for the first time seen in the virosphere, aminoacyl tRNA synthetases (aaRS)[4]. Although the very first discovered mimivirus (*Acanthamoeba polyphaga mimivirus*) encodes four different types of aaRS (Arg, Cys, Met, TyrRS), other mimivirus isolates genomes were described, containing up to seven types of aaRS, as Megavirus chilensis and LBA111 (Arg, Asn, Cys, Ile, Met, Trp, TyrRS)[5]. While amoeba-infecting mimiviruses present up to six copies of tRNA, *Cafeteria roenbergensis virus* (CroV), a group II algae-infecting of *Mimiviridae*, encodes 22 sequences for five different tRNAs[5]. Even more surprisingly, metagenomics data reveal that klosneuvirus genome may encodes aaRS with specificities for 19 different amino acids, over 10 translation factors and several tRNA-modifying enzymes[6]. However, klosneuviruses were not isolated and therefore there is no data regarding important biological features as virus particles, morphogenesis and host-range.

Here we report the discovery of two Tupanvirus strains, the longest tailed *Mimiviridae* members isolated in amoebae. Their genomes are 1.44–1.51 Mb linear double-strand DNA coding for 1276–1425 predicted proteins. Tupanviruses share the same ancestors with mimivirus lineages and these giant viruses present the largest translational apparatus within the known virosphere, with up to 70 tRNA, 20 aaRS, 11 factors for all translation steps, and factors related to tRNA/mRNA maturation and ribosome protein modification. Moreover, two sequences with significant similarity to intronic regions of 18 S rRNA genes are encoded by the tupanviruses and highly expressed. In this translation-associated gene set, only the ribosome is lacking. Tupanvirus is also cytotoxic and causes a severe shutdown of ribosomal RNA and a progressive degradation of the nucleus in host and non-host cells. The analysis of tupanviruses constitutes a new step towards understanding the evolution of giant viruses.

Results

Tupanviruses description and cycle. While attempting to find new and distant relatives of currently known giant viruses, we performed prospecting studies in special environments. Soda lakes (Nhecolândia, Pantanal biome, Brazil) are known as environments that conserve and/or mimic ancient life conditions (extremely high salinity and pH) and are considered some of the most extreme aquatic environments on Earth[7]. We also prospected giant viruses in ocean sediments collected at a depth of 3000 m (Campos dos Goytacazes, Brazilian Atlantic Ocean).

Both in soda lake and deep ocean samples, we found optically visible *Mimiviridae* members that surprisingly harbored a long, thick tail (Fig. 1a, b) as they grew on *Acanthamoeba castellanii* and *Vermamoeba vermiformis*. We named these strains Tupanvirus soda lake and Tupanvirus deep ocean as a tribute to the South American Guarani Indigenous tribes, for whom Tupan—or Tupã—(the God of Thunder) is one of the main mythological figures. Electron microscopy analyses revealed a remarkable virion structure. Tupanviruses present a capsid similar to that of amoebal mimiviruses in size (~450 nm) and structure, including a stargate vertex and fibrils[8] (Figs. 1a–d, 2a–q). However, the Tupanvirus virion presents a large cylindrical tail (~550 nm extension; ~450 nm diameter, including fibrils) attached to the base of the capsid (Figs. 1b–d, 2a,i–k). This tail is the longest described in the virosphere[9]. Microscopic analysis suggests that the capsid and tail are not tightly attached (Figs. 1e, f, 2a, i; Supplementary Movies 1 and 2), although sonication and enzymatic treatment of purified particles were not able to separate the two parts (Fig. 2f–h). The average length of a complete virion is ~1.2 µm, although some particles can reach lengths of up to 2.3 µm because of the variation in the tail's size; this makes them the one of the longest viral particles described to date (Figs. 1, 2i–k). Furthermore, there is a lipid membrane inside the capsid, which is associated with the fusion with the cellular membrane and the release of capsid content (Fig. 1f). Tail content appears to be released after an invagination of the phagosome membrane inside the tail (Fig. 1e). In contrast

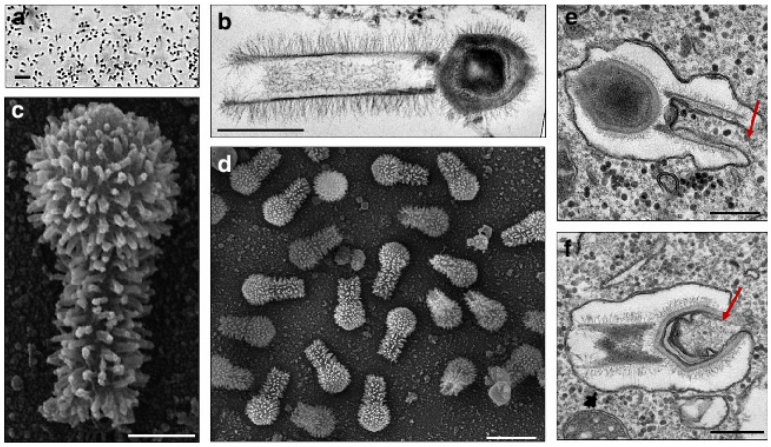

Fig. 1 Tupanvirus soda lake particles and cycle. **a** Optical microscopy of Tupanvirus particles after haemacolour staining (1000 ×). Scale bar, 2 µm. **b** Super particle (>1000 nm) observed by transmission electron microscopy (TEM). Scale bar, 500 nm. **c**, **d** Scanning electron microscopy (SEM) of Tupanvirus particles. Scale bars 250 nm and 1 µm, respectively. **e**, **f** The initial steps of infection in *A. castellanii* involve the release of both capsid (**e**) and tail (**f**) content into the amoeba cytoplasm (red arrows). Scale bars, 350 nm and 450 nm, respectively

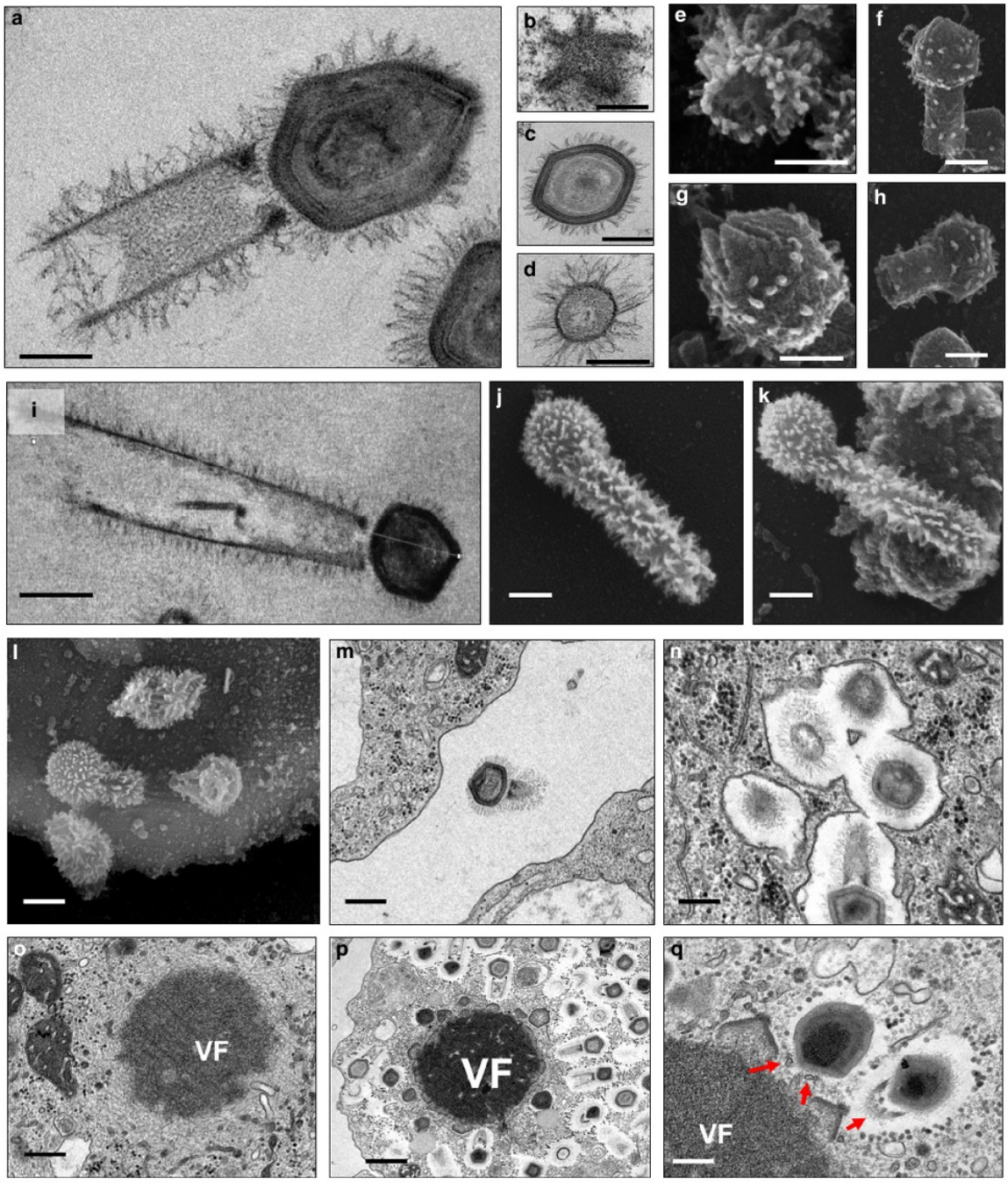

Fig. 2 Tupanvirus soda lake particles and cycle features. **a** Transmission electron microscopy (TEM) highlights the inner elements of the whole particle. Scale bar, 200 nm. **b** Star-gate vertex transversally cut. Scale bar, 100 nm. **c** Capsid transversally cut. Scale bar, 100 nm. **d** Tail transversally cut. Scale bar, 200 nm. **e**–**h** Scanning electron microscopy (SEM) of purified particles. Scale bars, 250 nm. The treatment of particles with lysozyme, bromelain and proteinase-K removed most of the fibers, revealing head and tail junction details. Super particles (>2000 nm) could be observed by TEM (**i**) and SEM (**j**, **k**). Scale bars, 400 nm. Cycle steps are shown from **l**–**r**. **l** Viral particle attachment to *Acanthamoeba castellanii* surface; scale bar, 500 nm; **m** phagocytosis; scale bar, 500 nm; **n** particles in a phagosome; scale bar, 500 nm; **o** early viral factory; scale bar, 500 nm; and **p**, **q** mature viral factories. Scale bars 1 µm and 250 nm, respectively. Arrows highlight tail formation associated with the viral factories. VF viral factory

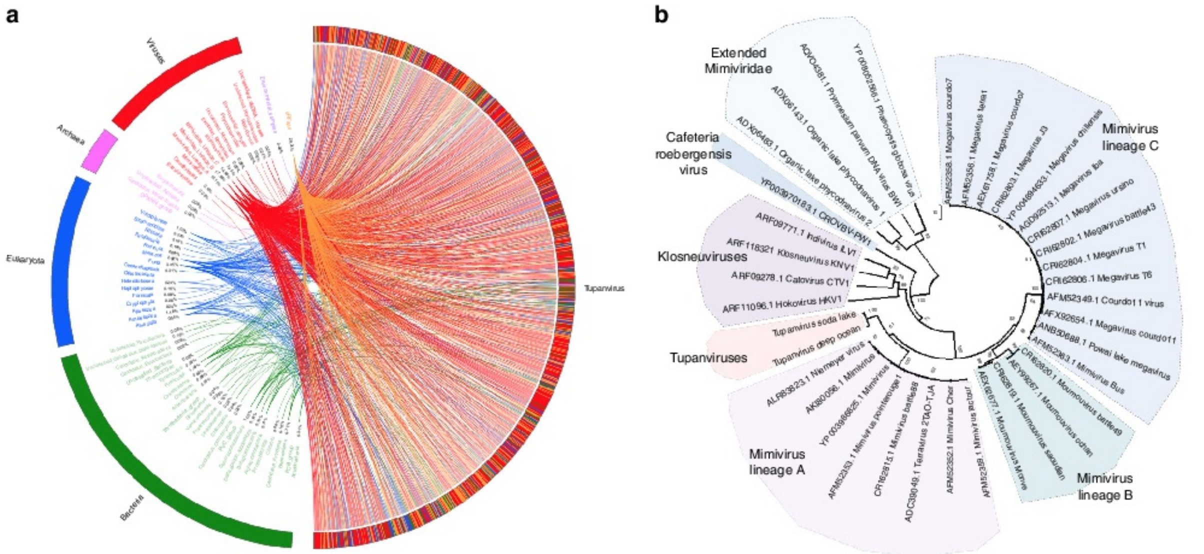

Fig. 3 Tupanvirus soda lake rhizome and Mimiviridae family B DNA polymerase tree. **a** The rhizome shows that most Tupanvirus soda lake genes have mimiviruses as best hits. However, correspondence among Tupanvirus and *Archaea*, *Eukaryota*, *Bacteria* and other viruses was also observed. **b** Family B DNA polymerase maximum likelihood phylogenetic tree demonstrating the position of Tupanvirus among *Mimiviridae* members, likely forming a new genus

to other giant viruses[10–14], Tupanviruses similarly replicate both in *A. castellanii* and *V. vermiformis*. Viral particles attach to the host-cell surface and enter through phagocytosis (1 h.p.i.) (Fig. 2 l,m,n). The inner membrane of the capsid merges with the amoebal host phagosome membrane, releasing the genome (2–6 h.p.i.) (Fig. 1f). A viral factory (VF) is then formed (7–12 h. p.i.)[15] where particle morphogenesis occurs (Fig. 2o–q; Supplementary Movies 1 and 2). During this step, the virion tail is attached to the capsid after its formation and closure. Later in the process (16–24 h.p.i.), the amoebal cytoplasm is filled with viral particles, followed by cell lysis and the release of viruses (Supplementary Fig. 1). This nucleus-like viral factory has also recently been reported in bacteria and fuels the concept of a virocell[16,17]. In that perspective, viral factories actively producing the progeny could be considered as the nuclei of virocells[16,17].

The genomes of tupanviruses. The tupanvirus soda lake and tupanvirus deep ocean genomes (GenBank accession number KY523104 and MF405918) are linear dsDNA molecules measuring 1,439,508 bp and 1,516,267 bp (GC% ~28%), respectively—the fourth largest viral genomes described to date[10,18]—containing a total of 1276 and 1425 predicted ORFs, 375 and 378 of which are ORFans (ORFs with no matches in current databases), respectively. To date, the largest genomes belong to pandoravirus isolates, and the largest one, *P. salinus*, has 2,473,870 bp and encodes 2,556 putative proteins[10]. The rhizome[19] of tupanvirus (graphical representation of gene-by-gene best hits) revealed sequences from mimiviruses of amoebae (~42%) and klosneuviruses (~8%) as their main best hits. Other best hits were mostly sequences from eukaryotes (~11%) and bacteria (~8%) (Fig. 3a; Supplementary Fig. 2A). Tupanviruses exhibited relatively close numbers of best matches to amoebal mimiviruses from lineages A (~10%), B (~18%) and C (~14%). These data and phylogenetic analyses demonstrate that they cluster with amoebal mimiviruses, suggesting that tupanviruses are distant relatives of, and comprise a sister group to, mimiviruses of amoeba (Figs. 3b, 4a). The 'AAAATTGA' promoter motif was found ~410 times in Tupanvirus deep ocean intergenic regions, a frequency similar to that of other *Mimiviridae* members, and ~600% more frequent than those coding regions ($p < 10^{-95}$, Fisher exact test)[20–22] (Fig. 4b). The pangenome of the family *Mimiviridae*, when taking into account the gene contents of tupanviruses, klosneuviruses and distant relatives to amoebal mimiviruses, was found by Proteinortho to comprise 8,753 groups of orthologues ($n = 3588$) or virus unique genes ($n = 5165$). A total of 189 groups were shared by at least one tupanvirus; one mimivirus of *Acanthamoeba* of each lineage A, B and C; and one klosneuvirus, and 100 of them were also shared with Cafeteria roenbergensis virus. In addition, a total of 757 groups were shared by a tupanvirus and at least another mimivirus: 477 were shared with Megavirus chiliensis, 434 with Moumouvirus, 431 with Mimivirus, 287 with Klosneuvirus, 126 with Cafeteria roenbergensis virus, and 59 with Phaeocystis globosa virus 12 T. Among these 757 groups, 583 corresponded to clusters of orthologous groups previously delineated for mimiviruses[19]. Finally, a total of 775 tupanvirus genes were absent from all other mimivirus genomes (Supplementary Data 1).

Proteomic analysis. Proteomic analysis of Tupanvirus soda lake particles revealed 127 proteins, nearly half ($67/127 = 52.8\%$) of which are unknown and eight of which are encoded by ORFans ($11/127 = 8.6\%$) (Supplementary Data 2; Supplementary Note 1). Although 62 Tupanvirus virion proteins homologous were not found by proteomics, either in Mimivirus or in *Cafeteria roenbergensis virus* particles, there are no distinct clues about which protein (s) could be associated with the tupanvirus fibrils and tail structure.

The most complete translational apparatus of the virosphere. Analyses of the tupanvirus gene sets related to energy production revealed a clear dependence of these viruses on host energy production mechanisms, similarly to other mimiviruses, because genes involved in glycolysis, the Krebs cycle and the respiratory chain are mostly lacking[22–24]. Astonishingly, Tupanvirus soda lake and Tupanvirus deep ocean exhibit the largest viral sets of genes involved in translation, with 20 ORFs related to aminoacylation (aaRS) and transport, and 67 and 70 tRNA associated with 46 and 47 codons, respectively (Fig. 5a; Supplementary

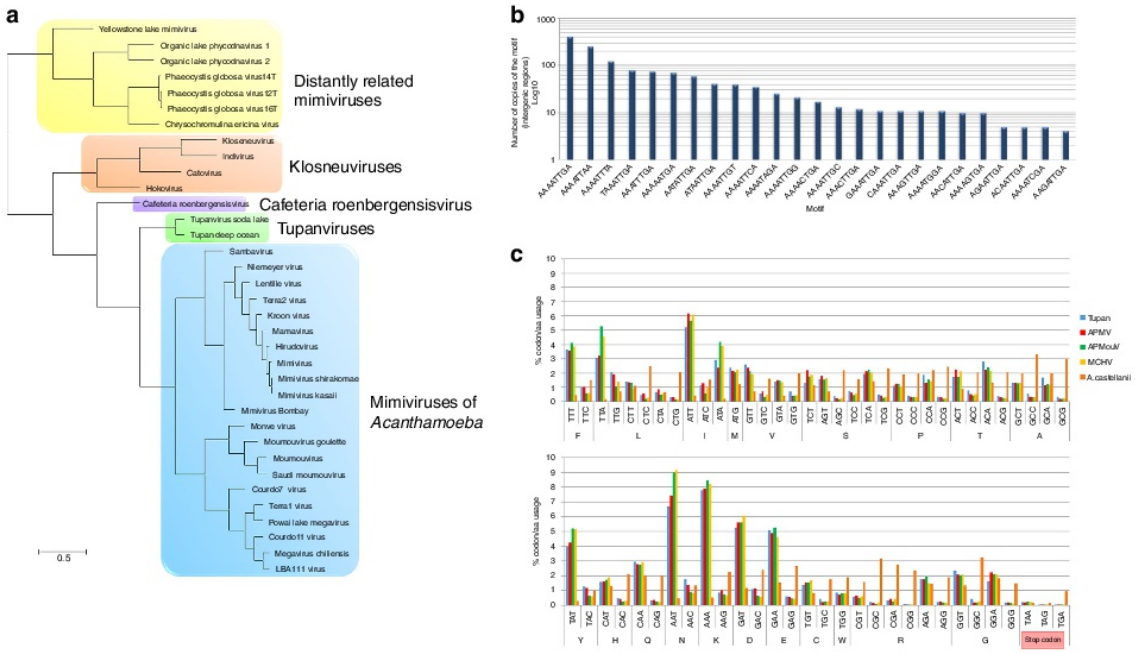

Fig. 4 Tupanvirus soda lake hierarchical clustering, promoter's motifs and amino-acid usage analysis. **a** Hierarchical clustering tree based on presence-absence matrix of cluster of orthologous genes shared by *Mimiviridae* members. **b** Frequency of mimivirus AAAATTGA canonical promoter motifs in Tupanvirus intergenic regions. We also analyzed the presence of the AAAATTGA motif with SNPs, considering each motif position. **c** Comparative amino-acid usage analysis of Tupan, *A. castellanii* and mimivirus lineages **a**, **b** and **c**. The amino-acid usage for protein sequences was calculated using the CGUA (General Codon Usage Analysis) tool

Fig. 2B, C, 3 and 7; Supplementary Datas 3 and 4). Tupanvirus deep ocean encodes an ambiguous tRNA related to the rare amino-acid pyrrolysine. Only selenocysteine-related genes are lacking, as previously observed for many cellular organisms[25]. Several translation factors were identified, including eight translation initiation factors (IF2 alpha, IF2 beta, IF2 gamma, IF4e (2 copies in Tupanvirus soda lake), IF5a (2 copies in Tupanvirus deep ocean), SUI1, IF4a), one elongation/initiation factor (GTP-binding elongation/initiation), one elongation factor (Ef-aef-2), and one release factor (ERF1) (Fig. 5a; Supplementary Fig 2B, C and 3; Supplementary Datas 3 and 4). Furthermore, we detected additional translation-related genes: factors related to tRNA maturation and stabilization (tRNA nucleotidyltransferase, tRNA guanylyltransferase, cytidine deaminase, RNA methyl transferase); mRNA maturation (poly(A) polymerase, mRNA capping enzyme) and splicing (RNA 2—phosphotransferase Tpt1 family protein); and ribosomal protein modification (ribosomal-protein-alanine N-acetyltransferase, FtsJ-like methyl transferase) (Fig. 5a; Supplementary Fig 2B; Supplementary Datas 3, 4). Phylogenies based on aaRS are acknowledged to be complex as they depend on sequence sampling, and natural and canonical taxonomical groups can be separated into different clades, as previously observed[6]. To reduce such disturbances in the trees during their construction, we selected the 100 best hits related to Tupanvirus soda lake, plus the sequences of 5–10 amoebozoa and those of klosneuviruses. In most of the trees, sequences from natural clades were clustered together, although some amoebozoa were separated into different clusters. Based on the 20 aaRS trees, it is not possible to state that the origin of most of these tupanvirus aaRS genes is cellular (Supplementary Fig. 4). Furthermore, the mosaic structure of aaRS gene reinforced the difficult to state on the origin of these genes, as illustrated in Supplementary Fig. 5. This contrasting result to that reported by Schultz et al.[6], 2017 for klosneuviruses may also be explained by the different sampling used for alignments and trees construction. In addition, the codon and amino-acid usage of tupanviruses is substantially different from that of *Acanthamoeba* spp. In tupanviruses, we observed a high correlation between tRNA isoacceptors and the most used codons, as these viruses present more tRNA isoacceptors for highly abundant codons (Fig. 4c; Supplementary Figs. 2C and 3). Surprisingly, we found two different copies of an 18 S rRNA intronic region in tupanviruses (Supplementary Fig. 6; Fig. 6a–e). In fact, such 18 S rRNA intronic regions are widespread in all mimiviruses (lineages A and B present only one copy in an intronic region and next to a self-splicing group I intron endonuclease) but are not found in klosneuviruses. Phylogenetic analyses revealed that the two copies found in tupanviruses had separate and different origins (Fig. 6f). Although Tupanvirus 18 S rRNA intronic sequences are located in intergenic regions, qPCR and FISH demonstrated that Tupanvirus soda lake 18 S rRNA intronic sequences are highly expressed during the entire replicative cycle but particularly during intermediate and late phases (6 and 12 h post-infection) (Fig. 7a; Supplementary Fig. 8). Furthermore, Tupanvirus soda lake is more tolerant to the translation-inhibiting drugs geneticin and cycloheximide than Mimivirus, an impressive characteristic considering the natural ribosomal RNA shutdown it performs in the permissive host (Fig. 8h). The functions of these 18 S rRNA intronic region sequences require further clarification. No exonic region of 18 S rRNA was found in the genomes of tupanviruses or any previously described mimivirus. The comparison between contents in translation-related categories of genes present in tupanviruses and cellular organisms reveals that tupanviruses present a richer gene set than *Candidatus Carsonella ruddii* (*Bacteria*) and *Nanoarchaeum equitans* (*Archaea*) (not considering ribosomal proteins). Tupanvirus deep ocean has even

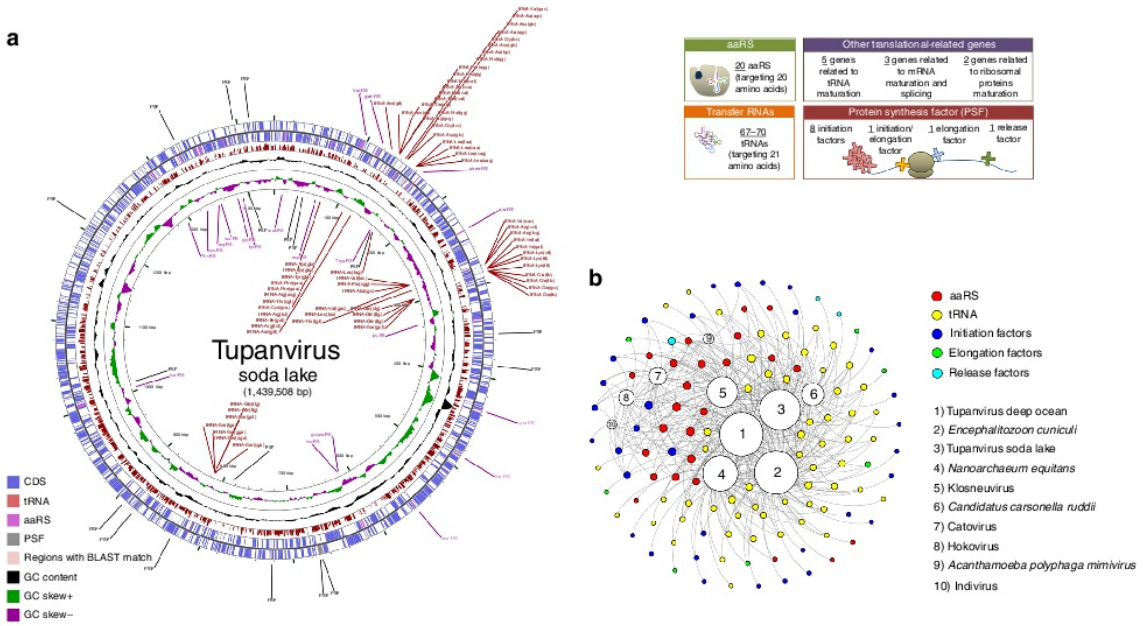

Fig. 5 Tupanvirus genome-translation-related factors. **a** Circular representation of Tupanvirus soda lake genome highlighting its translation-related factors (aaRS, tRNAs and PSF). The box (upright) summarizes this information and considers the Tupanvirus deep ocean data set. **b** Network of shared categories of translation-related genes (not considering ribosomal proteins) present in tupanviruses, Mimivirus (APMV), Klosneuvirus, Catovirus, Hokovirus, Indivirus and cellular world organism—*Encephalitozoon cuniculi* (*Eukaryota*), *Nanoarchaeum equitans* (*Archaea*) and *Candidatus Carsonella ruddii* (*Bacteria*). The diameter of the organism's circles (numbers) is proportional to the number of translation-related genes present in those genomes. CDS coding sequences, tRNA transfer RNA, aaRS aminoacyl tRNA synthetase, PSF protein synthesis factors

more such genes than *Encephalitozoon cuniculi*, a eukaryotic organism (Fig. 5b). Even if the impressive translation gene set recently described for klosneuviruses is taken into account, tupanviruses are the first viruses reported to harbor the complete set of the 20 aaRS (Fig. 5; Supplementary Figs. 3, 6 and 7).

Host range and host-ribosomal shutdown characterization. In contrast to other mimiviruses, Tupanvirus soda lake was able to infect a broad range of protist organisms in vitro. Surprisingly, we observed four distinct profiles of infectiveness: (i) productive cycle in permissive cells; (ii) abortive cycle; (iii) refractory cells; and (iv) most surprisingly, non-host cells exhibiting a cytotoxic phenotype in the presence of Tupanvirus without multiplication, a circumstance never previously reported—to the best of our knowledge (Supplementary table 1; Supplementary Notes 1). This latter profile was intriguing because toxicity was observed in *Tetrahymena* sp., a ravenous free-living protist[26]. This unusual phenotype was also observed in *A. castellanii* but only at higher multiplicities of infection (50 and 100; Fig. 8a). No such cytotoxicity was observed for Mimivirus (Fig. 8a). This toxic profile associated specifically with Tupanvirus appears to be related to shutting down host ribosomal RNA abundance, insofar that Tupanvirus leads to a reduction of host rRNA amounts by a mechanism not related to the canonical ribophagy/autophagy process (Figs. 7b–d, 8b–d; Supplementary Fig. 9). A remarkable acidification of amoebal cytoplasm is induced by Tupanvirus infection (but not mimivirus) (Fig. 7b; Supplementary Fig. 9A, B). The treatment of acanthamoeba with chloroquine, a lysosomal toxin, or bafilomycin did not prevent the Tupanvirus-induced rRNA shutdown (Supplementary Fig. 9A, C–H). Transfection with an siRNA targeting Atg8-2, a protein required for ribophagy/autophagy, failed to prevent Tupanvirus-induced ribosomal shutdown in *A. castellanii* (Fig. 7c, d). Transmission electron microscopy (TEM) of vesicles containing ribosomes after Tupanvirus infection (2 h.p.i.) revealed that these structures were formed close to the nuclear membrane after invagination and engulfment of ribosomes, mostly by single-membrane vesicles, rarely by double-membrane vesicles (Fig. 7e). These small vesicles then aggregated, accumulating more ribosomes and forming large structures containing ribosomes (Fig. 8d), which were fully depleted from the amoebal cytoplasm 6–9 h.p.i, when strong cellular rRNA shutdown could be detected (Fig. 8c). In addition, Tupanvirus infection induces nuclear/nucleolar progressive degradation, which is temporally associated with cellular rRNA shutdown (Fig. 7f). Mimivirus infection also caused changes in nucleolus architecture, but such alterations were not comparable to those observed upon Tupanvirus infection (Fig. 7e, f). Although the formation of vesicles containing ribosomes and nuclear degradation can be related to cellular rRNA shutdown during Tupanvirus infection, the mechanisms involved in cellular rRNA degradation after the formation of large vesicles containing ribosomes remain to be investigated. One possibility that should be explored is that Tupanvirus might preferentially target some ribosomes to favor the translation of its own (as opposed to cellular) proteins, as previously described for poxviruses[27].

The toxicity effect and rRNA shutdown are independent of Tupanvirus replication; instead, they are caused by the viral particle (Fig. 8e–g). UV-light-inactivated particles continued to induce the depletion of *Acanthamoeba* rRNA (Fig. 8g). Although Tupanvirus is not able to replicate within *Tetrahymena* sp., it is phagocytosed in a voracious manner (as are other available macromolecular structures) and forms large intracellular vesicles, where the capsid and tail release their content inside the protist cytoplasm (Fig. 8i–k). The virus induces gradual vacuolization (Fig. 8i), loss of motility, a decrease in the phagocytosis rate

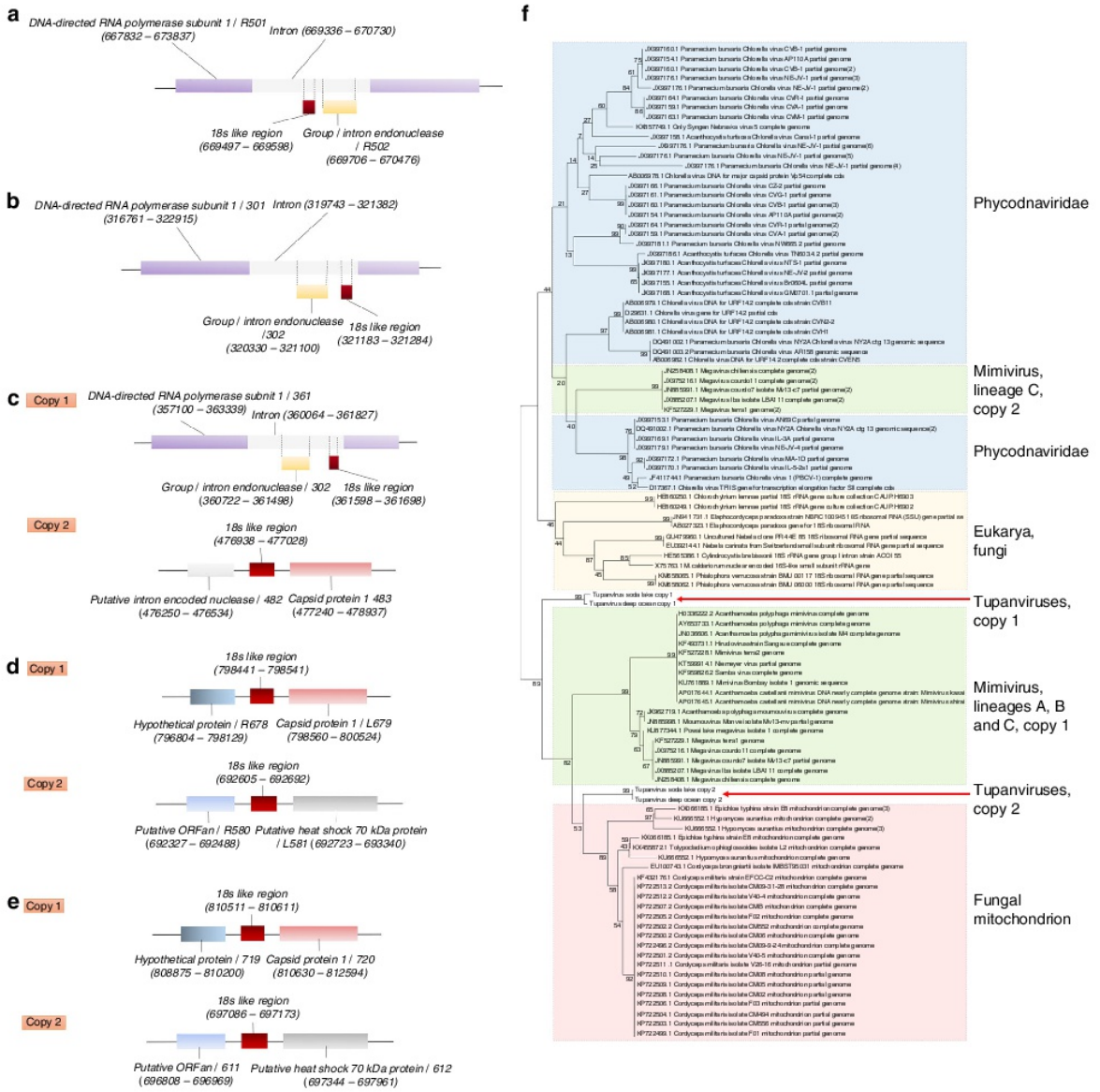

Fig. 6 Adjacent regions of 18S rRNA intronic sequences in the genus *Mimivirus* and Tupanvirus and maximum likelihood phylogenetic tree of 18S rRNA intronic region. Core sequences are represented for lineages A (**a**), B (**b**), C (**c**), Tupanvirus soda lake (**d**) and Tupanvirus deep ocean (**e**). Phylogenetic tree of 18S rRNA intronic region present in mimivirus (**e**), *Phycodnaviridae*, eukaryotes and fungi mitochondrion

(Fig. 8m), a decrease in rRNA abundance (Fig. 8l) and triggers nuclear degradation (Fig. 7g), similar to the effects observed in *A. castellanii* cells with high multiplicities of infection (Fig. 8a–d). We performed in vitro simulations to determine whether this toxicity could affect the maintenance of Tupanvirus populations in a solution containing both *Tetrahymena* and *Acanthamoeba*. Our data suggest that at M.O.I. of 10 the reduction of the physiological activity of *Tetrahymena* sp., a (non-host) predator, decreases the ingestion of Tupanvirus particles (Fig. 8n), improving their chances to find its host, *Acanthamoeba*, and keeping viral titers constant in the system. In contrast, mimivirus particles, which do not present any toxicity to *Tetrahymena* sp., are quickly predated, and the virus is eliminated from the system after some days (Fig. 8n). Although we have no clues about the hosts of tupanviruses at their original habitats nor if such high M. O.I. would be expected in nature, to our knowledge, a viral particle responsible for the modulation of host and non-host organisms independent of viral replication has not been previously described.

Discussion

Considering that tupanviruses comprise a sister group to amoebal mimiviruses, we can hypothesize that the ancestors of these clades of *Mimiviridae* could had a more generalist lifestyle and were able to infect a wide variety of hosts. In this view, the ancestors of tupanviruses (and maybe of amoebal mimiviruses) might have already been giant viruses that underwent reductive evolution,

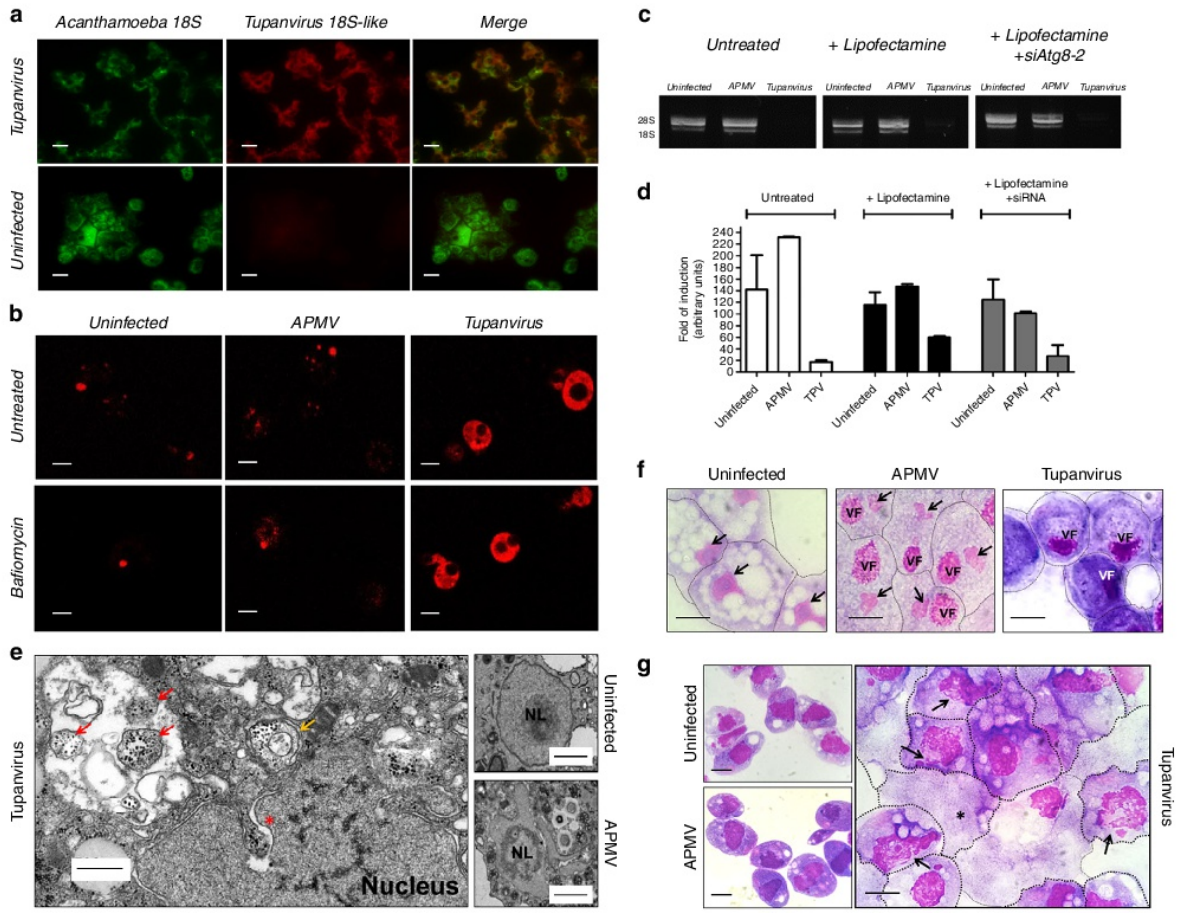

Fig. 7 Tupanvirus soda lake biological features in a host (*A. castellanii*) and non-host (*Tetrahymena* sp.). **a** Expression of Tupanvirus 18S intronic sequence-copy 1 transcript, 12 h post-infection observed by fluorescence in situ hybridization (FISH) (red). Tupanvirus-induced shutdown of *A. castellanii* ribosomal RNA18S transcripts (green). Scale bars, 10 µm. **b** Tupanvirus, but not mimivirus, induces strong acidification of *A. castellanii* cytoplasm (9 h.p.i.), even in the presence of bafilomycin A1. Scale bars, 10 µm. **c**, **d** The silencing of the canonical autophagy protein Atg8-2 does not prevent rRNA shutdown induced by Tupanvirus infection. Error bars, standard deviation. **e** Electron microscopy of *A. castellanii* infected by Tupanvirus (2 h.p.i.), highlighting the degradation of the nucleolus, nuclear disorganization and the formation of ribosome-containing vesicles near nuclear membranes. Scale bar, 500 nm. Red arrow: single-membrane vesicles containing ribosomes; orange arrow: double-membraned vesicles containing ribosomes; asterisk: ribosomes wrapping by the external nuclear membrane. Right: electron microscopy of uninfected amoebae and APMV infected cell (8 h.p.i.) showing a mild nucleolar disorganization in the presence of the virus. Scale bars: 1 µm. **f** Haemacolour staining showing the nuclear degradation of *A. castellanii* induced by Tupanvirus infection (9 h.p.i.) compared with infection by mimivirus (APMV) and uninfected cells. Tupanvirus-infected cells are purplish because of cytoplasm acidification. Scale bars, 5 µm. Arrows: nucleus, when present; VF: viral factory. **g** Haemacolour staining showing the nuclear degradation in *Tetrahymena sp.* induced by Tupanvirus infection (4 days post-inoculation) compared with mimivirus (APMV)-inoculated cells and uninfected cells. Tupanvirus-infected cells present an atypical shape and intense vacuolization, and some cells lack a nucleus (asterisk). Arrows: nucleus under degradation. Scale bars, 5 µm. The experiments were performed 3 times independently, with two replicates each

although some genes could have been acquired over time, as previously hypothesized for other mimiviruses[5,23,28,29]. A reductive evolution pattern is typical among obligatory intracellular parasites[30–32]. In these cases, the organisms lose genes related to energy production, which is one of the main reasons for their obligatory parasitic lifestyle. In an alternative scenario, a simpler ancestor could had substantially acquired genes over time and became more resourceful, being able to infect a broader host range[5,33]. Nevertheless, tupanvirus presents the most complete translational apparatus among viruses, and its discovery takes us one step forward in understanding the evolutionary history of giant viruses.

Methods

Virus isolation and host-range determination. In April 2014, a total of 12 sediment samples were collected from soda lakes in Southern Nhecolândia, Pantanal, Brazil. In 2012, 8 ocean sediments samples were collected from 3000 meters below water line surface at Bacia de Campos, in Campos dos Goytacazes, Rio de Janeiro, Brazil. The collection was performed by a submarine robot, during petroleum prospection studies performed by the Petrobras Company, and kindly provided to our group. The samples were stored at 4 °C until the inoculation process. The samples were transferred to 15 mL flasks, and 5 mL of Page's Amoebae Saline (PAS) was added. The solution was stored for 24 h to decant the sediment. The liquid was then subjected to a series of filtrations: first through paper filter and then through a 5 µm filter to remove large particles of sediment and to concentrate any giant viruses present. For co-culture, the cells used were *A. castellanii* (strain NEFF) and *V. vermiformis* (strain CDC 19), purchased from ATCC. These cell strains

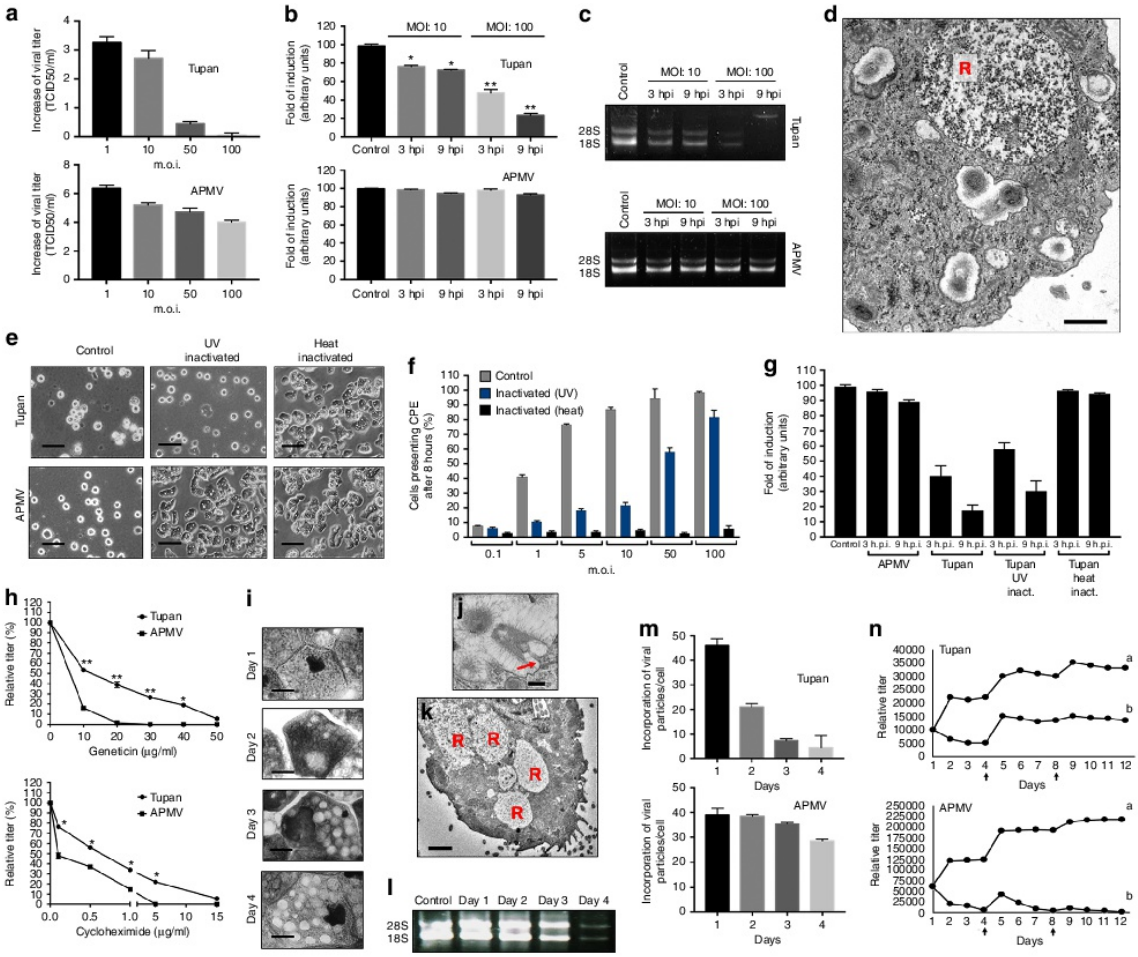

Fig. 8 rRNA shutdown induced by Tupanvirus and toxicity assays. **a** Tupanvirus and mimivirus titers (log_{10} values) 24 h.p.i. in *Acanthamoeba castellanii* at distinct MOIs. **b** Ribosomal 18S RNA relative measure by qPCR from *A. castellanii* infected by tupanvirus or mimivirus at an MOI of 10 or 100, 3 and 9 h post-infection. **c** Electrophoresis gel showing ribosomal 18S and 28S RNA from *A. castellanii* under the same conditions described in **b**. **d** Vesicle containing a large amount of *A. castellanii* ribosomes (R) 6 h after Tupanvirus infection. Scale bar, 1 µm. (**e**) Cytopathic effect of *A. castellanii* inoculated with Tupanvirus or mimivirus after UV or heat inactivation, MOI of 100, 8 h post-inoculation. Scale bar, 20 µm. **f** Counting of *A. castellanii* presenting cytopathic effect 8 h post-inoculation with tupanvirus inactivated by UV or heating under different MOIs. **g** Ribosomal 18S RNA relative measure by qPCR from *A. castellanii* infected by UV-inativated or heat-inactivated Tupanvirus, or APMV, at an MOI of 100, 3 and 9 h post-infection. **h** Dose-response of Tupanvirus and APMV in *A. castellanii* pre-treated with distinct doses of geneticin or cycloheximide. (**i**) Progressive vacuolization of tetrahymena after infection with Tupanvirus (days 1–4). Scale bars, 10 µm. **j** Tupanvirus tail content releasing in tetrahymena 1 h post-inoculation (TEM). Scale bar, 200 nm. **k** Vesicles containing large amounts of *Tetrahymena* ribosomes (R) after Tupanvirus infection. Scale bar, 3.5 µm. **l** Electrophoresis gel showing rRNA shutdown in tetrahymena inoculated with Tupanvirus at an MOI of 10 (days 1–4). **m** Rate of particles incorporation per tetrahymena cell (days 1–4). **n** Simulations showing the decrease in APMV and maintenance of Tupanvirus populations over the analyzed days after infection of a mix of *Acanthamoeba castellanii* and tetrahymena at an MOI of 10 (lines indicated by 'b' in both graphs of **n**). At days 4 and 8, fresh PYG medium and 10^5 *A. castellanii* were added to the systems (arrows). For the negative control of this experiment we pre-treated tetrahymena with 20 µg/ml of geneticin (lines indicated by 'a' in both graphs of **n**). In this case, both APMV and Tupanvirus were able to grow in the system. Statistical analyses in **b** and **h**: t-test based on control groups (**b**) or corresponding virus/drug concentrations (**h**). *:$p < 0.05$; **:$p < 0.01$. The experiments were performed 3 times independently, with two replicates each. Error bars (**a**, **b**, **f**, **g**, **h**, **m** and **n**), standard deviation

were stored in 75 cm^2 cell culture flasks containing 30 mL of peptone yeast extract glucose medium (PYG) at 28 °C. After 24 h of growth, cells were harvested and pelleted by centrifugation. The supernatant was removed, and the amoebae were resuspended three times in sterile PAS. After the third washing, 500,000 *A. castellanii* or *V. vermiformis* were resuspended in PAS or TS solutions and seeded in 24-well plates. The amoebae suspensions were added to an antibiotic mix containing ciprofloxacin (20 µg/mL; Panpharma, Z.I., Clairay, France), vancomycin (10 µg/mL; Mylan, Saint-Priest, France), imipenem (10 µg/mL; Mylan, Saint-Priest, France), doxycycline (20 µg/mL; Mylan, Saint-Priest, France), and voriconazole (20 µg/mL; Mylan, Saint-Priest, France). Each 100 µL of sample was mixed and inoculated in the numbered (1–12) wells and incubated at 30 °C in a humid chamber. A negative control was used in each plate. The wells were observed daily under an optical microscope. After 3 days, new passages of the inoculated wells were performed in the same manner until the third passage. In this passage, the content of the wells presenting lysis and cytopathic effects were collected and stored for production and analysis of the possible isolates by haemacolour staining and electron microscopy using the negative stain technique. Of the twelve tested samples from Pantanal, we found Tupanvirus (soda lake) in three. In only one

ocean sample we did isolate Tupanvirus (deep ocean). To evaluate the Tupanvirus soda lake host range, a panel of cell lines was subjected to virus infection at an multiplicity of infection (MOI) of 5: *Acanthamoeba castellanii* (ATCC30010), *Acanthamoeba royreba* (ATCC30884), *Acanthamoeba griffin* (ATCC50702), *Acanthamoeba* sp. E4 (IHU isolate), *Acanthamoeba* sp. Micheline (IHU isolate), *Vermamoeba vermiformis* (ATCC50237), *Dictyostelium discoideum* (ATCC44841), *Willartia magna* (ATCC50035), *Tetrahymena hyperangularis* (ATCC 50254), *Trichomonas tenax* (ATCC 30207), RAW264.7 (Mouse leukemic monocyte-macrophage) (ATCCTIB71) and THP-1 (human monocytic cell line) (ATCCTIB202). Cell lines were tested for mycoplasma. The assays were carried out in 24-well plates, and cells were incubated for 24 or 48 h. The tupanvirus titer was measured in *A. castellanii* by end-point and calculated by the Reed-Muench method[34]. In parallel, the samples were subjected to qPCR, targeting the tupanvirus tyrosyl RNA synthetase (5′-CGCAATGTGTGGAGCCTTTC-3′ and 5′-CCAAGA-GATCCGGCGTAGTC-3′) and aiming to verify viral genome replication (Biorad, CA, USA). Tupanvirus was propagated in 20 *A. castellanii* 175 cm^2 cell culture flasks in 50 mL PYG medium. The particles were purified by centrifugation through a sucrose cushion (50%), suspended in PAS and stored at −80 °C. Purified particles were used for genome sequencing, proteomic analysis[10], and microscopic and biological assays.

Cycle and virion characterization. All biological tests were performed with Tupanvirus soda lake only. To investigate the viral replication cycle by TEM, 25 cm^2 cell culture flasks were filled with 10×10^6 *A. castellanii* per flask, infected by Tupanvirus at a multiplicity of infection of 10 and incubated at 30 °C for 0, 2, 4, 6, 8, 12, 15, 18, and 24 h. One hour after virus-cell incubation, the amoeba monolayer was washed three times with PAS buffer to eliminate non-internalized viruses. A total of 10 mL of the infected cultures was distributed into new culture flasks. A culture flask containing only amoeba was used as the negative control. The infected cells and control sample were fixed and prepared for electron microscopy[14]. For immunofluorescence, *A. castellanii* cells were grown, infected by Tupanvirus at a multiplicity of infection of 1 as described and added to coverslips for 0, 2, 4, 6, 8, 12, 15, 18, and 24 h. After infection, the cells were rinsed in cold phosphate-buffered saline (PBS) and fixed with 4% paraformaldehyde (PFA) in PAS for 10 mins. After fixation, cells were permeabilized with 0.2% Triton X-100 in 3% bovine serum albumin (BSA)–PAS for 5 min, followed by rinsing with 3% BSA–PBS three times. Cells were then stained for 1 h at room temperature with an anti-tupanvirus antibody produced in mice (According Aix Marseille University ethics committee rules). After incubation with an anti-mouse secondary antibody, fluorescently labeled cells were viewed using a Leica DMI600b microscope. For Tupanvirus virion characterization, we also used scanning electron microscopy (SEM)[35]. Chemical treatment with proteases and sonication was performed as described elsewhere[35] to investigate fiber composition and the attachment between capsid and tail. For tomography videos, tilt series were acquired on a Tecnai G2 transmission electron microscope (FEI) operated at 200 keV and equipped with a 4096×4096 pixel resolution Eagle camera (FEI) and Explore 3D (FEI) software. The tilt range was 100°, scanned in 1° increments. The magnification ranged between 6,500 and 25,000, corresponding to pixel sizes between 1.64 and 0.45 nm, respectively. The image size was $4,096 \times 4,096$ pixels. The average thickness of the obtained tomograms was 298 ± 131 nm ($n = 11$). The tilt series were aligned using ETomo from the IMOD software package (University of Colorado, USA) by cross-correlation (http://bio3d.colorado.edu/imod/). The tomograms were reconstructed using the weighted-back projection algorithm in ETomo from IMOD. ImageJ software was used for image processing.

Genomes sequencing and analyses. The tupanviruses genomes were sequenced using an Illumina MiSeq instrument (Illumina Inc., San Diego, CA, USA) with the paired end application. The sequence reads were assembled de novo using ABYSS software and SPADES, and the resulting contigs were ordered by the Python-based CONTIGuator.py software. The obtained draft genomes were mapped back to verify the read assembly and close gaps. The best assembled genome was retained, and the few remaining gaps (three) were closed by Sanger sequencing. The gene predictions were performed using the RAST (Rapid Annotation using Subsystem Technology) and GeneMarkS tools. Transfer RNA (tRNA) sequences were identified using the ARAGORN tool. The functional annotations were inferred by BLAST searches against the GenBank NCBI non-redundant protein sequence database (nr) (*e*-value $< 1 \times 10^{-3}$) and by searching specialized databases through the Blast2GO platform. Finally, the genome annotation was manually revised and curated. The predicted ORFs that were smaller than 50 amino acids and had no hits in any database were ruled out. Tupanvirus codon and aa usages were compared with those of *A. castellanii* and other lineages of mimiviruses. Sequences were obtained from NCBI GenBank and subjected to CGUA (General Codon Usage Analysis). The global distribution of Tupanvirus tRNAs was analyzed and compared manually with viral aa usage considering the corresponding canonical codons related to each aa. Phylogenetic analyses were carried out based on the separate alignments of several genes, including family B DNA polymerase, 18 S rRNA intronic regions (copies 1/2) and 20 aminoacyl-tRNA synthetases (aaRS). The predicted aa sequences were obtained from NCBI GenBank and aligned using Clustal W in the Mega 7.0 software program. Trees were constructed using the maximum likelihood evolution method and 1000 replicates. The analysis of aaRS domains was carried out using NCBI Conserved Domain Search (https://www.ncbi.nlm.nih.gov/Structure/cdd/wrpsb.cgi). A search for promoter sequences was performed in intergenic regions based on a search for the mimivirus canonical AAAATTGA promoter sequence, as previously described[20]. Single-nucleotide polymorphisms (SNP) in the AAAATTGA promoter sequence were also considered for each base, considering all possibilities. Gene sets available for members of the family *Mimiviridae* and those of Tupanvirus soda lake and Tupanvirus deep ocean were used for analyses of the mimivirus pangenome. Groups of orthologues were determined using the Proteinortho tool V51 with 1*e*−3 and 50% as the *e*-value and coverage thresholds, respectively. Concurrently, BLAST searches were performed using ORFs of all mimivirus genomes available in the NCBI GenBank nucleotide sequence database against the set of clusters of orthologous groups previously delineated for mimiviruses (mimiCOGs) ($n = 898$), with 1*e*−3 and 50% as the *e*-value and coverage thresholds, respectively. For rhizome preparations, all coding sequences were blasted against the NR database, and results were filtered to retain the best hits. Taxonomic affiliation was retrieved from NCBI. For the construction of a translation-associated elements network, the different classes of translation elements of each organism included in the analysis were obtained by searching for each component within their genome, according to protein function annotation using Blastp searches against the GenBank NCBI non-redundant protein sequence database. The tRNA components were obtained using the ARAGORN tool. Different tRNA molecules were included in the analysis, considering the anti-codon sequence. Repeated elements were eliminated to avoid analysis of duplicate events. The layout of the network was generated by a force-directed algorithm—followed by local rearrangement for visual clarity, leaving the network's overall layout unperturbed—using the program Gephi (https://gephi.org).

Ribosomal RNA shutdown and toxicity assays. To investigate the toxicity of Tupanvirus particles, 1 million *A. castellanii* cells were infected with Tupanvirus or mimivirus at a multiplicity of infection of 1, 10, 50, or 100 and incubated at 32 °C. At 0 and 24 h post-infection, the cell suspensions were collected and titered as previously described. A fraction of this suspension (200 µL) was subjected to RNA extraction (Qiagen RNA extraction Kit, Hilden, Germany). The RNA was subjected to reverse transcription by using Vilo enzymes (Invitrogen, CA, USA) and then used as a template in qPCR targeting *A. castellanii* 18 S rRNA (5′-TCCAATTTTCTGCCACCGAA-3′ and 5′-ATCATTACCCTAGTCCTCGCG C-3′). The values were expressed as arbitrary units (delta-Ct). Normalized amounts of the original RNA extracted from each sample were electrophoresed in 1% agarose gel with TBE buffer and run at 150 V. TEM over the entire testing period was performed to evaluate the presence of ribosome-containing vesicles and other cytological alterations. To investigate the nature of virion toxicity, purified Tupanvirus was inactivated by UV light (1 h of exposure, 60 W/m^2) or heating (80 °C, 1 h)—inactivation was confirmed by inoculation on *Acanthamoeba castellanii*, CPE was observed for 5 days and lack of replication was confirmed by qPCR—and inoculated onto *A. castellanii* containing 500,000 cells at multiplicities of infection of 0.1, 1, 5, 10, 50, and 100. The assays were performed in PAS solution. The cytopathic effect was documented and quantified in a counting-cells chamber. Inactivated mimivirus was used for comparison. To determine whether Tupanvirus-induced shutdown of amoebal 18 S rRNA even after inactivation, 500,000 cells were infected (at a multiplicity of infection of 100) and collected at 3 and 9 h post-infection, and amoebal 18 S rRNA levels were measured by qPCR. APMV was used as the control. The sensitivity of Tupanvirus and mimivirus to the translation-inhibiting drugs geneticin and cycloheximide was tested. A total of 500,000 *A. castellanii* cells were pre-treated with different concentrations of the drugs (0–50 and 0–15 µg/ml, respectively) for 8 h and then infected at a multiplicity of infection of 10. Twenty-four hour post-infection, cells were collected, and the viral titers were measured. To investigate the toxicity effect of Tupanvirus particles in the non-host *Tetrahymena* sp., 1 million fresh cells were infected at a multiplicity of infection of 10 in a medium composed of 50% PYG and 50% PAS. The cytopathic effect was monitored for 4 days post-infection, given the reduction of cell movement and vacuolization (lysis or viral replication was not observed). Each day post-infection, 100 µL of infected cell suspension was collected and subjected to cytospin and haemacolour staining to observe vacuolization and other cytological alterations induced by the virus. Other 100 µL aliquots were used to investigate the occurrence of rRNA shutdown induced by Tupanvirus. To this end, the samples were subjected to RNA extraction and electrophoresis. Viral infection in *Tetrahymena* sp. was also observed by TEM at a multiplicity of infection of 10. To determine whether Tupanvirus particles affect the rate of *Tetrahymena* sp. phagocytosis because of toxicity, the rate of viral particle incorporation per cell was calculated during the period of infection. The ratio of TCID50 (infectious entities) and total particles was first calculated by counting the number of viral particles in a counting chamber (approximately 1 $TCID_{50}$ to 63 total particles). One million *Tetrahymena* cells were infected by Tupanvirus or mimivirus at an MOI of 10 $TCID_{50}$. Twelve hour post-infection, the number of viral particles in the medium was estimated by counting the remaining (non-phagocytized) particles. An input of 10 $TCID_{50}$ per cell was added each day post-infection (in separate flasks, one for each day), and the rate of particles phagocytosis was calculated 12 h post-input. For the calculation, the remaining particles from the day before were considered (counted immediately before the input). Considering the toxicity caused by Tupanvirus, but not APMV, in tetrahymena, we conducted an in vitro experiment

aiming to investigate the ability to maintain Tupanvirus or APMV in a system containing both *Acanthamoeba* (host) and *Tetrahymena* (non-host, predator of particles). Thus, *A. castellanii* (900,000 cells) and *Tetrahymena* (100,000 cells) were added simultaneously to the same flask, then infected by Tupanvirus or mimivirus at an MOI of 10 and observed for 12 days. One flask per observation day was prepared. At days 4 and 8, we added 500 µL of fresh medium (50% PYG and 50% PAS) and 100,000 *A. castellanii*, the permissive host. Each day post-infection, the corresponding flask was collected and subjected to titration as previously described. The same experiment was carried out by pre-treating *Tetrahymena* (8 h before infection) with 20 µg/ml of geneticin as negative controls.

Analysis involving Tupanvirus 18 S rRNA intronic region. All analyses involving the genomic environment of copies 1 and 2 were conducted based on the annotation of Tupanvirus. In the best-hits evaluation, the core sequences of copies 1 and 2 were used for nucleotide BLAST analysis using blastn. The resulting 100 best hits were tabulated, and the information was used to construct diagrams. For the phylogenetic analysis, the sequences of these best hits were also aligned, using Clustal W in the Mega 7.0 software, and constructed using the maximum likelihood evolution method of 1,000 replicates. To analyze subjacent regions of the core sequence of 18 S rRNA intronic regions in the *Mimiviridae* family, one member of the lineages A (HQ336222.2), B (JX962719.1) and C (JX885207.1) was chosen and analyzed. The expression of both copies was checked using fluorescence in situ hybridization (FISH) and qPCR. For this, *A. castellanii* cells were infected with Tupanvirus with a multiplicity of infection of 5 and collected at 30 min and at 6 and 12 h post-infection. As a control, *A. castellanii* cells were also incubated with PAS alone and collected. At the indicated times, cells and the supernatant were collected and centrifuged at 800 × g for 10 min. For FISH, the pellet was resuspended in 200 µL of PAS, submitted to cytospin and the cells were fixed in cold methanol for 5 min. Specific probes targeting the 18 S rRNA of *A. castellanii* (5′-TTCACGGTAAACGATCTGGGCC-3′-fluorophore Alexa 488), copy 1 RNA (5′-AGTGGAACTCGGGTATGGTAAAA-3′-fluorophore Alexa 555) and copy 2 RNA (5′-GGCCAAGCTAATCACTTGGG-3′-fluorophore Alexa 555) were diluted and applied at 2 µM in hybridization buffer (900 mM NaCl, 20 mM Tris/HCL, 5 mM EDTA, 0.01% SDS, 10–25% deionized-formamide in distilled-H_2O). The hybridization buffer containing the probes was added to the slides and the hybridization was carried out at 46 °C overnight in a programmable temperature-controlled slide-processing system (ThermoBrite StatSpin, IL, USA). Post-hybridization washes consisted of 0.45–0.15 M NaCl, 20 mM Tris/HCL, 5 mM EDTA, and 0.01% SDS at 48 °C for 10 min. Slides were analyzed using a DMI6000B inverted research microscope (Leica, Wetzlar, Germany). To qPCR the pellet of infected cells was also washed with PAS and then used for total RNA extraction using the RNeasy mini kit (Qiagen, Venlo, Netherlands). The extracted RNA was treated with the Turbo DNA-free kit (Invitrogen, CA, USA) and then used as a template in reverse transcription (RT) reactions carried out using SuperScript Vilo (Invitrogen, CA, USA). The resultant cDNA was used as a template for quantitative real-time PCR assays using the QuantiTect SYBr Green PCR Kit (Qiagen RNA extraction Kit, Hilden, Germany) and targeting copies 1 (primers 5′-GCATCAA GTGCCAACCCATC-3′ and 5′-CTGAAATGGGCAATCCGCAG-3′) and 2 (primers 5′-CCAAGTGATTAGCTTGGCCATAA-3′ and 5′-CGGGAAGTCCCTA AAGCTCC-3′) of the intergenic18S rRNA region in TPV. To normalize the results, primers targeting the GAPDH housekeeping gene of *Acanthamoeba* (primers 5′-GTCTCCGTCGTCGATCTCAC-3′ and 5′-GCGGCCTTAATCTCGTCGTA-3′) were also used. qPCR assays were performed in a BioRad Real-Time PCR Detection System (BioRad) using the following thermal conditions for all genes: 15 min of pre-incubation at 95 °C followed by 40 amplification cycles of 30 s at 95 °C, 30 s at 60 °C and 30 s at 72 °C. The results were analyzed using the relative quantification methodology of $2^{(-\Delta\Delta ct)}$.

Investigation of the nature of ribosomal RNA shutdown. To investigate the shutting down of the host rRNA and verify whether this phenomenon was related to the canonical ribophagy/autophagy process, tests using two acidification and lysosome-vesicle fusion inhibitors (chloroquine and bafilomycin A) were performed. The pH of infected cells and the effect of Atg8-2 silencing on shutdown were also tested. For the inhibitor assays, 5×10^5 *A. castellanii* cells cultured in PYG medium were infected with Tupanvirus or mimivirus at a multiplicity of infection of 100 and incubated at 32 °C. At 1 h post-infection, chloroquine (Sigma-Aldrich, MO, USA) at a final concentration of 100 µM or bafilomycin A (Sigma-Aldrich, MO, USA) at a final concentration of 10 nM was added to the infected cell suspensions. As a control, *A. castellanii* cells not infected were also treated with these inhibitors under the same conditions. After 3 and 9 h post-infection, cells and the supernatant were collected and centrifuged at 800 × *g* for 10 min. The supernatant was discarded, and the pellet was submitted to RNA extraction (Qiagen RNA extraction Kit, Hilden, Germany). From the extracted RNA, 10 µL of each sample was electrophoresed in 1.5% agarose gel with TBE buffer and run at 135 V, and 14 µL was submitted to reverse transcription to measure the amoebal 18 S rRNA levels by qPCR as previously described. To investigate the acidification caused by Tupanvirus or mimivirus infection, *A. castellanii* cells were also submitted to the same pattern of infection and treatment with bafilomycin A, as previously described. In addition, 1 h before the collection time, the cells were incubated with LysoTracker Red DND-99 (Thermo Fisher Scientific, Massachusetts, United States) at a final concentration of 75 nM. After 9 h post-infection, cells and the supernatant were collected and centrifuged at 800 × *g* for 10 min. The supernatant was discarded, and the pellet was resuspended in 1 mL of PAS medium containing only bafilomycin A (10 nM). A total of 20 µL of this suspension was added to glass slides and cover slipped. Analyses were performed using a confocal microscope (Zeiss, Jena, Germany). For gene silencing, small interfering RNA (siRNA) targeting the Atg8-2 gene of *A. castellanii* was synthesized by Eurogentec (Liège, Belgium) based on the cDNA sequence of the gene. The siRNA duplex with sense (5′-GAACUC AUGUCGCACAUCUTT-3′) and anti-sense (5′-AGAUGUGCGACAUGAGU UCTT-3′) sequences was used. The siRNA tagged with a fluorescence dye was transfected onto *A. castellanii* trophozoites at a density of 1×10^6 cells. The control of transfection was performed using fluorescence microscopy. The biological effect of siRNA was check by qPCR and by the observation of the inhibition of acanthamoebal encystment, which is dependent on Atg8-2. Finally, modifications of *A. castellanii* nucleus/nucleolus structure after infection with Tupanvirus and mimivirus were investigated. A total of 10^6 cells were infected with Tupanvirus or mimivirus at an MOI of 10, stained by haemacolour and treated with SYTO RNASelect Green Fluorescent cell stain (Invitrogen, USA) following the manufacturer's instructions. After 9 h.p.i., cells were observed under an immunofluorescence microscope to observe modifications to the nucleus /nucleolus of infected and control cells. In parallel, this preparation was submitted to electron microscopy.

Data availability. The Tupanvirus genome sequences have been deposited in GenBank under accession codes KY523104 (soda lake) and MF405918 (deep ocean). Proteomic data have been deposited in PRIDE archive under accession code PXD007583. All other data supporting the findings of this study are available within the article and its Supplementary Information, or from the corresponding author upon reasonable request.

Received: 3 October 2017 Accepted: 23 January 2018
Published online: 27 February 2018

References

1. Raina, M. & Ibba, M. tRNAs as regulators of biological processes. *Front. Genet.* **5**, 171 (2014).
2. Fournier, G. P., Andam, C. P., Alm, E. J. & Gogarten, J. P. Molecular evolution of aminoacyl tRNA synthetase proteins in the early history of life. *Orig. Life Evol. Biospheres.* **41**, 621–632 (2011).
3. Korobeinikova, A. V., Garber, M. B. & Gongadze, G. M. Ribosomal proteins: structure, function, and evolution. *Biochemistry* **77**, 562–574 (2012).
4. La Scola, B. et al. A giant virus in amoebae. *Science* **299**, 2033 (2003).
5. Abrahao, J. et al. The analysis of translation-related gene set boosts debates around origin and evolution of mimiviruses. *PLoS Genet.* **13**, e1006532 (2017).
6. Schulz, F. et al. Giant viruses with an expanded complement of translation system components. *Science* **356**, 82–85 (2017).
7. Sorokin, D. Y. et al. Microbial diversity and biogeochemical cycling in soda lakes. *Extremophiles* **18**, 791–809 (2014).
8. Xiao, C. et al. Structural studies of the giant mimivirus. *PLoS Biol.* **7**, e92 (2009).
9. Ageno, M., Donelli, G. & Guglielmi, F. Structure and physico-chemical properties of bacteriophage G. II. The shape and symmetry of the capsid. *Micron* **4**, 376–403 (1973).
10. Philippe, N. et al. Pandoraviruses: amoeba viruses with genomes up to 2.5 Mb reaching that of parasitic eukaryotes. *Science* **341**, 281–286 (2013).
11. Legendre, M. et al. Thirty-thousand-year-old distant relative of giant icosahedral DNA viruses with a pandoravirus morphology. *Proc. Natl. Acad. Sci. USA* **111**, 4274–4279 (2014).
12. Legendre, M. et al. In-depth study of Mollivirus sibericum, a new 30,000-y-old giant virus infecting Acanthamoeba. *Proc. Natl. Acad. Sci. USA* **112**, E5327–E5335 (2015).
13. Reteno, D. G. et al. Faustovirus, an asfarvirus-related new lineage of giant viruses infecting amoebae. *J. Virol.* **89**, 6585–6594 (2015).
14. Andreani, J. et al. Cedratvirus, a double-cork structured giant virus, is a distant relative of Pithoviruses. *Viruses* **8**, E300 (2016).
15. Suzan-Monti, M., La Scola, B., Barrassi, L., Espinosa, L. & Raoult, D. Ultrastructural characterization of the giant volcano-like virus factory of Acanthamoeba polyphaga Mimivirus. *PLoS ONE* **2**, e328 (2007).
16. Chaikeeratisak, C. et al. Assembly of a nucleus-like structure during viral replication in bacteria. *Science* **355**, 194–197 (2017).
17. Forterre, P. The virocell concept and environmental microbiology. *ISME J.* **7**, 233–236 (2013).
18. Antwerpen, M. H. et al. Whole-genome sequencing of a pandoravirus isolated from keratitis-inducing acanthamoeba. *Genome Announc.* **3**, e00136–15 (2015).

19. Raoult, D. The post-Darwinist rhizome of life. *Lancet* **375**, 104–105 (2010).
20. Suhre, K., Audic, S. & Claverie, J. M. Mimivirus gene promoters exhibit an unprecedented conservation among all eukaryotes. *Proc. Natl. Acad. Sci. USA* **102**, 14689–14693 (2005).
21. Fischer, M. G., Allen, M. J., Wilson, W. H. & Suttle, C. A. Giant virus with a remarkable complement of genes infects marine zooplankton. *Proc. Natl Acad. Sci. USA* **107**, 19508–19513 (2010).
22. Raoult, D. et al. The 1.2-megabase genome sequence of Mimivirus. *Science* **19**, 1344–1350 (2004).
23. Arslan, D., Legendre, M., Seltzer, V., Abergel, C. & Claverie, J. M. Distant mimivirus relative with a larger genome highlights the fundamental features of Megaviridae. *Proc. Natl Acad. Sci. USA* **108**, 17486–17491 (2011).
24. Assis, F. L. et al. Pan-genome analysis of Brazilian lineage A amoebal mimiviruses. *Viruses* **7**, 3483–3499 (2015).
25. Gonzales-Flores, J. N., Shetty, S. P., Dubey, A. & Copeland, P. R. The molecular biology of selenocysteine. *Biomol. Concepts* **4**, 349–365 (2013).
26. Csaba, G. Lectins and Tetrahymena—A review. *Acta Microbiol. Immunol. Hung.* **63**, 279–291 (2016).
27. Jah, S. et al. Trans-kingdom mimicry underlies ribosome customization by a poxvirus kinase. *Nature* **546**, 651–655 (2017).
28. Claverie, J. M. Viruses take center stage in cellular evolution. *Genome Biol.* **7**, 110 (2006).
29. Filée, J. Genomic comparison of closely related Giant Viruses supports an accordion-like model of evolution. *Front. Microbiol.* **6**, 593 (2015).
30. Smith, J. E. The ecology and evolution of microsporidian parasites. *Parasitology* **136**, 1901–1914 (2009).
31. Nunes, A. & Gomes, J. P. Gomes Evolution, phylogeny, and molecular epidemiology of Chlamydia. *Infect. Genet. Evol.* **23**, 49–64 (2014).
32. Raoult, D. & Forterre, P. Redefining viruses: lessons from Mimivirus. *Nat. Rev. Microbiol.* **6**, 315–319 (2008).
33. Yutin, N. et al. Origin of giant viruses from smaller DNA viruses not from a fourth domain of cellular life. *Virology* **0**, 38–52 (2014).
34. Reed, L. J. & Muench, H. A simple method of estimating fifty percent endpoints. *Am. J. Hyg.* **27**, 493–497 (1938).
35. Rodrigues, R. A. et al. Mimivirus fibrils are important for viral attachment to the microbial world by a diverse glycoside interaction repertorie. *J. Virol.* **89**, 1182–1189 (2015).

Acknowledgements

We thank our colleagues from URMITE and Laboratório de Vírus of Universidade Federal de Minas Gerais for their assistance, particularly Julien Andreani, Jean-Pierre Baudoin, Gilles Audoly, Amina Cherif Louazani, Lina Barrassi, Priscilla Jardot, Eric Chabrières, Philippe Decloquement, Nicholas Armstrong, Said Azza, Emeline Baptiste, Claudio Bonjardim, Paulo Ferreira, Giliane Trindade and Betania Drumond. In addition, we thank the Méditerranée Infection Foundation, Centro de Microscopia da UFMG, CNPq (Conselho Nacional de Desenvolvimento Científico e Tecnológico), CAPES (Coordenação de Aperfeiçoamento de Pessoal de Nível Superior) and FAPEMIG (Fundação de Amparo à Pesquisa do estado de Minas Gerais) for their financial support. We thank Petrobras for the collection of sediments from ocean. This work was also supported by the French Government under the « Investissements d'avenir » (Investments for the Future) program managed by the Agence Nationale de la Recherche (ANR, fr: National Agency for Research), (reference: Méditerranée Infection 10-IAHU-03). J.A., B.R. and E.K. are CNPq researchers. B.L.S., J.A., L.S., P.C., and E.G.K. are members of a CAPES-COFECUB project.

Author contributions

D.R., B.L.S., J.S.A., A.L., P.C., E.G.K, and E.G. designed the study and experiments. L.S., J. S.A, J.B.K., R.R., L.S., L.S.S., T.A., P.C., F.A. P.B., M.A., I.B., B.R., A.L., and H.S. performed sample collection, virus isolation, experiments and/or analyses. D.R., B.L.S., A.L., J.S.A., P.C., G.K., R.R., L.S., and L.S.S. wrote the manuscript. All authors approved the final manuscript.

Additional information

Supplementary Information accompanies this paper at https://doi.org/10.1038/s41467-018-03168-1.

Competing interests: The authors declare no competing financial interests.

Reprints and permission information is available online at http://npg.nature.com/reprintsandpermissions/

Publisher's note: Springer Nature remains neutral with regard to jurisdictional claims in published maps and institutional affiliations.

SUPPLEMENTARY INFORMATION

SUPPLEMENTARY NOTE 1

Proteomic analysis of Tupanvirus particles

Proteomic analysis of Tupanvirus soda lake particles revealed 127 proteins, nearly half (32/127 = 25.1%) of which are unknown and eight of which are encoded by ORFans (11/87 = 12.6%). Besides the expected major structural components [major capsid protein (L679) and core protein (L614)], transcription components constitute the largest functional category associated to the viral particle (13 gene products, including subunits of DNA-dependent RNA polymerase, RNA helicases, and mRNA capping enzyme). Moreover, other functional categories were detected in Tupanvirus particles, including protein/lipid modification (14), oxidative pathways (6), DNA topology and repair (3), particle structure (4), and others (87). 59 and 25 out of 127 TPV virion-associated proteins are shared with mimivirus (APMV) and Cafeteria roenbergensis virus respectivelly, out spanning all functional categories analyzed (Supplementary Data 2).

18S rRNA intronic sequence within Mimiviridae and Tupanvirus

The study of 18S rRNA sequences in tupanviruses showed that both copies are located in an intergenic region (Fig. 6; Supplementary Fig. 6A,B). The genomic environment analysis revealed the presence of many hypothetical proteins and ORFans next to the two copies and a tRNA island, composed of seven tRNAs, 15 kbp away from the core sequence of copy 1 (Supplementary Fig. 6A,B). Best hit analysis showed that the first 100 sequences, for both copies, belong mainly to the intronic regions of 18S sequences from different organisms such as fungi, amoebas and algae (Supplementary Fig. 6C,D). The presence of the 18S rRNA intronic sequence was also observed in members of lineages A, B and C of the *Mimiviridae* family (Fig. 6) Lineages A and B presented just

one copy which is located in an intronic region next to a self-splicing group I intron endonuclease. Lineage C presented two copies of the 18S rRNA sequence: copy 1 was disposed in a similar pattern of the copies presented in both tupanviruses (in intergenic regions) and copy 2 showed a most similar pattern to the unique copies of lineages B and C (in an intronic region also next to a self-splicing group I intron endonuclease) (Fig. 6 A-E). Phylogenetic analyses suggested that 18S rRNA copies 1 and 2 of mimiviruses lineage C had separate and different origins. However, Tupanvirus 18S rRNA copy 1 and 2 seem to be related to mimiviruses lineage A and B (single copy) and fungi mitochondrial 18S rRNA intronic region (Fig. 6F). We also observed the presence of three or four copies of the 18S-like sequences in some *Chlorella virus*, which were all phylogenetically inter-related (Fig. 6F). Analyses involving FISH and qPCR of the intronic 18S ribosomal region in tupanvirus soda lake demonstrated that, although these 18S rRNA copies are located in intergenic regions, they are highly expressed during the entire infection, especially in intermediate and later phases (6 and 12 hours post infection) (Supplementay Fig. 8).

Profile of infectiveness of Tupanvirus

Tupanvirus was first isolated in both *Acanthamoeba castellanii* and *Vermamoeba vermiformis,* suggesting a broader host-range compared to other previously described amoebal giant viruses. In light of this, we tested the infectiveness of the new isolate on a large panel of protozoa. Four distinct infectiveness profiles were observed (Supplementary Table 1). Cytopathic effect (CPE), increase of viral titer, and genome replication were observed in *A. castellanii, A. polyphaga, A. sp E4, A. griffini, V. vermiformis, Dysctiostelium discoideum*, and *Willartia magna*, characterizing a productive cycle wherein these hosts were permissive to Tupanvirus. An abortive cycle

was observed in *Acanthamoeba sp michelline* and *A. royreba,* wherein CPE and Tupanvirus genome replication were observed, but there was no particle formation since the viral titer did not increase. *Trichomonas tenax* were completely refractory to Tupanvirus, since CPE, genome replication and increase of viral titer were not observed. The fourth profile was observed in RAW247, THP-1 cells and in *Tetrahymena hyperangularis*, a ravenous free-living protist, wherein Tupanvirus was able to induce a cytopathic effect, but neither an increase of viral titer nor genome replication were observed, thus we concluded that TPV was toxic to the susceptible cell - an unprecedented profile among amoebal giant viruses.

Tupanvirus modulates a non-host organism

Tetrahymena sp was susceptible to Tupanvirus, which caused several effects (Fig. 7G; Fig. 8); however it could not replicate within the protist. In light of this, we hypothesized that the reduction of physiological activity of a (non-host) predator could increase the virus' fitness. We put it to the test by performing *in vitro* simulations, wherein *Acanthamoeba castellanii* (AC) and *Tetrahymena* sp cells were put together and infected at M.O.I. of 10 (Tupanvirus or APMV), and observed over 12 days. Input of fresh medium and permissive host (AC) was done at days four and eight post infection. After the input, Tupanvirus reached higher titers while APMV was extinguished, since the latter was not able to modulate the predator organism, unlike Tupanvirus (Fig. 8N). When we induced a previous ribosomal RNA shutdown in Tetrahymena with geneticin, APMV was able to survive until the last day of observation, similar to tupanvirus. This indicates that viral particles' toxicity confers an advantage in a habitat of intense competition where giant viruses are abundant (e.g. water environment), favoring the encounter between the virus and a permissive host.

Altogether, this data suggest that viral particles can act as active "non-alive" players favoring viral progeny maintenance, in a distinct way of their canonical role of transmitting genetic information. Considering that Tupanvirus is sister group of mimivirus, such modulation mechanism could be an ancient inheritance from an ancestor of *Mimivirus* or *Mimiviridae*. This new mechanism demonstrates that selective pressures over virion content go beyond the metastability properties in early steps of host infection, and can act as unexpected players to protect the rest of the viral progeny against predation.

rRNA shutdown does not seems to be related to ribophagy

The cytotoxic phenotype caused by Tupanvirus in host (*A. castellanii*) and non-host cells (*Tetrahymena*) is a circumstance never previously described and seems to be related to the shutting down of host ribosomal amounts (Fig. 7C; Fig. 8B,C,D,K,L). In a first moment, we believed that the autophagy might be related to Tupanvirus infection. In order to corroborate or not this hypothesis, we developed other several experiments involving the use of acidification inhibitors (chloroquine and bafilomycin A), the observation of acidification of infected cells, as well as the silencing of the gene that encodes an autophagy-related protein, Atg8-2. The treatment of amoebas with chloroquine (a lysosomotropic agent that accumulates inside the acidic parts of the cell, including endosomes and lysosomes, preventing acidification and, consequently, the fusion of endosomes and lysosomes) or bafilomycin A (a vacuolar H+ ATPase inhibitor that acts in the late phase of autophagy) did not prevented the occurrence of the ribosomal shutdown caused by tupanvirus infection, suggesting that this phenomenon is not dependent of the autophagosomes formation, a hallmark of ribophagy (Fig. 7C,D; Supplementary Fig. 9). In order to confirm this first experiment, we also opted to do the

silencing (siRNA) of Atg8-2, that is one of the ubiquitin-like proteins required for autophagosome formation, representing thus a cell marker related to ribophagy. Curiously, the gene silencing also does not prevent viral induced ribosomal shutdown in *Acanthamoeba castellanii*, corroborating the results observed with the inhibitors treatment (Fig. 7C,D). We also checked the pH of cells infected by tupanvirus or mimivirus, in presence or absence of bafilomycin A. Tupanvirus, in contrast to mimivirus, induces a strong acidification of whole amoebal cytoplasm at the time of 9 hours after infection (Fig. 7B; Suppementay Fig.9A,B). In mimivirus-infected amoebas and non-infected amoebas, it was possible visualize only localized acidic vacuoles, but in a scale quite smaller than that observed to tupanvirus infected cells (Fig 7B; Suppementay Fig.9A,B). Interestingly, the intense acidification caused by tupanvirus is not affected by the bafilomicyn A treatment, suggesting that this decrease in pH could be induced by an another acidification mechanisms not related to H+ ATPase pump (Fig. 7B; Suppementay Fig.9A,B). Although tupanvirus induces a remarkable acidification of host cells concomitantly with the ribosomal RNA shutdown, the biological meaning of such acidification and its possible relation to ribosomal shutdown remain to be investigated. As demonstrated in main data, Tupanvirus (inactivated or not) also causes degradation of host (*Acanthamoeba castellanii*) and non-host (*Tetrahymena*) nucleolus/nucleus (Fig. 7F,G), which may contribute to rRNA shutdown, since the nucleolus is important to ribosomal biogenesis. Taken together, these results indicate that this cytotoxic phenotype caused by tupanvirus is a mechanism not-related to the canonical ribophagy/autophagy process.

SUPPLEMENTARY FIGURES

Supplementary Figure 1: Tupanvirus soda lake cycle in *A. castellanii* observed by immunofluorescence. Cells were infected at a multiplicity of infection of 1 and observed at different time points post-infection. In green, viral particles detected by anti-tupan particle antibody produced in mouse; in red, amoeba cytoskeleton. H: hours post-infection. Scale bar, 10 µm.

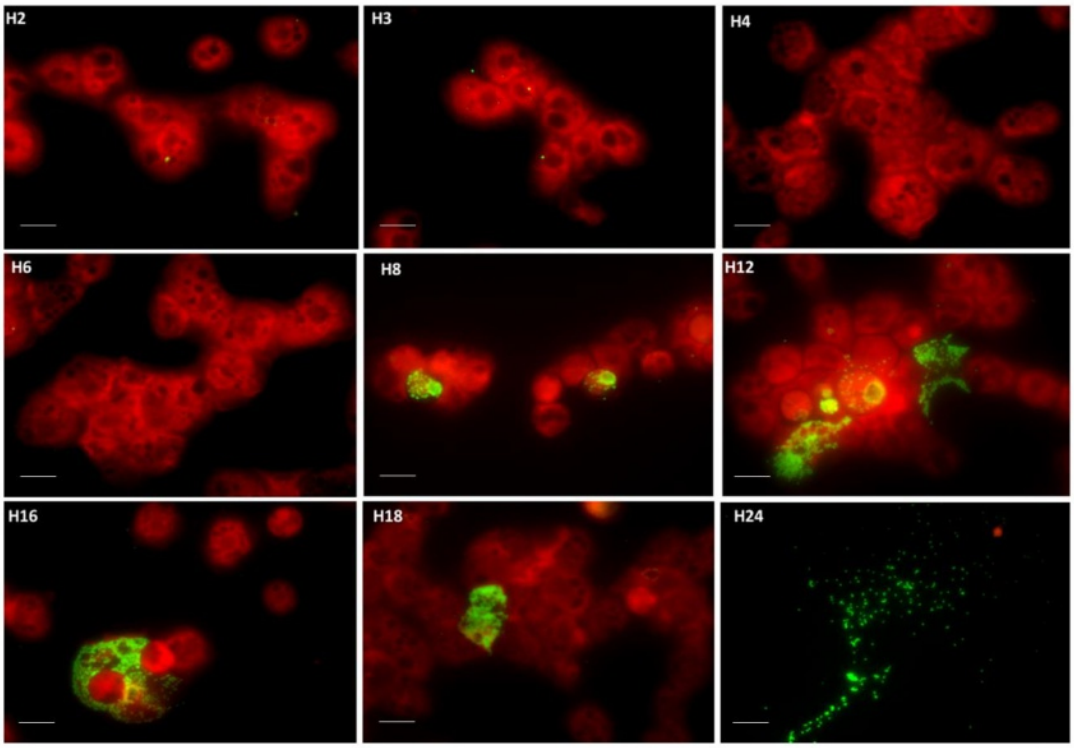

7

Supplementary Figure 2: Tupanvirus deep ocean genomic information. (a) Rhizome; (b) circular representation of the genome highlighting the translation-related factors; and (c) analysis of Tupanvirus deep ocean 70 tRNAs distribution among amino acid (aa) categories, isoacceptors and their relation to viral aa usage. Bars represent the percentage of use of a given codon (isoacceptor) related to a given aa. Dots above bars represent codons in which Tupanvirus deep ocean presents one or more related tRNAs. *Ambiguous tRNA – also predicted for pyrrolysine.

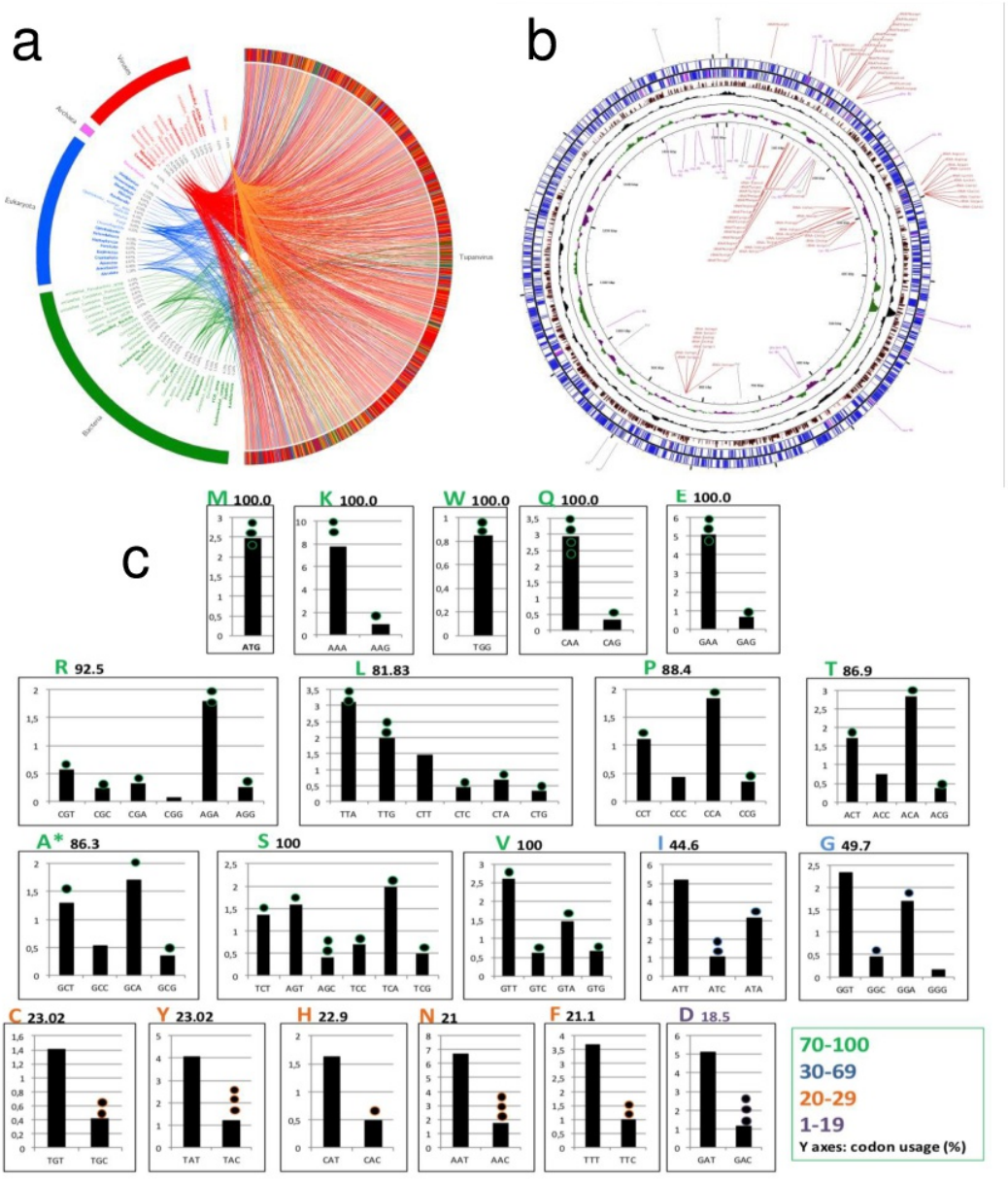

Supplementary Figure 3: Analysis of 67 tRNA distribution in tupanvirus soda lake among amino acid (aa) categories, isoacceptors and their relation to viral aa usage. Bars represent the percentage of use of a given codon (isoacceptor) related to a given aa. Dots above bars represent codons in which Tupanvirus presents one or more related tRNAs. Numbers above the squares represent the percentage of codon occurrence covered by tupanvirus tRNA, considering each aa. These numbers determined the colours, according to the legend at the bottom right corner of the figure.

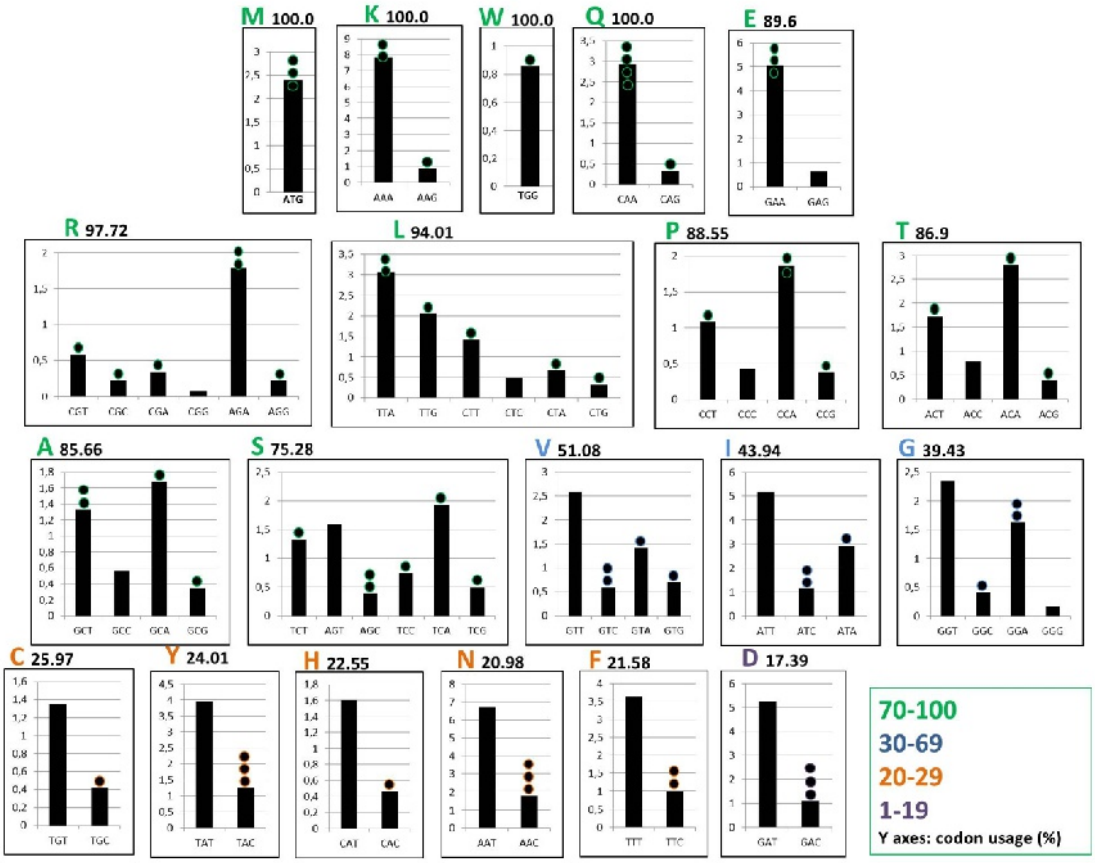

29

Supplementary Figure 5: The rhizome of the glutaminyl-tRNA synthetase of Tupanvirus soda lake. The sequence of the glutaminyl-tRNA synthetase was split into short fragments and blasted against the NR database. Best hit was selected and integrated in a circular gene data image. Taxonomic origins are colored in blue for eukaryote, green for bacteria and orange for viruses.

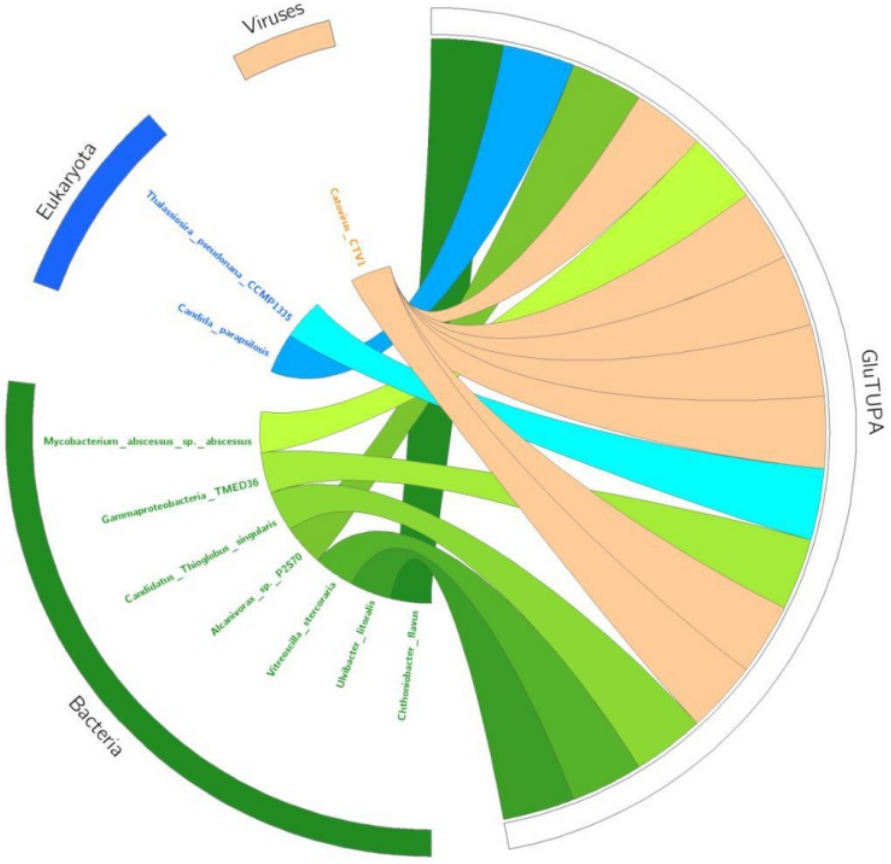

Supplementary Figure 6: Genomic environment and best-hit analyses of Tupanvirus soda lake 18S rRNA intronic regions. Genomic environment of copy 1 (a) and copy 2 (b). The 100 best hits for copies 1 (c) and 2 (d).

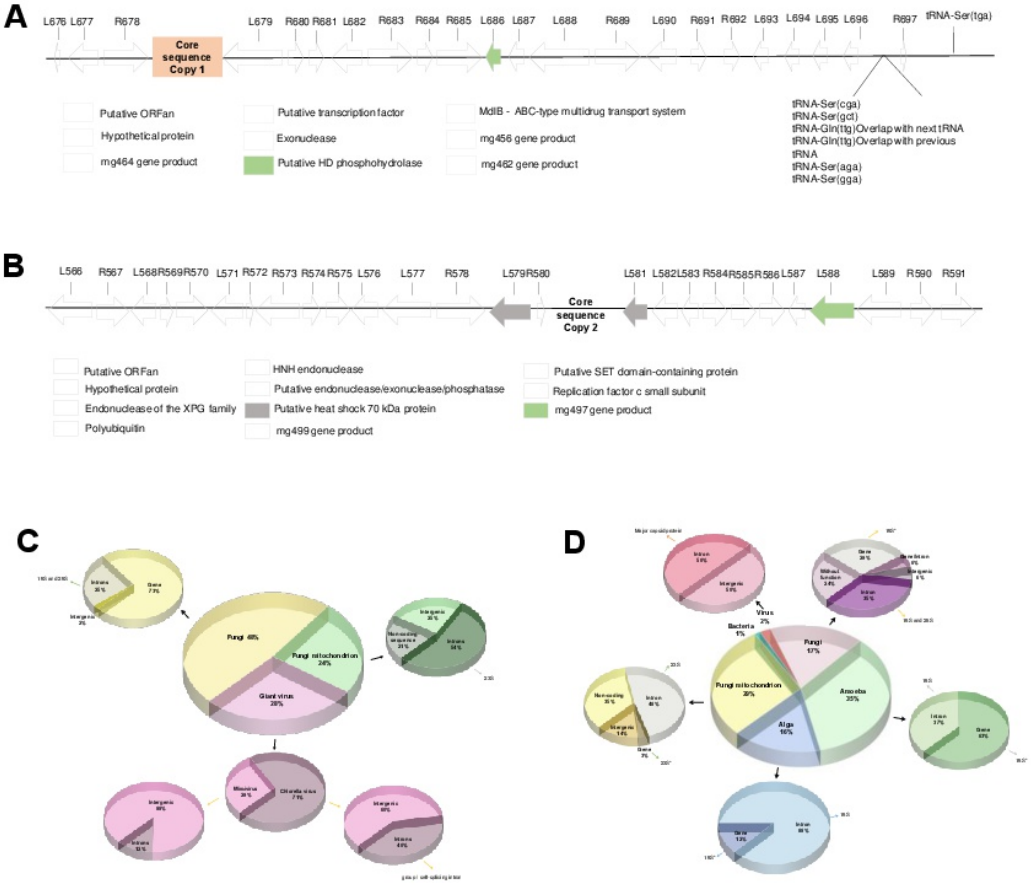

31

Supplementary Figure 7: Networks of translation-related category of genes of tupanviruses, Klosneuviruses, other mimiviruses and cell organisms.

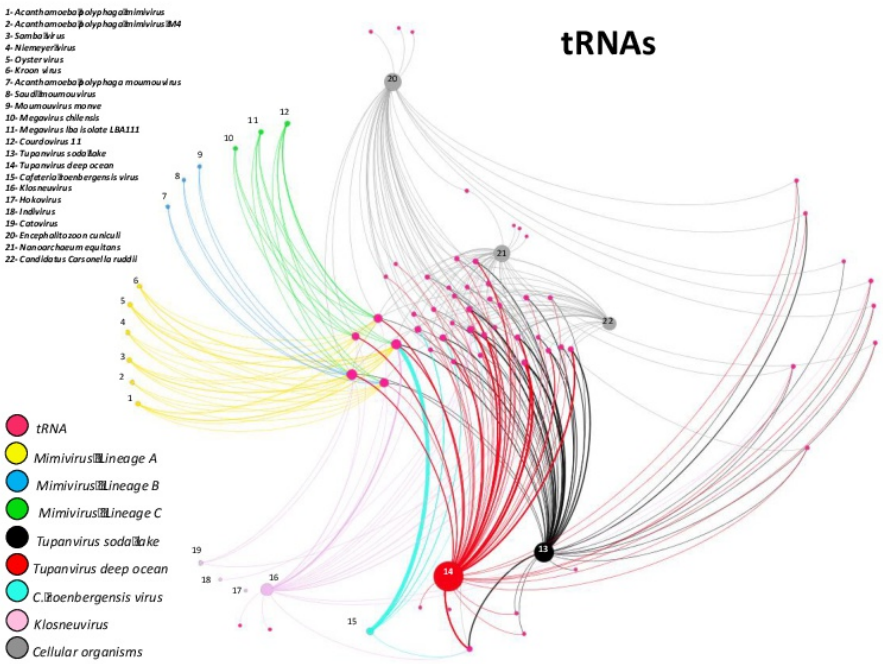

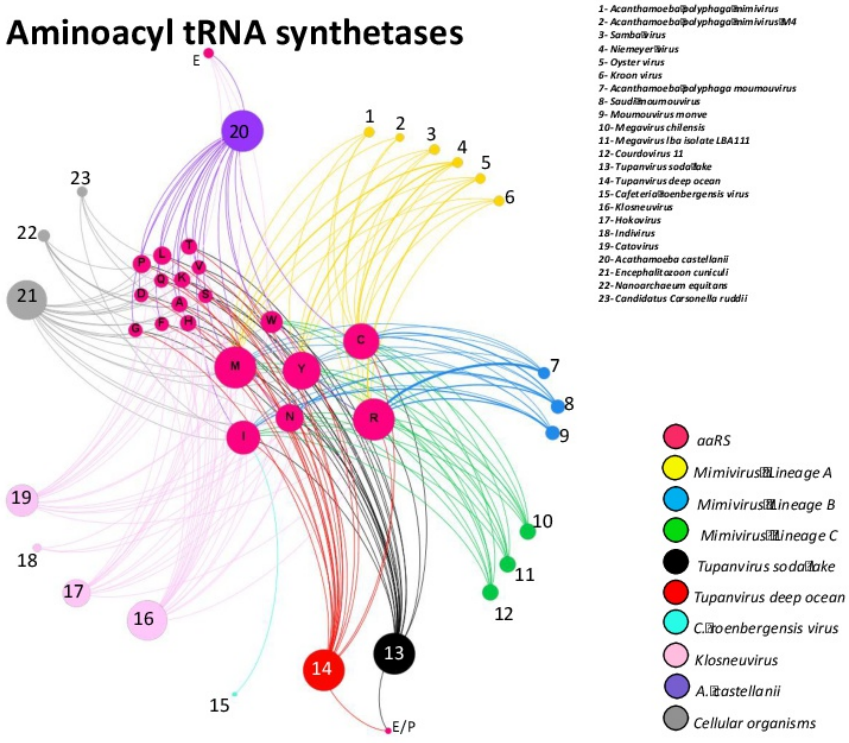

32

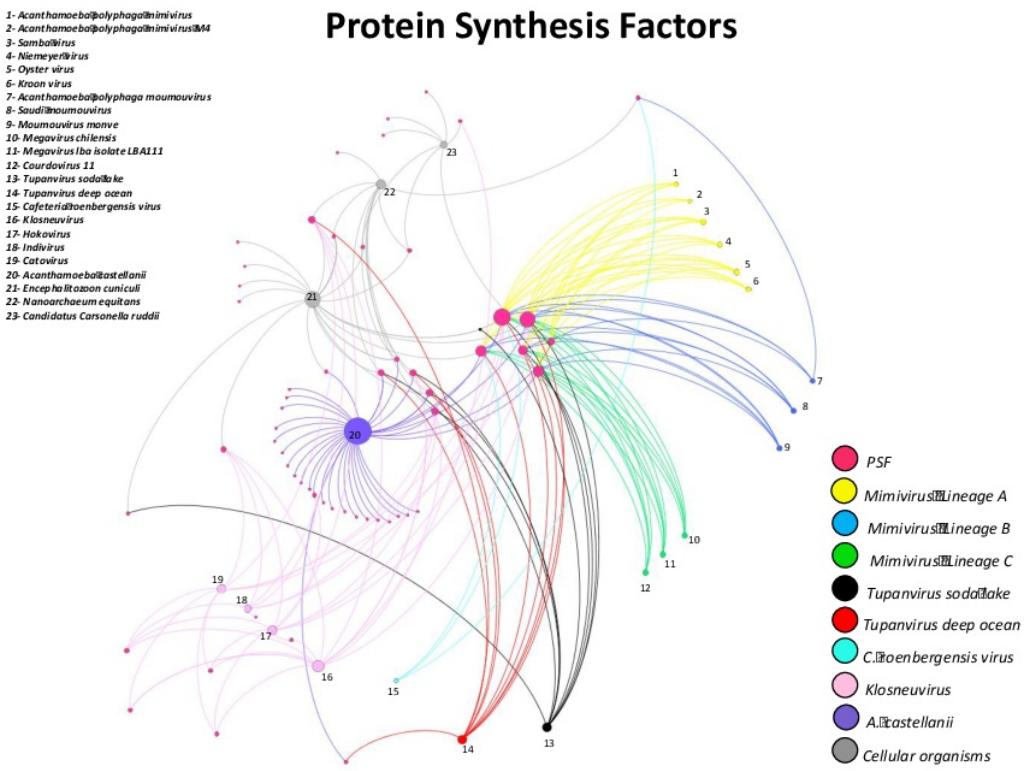
Protein Synthesis Factors
1- Acanthamoeba polyphaga mimivirus
2- Acanthamoeba polyphaga mimivirus M4
3- Samba virus
4- Niemeyer virus
5- Oyster virus
6- Kroon virus
7- Acanthamoeba polyphaga moumouvirus
8- Saudi moumouvirus
9- Moumouvirus monve
10- Megavirus chilensis
11- Megavirus lba isolate LBA111
12- Courdovirus 11
13- Tupanvirus soda lake
14- Tupanvirus deep ocean
15- Cafeteria roenbergensis virus
16- Klosneuvirus
17- Hokovirus
18- Indivirus
19- Catovirus
20- Acanthamoeba castellanii
21- Encephalitozoon cuniculi
22- Nanoarchaeum equitans
23- Candidatus Carsonella ruddii
PSF
Mimivirus Lineage A
Mimivirus Lineage B
Mimivirus Lineage C
Tupanvirus soda lake
Tupanvirus deep ocean
C. roenbergensis virus
Klosneuvirus
A. castellanii
Cellular organisms

33

Supplementary Figure 8: Analysis of Tupanvirus 18S rRNA intronic region (copies 1 or 2) expression in infected *Acanthamoeba castellanii* cells at 30 minutes and at 6 and 12 hours post-infection. Fluorescence in situ hybridization (FISH) (a and b) and qPCR (c – copy 1 and d – copy 2). In red, viral 18S rRNA intronic copies; in green *Acanthamoeba* 18S rRNA region (a and b). FISH analysis related to 24 hours post-infection; copy 1 is also shown in Figure 7a. Scale bar, 10 µm. Error bars (c and d), standard deviation. The experiments were performed 3 times independently, with two replicates each.

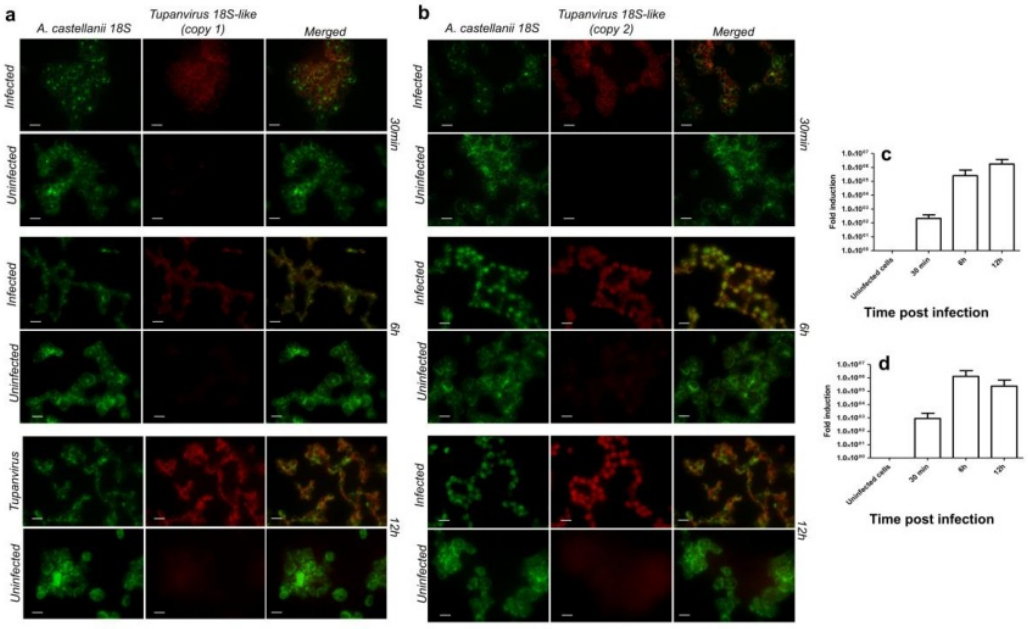

34

Supplementary Figure 9: Acidification of *Acanthamoeba castellanii* cytoplasm after Tupanvirus soda lake and mimivirus infection (9 h.p.i.). (a) Tupanvirus causes strong acidification of amoebal cytoplasm even in the presence of bafilomycin A. (b) Quantification of the acidification demonstrated in (a). (c-f) Even in the presence of chloroquine or bafilomycin A, the rRNA shutdown induced by Tupanvirus is not prevented (3 and 9 h.p.i.). (g-j) qPCR results related to the cells infected and treated as presented in (c-f). Scale bar, 5 µm. Error bars (b, g-j), standard deviation. Statistical analyses were performed on the data shown in (b) using a t-test based on control groups. **:p<0.01; ***:p<0.001. The experiments were performed 3 times independently, with two replicates each.

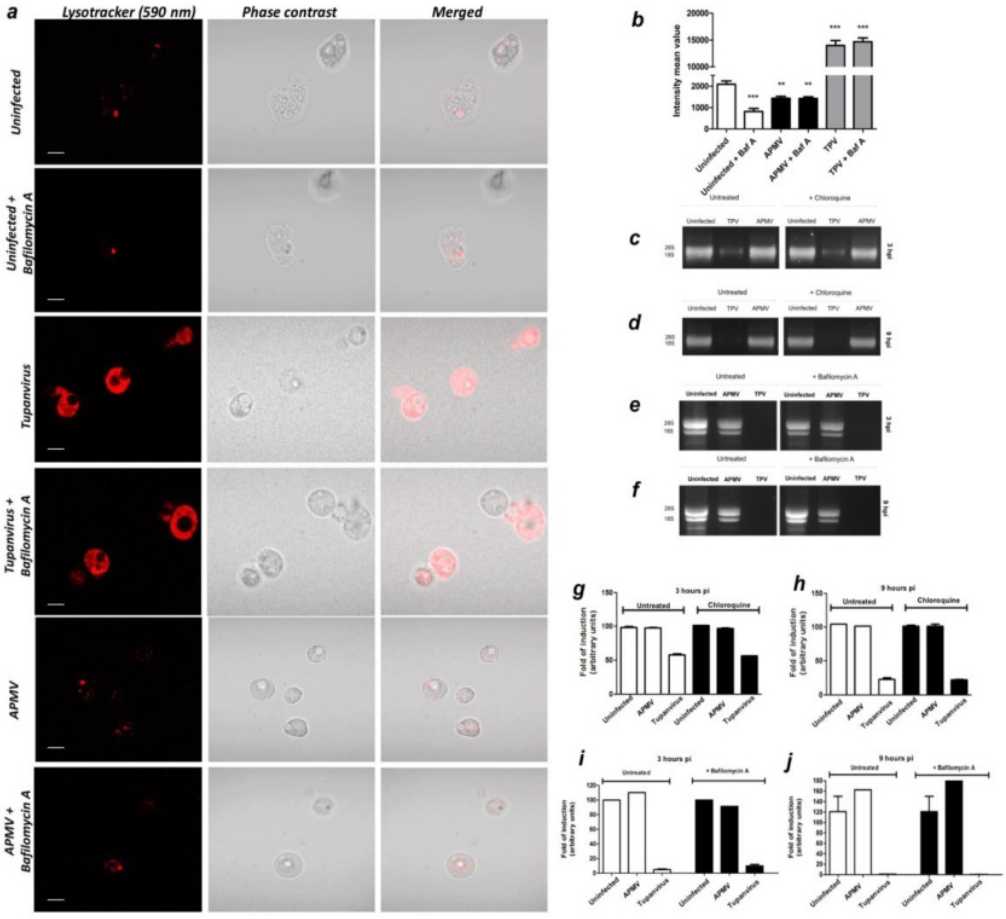

SUPPLEMENTARY TABLE

Supplementary Table 1: Permissiveness profile of Tupanvirus in different cells.

Cell	CPE	Viral titer increasing	Viral genome replication	Infection profile
Acanthamoeba castellanii	+	$3\log_{10}$, after 24 hours	5 x $3\log_{10}$, after 24 hours	productive
Acanthamoeba sp E4	+	$1\log_{10}$, after 24 hours	6 x $3\log_{10}$, after 24 hours	productive
Acanthamoeba sp. micheline	+	No	2 x $1\log_{10}$, after 24 hours	abortive
Acanthamoeba polyphaga	+	$1\log_{10}$, after 24 hours	4 x $1\log_{10}$, after 24 hours	productive
Acanthamoeba royreba	+	No	2 x $1\log_{10}$, after 24 hours	abortive
Acanthamoeba griffini	+	$1{,}5\log_{10}$, after 24 hours	7 x $1{,}5\log_{10}$, after 24 hours	productive
Vermamoeba vermiformis	+	$1\log_{10}$, after 24 hours	6 x $1\log_{10}$, after 24 hours	productive
Dyctiostelium discoideum	+	$1\log_{10}$ after 48 hours	2 x $1\log_{10}$ after 48 hours	productive
Willartia magna	+	$0{,}5\log_{10}$ after 24 hours	$0{,}8\log_{10}$ after 24 hours	productive
Tetrahymena hyperangularis	+	No	No	cytotoxic
THP-1	+	No	No	cytotoxic
RAW264.7	+	No	No	cytotoxic
Trichomonas tenax	-	No	No	resistant

CPE: cytopathic effect

www.nature.com/scientificreports

OPEN

Cedratvirus getuliensis replication cycle: an in-depth morphological analysis

Received: 9 January 2018
Accepted: 22 February 2018
Published online: 05 March 2018

Ludmila Karen dos Santos Silva[1], Ana Cláudia dos Santos Pereira Andrade[1], Fábio Pio Dornas[1,2], Rodrigo Araújo Lima Rodrigues[1], Thalita Arantes[1], Erna Geessien Kroon[1], Cláudio Antônio Bonjardim[1] & Jônatas Santos Abrahão[1]

The giant viruses are the largest and most complex viruses in the virosphere. In the last decade, new members have constantly been added to this group. Here, we provide an in-depth descriptive analysis of the replication cycle of Cedratvirus getuliensis, one of the largest viruses known to date. We tracked the virion entry, the early steps of virus factory and particles morphogenesis, and during this phase, we observed a complex and unique sequential organization of immature particle elements, including horseshoe and rectangular compartments, revealed by transverse and longitudinal sections, respectively, until the formation of the final ovoid-shaped striped virion. The genome and virion proteins are incorporated through a longitudinal opening in the immature virion, followed by the incorporation of the second cork and thickening of the capsid well. Moreover, many cell modifications occur during viral infection, including intense membrane trafficking important to viral morphogenesis and release, as evidenced by treatment using brefeldin A. Finally, we observed that Cedratvirus getuliensis particles are released after cellular lysis, although we obtained microscopic evidence that some particles are released by exocytosis. The present study provides new information on the unexplored steps in the life cycle of cedratviruses.

The study of giant viruses has been intensified after the isolation of Acanthamoeba polyphaga mimivirus, a virus of outstanding dimensions, capable of infecting amoebas of the genus *Acanthamoeba*[1]. Since then, the intense prospection and improvement of isolation techniques has made possible the discovery of new viruses[2,3]. The presence of these viruses has been observed in rather diverse environments, such as water, soil, sewage, and clinical samples, as well as in extreme environments, including permafrost and soda lakes, for example[4–6]. These discoveries have revealed a wide diversity and variety of species not previously observed in the virosphere, challenging the concepts and paradigms concerning the canonical definition of viruses[7]. Currently, the International Committee of Taxonomy of Viruses (ICTV) officially recognizes two families of giant virus of amoebas: *Mimiviridae* and *Marseilleviridae*. In addition to these families, other giant viruses (not assigned yet) have been isolated, such as Faustovirus and Kaumoebavirus, the first giant viruses described to replicate in *Vermoamoeba vermiformes*[8,9]. The tupanviruses, recently isolated from Brazilian environments, present a complex virion structure, with a mimivirus-like capsid attached to a long tail, and these viruses replicate in a broad range of protists (unpublished data). Other isolated viruses, such as Pandoravirus, Pithovirus, Mollivirus and Cedratvirus, also have atypical virion morphologies, exhibiting amphora-shaped, spherical or ovoid structures[4,6,10,11].

Among these viruses, the cedratvirus has an ovoid viral particle, morphologically similar to that of pithovirus but presenting two corks, one at each apex[4,10]. The first Cedratvirus, A11, was isolated from environmental samples from Algeria[10]. Then, a second isolate, Cedratvirus lausannensis, was recovered from a water treatment plant in Morsang-sur-Seine, France[12]. Through an extensive prospective study, we isolated the first cedratvirus from Brazil, named Cedratvirus getuliensis. Although studies on the prospection of giant viruses have advanced over the years, enabling the isolation of new viruses, information regarding their biology remains scarce. In the present study, we present an in-depth investigation of the replication cycle of Cedratvirus getuliensis (C. getuliensis). Through transmission electron microscopy and biological assays using different pharmacological

[1]Departamento de Microbiologia, Instituto de Ciências Biológicas, Universidade Federal de Minas Gerais, Belo Horizonte, Minas Gerais, Brazil. [2]Centro de Microscopia da Universidade Federal de Minas Gerais, Belo Horizonte, Minas Gerais, Brazil. Correspondence and requests for materials should be addressed to J.S.A. (email: jonatas.abrahao@gmail.com)

inhibitors, we elucidated different steps of the replication cycle. We provided the first evidence of a complex and unique sequential organization of immature particles elements, including transverse-sectioned horseshoe and longitudinal-sectioned rectangular compartments, until the formation of the final striped, ovoid-shaped virion. Moreover, many cell modifications occur during viral infection, raising questions about the role of some organelles during the replication of Cedratvirus getuliensis. Amorphous particles were observed in many cells, similar to those previously observed for Pithovirus, but these particles were homogeneously diffused throughout the host cytoplasm, suggesting that deformed particles are naturally formed by Cedratvirus getuliensis. Finally, we observed that Cedratvirus getuliensis particles are released after cellular lysis, although we obtained microscopy evidence that some particles are released by exocytosis. These results provide new information on the unexplored steps in the life cycle of cedratviruses.

Material and Methods

Virus isolation, cell culture, production and titration. Cedratvirus getuliensis was previously isolated in 2017 from sewage samples collected in the city of Itaúna, Minas Gerais, Brazil. After isolation, the virus genome was sequenced, and subsequent bioinformatics analyses were developed; we observed high homology and synteny among the genomes of Cedratvirus getuliensis and other Cedratviruses (in preparation). For co-culture and isolation procedures, *Acanthamoeba castellanii* cells (ATCC 30010) were cultivated in Peptone-yeast extract with glucose (PYG)[13] medium supplemented with 25 mg/ml amphotericin B (Fungizone; Cristalia, São Paulo, Brazil), 500 U/ml penicillin (Schering-Plough, Brazil) and 50 mg/ml gentamicin (Schering-Plough, Brazil). A total of 7×10E6 cells was infected with *C. getuliensis* at a multiplicity of infection (MOI) of 0.01 and incubated at 32 °C. After the appearance of a cytopathic effect, the cells and supernatants were collected, with sterile serological pipettes, stored in conic sterile tubes and the viruses were subsequently purified through ultracentrifugation with a 40% sucrose cushion at 36,000 *g* for 1 h. After purification, the viruses were serially diluted, and multiple replicate samples of each dilution were inoculated into *A. castellanii* monolayers. After 72–96 h of incubation, the amoebas were analyzed to determine whether infection occurred. Based on these data, the virus titers were determined using the endpoint method[13,14].

Entry and traffic membrane assays. In these experiments, we first evaluated the primary mechanism used by C. getuliensis to enter *A. castellanii* cells. For that we used different chemical inhibitors in order to investigate different endocytic pathways commonly explored by viral particles to enter in host cells, such as cytochalasin D – a phagocytosis inhibitor, chloroquine – clathrin and caveolin -dependent of acidification pathways inhibitors, and 5-(N-ethyl-N-isopropyl) amiloride (EIPA) – a specific macropinocytosis inhibitor. Cytochalasin D and chloroquine had already been confirmed as inhibitors of endocytic pathways in *Acanthamoeba*. However, the micropinocytosis inhibition effect induced by EIPA (observed in other systems) remains to be molecularly investigated in *Acanthamoeba*. A total of 5×10^5 *A. castellanii* cells was pre-treated with 2 μM of cytochalasin (Sigma-Aldrich, United States), 100 μM of chloroquine (Sigma-Aldrich, United States) or 1 μM of EIPA (Sigma-Aldrich, United States). The cytotoxicity of the inhibitors was tested in *Acanthamoeba* and the choice by inhibitors concentrations was based on previous studies[15–22]. After 1 h, the cells were infected with C. getuliensis at an MOI of 5. Control groups of untreated infected amoebas were also prepared. Thirty minutes post-infection, cells and supernatant were collected and centrifuged at 800 g per 10 minutes. The resultant pellet was washed three times with Page's amoeba saline (PAS)[13]. After, cells were submitted to three rounds of freezing and thawing, to allow the viral particles release, and then subjected to titration using the endpoint method[13,14]. In parallel, the supernatant of cytochalasin assay was also submitted to titration for comparison.

To evaluate the role of cell membranes in the viral replication cycle, 5×10^5 *A. castellanii* cells were also infected with C. getuliensis at an MOI of 5. Thirty minutes post-infection, the amoebas were washed with PAS and then transferred to 6-well microplates containing 1 mL of PYG medium and maintained at 32 °C. After 1 h, brefeldin A (BFA), an inhibitor of membrane traffic, was added at a final concentration of 10 μM, and at 8 and 24 h post-infection, the amoebas were collected for TEM analysis and titration, respectively.

All experiments were performed in triplicate. Graphs were constructed using GraphPad Prism version 7.00 for Windows (GraphPad Software).

Transmission electron microscopy and Scanning electron microscopy. For transmission electron microscopy (TEM), 7×10^6 *Acanthamoeba castellanii* cells were subjected to an asynchronous viral infection using a low MOI of 0.1, and 24 hours post-infection they were recovered and pelleted for 10 min at 800 g. The pellet was washed twice with 0.1 M phosphate buffer (pH 7.4) and fixed with 2.5% glutaraldehyde in 0.1 M phosphate buffer for 1 h at room temperature. The pellet was then washed twice with 0.1 M phosphate buffer and resuspended in the same buffer. After repelleting, the amoebas were embedded in Epon resin by using a standard method, as follows: 2 h of fixation in 2% osmium tetroxide, five washes in distilled water, overnight incubation in uranyl acetate 2% at 2–8 °C, two washes in distilled water, 10 min dehydration in increasing ethanol concentrations (35%, 50%, 70%, 85%, 95% and 100% ethanol), 20 min incubation in acetone and embedding in EPON resin. Ultrathin sections were subsequently analyzed under transmission electron microscopy (TEM; Spirit Biotwin FEI-120 kV).

For scanning electron microscopy assays, 10 μL of purified particles of C. getuliensis were added to round glass coverslips covered with poly-l-lysine and fixed with 2.5% glutaraldehyde in 0.1 M cacodylate buffer for at least 1 h at room temperature. The same procedure was performed to observe *Acanthamoeba* cell interactions with C. getuliensis during the early (1 h.p.i) and late stages (24 h.p.i.) of infection. The samples were washed three times with 0.1 M cacodylate buffer and post-fixed with 1.0% osmium tetroxide for 1 h at room temperature. After a second fixation, the samples were washed three times with 0.1 M cacodylate buffer and immersed in 0.1% tannic acid for 20 min. The samples were then washed in cacodylate buffer and 10 min dehydrated by serial passages in ethanol solutions (35%, 50%, 70%, 85%, 95% and 100%). Samples were subsequently subjected to critical point drying

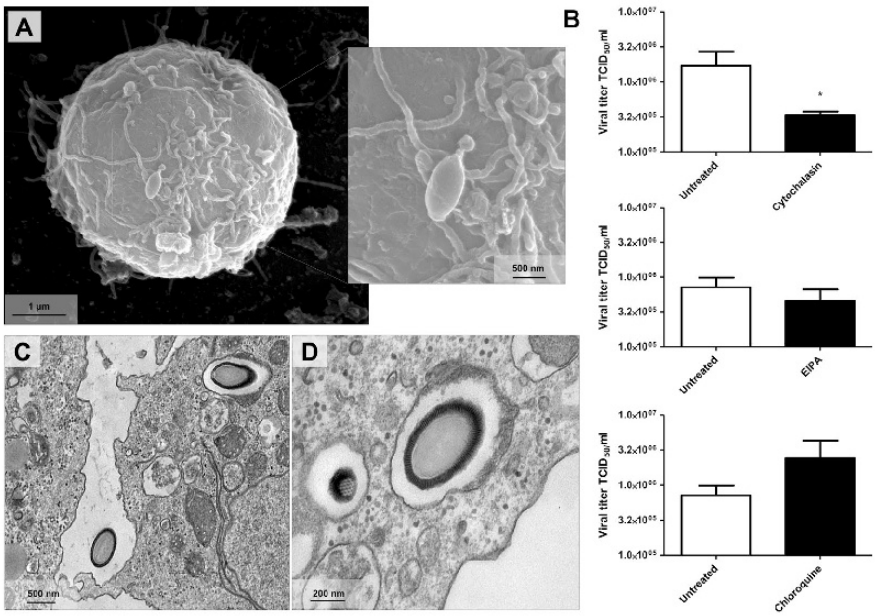

Figure 1. Cedratvirus getuliensis entry in Acanthamoeba castellanii cells. (**A**) Scanning microscopy showing a C. getuliensis particle attached to an *Acanthamoeba* cell. (**B**) The impact of different inhibitors of endocytic pathways in C. getuliensis entry. Treatment of amoebas with cytochalasin D reduced Cedratvirus getuliensis virion incorporation, indicating that particles can enter amoebas by phagocytosis. (**C**) and (**D**) TEM of C. getuliensis particles inside vesicles that strong resemble phagosomes.

using CO_2, placed in stubs and metalized with a 5 nm gold layer. The analyses were completed using scanning electron microscopy (FEG Quanta 200 FEI).

Results

Cytochalasin impacts the incorporation of cedratvirus getuliensis particles by *Acanthamoeba castellanii* cells. Upon discovery of the first cedratviruses[10], analyses involving transmission electron microscopy and scanning electron microscopy[12] revealed the presence of particles with a similar morphology presented by other described viruses, such as pandoravirus and pithovirus. In addition to the morphological similarity, other aspects involving the replication cycle of these viruses were extrapolated and applied to characterize the cedratviruses, such as the internalization of viral particles in amoeba cells by phagocytosis. Our data indicate that Cedratvirus getuliensis can explore phagocytic pathways to enter *A. castellanii* cells, since the titration of pellet cells pretreated with cytochalasin D revealed a significantly decrease (p-value = 0.0385) in the viral titer, when compared to the untreated cells (Fig. 1A and B). Corroborating with those results, when we performed the titration of the supernatant, we observed a higher viral titer for samples pretreated with cytochalasin D, evidencing that a significant number of particles were not phagocytosed (p-value = 0.0243). Transmission electron microscopies of infected particles also corroborate this hypothesis, once C. getuliensis particles could be observed inside vesicles that strong resemble phagosomes (>500 nm), which is consistent with previous studies in which phagocytosis was investigated in amoebas (Fig. 1C and D)[23,24]. In contrast to cytochalasin D, pretreatment with EIPA did not result in a significant reduction in viral titer, indicating that the macropinocytosis is not essential for Cedratvirus getuliensis entry (Fig. 1B). However, as the effects of EIPA has not been previously studied in *Acanthamoeba*, the entry of cedratvirus getuliensis by macropinocytosis cannot be ruled out. In addition, some works have demonstrated that cytochalasin can also interfere on macropinocytosis, that's why a in depth characterization of EIPA in *Acanthamoeba* would be important. Interestingly, we also observed a strong biological tendency of viral title increasing when *Acanthamoeba* cells were treated with chloroquine, an inhibitor of clathrin and caveolin pathways (Fig. 1B).

Cedratvirus getuliensis infection induces the formation of an electron-lucent viral factory and causes cytoplasmic modifications involving different organelles. The replication of many viruses occurs in subcellular microenvironments designated viral factories that originate from the reorganization of cytoskeleton, organelles and cellular membrane compartments[25]. Similarly, the morphogenesis of cedratviruses, as other giant viruses[15,26], occurs in a viral factory located in the cytoplasm of host cells. Using TEM images of Cedratvirus getuliensis replication cycle, we observed the presence of an evident viral factory that in general is as large as the cellular nucleus. Different from mimiviruses, which present an electron-dense viral factory

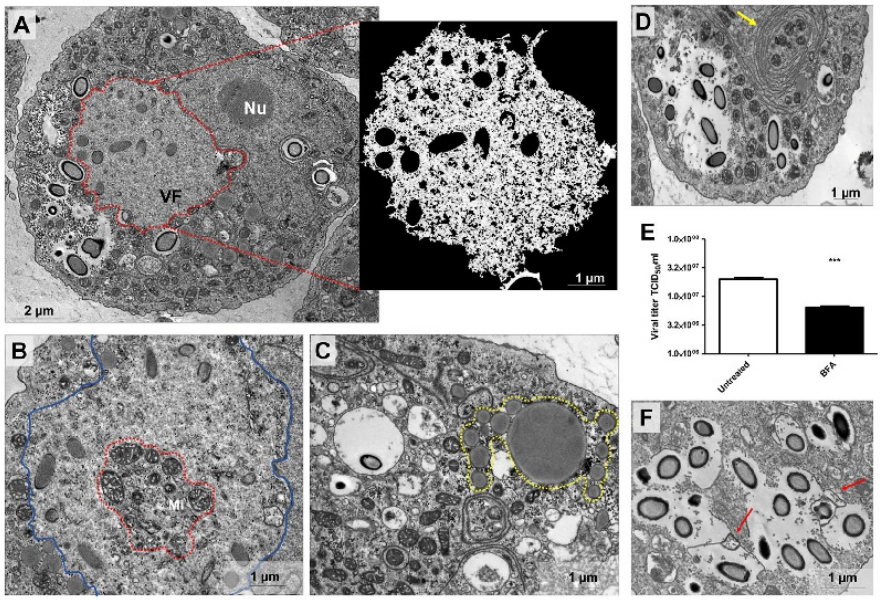

Figure 2. Electron-lucent viral factory and cytoplasmic modifications induced by Cedratvirus getuliensis modification. (**A**) C. getuliensis presents an electron-lucent viral factory (contoured in red and in detail) not easily distinguished from the rest of the cytoplasm and observed at the perinuclear region. Different stages of viral particle morphogenesis could also be observed within the viral factory. (**B**) Abundant presence of mitochondria inside (contoured in red) the viral factory (contoured in blue). (**C**) Lysosomal accumulation and polarization in the host cytoplasm (contoured in yellow). (**D**) Intensified membrane traffic in the host cytoplasm (yellow arrow). (**E**) Treatment with BFA reduces the viral titer after 24 hours of infection. (**F**) Infected cells treated with BFA presented membrane degradation after 8 hours of infection. VF: Viral factory. Nu: Nucleus. Mi: Mitochondria. Image A-right was obtained by TEM and graphically highlighted by using IOS image visualization software.

divided into different parts (one related to genome replication and morphogenesis and another one associated with fibrils acquisition) and are easily distinguished from the rest of the host cytoplasm, the C. getuliensis viral factory is electron-lucent and does not exhibit well-defined zones, thus preventing its prompt distinction from the remaining cytoplasm (Fig. 2A)[26-28]. Moreover, the morphogenesis of C. getuliensis progeny could be observed in the periphery and in the middle of the viral factory, where some electron-dense structures were observed, in contrast to the results observed for mimiviruses, for which the final assembly of new particles occurs at the edge of the factory (Fig. 2A).

Interestingly, we observed that the C. getuliensis viral factory is typically situated at the perinuclear region. During the cycle, the nucleus was consistently present and apparently not affected by the virus, different from that described for pandoraviruses, in which some nuclear disorganization with numerous membrane invaginations were observed in infected cells[11,29]. In addition, during C. getuliensis replication, some absorbing cellular alterations were observed (Fig. 2B,C and D). One alteration was the abundant presence of mitochondria inside and around the viral factory (Fig. 2B). Another interesting change was the intense accumulation and polarization of structures that resemble lysosomal vesicles in the host cytoplasm, particularly during the late steps of the cycle (Fig. 2C). Finally, we also observed exacerbated membrane traffic (Fig. 2D), revealed as important for the morphogenesis and/or exocytosis release of virions, upon the treatment of amoebas with BFA, which significantly impacts the viral titer after 24 hours of infection (Fig. 2E). TEM images also showed a decrease of membrane traffic, as well as membrane degradation in BFA-treated cells, after 8 h of infection (Fig. 2F).

Cedratvirus getuliensis morphogenesis involves the complex and unique sequential organization of immature particles. C. getuliensis morphogenesis is a complex process involving the formation of subsequent structures that could be clearly visualized as electron-dense materials within and at the periphery of the viral factory in TEM images (Fig. 3). TEM images should be analyzed with cautious, since 2D perspective can lead to misinterpretation. However, the obtained images suggest that the first discernible viral particle structures are crescent-shaped ~100 nm precursors developed in the middle of viral factory (Fig. 3A). Similar structures, described as open membrane intermediates or precursors, have been also observed during Vaccinia virus, Mimivirus and African Swine fever virus replication, suggesting the occurrence of a common assembly steps for NCLDVs[30–33]. The following observed differentiation is the longitudinal elongation of the particle (~600 nm),

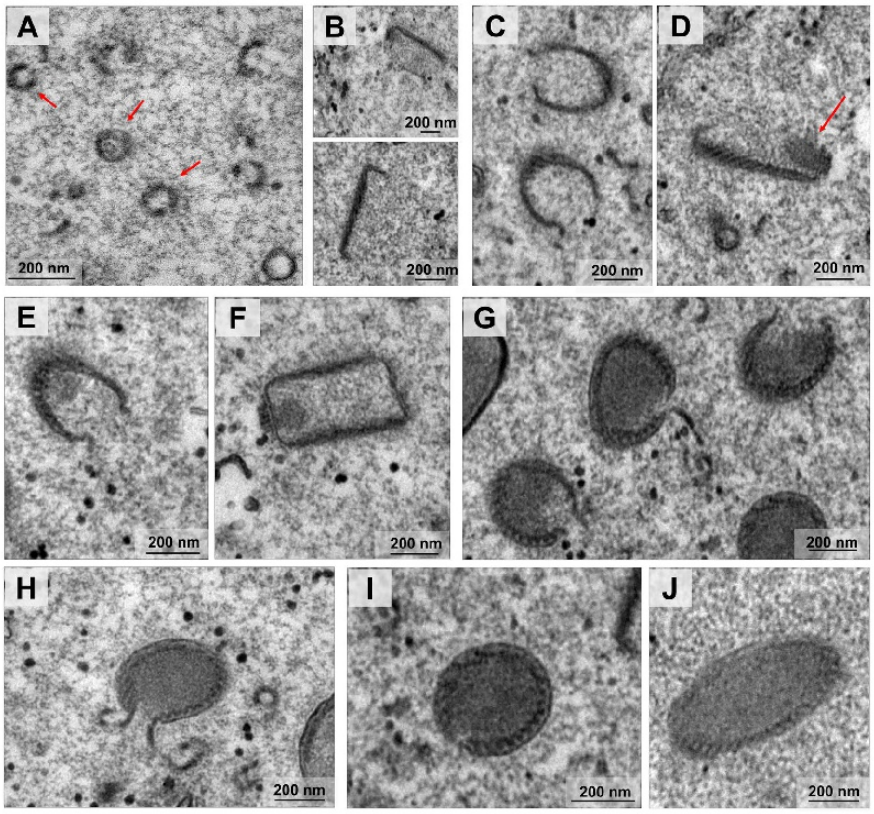

Figure 3. Cedratvirus getuliensis morphogenesis involves the occurrence of subsequent complex structures. (**A**) First discernible viral structures showing a crescent-shaped capsid precursor. (**B**) Longitudinal sections revealed the longitudinal-elongation of the particle and capsids assuming a staple-shaped conformation. (**C**) Transversal sections showed empty capsids with a horseshoe conformation. (**D**) Longitudinal sections showed staple-shaped with the first cork evident (red arrow). The particle may be an open cylinder at this moment, since transversal-sectioned particles appears as rectangles (**F**) and transversal-sectioned particles still reveals horseshoe-like structures (**E**). Progressive filling of the capsid (**G,H**). (**J**) Complete closure of the capsids.

when the precursor capsid assumes a staple-shaped conformation, as visualized by longitudinal sections (Fig. 3B). Transversal sections revealed empty capsids with a similar horseshoe conformation and an evident striated wall, a characteristic feature of pithoviruses as also observed[4,34] (Fig. 3C). At this stage, only one cork region is clearly visible in the longitudinal cut, at the pole where the morphogenesis probably started (Fig. 3D). The particle appears to be an open cylinder at this moment, since longitudinal-sectioned particles appear as rectangles (Fig. 3F) and transversal-sectioned particles still reveal horseshoe-like structures (Fig. 3E). Next, we observed a progressive filling of the capsid (Fig. 3G,H and I), followed by the complete closure of the capsid (Fig. 3J) and the emergence/incorporation of the second cork.

Following the total closure of the capsid, we observed that this structure undergoes some degree of differentiation related to the capsid wall thickness. Immediately after capsid closure, some ovoid particles are observed in the periphery of the viral factory and particle thickening occurs in an area at the edge of or surrounding the viral factory (Fig. 4A and B). Initially, the capsid presents a thin wall and the two corks are not completely laterally covered (Fig. 4C,D and E). As the maturation progresses, the capsid wall becomes thicker until it acquires the same thickness presented by both corks (Fig. 4F,G and H).

Misshapen Cedratvirus getuliensis particles could be observed during virus morphogenesis. We also observed the appearance of some misshapen structures as blobs comprising portions of corks, capsids, membrane and electron-dense material (Fig. 5A and B). These unusual structures have previously been described by Legendre and colleagues in the Pithovirus sibericum replication cycle as "possible reservoirs of partially organized virion building blocks"[4]. We could not discard the hypothesis that these structures might be premature or defective particles, as the occurrence of abnormal particles has previously been reported for other viruses,

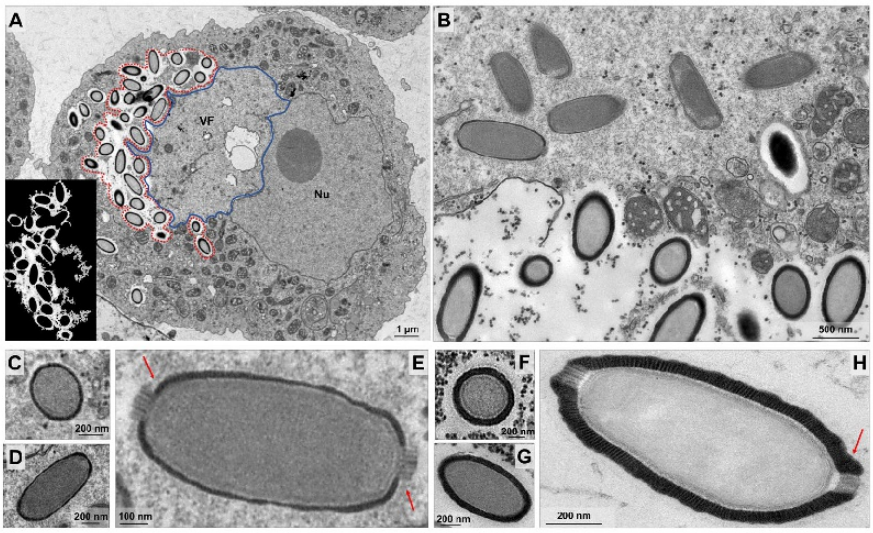

Figure 4. Particle wall thickening after capsids closure. (**A**) Viral particles suffer differentiation related to the thickness in a specific area at the edge of the viral factory (contoured in red and in detail). (**B**) Viral factory periphery evidencing the capsid wall thickness. Cross (**C**) and longitudinal (**D**) sections of capsids presenting a thin thickness and the corks not completely laterally covered (**E**) (red arrows). (**F**) and (**G**) The capsids become thicker with the progression of maturation and acquire the same thickness presented by both corks (**H**) (red arrow). VF: Viral factory. Nu: Nucleus. Image A-left was obtained by TEM and graphically highlighted by using IOS image-visualize software.

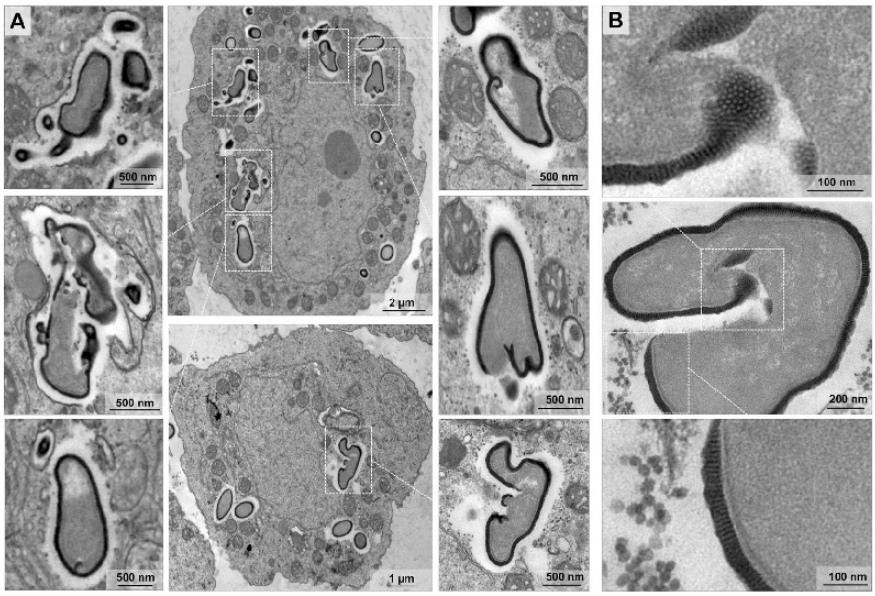

Figure 5. Misshapen structures observed during C. getuliensis multiplication. (**A**) and (**B**) Amorphous structures resembling defective particles and composed by portions of corks, striated capsids, membrane and electron-dense material could be visualized in different regions of the host cytoplasm alongside mature virus.

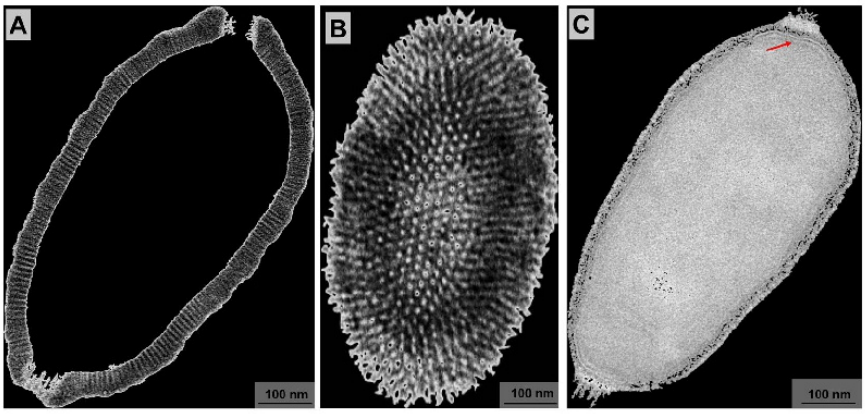

Figure 6. Cedratvirus getuliensis particles present a striped amphora-shaped format and a size plasticity. (**A**) Typical capsid presenting parallel stripes and not completely opposite corks. (**C**) Superficial section of a mature particle evidencing the striped wall. (**D**) Capsid interior composed by a membrane (red arrow) that delimits the internal homogeneous compartment. Images were obtained by TEM and graphically highlighted by using IOS image visualization software.

including giant viruses[26,35]. Notably, the quantification of occurrence of these misshapen structures revealed that 7% of the cells presented at least one of these elements detected in different regions of the host cytoplasm alongside mature virions; thus, these particles are not confined to a viral factory, suggesting that these elements might be defective particles and not particles under morphogenesis.

Viral progeny present ovoid-shaped format, striped capsid and size plasticity. As mentioned, the end of the C. getuliensis replication cycle is characterized by cell lysis with the consequent release of viral particles. An observation of the viral progeny revealed mature particles measuring ~1 µm in size and ~0.5 µm in diameter and showing an ovoid-shaped format with a typical capsid presenting parallel stripes (Fig. 6A). We sagittally sectioned the lateral top, revealing that the virion subunits appear as organized dots (Fig. 6B). Inside this capsid, we observed a putative membrane delimiting the internal compartment without substructures (Fig. 6C). We believe that this putative inner membrane is acquired during the first steps of morphogenesis, prior to the filling of the particles with the viral genome and virion proteins. Unlike that observed for pithovirus, the interior of Cedratvirus getuliensis virions does not harbor episodic electron-dense spheres or tubular structures but is rather homogeneous[4].

As a hallmark of cedratvirus virions, C. getuliensis particles also showed two characteristic protruding striped corks at each apex (Fig. 6A and C). However, although these corks are located at the apices, these structures are not antipodally aligned to each other (Fig. 6A and B) and we observed the existence of a misalignment between the centers of the opposite corks.

Although most of the C. getuliensis particles present a similar morphological pattern, different mature particles were also present. This variation is primarily related to the size of the particles, as shown by scanning electron microscopy analyses that revealed the presence of virions up to 2.04 µm, almost the double the size observed for the majority of particles. Therefore, these data provide evidence of size plasticity for the progeny of Cedratvirus getuliensis, as demonstrated for Pithovirus sibericum[36].

Cedratvirus getuliensis virions can be released after cell lysis or by exocytosis. After the capsid thickening process, the viral morphogenesis and maturation is now complete and new virions are found immersed in the host cytoplasm surrounded by a halo that, despite could be an artefact of epon embedding, is recurrently observed around other giant viruses particles studies[4,6,10,12,37]. Furthermore, new viruses were also observed embedded within membranes (Fig. 7A). Interestingly, these data revealed the presence of one or more particles inside the same vacuole (Fig. 7B,C and D), which could also present more than one membrane (Fig. 7E). We also observed some particles insides vacuoles and outside the cell membrane, but based only in a 2D perspective we could not affirm that the particles are indeed outside of the amoebas or inside some membrane protrusions (Fig. 7F). The presence of the giant virus progeny inside vacuoles has previously been described for Pithovirus sibericum, suggesting that these particles could be released from the cell by exocytosis[4]. Although exocytosis could be an alternative mechanism used for releasing viral progeny, the main strategy used for Cedratvirus getuliensis is cell lysis. Scanning electron microscopy analyses of the late steps of the C. getuliensis cycle reveals the presence of many cells with substantial damage in the plasmatic membrane, where new viral particles are released (Fig. 7G). Furthermore, the cell lysis is accompanied by plasma membrane blebbing (Fig. 7H), that was not visible in control cells not infected by C. getuliensis (Fig. 7I). However, the causes of these blebs induced upon Cedratvirus getuliensis infection deserve further investigation.

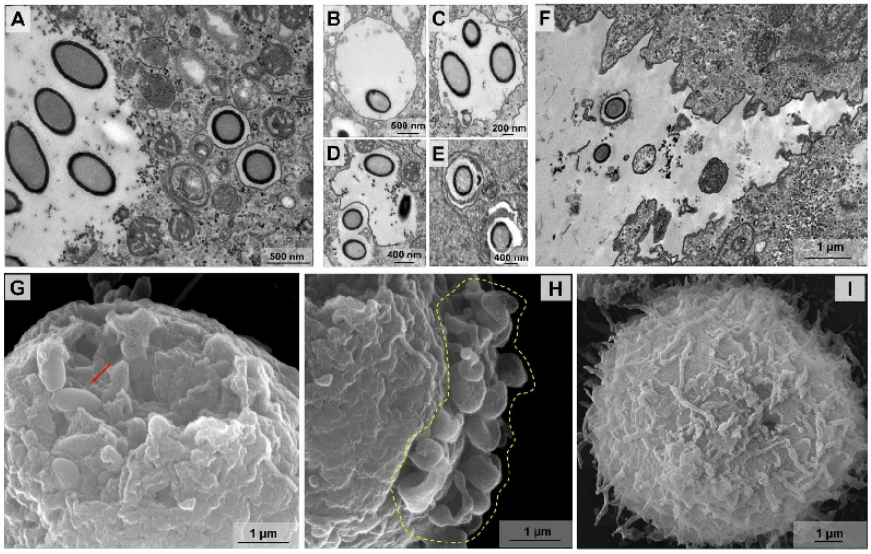

Figure 7. Cedratvirus getuliensis virions can be released after cell lysis or by exocytosis. (**A**) New Cedratvirus getuliensis particles are found immersed in the host cytoplasm or inside vacuoles. (**B–C**) Vacuoles presenting one or more visible particles. (**D**) Particles being engulfed by a membrane. (**E**) Vacuole with more than one membrane. (**F**) Particle insides vacuole apparently outside the cell membrane. (**G**) Scanning microscopy of a host cell presenting a huge damage in the membrane from where new viral particles were released (red arrow). (**H**) Many blebs in the plasma membrane can be observed at the end of infection. (**I**) Cell control not presenting blebs formation in membrane.

Discussion

The current understanding of the virosphere has dramatically changed after the discovery of mimivirus, which paved the way for the discovery of other giant and complex amoeba-infecting viruses[29]. Although many studies have highlighted that giant viruses can be phylogenetically related and may form a new putative viral order 'Megavirales' along with other large DNA viruses[38], these viruses present a plethora of virion structures and remarkable differences regarding their developmental cycles. In the present study, we present the first in-depth description of Cedratvirus getuliensis replication cycle, providing valuable information to better understand the biology of this new group of viruses.

Cedratviruses are ~1.4 µm in size and ~0.5 µm in diameter, representing one of the longest viruses described thus far, along with their close relative pithoviruses[4,10,12,34]. Due to their huge size, it was initially proposed that these viruses started their replicative cycle by entering the hosts through phagocytosis, but no experimental data was provided to support this hypothesis, except for a few microscopy images. Here, we demonstrated that the inhibition of phagocytosis with cytochalasin D results in a reduction of Cedratvirus getuliensis virion incorporation by amoebas, suggesting that this virus may enter by this pathway (Fig. 1B,C and D). However, the inhibition of macropinocytosis by EIPA does not affect the entry of Cedratvirus getuliensis particles (Fig. 1B). Interestingly, *Acanthamoeba* cells treatment with chloroquine increased C. getuliensis viral titer, suggesting that this inhibitor could accumulates inside the phagosomes, resulting in pH increasing and consequent prevention of uncoating process; thus preserving a higher number of not uncoated virions inside phagosomes. Following entry, one of the corks is expelled, enabling the fusion of the internal membrane with the phagosome membrane and further releasing the genome into the host cytoplasm[10]. The precise mechanism that triggers these events remains unclear, but it may be related to the low pH environment of phagosomes, similar to the mechanism observed for mimiviruses[26].

After an eclipse phase, a large electron-lucent viral factory (VF) is formed, wherein genome replication and virion morphogenesis occur. It is still uncertain whether the host nucleus is involved in the replication of the cedratvirus genome, since the nucleus remains apparently unaltered during the entire viral cycle, different from other giant viruses[6,11]. Similar to pithovirus, no delimiting structure was observed around the VF of Cedratvirus getuliensis, which is perinuclearly located[4]. Cedratviruses present a gene-set related to DNA replication and transcription[10,12], and it is possible that these elements are packaged into mature virions, similar to its closest relative Pithovirus sibericum[4]; no nuclear machinery is required during cedratvirus replication, in contrast to that described for marseillevirus[39]. The morphogenesis of cedratviruses is complex, wherein different structures are observed until the full maturation of the virion, which exclusively occurs within the VF (Figs. 3 and 4). Similar to other large and giant DNA viruses, cedratviruses form crescent-like structures and may exhibit an internal membrane, although its origin is still unknown[15,26,30–33,39]. Besides to this putative intern membrane, we also observed transversal-sectioned capsids been filled with an electron-dense material that suggest the occurrence of genome and virion protein acquisition (Fig. 3G,H and I). The complete morphogenesis of the virion resembles that of

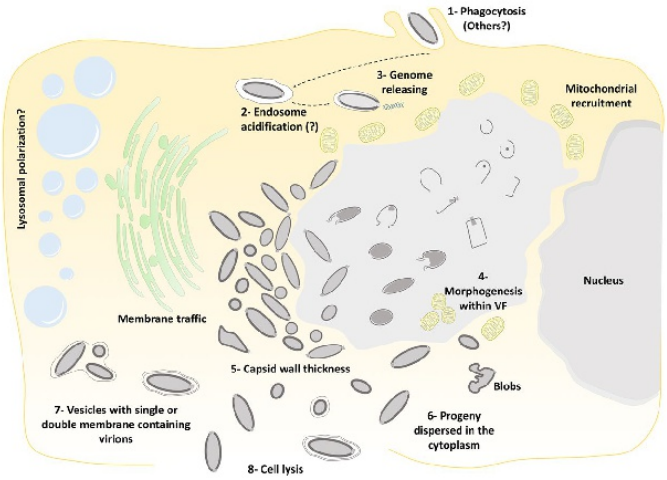

Figure 8. Schematic representation of the Cedratvirus getuliensis replication cycle. Infectious particles enter their host cells by phagocytosis (1). Following entry, one cork is expelled and the fusion of the internal membrane with the phagosome membrane occurs with the release of the genome into the cytoplasm, as demonstrated by Andreani *et al*. (2016) and Bertelli *et al.* (2017) (2–3). The precise mechanism that triggers the cork expelling and membrane fusion remains unknown, but it may be related to the low pH environment of phagosome. After an eclipse phase, a large electron-lucent viral factory is formed, wherein the virion morphogenesis occurs (4). This process is complex and involves sequential structures starting with crescent-shaped precursors, followed by longitudinal-elongation, first cork acquisition, and the presence of structures with a horseshoe-like and rectangular shape (4). Next, a progressive filling of the capsid is observed, followed by the complete closure of the capsid and the emergence of the second cork (4). Thickening of the capsid wall (5) also occurs, and new viral particles are observed dispersed throughout the cytoplasm (6) or taken up by vesicles with one or two membranes (7). The viral progeny are primarily released through cell lysis (8), but exocytosis is also likely to occur.

pithoviruses, with a rectangular shape initially emerging, followed by a thickening of the capsid and subsequent acquisition of an oval shape[4]; but differently from its relative, cedratviruses acquire a second cork at the end of the process. Furthermore, no horseshoe structure has been described for pithoviruses. It is likely that this feature is shared by the members of the putative '*Pithoviridae*' family, but additional studies on the morphogenesis of pithoviruses are needed to corroborate this hypothesis. The replication cycle is completed with the release of new viral particles primarily through cell lysis, but exocytosis is likely to occur, since we observed some viral particles embedded in the membranes and outside the host cells. The origin of these membranes is not clear, but we observed that treatment with BFA significantly impacted the viral titer, showing that membrane traffic is important for the occurrence of virion morphogenesis and/or exocytosis. Although no specific labeling for lysosomes was used, we observed the polarization of structures that resemble these organelles during cedratviruses infection, that could suggest the occurrence of autophagy of target viral components or virions, once this organelle acts as an end point degradative structure (Fig. 2)[40]. Moreover we also noted the recruitment of mitochondria, which could be related to the optimization of energy acquisition, required for viral replication (Fig. 2)[40]. However, the actual impact of these organelles on the viral replication cycle remains unknown. Finally, based on the present data, we provide a general view of the entire life cycle of cedratviruses (Fig. 8 – see legend for details).

There are still some unanswered questions concerning the replication cycle of this new group of viruses, especially at the molecular level. Further investigation using different imaging techniques, combined with transcriptomics and proteomics data, will certainly provide valuable insights into the virus-host interaction dynamics and fill some remaining gaps concerning the life cycle of cedratviruses. The world of giant viruses is constantly increasing, and investigating their infectious biology will provide a better understanding of the ecology and evolution of these complex organisms.

References

1. La Scola, B. *et al*. A giant virus in amoebae. *Science* **299**, 2033, https://doi.org/10.1126/science.1081867 (2003).
2. Pagnier, I. *et al.* A decade of improvements in Mimiviridae and Marseilleviridae isolation from amoeba. *Intervirology* **56**, 354–363, https://doi.org/10.1159/000354556 (2013).
3. Dornas, F. P. *et al.* Isolation of new Brazilian giant viruses from environmental samples using a panel of protozoa. *Frontiers in microbiology* **6**, 1086, https://doi.org/10.3389/fmicb.2015.01086 (2015).
4. Legendre, M. *et al.* Thirty-thousand-year-old distant relative of giant icosahedral DNA viruses with a pandoravirus morphology. *Proceedings of the National Academy of Sciences of the United States of America* **111**, 4274–4279, https://doi.org/10.1073/pnas.1320670111 (2014).

5. Saadi, H. *et al.* First isolation of Mimivirus in a patient with pneumonia. *Clinical infectious diseases: an official publication of the Infectious Diseases Society of America* **57**, e127–134, https://doi.org/10.1093/cid/cit354 (2013).
6. Legendre, M. *et al.* In-depth study of Mollivirus sibericum, a new 30,000-y-old giant virus infecting Acanthamoeba. *Proceedings of the National Academy of Sciences of the United States of America* **112**, E5327–5335, https://doi.org/10.1073/pnas.1510795112 (2015).
7. Lwoff, A. Interaction among virus, cell, and organism. *Science* **152**, 1216–1220 (1966).
8. Bajrai, L. H. *et al.* Kaumoebavirus, a New Virus That Clusters with Faustoviruses and Asfarviridae. *Viruses* **8**, https://doi.org/10.3390/v8110278 (2016).
9. Reteno, D. G. *et al.* Faustovirus, an asfarvirus-related new lineage of giant viruses infecting amoebae. *Journal of virology* **89**, 6585–6594, https://doi.org/10.1128/JVI.00115-15 (2015).
10. Andreani, J. *et al.* Cedratvirus, a Double-Cork Structured Giant Virus, is a Distant Relative of Pithoviruses. *Viruses* **8**, https://doi.org/10.3390/v8110300 (2016).
11. Philippe, N. *et al.* Pandoraviruses: amoeba viruses with genomes up to 2.5 Mb reaching that of parasitic eukaryotes. *Science* **341**, 281–286, https://doi.org/10.1126/science.1239181 (2013).
12. Bertelli, C. *et al.* Cedratvirus lausannensis - digging into Pithoviridae diversity. *Environmental microbiology* **19**, 4022–4034, https://doi.org/10.1111/1462-2920.13813 (2017).
13. Abrahao, J. S. *et al.* Mimiviruses: Replication, Purification, and Quantification. *Current protocols in microbiology.* **41**(14G), 11 11–14G 11 13, https://doi.org/10.1002/cpmc.2 (2016).
14. Reed, L. J. M. H. A simple method of estimating fifty percent endpoints. *Am. J. Hyg* **27**, 493–497 (1938).
15. Arantes, T. S. *et al.* The Large Marseillevirus Explores Different Entry Pathways by Forming Giant Infectious Vesicles. *Journal of virology* **90**, 5246–5255, https://doi.org/10.1128/JVI.00177-16 (2016).
16. Moon, E. K. *et al.* Autophagy inhibitors as a potential antiamoebic treatment for Acanthamoeba keratitis. *Antimicrobial agents and chemotherapy* **59**, 4020–4025, https://doi.org/10.1128/AAC.05165-14 (2015).
17. Jha, B. K. *et al.* Chloroquine has a cytotoxic effect on Acanthamoeba encystation through modulation of autophagy. *Antimicrobial agents and chemotherapy* **58**, 6235–6241, https://doi.org/10.1128/AAC.03164-14 (2014).
18. Ghigo, E. *et al.* Ameobal pathogen mimivirus infects macrophages through phagocytosis. *PLoS pathogens* **4**, e1000087, https://doi.org/10.1371/journal.ppat.1000087 (2008).
19. Alsam, S., Sissons, J., Dudley, R. & Khan, N. A. Mechanisms associated with Acanthamoeba castellanii (T4) phagocytosis. *Parasitology research* **96**, 402–409, https://doi.org/10.1007/s00436-005-1401-z (2005).
20. Chrisman, C. J., Alvarez, M. & Casadevall, A. Phagocytosis of Cryptococcus neoformans by, and nonlytic exocytosis from, Acanthamoeba castellanii. *Applied and environmental microbiology* **76**, 6056–6062, https://doi.org/10.1128/AEM.00812-10 (2010).
21. Soto-Arredondo, K. J., Flores-Villavicencio, L. L., Serrano-Luna, J. J., Shibayama, M. & Sabanero-Lopez, M. Biochemical and cellular mechanisms regulating Acanthamoeba castellanii adherence to host cells. *Parasitology* **141**, 531–541, https://doi.org/10.1017/S0031182013001923 (2014).
22. Taylor, W. M., Pidherney, M. S., Alizadeh, H. & Niederkorn, J. Y. *In vitro* characterization of Acanthamoeba castellanii cytopathic effect. *The Journal of parasitology* **81**, 603–609 (1995).
23. Korn, E. D. & Weisman, R. A. Phagocytosis of latex beads by Acanthamoeba. II. Electron microscopic study of the initial events. *The Journal of cell biology* **34**, 219–227 (1967).
24. Wetzel, M. G. & Korn, E. D. Phagocytosis of latex beads by Acahamoeba castellanii (Neff). 3. Isolation of the phagocytic vesicles and their membranes. *The Journal of cell biology* **43**, 90–104 (1969).
25. de Castro, I. F., Volonte, L. & Risco, C. Virus factories: biogenesis and structural design. *Cellular microbiology* **15**, 24–34, https://doi.org/10.1111/cmi.12029 (2013).
26. Andrade, A. *et al.* Filling Knowledge Gaps for Mimivirus Entry, Uncoating, and Morphogenesis. *Journal of virology* **91**, https://doi.org/10.1128/JVI.01335-17 (2017).
27. Suzan-Monti, M., La Scola, B., Barrassi, L., Espinosa, L. & Raoult, D. Ultrastructural characterization of the giant volcano-like virus factory of Acanthamoeba polyphaga Mimivirus. *PloS one* **2**, e328, https://doi.org/10.1371/journal.pone.0000328 (2007).
28. Kuznetsov, Y. G., Klose, T., Rossmann, M. & McPherson, A. Morphogenesis of mimivirus and its viral factories: an atomic force microscopy study of infected cells. *Journal of virology* **87**, 11200–11213, https://doi.org/10.1128/JVI.01372-13 (2013).
29. Colson, P., La Scola, B. & Raoult, D. Giant Viruses of Amoebae: A Journey Through Innovative Research and Paradigm Changes. *Annual review of virology* **4**, 61–85, https://doi.org/10.1146/annurev-virology-101416-041816 (2017).
30. Suarez, C. *et al.* African swine fever virus assembles a single membrane derived from rupture of the endoplasmic reticulum. *Cellular microbiology* **17**, 1683–1698, https://doi.org/10.1111/cmi.12468 (2015).
31. Suarez, C. *et al.* Open membranes are the precursors for assembly of large DNA viruses. *Cellular microbiology* **15**, 1883–1895, https://doi.org/10.1111/cmi.12156 (2013).
32. Mutsafi, Y., Shimoni, E., Shimon, A. & Minsky, A. Membrane assembly during the infection cycle of the giant Mimivirus. *PLoS pathogens* **9**, e1003367, https://doi.org/10.1371/journal.ppat.1003367 (2013).
33. Mutsafi, Y., Zauberman, N., Sabanay, I. & Minsky, A. Vaccinia-like cytoplasmic replication of the giant Mimivirus. *Proceedings of the National Academy of Sciences of the United States of America* **107**, 5978–5982, https://doi.org/10.1073/pnas.0912737107 (2010).
34. Levasseur, A. *et al.* Comparison of a Modern and Fossil Pithovirus Reveals Its Genetic Conservation and Evolution. *Genome biology and evolution* **8**, 2333–2339, https://doi.org/10.1093/gbe/evw153 (2016).
35. Abrahao, J. S. *et al.* Acanthamoeba polyphaga mimivirus and other giant viruses: an open field to outstanding discoveries. *Virology journal* **11**, 120, https://doi.org/10.1186/1743-422X-11-120 (2014).
36. Okamoto, K. *et al.* Structural variability and complexity of the giant Pithovirus sibericum particle revealed by high-voltage electron cryo-tomography and energy-filtered electron cryo-microscopy. *Scientific reports* **7**, 13291, https://doi.org/10.1038/s41598-017-13390-4 (2017).
37. Campos, R. K. *et al.* Samba virus: a novel mimivirus from a giant rain forest, the Brazilian Amazon. *Virology journal* **11**, 95, https://doi.org/10.1186/1743-422X-11-95 (2014).
38. Colson, P., de Lamballerie, X., Fournous, G. & Raoult, D. Reclassification of giant viruses composing a fourth domain of life in the new order Megavirales. *Intervirology* **55**, 321–332, https://doi.org/10.1159/000336562 (2012).
39. Fabre, E. *et al.* Noumeavirus replication relies on a transient remote control of the host nucleus. *Nature communications* **8**, 15087, https://doi.org/10.1038/ncomms15087 (2017).
40. Novoa, R. R. *et al.* Virus factories: associations of cell organelles for viral replication and morphogenesis. *Biology of the cell* **97**, 147–172, https://doi.org/10.1042/BC20040058 (2005).

Acknowledgements

The authors would like to thank our colleagues from Gepvig and the Laboratório de Vírus for their excellent technical support. The authors would also like to thank the CNPq, CAPES and FAPEMIG for scholarships and the Center of Microscopy of UFMG. J.S.A., C.A.B. and E.G.K. are CNPq researchers.

Author Contributions

L.K.S.S., A.C.S.P.A., F.P.D., R.A.L.R., T.A.: performed experiments; J.S.A., C.A.B. and E.G.K.: designed the study. L.K.S.S.: made the Fig. 8; L.K.S.S., R.A.L.R., J.S.A.: wrote the manuscript. All the authors read the final version of the manuscript.

Additional Information

Competing Interests: The authors declare no competing interests.

Publisher's note: Springer Nature remains neutral with regard to jurisdictional claims in published maps and institutional affiliations.

11.4. Outros artigos publicados durante o doutorado

OLIVEIRA, GRAZIELE; ANDRADE, ANA; RODRIGUES, RODRIGO; ARANTES, THALITA; BORATTO, PAULO; SILVA, LUDMILA; DORNAS, FÁBIO; TRINDADE, GILIANE; DRUMOND, BETÂNIA; LA SCOLA, BERNARD; KROON, ERNA; ABRAHÃO, JÔNATAS. **Promoter Motifs in NCLDVs: An Evolutionary Perspective.** Viruses, v. 9, p. 16, 2017.

ARANTES, THALITA SOUZA; RODRIGUES, RODRIGO ARAÚJO LIMA; SILVA, LUDMILA KAREN DOS SANTOS; OLIVEIRA, GRAZIELE PEREIRA; DE SOUZA, HELTON LUÍS; B. KHALIL, JACQUES Y.; OLIVEIRA, DANILO BRETAS DE; TORRES, ALICE ABREU; DA SILVA, LUIS LAMBERTI; COLSON, PHILIPPE; KROON, ERNA GEESSIEN; DA FONSECA, FLÁVIO GUIMARÃES; BONJARDIM, CLÁUDIO ANTÔNIO; LA SCOLA, BERNARD; ABRAHÃO, JÔNATAS SANTOS. **The large marseillevirus explores different entry pathways by forming giant infectious vesicles.** Journal of Virology (Print), v. 90, p. JVI.00177-16, 2016.

ABRAHAO, J. S.; OLIVEIRA, GRAZIELE PEREIRA; SILVA, L. C. F.; SILVA, L. K. S.; KROON, ERNA; LA SCOLA, BERNARD. **Mimiviruses: Replication, Purification, and Quantification.** Current Protocols in Microbiology. 14Ged.New Jersey: John Wiley & Sons, 2016, v. 41, p. 1-13.

viruses

MDPI

Review

Promoter Motifs in NCLDVs: An Evolutionary Perspective

Graziele Pereira Oliveira [1,†], Ana Cláudia dos Santos Pereira Andrade [1,†], Rodrigo Araújo Lima Rodrigues [1], Thalita Souza Arantes [1], Paulo Victor Miranda Boratto [1], Ludmila Karen dos Santos Silva [1], Fábio Pio Dornas [1], Giliane de Souza Trindade [1], Betânia Paiva Drumond [1], Bernard La Scola [2], Erna Geessien Kroon [1] and Jônatas Santos Abrahão [1,*]

[1] Laboratório de Vírus, Departamento de Microbiologia, Instituto de Ciências Biológicas, Universidade Federal de Minas Gerais, Belo Horizonte 31270-901, Minas Gerais, Brazil; graziufmg@yahoo.com.br (G.P.O.); ana.andrade2008@hotmail.com (A.C.d.S.P.A.); rodriguesral07@gmail.com (R.A.L.R.); tsarantes@gmail.com (T.S.A.); pvboratto@gmail.com (P.V.M.B.); ludmilakaren@gmail.com (L.K.d.S.S.); fabiopiod154@gmail.com (F.P.D.); gitrindade@yahoo.com.br (G.d.S.T.); betaniadrumond@gmail.com (B.P.D.); ernagkroon@gmail.com (E.G.K.)

[2] Unité de Recherche sur les Maladies Infectieuses et Tropicales Emergentes (URMITE) UM63 CNRS 7278 IRD 198 INSERM U1095, Aix-Marseille Université., 27 Boulevard Jean Moulin, Faculté de Médecine, 13385 Marseille Cedex 05, France; bernard.la-scola@univ-amu.fr

* Correspondence: jonatas.abrahao@gmail.com; Tel.: +55-031-3409-3002

† These authors contributed equally to this work.

Academic Editor: Eric Freed

Received: 14 November 2016; Accepted: 5 January 2017; Published: 20 January 2017

Abstract: For many years, gene expression in the three cellular domains has been studied in an attempt to discover sequences associated with the regulation of the transcription process. Some specific transcriptional features were described in viruses, although few studies have been devoted to understanding the evolutionary aspects related to the spread of promoter motifs through related viral families. The discovery of giant viruses and the proposition of the new viral order Megavirales that comprise a monophyletic group, named nucleo-cytoplasmic large DNA viruses (NCLDV), raised new questions in the field. Some putative promoter sequences have already been described for some NCLDV members, bringing new insights into the evolutionary history of these complex microorganisms. In this review, we summarize the main aspects of the transcription regulation process in the three domains of life, followed by a systematic description of what is currently known about promoter regions in several NCLDVs. We also discuss how the analysis of the promoter sequences could bring new ideas about the giant viruses' evolution. Finally, considering a possible common ancestor for the NCLDV group, we discussed possible promoters' evolutionary scenarios and propose the term "MEGA-box" to designate an ancestor promoter motif ('TATATAAAATTGA') that could be evolved gradually by nucleotides' gain and loss and point mutations.

Keywords: megavirales; NCLDV; giant viruses; promoter; transcription; evolution; MEGA-box

1. Introduction

For decades, viruses have been strictly considered intracellular parasites, filterable in membranes of 0.22 nm, composed by genomes of DNA or RNA encoding only a few proteins, being entirely dependent on the metabolic machinery of the host cell [1]. However, viruses show a large diversity of genome size and organization, capsid architecture, mechanisms of replication, and interactions with host cells. The extreme diversity of viruses suggests that they must have had multiple evolutionary origins, thus being polyphyletic [2]. In 2001, a supposedly monophyletic

group named nucleo-cytoplasmic large DNA viruses (NCLDV) was proposed, composed of families *Poxviridae*, *Asfarviridae*, *Iridoviridae* and *Phycodnaviridae* [3]. This group gained notoriety two years later with the discovery of *Acanthamoeba polyphaga mimivirus* [4] and it is currently composed of the families mentioned above, as well as *Ascoviridae*, and the more recently incorporated *Mimiviridae* and *Marseilleviridae* [5]. Moreover, other recently discovered giant viruses such as pandoraviruses, faustoviruses and pithoviruses were classified as members of the NCLDV group [6–9]. This group has single features such as large genomes and a diverse gene repertoire, which encode some proteins never identified previously in viruses. Therefore, the creation of a new viral order named 'Megavirales', encompassing all families of the NCLDV group was proposed [5].

This proposed order comprises viruses with large double-stranded DNA (dsDNA) genomes, encoding hundreds of proteins and capable of infecting a wide-range of eukaryotic organisms. These viruses replicate completely or partly, in the cytoplasm of eukaryotic cells and some of them are able to synthesize RNA polymerases (RNA pol), helicases and transcription factors involved in the transcription initiation and elongation steps with lower dependence of the host's transcriptional machinery [3]. The presence of a robust transcriptional apparatus in some Megavirales members, along with a quasi-autonomous glycosylation and translational machinery, especially in mimiviruses, boosted the discussion about the origin and evolution of giant viruses and their genome. Recent evolutionary reconstructions mapped about 25–50 genes encoding essential genes for the probable most recent common ancestor [10]. Concerning the origin of such giant genomes, different hypotheses have been proposed. Some authors suggest a "genome degradation hypothesis", wherein the giant viruses are derived from a cellular ancestor through genome simplification linked to the adaptation to some host lineage [11,12]. Other authors argue in favor of a "genome expansion hypothesis", wherein the giant viruses evolved from a smaller viral ancestor and the universal genes have been independently acquired from their eukaryotic hosts by progressive gene accretion and duplication. According to this theory, the genes of giant viruses have several origins and the origin of giant viruses is probably from a simpler ancestor [13,14].

On the other hand, the accordion-like model of evolution proposes that there is no trend of genome expansion or general tendency of genome contraction. Instead, viruses evolving by constant gene gain and loss originated from an ancestor giant virus [10]. All these theories are often contradictory and have stimulated discussion about the establishment of a fourth domain of life where the giant viruses of the proposed order Megavirales were suggested to share a common ancestral origin based on analyses of their sequences and gene repertoires and compose a new domain aside Bacteria, Archaea and Eukarya [14–16].

During the last years, a huge effort has been made to better understand the virus–host interaction on many levels. One of the most interesting research fields is how the viruses can explore host transcriptional machinery to express their genes. Nevertheless, it is important also to look into the transcription process of the cellular organisms. The upstream regions of eukaryotes and prokaryotes genes have been studied in different organisms in an attempt to discover sequences associated with the regulation of the transcription process. The same has been done for viruses, especially considering the proposed Megavirales order, where some putative promoter sequences have already been described. In this review, we summarize the main aspects of the transcription regulation process in the three domains of life, followed by a systematic description of current knowledge of the promoter regions of all members within Megavirales order. Finally, we discuss how the analysis of the promoter sequences found in giant viruses provides new insights into the evolutionary history of these complex and intriguing agents.

2. Gene Expression in Cells

In all cells, thousands of genes encoded in the DNA are transcribed into RNA and for the efficient occurrence of this process, multiple events must be triggered. In eukaryotes, the genome is coupled to histones and other proteins, forming the chromatin compact complex. Since wrapping

DNA around histones blocks the access to the genetic information, decondensation of DNA is required, to allow physical access to the the gene locus and the transcription initiation machinery formation [17–19]. The transcription initiation machinery is formed over a region of the genome, the promoter. The promoter is typically located 40 bp upstream and downstream of the transcription start of a gene, called transcription start sites (TSS). Several transcription factors mediate the transcription machinery assembly on the promoter region. There are thousands of transcription factors involved in the transcription process, such as TFIIA, TFIIB, TFIID, TFIIE, TFIIF and TFIIH that recognize and bind the promoter region, called the core promoter, and recruit RNA polymerase (RNA pol) [20]. Eukaryotes have five types of RNA pol (I to V). RNA pol I transcribes ribosomal RNA, whereas the type II is the best characterized one and responsible for transcribing genes encoding proteins, and several noncoding RNA classes [18,21,22]. RNA pol III transcribes genes encoding short, untranslated RNAs, such as tRNAs, 5S ribosomal RNA (rRNA) and the spliceosomal U6 small nuclear RNA (snRNA) [23]. RNA pol IV and V transcribe siRNA in plants [24].

One classical element of the core promoter is the TATA-box, which is a consensus sequence (TATAAAT) located at −25 to −30 bp upstream of the TSS. Although the TATA-box sequence is a well-known promoter core motif, it is present only in a minority of mammalian promoters. This sequence is commonly associated with tissue-specific gene transcription and high conservation within species [25,26]. Other eukariotic promoter elements are Initiator (Inr); Downstream Promoter Element (DPE), Core Element Downstream (CED), TFIIB-Recognition Element (TRE), and Motif Ten Element (MTE) [20,27,28]. Together, these components act synergistically to increase transcription efficiency by providing recognition sites for transcription factors, and indicate the direction of transcription and also the DNA strand to be transcribed [20]. The transcription starts with the binding of the TFIID to the TATA-box region, the Inr sequence and/or other core promoter elements [27]. TFIID is a multiprotein complex comprising the TATA-box binding protein (TBP) and more than 10 different TBP associated factors (TAFs) [22]. After binding TBP to the TATA-box motif, the RNA pol II is recruited, and the transcription is triggered (Figure 1A).

Nevertheless, the transcription in eukaryotes is a much more complex process than previously thought and various strategies are used to increase the diversity of transcripts produced. Among mammals, previous analysis has shown that a large proportion of protein-coding genes (58%) use alternative promoters during transcription [25]. These alternative promoters may have different combinations of core promoter elements to increase the variability of transcripts [20,29,30].

There are many differences between the transcription process of eukaryotic and bacteria cells. The bacterial transcription is much simpler compared to the eukaryotic process since the transcription occurs using a single type of RNA pol and there are no transcription factors [31]. This enzyme is capable of synthesizing RNA from a DNA template, but it is unable to locate the promoter and transcription initiation site. Thus, a key factor to transcription is the free subunit named σ (sigma), which is responsible for recognizing the promoter region (Figure 1B) [32,33]. Although the majority of nucleotides within bacteria promoters vary in sequence, several short motifs are conserved. These include the hexamer (TATAAT), located 10 base pairs (bp) upstream of the TSS and is recognized by domain 2 of RNA pol σ subunit. Another motif is the the hexamer (TTGACA), located 35 base pairs (bp) upstream of the TSS and recognized by domain 4 of the RNA pol σ subunit [31,34,35]. In Archaea, there is a mix of eukarya and bacteria translational apparatus. Just as in eukaryotes, the archaea RNA pol is not able to recognize promoter sequences by itself and at least two transcription factors analogous to TBP and TFIIB are required [36–38]. The archeal TBP also recognizes specifically an AT-rich sequence, homologous to the TATA-box region of eukaryotes [39,40]. Although archaea transcription machinery is similar to that of eukaryotes, the characterization of transcription regulators of some archaeas showed that most of the transcriptional regulation in archaea is done by "bacterial-like" regulators, as two homologues of bacterial leucine-responsive regulatory protein (Lrp)—Lrs14 and Sa-Lrp and metal-dependent repressor 1 (MDR1) homologous to bacterial metal-dependent regulators (Figure 1C) [41–43].

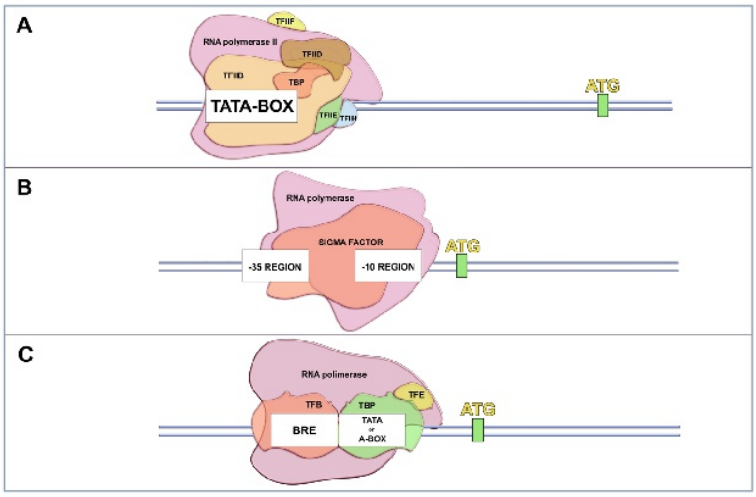

Figure 1. Main features in the transcription initiation machinery presented in the canonical Domains of Life. (**A**) In Eukarya, several components, called general transcription factors (represented as TFIIB, TFIID, TFIIE, TFIIF, TFIIH and TBP), are responsible for assembling over a region called the promoter, where they recruit an RNA polimerase to initiate the transcription process. A classical promoter presented in this group is the TATA-BOX region, located at the positions −25 and −30 from the initial transcription site; (**B**) In Bacteria, the sigma factor recognizes and recruits the RNA polimerase over the promoter regions. These regions are well conserved over the positions −35 and −10 upstream of the initial transcription site; (**C**) Archaea present a mixture of the transcription apparatus of the two other Domains. While the machinery itself is similar to that found in eukaryotes (the general transcription factors, a homologous TATA-BOX region and the RNA polimerase), the archaeal transcription regulators, activators and repressors are homologous to the bacterial ones.

Hypotheses regarding the evolutionary history of translational machinery among the living organisms have been raised during the last years, but the theme is still under debate [44]. Even considering the most recent proposals, the translational process of viruses remains out of the discussion, basically because these organisms are traditionally excluded from the canonical tree of life. However, this scenario has been changing since the discovery of giant viruses [16]. Therefore, it becomes interesting to examine if NCLDV members share similar transcription initiation strategies that could bring insights about how this correlates to giant viruses' evolution.

Gene Expression in NCLDVs

In contrast to cellular genomes, which are formed by dsDNA, viral genomes show a large diversity genome composition, structures, replication and transcription strategies with great implications in virus biology, as virus–host interactions [45]. The majority of the RNA viruses employ virus-coded specific enzymes (RNA-dependent RNA polymerases) to synthesize and modify their mRNA. DNA viruses showing small and intermediate size genomes such as the parvoviruses, papillomaviruses, and adenoviruses, depend on host-cell enzymes for transcription, including the RNA pol [45]. However, viruses with a large genome such as the giant viruses, mostly encode their transcriptional apparatus, which make them relatively independent from their host transcription machinery [15,46].

The transcription of a typical large DNA virus occurs in a temporal pattern in the host cytoplasm (Figure 2). At the start of infection, a subset of immediate early viral proteins is required for DNA replication and host cell manipulation [47,48]. The early mRNAs also encode enzymes and factors needed for transcription of the intermediate genes. Concomitantly with the expression of intermediate genes, the expression of the early genes is often repressed. Finally, late genes are transcribed, directing the synthesis of structural proteins, non-structural proteins and enzymes present in the mature particle

required for viral assembly [45,48]. The efficient transcription of late mRNA usually depends on intermediate gene products, as well as cellular transcription factors that may differ from those used by the early promoters. The products of the late genes include the immediate early transcription factors, which are packaged along with RNA pol and other enzymes within the virus progeny [47–50].

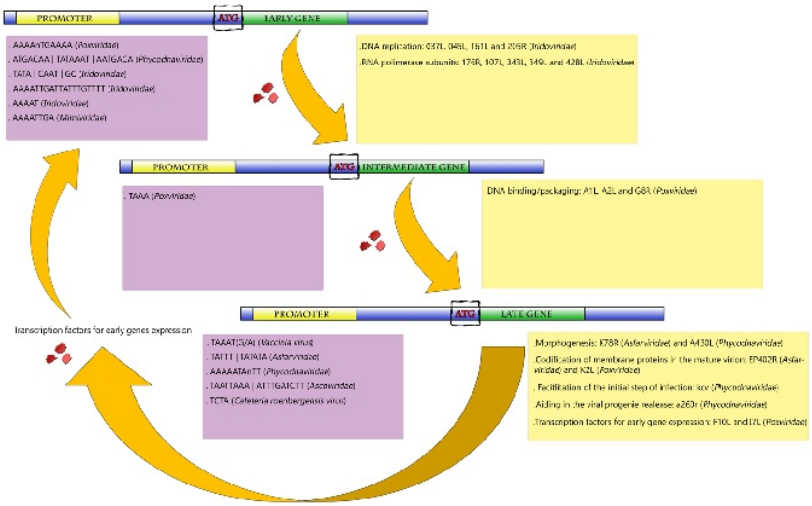

Figure 2. Representative scheme of the temporal gene expression in NCLDVs. During initial times of infection, the expression of genes related to the metabolism of nucleic acids is primarily activated (early and intermediate genes). After DNA replication, the activation of late genes is initiated. Those genes are involved in the production of viral structural proteins, in transcription factors used for early gene expression and also in proteins that facilitate the initial step of infection of the viral progeny in the next round of multiplication. Purple boxes represent the promoters described for giant viruses according to each gene category (early, intermediate and late genes). Yellow boxes exemplify the biological functions involved in each category, with some genes represented inside the parentheses.

This ability to regulate temporally the transcription of genes is characterized as an evolutionary advantage. This strategy is possible due to the presence of promoter codes that dictate when, where, and at what level the classes of early, intermediate, and late genes are transcribed [45,48]. These promoter sequences are different between the three genes classes, but there is a pattern of conservation within the same group. This indicates that during the evolution the gene promoters were selected to ensure the temporal gene expression, and therefore ensure the gene expression in the host cell during its replication [45,47,48,50].

In the following sections, we look closer at how the gene transcription is carried out in each family of the proposed Megavirales order, focusing on the current knowledge about the promoter sequence of these viruses.

3. *Poxviridae* Family

Among NCLDVs, the *Poxviridae* family is one of the most studied. These viruses have enveloped ovoid particles of around 200 nm in diameter and 300 nm in length and present a linear dsDNA genome of approximately 200 kbp coding nearly 200 open reading frames (ORFs). Poxviruses can infect a wide range of hosts, such as insects, birds, and mammals [48,51]. Extensive study of the poxvirus genome and replication cycle allowed a detailed identification of its promoters, as well as important transcription factors. Poxviruses possess their own DNA-dependent RNA polymerase (RNA pol) that is very similar to the eukaryotic protein, regarding size and subunit complexity. In the case of *Vaccinia virus* (VACV), a poxvirus prototype, the enzyme subunits are encoded by eight viral VACV genes

which, in most cases, are homologous to cellular RNApol [52,53]. Gene transcription in poxviruses follows a typical temporal profile regulated by well-conserved promoters of early, intermediate and late genes (Figure 2) [47,48].

The transcription of early genes is characterized by an A/T-rich motif upstream of transcriptional start site with a critical core region located from −13 to −25 to that region. Figure 3 illustrates the promoter motifs described in megavirales members. The representative consensus sequence of the early promoter region is 'AAAANTGAAAA'. Mutagenesis in this promoter region of VACV causes a drastic negative effect on VACV gene transcription [54]. The intermediate genes are transcribed after DNA replication, before the transcription of the late genes. The intermediate core promoter is similar to the early promoter due to the A/T-rich content, but its specific sequence is given by the tetranucleotide 'TAAA'. Furthermore, the intermediate promoter sequence has a bipartite structure presenting a core and an initiator region with similar sequences (TAAA) [55–57]. Three (*A1L*, *A2L*, and *G8R*) of the 53 genes that compose the set of intermediate genes encode transcription factors that are directly related to the late stage of the replication cycle, important to DNA binding/packaging processes and to core-associated proteins [58].

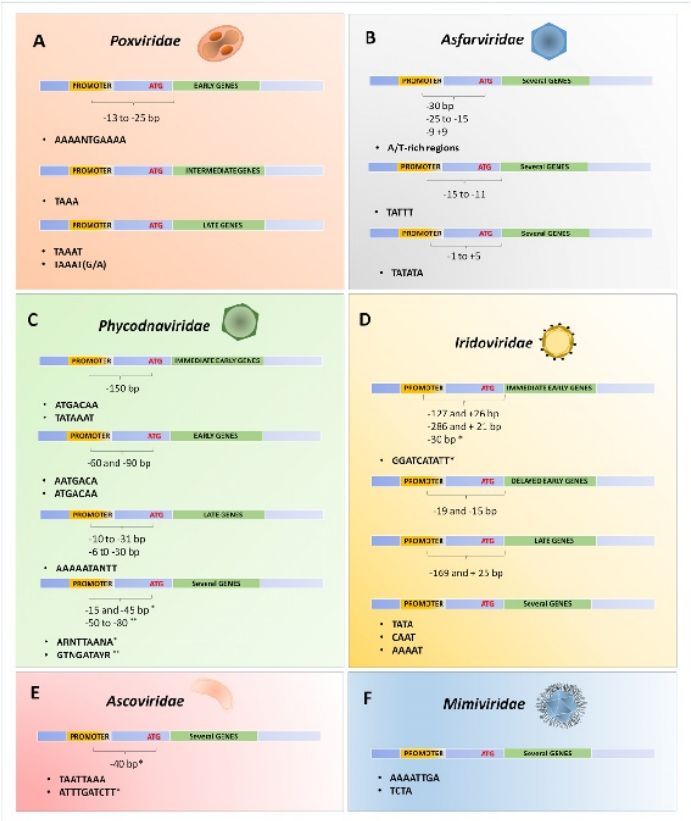

Figure 3. Schematic representation of the promoter's sequences described for different NCLDVs. Compilation of the described promoters for some viral families belonging to the proposed order Megavirales: *Poxviridae* (**A**); *Asfarviridae* (**B**); *Phycodnaviridae* (**C**); *Iridoviridae* (**D**); *Ascoviridae* (**E**) and *Mimiviridae* (**F**). Each promoter was related to the expression of immediate early, early, delayed early, intermediate and late genes, or related to the expression of genes independent of temporal expression (several genes). The distances between the transcription start site or translate start site (ATG) until the promoters are also indicated by brackets.

The transcription of late genes persists until the end of the replication cycle. Around 38 late genes have already been identified, with their main functions related to the codification of membrane proteins in the virion, morphogenesis steps, and also to the production of immediate early transcription factors [57,59]. Most of them are clustered in the central region of the poxviruses genome and also have A/T-rich sequence promoters. These regions consist of a core sequence of about 20 bp with some 'T' residues, separated by a region of about 5–7 bp of a conserved 'TAAAT' motif, which regulates the transcription initiation. Usually, G or A follows the late promoter sequence, performing a 'TAAAT (G/A)' transcription initiation sequence. This sequence is conserved among VACV late promoters, overlapping the site of transcription initiation that is absent in 5' untranslated regions (5'-UTR) [48,54]. Mutations within this conserved element were demonstrated to cause complete inactivation of the promoter, and almost 25% of the 'AAA' sequences are used as transcription initiation sites in VACV. Along with other factors, the viral RNA pol directs the synthesis of late mRNAs, finishing the transcription process [54,60–62].

The presence of complete transcriptional machinery in poxviruses allows a lower dependency of these viruses on their hosts. It permits that the mRNA transcription totally occurs in the host's cytoplasm, right after the virus entry. Addionally, the presence of well conserved promoter regulatory sequences in different poxviruses suggests a conserved evolutionary pattern among them. It is likely that such a complete transcriptional set was already present in their ancestor and was maintained over time. Alternatively, the presence of a robust transcriptional apparatus in all members of the *Poxivirdae* family might be a result of evolutive convergence. Although less parcimonious, the different poxviruses might have had different evolutionary histories regarding the transcription process, including both protein-related elements and promoter sequence regions, but in the course of evolution, they became more similar to each other. It is not yet possible to determine which hypothesis is the correct, or even if other possibilities correspond to the real history of these complex viruses, and this discussion shall continue for a while.

4. *Asfarviridae*

African swine fever virus (ASFV), a large (~200 nm), icosahedral, and enveloped virus is currently the single member of the *Asfarviridae* family, infecting members of the *Suidae* family (pigs, hogs and boars) [63]. The genome is composed of a linear dsDNA molecule of approximately 170 kbp with terminal inverted repeats. It encodes approximately 150 ORFs separated by short intergenic regions [64,65]. ASFV encodes its own RNA pol and all ASFV genes are transcribed by its enzyme [66,67].

Similar to poxviruses, the ASFV gene transcription follows a temporal profile, where immediate early and early genes are expressed before the DNA replication that is followed by the expression of intermediate, late and immediate early genes. Transcription initiation and termination occurs at very precise positions in the genome, encoding a several genes involved in the transcription and modification of viral mRNAs. The transcriptional machinery of ASFV provides an accurate temporal control of gene expression regulated by cis-DNA elements, enhancers, and promoters together with a structural complexity of transcription factors [68]. Analysis of the base composition of the intergenic regions shows that they are rich in A/T sequences, similar to that observed in poxviruses [69–71]. A/T-rich regions located at approximately −30 bp upstream of the ATG translation start site are essential for the expression of the K9L gene, which encodes a protein with similarity to mammalian transcription elongation factor IIS [72]. Furthermore, upstream sequences presented in two intermediate genes exhibit highly conserved sequences at positions −25 to −15, and −9 to +9 to the translational start codon [70]. Experiments involving genetic deletions, linker scan substitutions and point mutations in the promoter sequence of the *p72* gene (major capsid protein) revealed that the replacement of the A/T-rich region by G/C residues strongly reduced the transcription rate, demonstrating the importance of this sequence for efficient late viral transcription [71].

Two other major essential regions for promoter activity are described: one region is located at position −15 to −11 upstream of the transcription start site (TATTT); and the second region at positions −1 to +5 (TATATA) [71]. Mutants presenting the 'TATATA' motif replaced by a G/C-rich sequence had the promoter activity completely abolished, suggesting that ASFV transcription is dependent on such sequence at (or near) the region of transcriptional initiation, similar to what is found in other large viruses [71]. The replacement of the equivalent 'TATATA' sequence on the late genes *K78R*, *EP402R* and *A137R* by the 'GCGC' motif was also demonstrated to be deleterious, suggesting that the A/T-rich sequence could be a motif for late promoter function as well [68,71]. Interestingly, the bipartite structure seen in the late promoter of ASFV is similar to the late and intermediate promoters in poxviruses that contain a core and an initiator region [54,55,62,71]. The similarities found in the transcriptional strategies reinforce the genetic data, indicating a close relationship between poxviruses and asfavirus, pointing to a common ancestor for both viral families.

5. *Phycodnaviridae*

The phycodnaviruses are large and icosahedral viruses (~100–220 nm), with dsDNA genomes ranging from 180 to 560 kbp [73]. Since they infect a diverse group of eukaryotic algae, they are one of the most important groups of organisms regulating the oxygen cycle in the Earth [74,75]. The family *Phycodnaviridae* consists of six genera, named according to the hosts that they infect: *Chlorovirus*, *Coccolithovirus*, *Prasinovirus*, *Prymnesiovirus*, *Phaeovirus*, and *Raphidovirus* [76]. As demonstrated by other giant viruses, the phycodnaviruses exhibit a temporal transcription profile. Early genes are transcribed within 5 to 60 min post-infection (p.i), and transcripts of late genes begin to appear around 60–90 min p.i. However, some early genes can also be detected in later stages of infection [77,78].

The presence of A/T-rich promoters was also observed in phycodnaviruses. Analysis of the *kcv* gene, encoding a potassium ion channel protein in chlorella viruses, revealed a highly conserved 10-nt sequence (AAAAATANTT) in the promoter region of this gene, present in 16 out of 17 chlorellaviruses [77]. This sequence is located at 10–31 nucleotides upstream of the ATG translation start codon in all of the analyzed viruses, and it was associated with late gene transcription, since, apparently, *kcv* transcripts are produced during the late steps of infection. Furthermore, the region that precedes seven genes expressed at later times during the *Paramecium bursaria chlorella virus 1* (PBCV-1) replication cycle (*a85r*, *a237r*, *a248r*, *a260r*, *a292l*, *a430l*, and *a530r*) contain the same sequence or at least a subset of this sequence located at 6–30 nucleotides upstream of the ATG start codon [77]. The study of immediate early genes expressed in chlorovirus infections also revealed A/T-rich sequences as putative promoter regions. Two sequences determined by 'ATGACAA' and 'TATAAAT' (such as the eukaryotic "TATA-box") were located in a 150 bp region from the translation start codon in the upstream regions of almost all immediate early genes (20 of 23 studied) [78]. These elements, especially 'ATGACAA', were absent in all genes so far examined, expressed after 40 min p.i, including *A122R* (Vp260) [79], *A181-182R* (chitinase), *A292L* (chitosanase) [80], *A430L* (major capsid protein) [81], *vAL-1* [82].

Bioinformatics analysis revealed highly conserved nucleotide sequences in putative promoter regions involving three different chlorella viruses: PBCV-1, virus MT325 [83], and *Paramecium bursaria chlorella virus* NY-2A [84]. Three putative AT-rich sequence promoters, comprising seven to nine nucleotides (ARNTTAANA, AATGACA and GTNGATAYR), located at 150-nt upstream of the translation start codon of many ORFs were observed [85]. The 'ARNTTAANA' sequence is found between nucleotides −15 and −45 relative to the ATG translation start codon. This sequence occurs in the promoter region of 25% of PBCV-1 genes, 22% of NY-2A genes and 12% of MT325 genes. Regarding the entire genome, this sequence is present within the 200-nt promoter region during 44% of the time in PBCV-1, 49% of the time in NY-2A, and 37% of the time in MT325. The hotspot for the presence of the 'AATGACA' sequence is located between nucleotides −60 and −90 from the translational start codon. This sequence occurs in the promoter region of 16% of the PBCV-1 genes, 18% of NY-2A genes and 8% of MT325 genes. Regarding the entire genome, this sequence is present within the 200-nt promoter region in 54% of the PBCV-1 genes, 53% of the NY-2A genes, and 25% of the MT325 genes [85].

The 'AATGACA' sequence in PBCV-1 is associated with early genes during the replication cycle [85]. This sequence is very similar to a motif previously identified in some chlorella viruses (ATGACAA), which is also correlated with early transcripts [78]. Finally, the 'GTNGATAYR' sequence is mainly located at nucleotide positions −50 to −80 from the ATG initiation codon, occurring in the promoter region of 13% of PBCV-1 genes, 14% NY-2A genes, and in 11% of MT325 genes. Regarding the entire genome, this sequence is found specifically within the 200-nt promoter region in 28% of the PBCV-1 genes, 22% of the NY-2A genes, and 21% of the MT325 genes [85].

Unlike other members of the NCLDVs, phycodnaviruses do not encode their own RNA pol and need to appropriate the host's RNA pol to properly make their transcripts [86]. However, uniquely for the *Phycodnaviridae* family, *Emiliania huxleyi virus 86* (EhV-86), a coccolithovirus that infects the marine calcifying microalga *Emiliania huxleyi*, contains a total of six RNA pol subunits, which suggests that this virus partially encodes its own transcription machinery [87]. Although these viruses present some important elements for the mRNA synthesis, it is not possible to state that they have their own transcriptional complete apparatus, at least for the majority of them. Therefore, concerning the transcriptional process, the phycodnaviruses seem to present a different evolutionary history.

6. *Iridoviridae*

The *Iridoviridae* family is composed by five genera: *Ranavirus*, *Megalocytivirus* and *Lymphocystivirus* that infect vertebrates; *Iridovirus* and *Chloriridovirus* that infect invertebrates [88]. Iridoviruses have a linear dsDNA genome varying from 105 to 212 kbp, coding between 92 and 211 putative proteins. They present a non-enveloped icosahedral particle of 300 nm in size [89–92]. These large viruses also display a pattern of temporal gene expression regulation, wherein the genes are divided into three classes: immediate-early (IE or α), delayed-early (DE or β), and late (L or γ) genes [93–95]. Iridoviruses are typical nucleo-cytoplasmic viruses. They begin the replication cycle in the nucleus, followed by the second phase of genome replication in the cytoplasm [90].

Gene transcription and promoter sequences studies have been performed for only a few genes in members of the *Iridoviridae* family. The study of promoter sequences in iridovirus is focused mainly in the *Ranavirus* genus (using type species *Frog virus 3* (FV3)) and *Iridovirus* genus (using type species *Invertebrate iridescent virus 6* (IIV-6)), the type species of the *Iridovirus* genus. Notwithstanding, both the gene expression and promoter sequences studies have been performed for only a few genes in the *Iridoviridae* family. The most complex studies were performed with immediate-early *ICR-169* and *ICR-489* genes of FV3 [96,97]. Those studies revealed the importance of a 78 bp sequence before the transcription start site of an IE gene of the FV3 promoter. It was shown that an FV3 protein acts in trans to induce the transcription of the major FV3 IE gene, *ICR-169*, and is dependent on the 78 bp sequence located at the 5′ position from the start site of the transcription of this gene [98]. Two years later, the same group demonstrated that a 23 bp sequence was possibly a critical *cis*-regulatory element for the occurrence of FV3 *trans*-activation, since a significant reduction of transcription occurred after its deletion, located at the 5′ region, showing the sequence 'ATATCTCACAGGGGAATTGAAAC' [96]. Despite the importance of the approximately 23-nt sequence upstream of the transcription start site in the IE *ICR-169* gene of FV3, this sequence had no similarity with the promoter region of the intermediate gene *ICR489*. This lack of similarity indicated that the contemporary regulation of these two promoters is not controlled by sequences upstream of the start point of transcription [97]. It is worthy to note that in the *ICR489* gene, in an upstream region, 'TATA', 'CAAT', and 'GC' motifs were identified, which are similar to those of typical eukaryotic promoters [97].

Another study analyzed three genes—two early (*ICP-18* and *ICP-46*) and a late one [major capsid protein (MCP)] of *Bohle iridovirus* (another *Ranavirus* member)—looking for conserved regions to be considered as regulatory elements [99]. The authors demonstrated that all gene promoters included sequences located 127 to 281 bases upstream of the transcription initiation site (127 pb or ICB-18, 281 pb for ICP46, and 169 pb for MCP), but also sequences located from 21 to 26 bases downstream of this site (26 bases for *ICP-18*, 21 bases for ICP 46 and 25 bases for MCP) [99].

Moreover, a detailed study conducted in the following years identified an essential 'AAAAT' motif in a DE gene of IIV-6 (*Iridovirus*) [100]. The authors described a sequence of 19 bp (AAAATTGATTATTTGTTTT), located between −19 and −2 relative to the mRNA transcription start site, which is the putative region responsible for promoter activity of the DNApol gene. Deletions and point mutations in the DNApol promoter of IIV-6 showed that each of the 5-nt of 'AAAAT' motif located between −19 and −15 were equally essential for promoter activity. Mutations at the downstream side had a lower effect, but the role of individual nucleotides positioned at −14 to −5 was not analyzed in this study [100].

It is noteworthy that the same critical 'AAAAT' motif was found in the 100-nt upstream of the putative translational start codons of several other putative DE IIV-6 genes [91]. In *Invertebrate iridescent virus 3* (IIV-3), many homologues of these genes also presented the 'AAAAT' motif in proximity to their start codon. A great similarity was also found between the region upstream of the DNApol ORF and the corresponding region in 12 iridovirus genomes [101]. Eight of these genomes showed a similar 'AAAAT' motif in the DNApol upstream region and three sequenced ranavirus genomes also shared the related 'TAAAT' motif in their DNA pol promoter region, which may indicate a conserved regulation of DE promoter activity in iridoviruses [101].

A study that targeted a IE gene (012L) of IIV-6 showed that the transcription start site is located 30-nt upstream of the ATG translational start codon. Analyzing mutants (produced by deletion), it was established that the intergenic region located between −21 and −10 (GGATCATATT) upstream of the transcription start site comprised the promoter sequence promoter 012L gene. This type of sequence was not observed in upstream regions of other IE genes of IIV-6, such as 468R, 006L and 010R. The 'TATA' and 'CAAT' sequences were also identified in the intergenic region of this gene, as well as sequences similar to the 'AAAAT' motif described to the DNA pol gene, but this sequence had no promoter activity for the 012L, differently than demonstrated for the DNA pol gene. The 037L and 012L genes of IIV-6, both early genes, do not share conserved key promoter motifs. However, DNA pol is considered a DE gene and 012L an IE gene [100,102].

Despite the presence of homologs of RNA pol subunits in the iridoviruses genome, host RNA pol II is required for the synthesis of *Ranavirus* IE transcripts, and it is likely that the same is true from *Iridovirus* IE genes, contrasting to pox- and asfaviruses [103–106]. It has been proposed that the RNA pol subunits found in members of the *Iridoviridae* family are probably involved in the cytoplasmic phase of transcription in later stages of infection [91,107]. Such a paradox may reflect the long co-evolution period that these viruses had been through. It is possible that the ancestor of iridoviruses presented a complete transcription apparatus, but some elements were lost due to the adaptation to a more parasitic lifestyle. Other possibilities are the occurrence of events of horizontal gene transfer (HGT) between the viruses and their hosts. However, the lack of information about such events involving members of the *Iridoviridae* family prevents further insights into this alternative for the evolution of the transcription apparatus of these viruses.

7. *Ascoviridae*

The *Ascoviridae* family has two genera that include *Ascovirus*, with three species including *Spodoptera frugiperda ascovirus 1a* (SfAV-1a), the prototype of the genus, *Trichoplusia ni ascovirus 2a* (TnAV-2a), and *Heliothis virescens ascovirus 3a* (HvAV-3a), and the *Toursvirus* genus, with only one representative, *Diadromus pulchellus ascovirus 4a* (DpAV-4a) [108,109]. Ascoviruses are enveloped viruses, 300–400 nm long by 100–150 nm in diameter, with a circular dsDNA genome with sizes ranging from 116 to 185 kb, infecting arthropods, mainly lepidopterans [110–112].

The studies regarding the ascoviruses are still in their infancy. Information about the replication and more specifically, the transcription process, are extremely scarce. The current knowledge about transcription in ascoviruses come from the analyses of the *Ascovirus* genus [110,113]. A study performed using a possible variant of HvAV-3, the *Spodoptera exigua ascovirus 5a* (SeAV-5a) showed that the 5'-UTR region of the SeAV-5a MCP gene is composed of 25-nt [114]. The upstream region

of this gene does not present a typical eukaryotic class II promoter motif sequence 'TATAAAT' (TATA box). However, the putative 5' transcription control region of the SeAV-5a MCP gene shares similarities with other ascoviruses and iridoviruses, containing a conserved TATA-box like motif (TAATTAAA) and an 'ATTTGATCTT' motif within 40-nt upstream of the translation initiation codon ATG [114]. The 'TAATTAAA' and 'ATTTGATCTT' motifs are located downstream and upstream of the transcription initiation site, respectively. Furthermore, the ORF p27 presents a similar 5' downstream transcription promoter region, suggesting that such a region might be a truly regulatory sequence within ascoviruses [114].

Sequences from the promoter regions of the MCP genes from ascoviruses and IIV-6 (late genes), showed that ascoviruses and iridoviruses are closely related in this aspect, suggesting that the transcription regulation could be maintained during the viral evolution process in closely related viruses [115,116]. Furthermore, phylogenetic studies showed that ascoviruses probably evolved from the iridoviruses [116–118]. It is possible that the same pattern of temporary gene expression exhibited in iridoviruses (and the other members of proposed Megavirales order) was conserved in the ascoviruses lineage, and that such a mechanism might have been present in their common ancestor.

8. *Mimiviridae* and Other Amoebal Giant Viruses

The discovery of mimiviruses in 2003 and the establishment of the *Mimiviridae* family astonished the scientific community, making the term 'giant virus' more appropriated than ever. These viruses have particles visible in light microscopy, with sizes of ~700 nm in diameter. Viral particles have characteristics never described before in the virosphere, such as long proteic fibrils (~125 nm in length) immersed in a peptidoglycan matrix, and a star-shaped face, named stargate, responsible for the releasing of the genome inside the cytoplasm of their host (*Acanthamoeba* genus) [4,119–121]. The genome is a linear dsDNA molecule of about 1.2 Mbp, coding more than 1000 proteins, including a large set of transcriptional elements [15,122].

Similar to other NCLDVs members, mimiviruses genes can be divided into early, intermediate and late categories according to three major temporal classes of transcription determined by mRNA deep sequencing [49]. The analysis of the intergenic regions of *Acanthamoeba polyphaga mimivirus*, the prototype species of *Mimivirus* genus, showed a conserved 'AAAATTGA' motif in nearly 50% of genes [50]. The intergenic regions of the genome of mimiviruses have an average size of 157-nt. In silico analyses showed that the conserved 'AAAATTGA' motifs are present within the 150-nt upstream regions of the translation start codon in 45% of all predicted mimivirus genes [50]. This motif is mainly associated to early (or the late-early) genes during the viral infectious cycle, and it is absent from the upstream regions of mimivirus late genes, such as DNA replication and particle morphogenesis and assembly. It is noteworthy that similar sequences were described regulating the early genes in other giant viruses, such as iridoviruses and phycodnaviruses, as described in the topics above. Besides the early promoter sequence, another A/T-rich motif (two 10-nt informative segments separated by a highly degenerated 4-nt sequence) was identified as a putative late promoter within mimiviruses, which is present in 24.2% of the considered late class genes. To the best of our knowledge, an intermediate promoter sequence has not already been described in mimiviruses [49,50].

In a distant relative, the *Cafeteria roenbergensis virus* [CroV (*Cafeteria* genus)], *Mimiviridae* family; the same early promoter motif was identified in the upstream region of 35% of genes [123]. However, considering the late promoter motif, this virus exhibits a different putative regulatory sequence compared to other mimiviruses, wherein the 'TCTA' tetramer flanked by A/T-rich regions on either side was found in the 5' upstream of 124 late genes [123]. Moreover, CroV present eight RNA pol II subunits, six transcription factors, several helicases, among others, indicating the presence of nearly complete transcriptional machinery. This feature seems to be a mark to all members of the *Mimiviridae* family, which suggests that such a robust transcriptional apparatus was already present in the last common ancestor.

After the discovery of mimiviruses, other giant viruses infecting amoebae were described, such as marseilleviruses, which is currently classified in the family *Marseilleviridae* [124]. Other viruses have also been isolated but still not properly classified, namely faustoviruses [125], pandoraviruses [8,126], phitoviruses [127,128] and mollivirus [129]. Although these viruses are not yet officially recognized by the ICTV, they are genuine members of the NCLDVs [6,7,9]. In all of these giant viruses, a set of transcriptional elements has already been identified, including many RNA pol subunits, indicating a nearly autonomous process in these viruses. However, analysis of promoters and studies aiming to understand how gene expression is regulated in those newly discovered viruses remain to be performed.

9. MEGA-Box: A Putative Promoter Region in the Common Ancestor of Megavirales

The proposed Megavirales order comprises viral families that exhibit some unique features that allow their clustering into a monophyletic group [5]. In addition to some core genes that are shared among these viruses, they present other similarities, such as a temporal transcription profile. As described above, all viruses present elements to the transcriptional apparatus, most of them reaching up to the independence from their host in this step of the viral life cycle. Also, the presence of an A/T-rich promoter sequence has been described in many representatives of each family, even in those in which the genome presents a high G/C content. More interesting is the fact that some promoter sequences found in one family are very similar to others found in their relatives (Figure 3). This fact suggests that a possible common ancestor of the Megavirales order likely had an A/T-rich promoter sequence. More interesting is the fact that some promoter sequences found in one family are very similar to others found in their giant relatives. This fact suggests that such a common ancestor of Megavirales likely had an A/T-rich promoter sequence.

The origin of the members of the Megavirales order is still under debate, but the evolutionary history of some of its members is already being told, at least concerning genome evolution. The first members to be analyzed were the poxviruses. It has been demonstrated by phylogenetic analysis based on the presence/absence of genes that genomes from this family have been subject to frequent events of gene duplication, deletion, and HGT from their hosts. Many of these genes can interfere with host immune signaling, such as homologues of cytokines receptors which could confer some advantages in the interaction with the hosts [130–132]. By analyzing the poxviruses' closest relative, ASFV, it seems that it has been through the same pattern of evolution, at least considering the multigene and p22 gene families [133,134].

The "accordion-like" pattern of evolution was also identified in different members of the *Iridoviridae* family. It is particularly interesting the fact that iridoviruses infecting the same host-range exhibited a similar pattern of gene gain and loss, but this was slightly different when the viruses infected different hosts (fish vs. insect-infecting viruses), suggesting that such a pattern was driven by host–virus co-evolution [135]. Finally, the same evolutionary model for members of the families *Phycodnaviridae* and *Mimiviridae* has recently been described. The genomic comparisons of closely related viruses belonging to the *Mimiviridae* and *Phycodnaviridae* families show that genomes accumulating genomic mutations occur on successive cycles of genome expansion and reduction. In addition, there is no general tendency of genome expansion or contraction. Each family exhibits a specific pattern for gene acquisition, which might be a reflex of interaction with distinct hosts [10]. Since these viruses seem to exhibit a similar pattern of genome evolution, it is possible that a similar scenario has also happened with their promoter sequences. In the same way, it is reasonable to consider that NCLDVs' common ancestor evolved by the same "accordion-like" pattern, and thus it presented a promoter region that underwent an analogous mechanism.

Considering a common origin for the NCLDVs, a possible scenario is that the Megavirales' common ancestor presented a 'TATATAAAATTGA' promoter motif, which we named here as the "MEGA-box" (an allusion to the conserved TATA-box promoter found in cellular organisms). Over time, with the Megavirales' order radiation, the MEGA-box has been gradually evolved by nucleotides'

gain and loss, analogously to that reported for the entire genome, which evolved through gene gain and loss. The MEGA-box was slightly modified in the poxviruses lineage, at least concerning the early promoter motif. Considering the intermediate and the late promoter motifs of poxviruses, if they truly came from the MEGA-box, this could have happened through a series of nucleotide loss. However, it is also possible that the emergence of other promoters, rather than the early one, have emerged after the establishment of the poxvirus' lineage, thus not originating from the ancestral promoter sequence. The same might be true for mimiviruses, phycodnaviruses and iridoviruses. Considering asfavirus and ascoviruses, their promoter sequences might have originated from the MEGA-box through successive gain and loss of nucleotides. However, another scenario is also possible, wherein their promoter motifs emerged from the poxviruses and iridoviruses lineages respectively (closest evolutionary groups). This scenario is in agreement with the proposition that the Megavirales' ancestor was already a giant virus with a large genome [10]. In this aspect, the giant ancestor also had a large promoter sequence that evolved through constant nucleotide gain and loss, a pattern analogous to the accordion-like model of genome evolution. However, other scenarios are also possible, although less probable, considering the evolutionary data currently available for these viruses. One is that the ancestor had a very short promoter sequence, like a poxvirus intermediate promoter (TAAA), that underwent massive nucleotide gain over time, leading to very large promoter sequences in the majority of the giant viruses. Another one is just the opposite; wherein the ancestor had a very large promoter region that had been losing nucleotides during evolution. A third pathway, equally unlikely, would be the acquisition of promoter sequences by horizontal/lateral transfer. Similar to different genes, the MEGA-box promoter evolutionary pattern during the radiation of NCLDVs members could be related to the co-evolution with different hosts over time.

Whether the NCLDVs came from a simple entity [14,136], or from an already complex organism [10,16,137], is still under debate. Despite this, increasing evidence that they originated from a common ancestor is emerging, and it suggests that such an ancestor evolved through an "accordion-like" pattern. By analyzing the promoter regions currently known for different giant viruses, we provide another piece of evidence to support this statement. Further, we propose how a conserved A/T-rich promoter sequence was present in the possible common ancestor, which might have evolved by continuous gain and loss of nucleotides, in addition to some point mutations in the MEGA-box original sequence. Other scenarios could also be discussed for the evolution of the promoter sequences of the NCLDVs, including selective sweep or convergence. However, these alternatives run off the diffused hypothesis of a common origin for the putative Megavirales order.

10. What Comes Next?

Most of the giant viruses have a powerful genetic arsenal, encoding several proteins necessary for the transcription system which provides a relative independence of their hosts for this process. In addition, the transcription of this high gene content is temporally regulated by promoter regions that exhibit some similarities, indicating a common origin of these regulatory elements. Although many studies have already been done in relation to almost all viral families of the Megavirales order, most of them remain without biological confirmation; i.e., the promoter motifs in many giant viruses were predicted, but not experimentally validated. Therefore, the performance of biological studies to confirm the existence and the effect of all promoter motifs described so far in giant viruses is imperative. This analysis will truly establish the common temporal regulation pattern predicted in these viruses, and will also corroborate (or even refute) the hypothesis of an A/T-rich promoter in the Megavirales common ancestor. Moreover, the deep analysis of the genome of the recently described giant viruses (Marseilleviruses, Pandoraviruses, Pithoviruses, Faustoviruses and Mollivirus), and also the discovery of new complex viruses, will strongly contribute to complete the puzzle of the origin and evolution of Megavirales.

On the other hand, the biotechnology field will also be boosted by the advance in the studies of promoters and gene expression in giant viruses. Among the NCLDVs, the poxviruses are by far the best

characterized group regarding the genome expression, especially the VACV. These viruses have been used as expression vectors for the synthesis of proteins and as vaccine candidates to prevent infectious diseases and treat cancer, mainly due to their high gene expression levels [69,138]. This attribute is clearly shared with other giant viruses that were recently described, and the real comprehension of their gene regulation and expression will bring uncountable possibilities for biotechnology purposes. Finally, the impact of the giant viruses on the basic comprehension of the origin and evolution of life is undeniable, as well as for their ecological, medical and technological importance. The discovery of even more complex viruses associated with the advance of many techniques used for genomic studies will certainly answer those remaining questions around the NCLDVs, and will surely bring new exciting challenges for the whole scientific community.

Acknowledgments: We would like to thank our colleagues from GEPVIG (Grupo de Estudo e Prospecção de Vírus Gigantes) and Laboratório de Vírus of Universidade Federal de Minas Gerais. In addition, CNPq (Conselho Nacional de Desenvolvimento Científico e Tecnológico), CAPES (Coordenação de Aperfeiçoamento de Pessoal de Nível Superior) and FAPEMIG (Fundação de Amparo à Pesquisa do estado de Minas Gerais). G.S.T., E.G.K. and J.S.A. are CNPq researchers. B.L.S., J.S.A. and E.G.K. are members of a CAPES-COFECUB project.

Author Contributions: G.P.O.; A.C.S.P.A.; R.A.L.R.; T.S.A.; P.V.M.B.; L.K.S.S. and F.P.D. wrote the paper. B.P.D., G.S.T., B.L.S., E.G.K. and J.S.A. approved and reviewed the final version.

Conflicts of Interest: The authors declare no conflict of interest.

References

1. Lwoff, A. The concept of virus. *J. Gen. Microbiol.* **1957**, *17*, 239–253. [CrossRef] [PubMed]
2. Durzyńska, J.; Goździcka-Józefiak, A. Viruses and cells intertwined since the dawn of evolution. *Virol. J.* **2015**, *16*, 169. [CrossRef] [PubMed]
3. Iyer, L.M.; Aravind, L.; Koonin, E.V. Common origin of four diverse families of large eukaryotic DNA viruses. *J. Virol.* **2001**, *75*, 11720. [CrossRef] [PubMed]
4. La Scola, B.; Audic, S.; Robert, C.; Jungang, L.; de Lamballerie, X.; Drancourt, M.; Birtles, R.; Claverie, J.M.; Raoult, D. A giant virus in amoebae. *Science* **2003**, *299*. [CrossRef] [PubMed]
5. Colson, P.; de Lamballerie, X.; Fournous, G.; Raoult, D. Reclassification of giant viruses composing a fourth domain of life in the new order Megavirales. *Intervirology* **2012**, *55*, 321–332. [CrossRef] [PubMed]
6. Sharma, V.; Colson, P.; Chabrol, O.; Pontarotti, P.; Raoult, D. *Pithovirus sibericum*, a new bona fide member of the "Fourth TRUC" club. *Front. Microbiol.* **2015**, *4*, 722. [CrossRef] [PubMed]
7. Sharma, V.; Colson, P.; Chabrol, O.; Scheid, P.; Pontarotti, P.; Raoult, D. Welcome to pandoraviruses at the "Fourth TRUC" club. *Front. Microbiol.* **2015**, *18*, 423.
8. Scheid, P. A strange endocytobiont revealed as largest virus. *Curr. Opin. Microbiol.* **2016**, *31*, 58–62. [CrossRef] [PubMed]
9. Benamar, S.; Reteno, D.G.; Bandaly, V.; Labas, N.; Raoult, D.; la Scola, B. Faustoviruses: Comparative genomics of new Megavirales family members. *Front. Microbiol.* **2016**, *5*, 3. [CrossRef] [PubMed]
10. Filée, J. Genomic comparison of closely related Giant Viruses supports an accordion-like model of evolution. *Front. Microbiol.* **2015**, *16*, 593. [CrossRef] [PubMed]
11. Suzan-Monti, M.; la Scola, B.; Raoult, D. Genomic and evolutionary aspects of Mimivirus. *Virus Res.* **2006**, *117*, 145–155. [CrossRef] [PubMed]
12. Claverie, J.M. Viruses take center stage in cellular evolution. *Genome Biol.* **2006**, *7*, 110. [CrossRef] [PubMed]
13. Moreira, D.; López-García, P. Comment on "The 1.2-megabase genome sequence of Mimivirus". *Science* **2005**, *20*, 1114. [CrossRef] [PubMed]
14. Yutin, N.; Wolf, Y.I.; Koonin, E.V. Origin of giant viruses from smaller DNA viruses not from a fourth domain of cellular life. *Virology* **2014**, *38–52*, 466–467. [CrossRef] [PubMed]
15. Raoult, D.; Audic, S.; Robert, C.; Abergel, C.; Renesto, P.; Ogata, H.; la Scola, B.; Suzan, M.; Claverie, J.M. The 1.2-megabase genome sequence of Mimivirus. *Science* **2004**, *306*, 1344–1350. [CrossRef] [PubMed]
16. Boyer, M.; Madoui, M.A.; Gimenez, G.; La Scola, B.; Raoult, D. Phylogenetic and phyletic studies of informational genes in genomes highlight existence of a 4 domain of life including giant viruses. *PLoS ONE* **2010**, *2*, e15530. [CrossRef] [PubMed]

17. Schones, D.E.; Cui, K.; Cuddapah, S.; Roh, T.-Y.; Barski, A.; Wang, Z.; Wei, G.; Zhao, K. Dynamic regulation of nucleosome positioning in the human genome. *Cell* **2008**, *132*, 887–898. [CrossRef] [PubMed]
18. Fuda, N.J.; Ardehali, M.B.; Lis, J.T. Defining mechanisms that regulate RNA polymerase II transcription in vivo. *Nature* **2009**, *10*, 186–192. [CrossRef] [PubMed]
19. Lacadie, S.A.; Ibrahim, M.M.; Gokhale, S.A.; Ohler, U. Divergent transcription and epigenetic directionality of human promoters. *FEBS J.* **2016**, *283*, 4214–4222. [CrossRef] [PubMed]
20. Haberle, V.; Lenhard, B. Promoter architectures and developmental gene regulation. *Semin. Cell Dev. Biol.* **2016**, *57*, 11–23. [CrossRef] [PubMed]
21. Weiss, S.; Gladstone, L. A mammalian system for the incorporation of cytidine triphosphate into ribonucleic acid. *J. Am. Chem. Soc.* **1959**, *81*, 4118–4119. [CrossRef]
22. Thomas, M.C.; Chiang, C.M. The general transcription machinery and generalcofactors. *Crit. Rev. Biochem. Mol. Biol.* **2006**, *41*, 105–178. [CrossRef] [PubMed]
23. Sabin, L.R.; Delás, M.J.; Hannon, G.J. Dogma derailed: The many influences of RNA on the genome. *Mol. Cell* **2013**, *49*, 783–794. [CrossRef] [PubMed]
24. Vannini, A.; Ringel, R.; Kusser, A.G.; Berninghausen, O.; Kassavetis, G.A.; Cramer, P. Molecular basis of RNA polymerase III transcription repression by Maf1. *Cell* **2010**, *143*, 59–70. [CrossRef] [PubMed]
25. Carninci, P.; Sandelin, A.; Lenhard, B.; Katayama, S.; Shimokawa, K.; Ponjavic, J.; Semple, C.A.; Taylor, M.S.; Engström, P.G.; Frith, M.C. Genome-wide analysis of mammalian promoter architecture andevolution. *Nat. Genet.* **2006**, *38*, 626–635. [CrossRef] [PubMed]
26. Cooper, S.J.; Trinklein, N.D.; Anton, E.D.; Nguyen, L.; Myers, R.M. Comprehensive analysis of transcriptional promoter structure and functionin 1% of the human genome. *Genome Res.* **2006**, *16*, 1–10. [CrossRef] [PubMed]
27. Smale, S.T.; Kadonaga, J.T. The RNA polymerase II core promoter. *Annu. Rev. Biochem.* **2003**, *72*, 449–479. [CrossRef] [PubMed]
28. Maston, G.A.; Evans, S.K.; Green, M.R. Transcriptional regulatory elements in the human genome. *Annu. Rev. Genom. Hum. Genet.* **2006**, *7*, 29–59. [CrossRef] [PubMed]
29. Hansen, S.K.; Tjian, R. TAFs and TFIIA mediate differential utilization of thetandem Adh promoters. *Cell* **1995**, *82*, 565–575. [CrossRef]
30. Ren, B.; Maniatis, T. Regulation of Drosophila Adh promoter switching by aninitiator-targeted repression mechanism. *EMBO J.* **1998**, *17*, 1076–1086. [CrossRef] [PubMed]
31. Browning, D.F.; Busby, S.J. Local and global regulation of transcription initiation in bacteria. *Nat. Rev. Microbiol.* **2016**, *14*, 638–650. [CrossRef] [PubMed]
32. Burgess, R.R.; Travers, A.A.; Dunn, J.J.; Bautz, E.K. Factor stimulating transcription by RNA polymerase. *Nature* **1969**, *221*, 43–46. [CrossRef] [PubMed]
33. Lee, D.J.; Minchin, S.D.; Busby, S.J. Activating transcription in bacteria. *Annu. Rev. Microbiol.* **2012**, *66*, 125–152. [CrossRef] [PubMed]
34. Murakami, K.S.; Masuda, S.; Campbell, E.A.; Muzzin, O.; Darst, S.A. Structural basis of transcription initiation: An RNA polymerase holoenzyme–DNA complex. *Science* **2002**, *296*, 1285–1290. [CrossRef] [PubMed]
35. Browning, D.F.; Busby, S.J. The regulation of bacterial transcription initiation. *Nat. Rev. Microbiol.* **2004**, *2*, 57–65. [CrossRef] [PubMed]
36. Hausner, W.; Wettach, J.; Hethke, C.; Thomm, M. Two transcription factors related with the eucaryal transcription factors TATA binding protein and transcription factor IIB direct promoter recognition by an archaeal RNA polymerase. *J. Biol. Chem.* **1996**, *271*, 30144–30148. [CrossRef] [PubMed]
37. Bell, S.D.; Jaxel, C.; Nadal, M.; Kosa, P.F.; Jackson, S.P. Temperature template topology, and factor requirements of archaeal transcription. *Proc. Natl. Acad. Sci. USA* **1998**, *95*, 15218–15222. [CrossRef] [PubMed]
38. Darcy, T.J.; Hausner, W.; Awery, D.E.; Edwards, A.M.; Thomm, M.; Reeve, J.N. Methanobacterium thermoautotrophicum RNA polymerase and transcription in vitro. *J. Bacteriol.* **1999**, *181*, 4424–4429. [PubMed]
39. Reiter, W.D.; Hudepohl, U.; Zillig, W. Mutational analysis of an archae bacterial promoter—Essential role of a TATA Box for transcription efficiency and start-site selection in vitro. *Proc. Natl. Acad. Sci. USA* **1990**, *87*, 9509–9513. [CrossRef] [PubMed]

40. Palmer, J.R.; Daniels, C.J. In vivo definition of an archaeal promoter. *J. Bact.* **1995**, *177*, 1844–1849. [CrossRef] [PubMed]
41. Kyrpides, N.C.; Ouzounis, C.A. Transcription in Archaea. *Proc. Natl. Acad. Sci. USA* **1999**, *96*, 8545–8550. [CrossRef] [PubMed]
42. Aravind, L.; Koonin, E.V. DNA-binding proteins and evolution of transcription regulation in the *Archaea*. *Nucleic Acids Res.* **1999**, *27*, 4658–4670. [CrossRef] [PubMed]
43. Bell, S.D.; Jackson, S.P. Mechanism and regulation of transcription in *Archaea*. *Curr. Opin. Microbiol.* **2001**, *4*, 208–213. [CrossRef]
44. Werner, F.; Grohmann, D. Evolution of multisubunit RNA polymerases in the three domains of life. *Nat. Rev. Microbiol.* **2011**, *9*, 85–98. [CrossRef] [PubMed]
45. Whelan, S. Viral Replication Strategies. In *Fields Virology*, 6th ed.; Knipe, D.M., Howley, P.M., Eds.; Lippincott, Williams and Wilkins: Philadelphia, PA, USA, 2014; Volume 2, p. 2160.
46. Abergel, C.; Rudinger-Thirion, J.; Giege, R.; Claverie, J.M. Virus-encoded aminoacyl-tRNA synthetases: Structural and functional characterization of mimivirus TyrRS and MetRS. *J. Virol.* **2007**, *81*, 12406–12417. [CrossRef] [PubMed]
47. Broyles, S.S.; Knutson, B.A. Poxvirus transcription. *Future Virol.* **2010**, *5*, 639–650. [CrossRef]
48. Moss, B. Poxviridae. In *Fields Virology*, 6th ed.; Knipe, D.M., Howley, P.M., Eds.; Lippincott, Williams and Wilkins: Philadelphia, PA, USA, 2014; Volume 2, p. 2129.
49. Legendre, M.; Audic, S.; Poirot, O.; Hingamp, P.; Seltzer, V.; Byrne, D.; Lartigue, A.; Lescot, M.; Bernadac, A.; Poulain, J.; et al. mRNA deep sequencing reveals 75 new genes and a complex transcriptional landscape in Mimivirus. *Genome Res.* **2010**, *20*, 664–674. [CrossRef] [PubMed]
50. Suhre, K.; Audic, S.; Claverie, J.M. Mimivirus gene promoters exhibit an unprecedented conservation among all eukaryotes. *Proc. Natl. Acad. Sci. USA* **2005**, *102*, 14689–14693. [CrossRef] [PubMed]
51. Damon, I.K. Poxviruses. In *Fields Virology*, 6th ed.; Knipe, D.M., Howley, P.M., Eds.; Lippincott, Williams and Wilkins: Philadelphia, PA, USA, 2014; Volume 2, p. 2160.
52. Baroudy, B.M.; Moss, B. Purification and characterization of a DNA dependent RNA polymerase from vaccinia virions. *J. Biol. Chem.* **1980**, *255*, 4372–4380. [PubMed]
53. Knutson, B.A.; Broyles, S.S. Expansion of poxvirus RNA polymerase subunits sharing homology with corresponding subunits of RNA polymerase II. *Virus Genes* **2008**, *36*, 307–311. [CrossRef] [PubMed]
54. Davison, A.J.; Moss, B. The structure of vaccinia virus early promoters. *J. Mol. Biol.* **1989**, *210*, 749–769. [CrossRef]
55. Baldick, C.J.; Keck, J.G.; Moss, B. Mutational analysis of the core, spacer and initiator regions of vaccinia virus intermediate class promoters. *J. Virol.* **1992**, *66*, 4710–4719. [PubMed]
56. Knutson, B.A.; Liu, X.; Oh, J. Vaccinia virus intermediate and late promoter elements are targeted by the TATA-binding protein. *J. Virol.* **2006**, *80*, 6784–6793. [CrossRef] [PubMed]
57. Yang, Z.; Bruno, D.P.; Martens, C.A.; Porcella, S.F.; Moss, B. Genome-wide analysis of the 5′ and 3′ ends of vaccinia virus early mRNAs delineates regulatory sequences of annotated and anomalous transcripts. *J. Virol.* **2011**, *85*, 5897–5909. [CrossRef] [PubMed]
58. Keck, J.G.; Baldick, C.J.; Moss, B. Role of DNA replication in vaccinia virus gene expression: A naked template is required for transcription of three late transactivator genes. *Cell* **1990**, *61*, 801–809. [CrossRef]
59. Yang, Z.; Reynolds, S.E.; Martens, C.A.; Bruno, D.P.; Porcella, S.F.; Moss, B. Expression profiling of the intermediate and late stages of poxvirus replication. *J. Virol.* **2011**, *85*, 9899–9908. [CrossRef] [PubMed]
60. Yang, Z.; Martens, C.A.; Bruno, D.P.; Porcella, S.F.; Moss, B. Pervasive initiation and 3′-end formation of poxvirus postreplicative RNAs. *J. Biol. Chem.* **2012**, *287*, 31050–31060. [CrossRef] [PubMed]
61. Broyles, S.S.; Liu, X.; Zhu, M.; Kremer, M. Transcription factor YY1 is a vaccinia virus late promoter activator. *J. Biol. Chem.* **1999**, *274*, 35662–35667. [CrossRef] [PubMed]
62. Hänggi, M.; Bannwarth, W.; Stunnenberg, H.G. Conserved TAAAT motif in vaccinia virus late promoters: Overlapping TATA box and site of transcription initiation. *EMBO J.* **1986**, *5*, 1071–1076. [PubMed]
63. International Committee on Taxonomy of Viruses. Available online: http://www.ictvonline.org/taxonomyHistory.asp?taxnode_id=20151927&taxa_name=Asfarviridae (accessed on 22 September 2016).
64. Sogo, J.M.; Almendral, J.M.; Talavera, A.; Vinuela, E. Terminal and internal inverted repetitions in African swine fever virus DNA. *Virology* **1984**, *133*, 271–275. [CrossRef]

65. Tulman, E.R.; Delhon, G.A.; Ku, B.K.; Rock, D.L. African swine fever virus. *Curr. Top. Microbiol. Immunol.* **2009**, *328*, 43–87. [PubMed]
66. Kuznar, J.; Salas, M.L.; Vinuela, E. DNA-dependent RNA polymerase in African swine fever virus. *Virology* **1980**, *101*, 169–175. [CrossRef]
67. Salas, J.; Salas, M.L.; Vinuela, E. Effect of inhibitors of the host cell RNA polymerase II on African swine fever virus multiplication. *Virology* **1988**, *164*, 280–283. [CrossRef]
68. Rodríguez, J.M.; Salas, M.L. African swine fever virus transcription. *Virus Res.* **2013**, *173*, 15–28. [CrossRef] [PubMed]
69. Moss, B. Genetically engineered poxviruses for recombinant gene expression, vaccination, and safety. *Proc. Natl. Acad. Sci. USA* **1996**, *15*, 11341–11348. [CrossRef]
70. Rodríguez, J.M.; Salas, M.L.; Vinuela, E. Intermediate class of mRNAs in African swine fever virus. *J. Virol.* **1996**, *70*, 8584–8589. [PubMed]
71. Garcia-Escudero, R.; Vinuela, E. Structure of African swine fever virus late promoters: Requirement of a TATA sequence at the initiation region. *J. Virol.* **2000**, *74*, 8176–8182. [CrossRef] [PubMed]
72. Yates, P.R.; Dixon, L.K.; Turner, P.C. Promoter analysis of an African swine fever virus gene encoding a putative elongation factor. *Biochem. Soc. Trans.* **1995**, *23*, 139S. [CrossRef]
73. Van Etten, J.L.; Graves, M.V.; Müller, D.G.; Boland, W.; Delaroque, N. Phycodnaviridae—Large DNA algal viruses. *Arch. Virol.* **2002**, *147*, 1479–1516. [CrossRef] [PubMed]
74. Van Etten, J.L.; Meints, R.H. Giant viruses infecting algae. *Annu. Rev. Microbiol.* **1999**, *53*, 447–494. [CrossRef] [PubMed]
75. Wilson, W.H.; van Etten, J.L.; Allen, M.J. The *Phycodnaviridae*: The story of how tiny giants rule the world. *Curr. Top. Microbiol. Immunol.* **2009**, *328*, 1–42. [PubMed]
76. International Committee on Taxonomy of Viruses. Available online: http://www.ictvonline.org/taxonomyHistory.asp?taxnode_id=20153552&taxa_name=Phycodnaviridae (accessed on 22 September 2016).
77. Kang, M.; Graves, M.; Mehmel, M.; Moroni, A.; Gazzarrini, S.; Thiel, G.; Gurnon, J.R.; van Etten, J.L. Genetic diversity in chlorella viruses flanking *kcv*, a gene that encodes a potassium ion channel protein. *Virology* **2004**, *326*, 150–159. [CrossRef] [PubMed]
78. Kawasaki, T.; Tanaka, M.; Fujie, M.; Usami, S.; Yamada, T. Immediate early genes expressed in chlorovirus infections. *Virology* **2004**, *318*, 214–223. [CrossRef] [PubMed]
79. Chuchird, N.; Nishida, K.; Kawasaki, T.; Fujie, M.; Usami, S.; Yamada, T. A variable region on the chlorovirus CVK2 genome contains five copies of the gene for Vp260, a viral-surface glycoprotein. *Virology* **2002**, *10*, 289–298. [CrossRef] [PubMed]
80. Yamada, T.; Hiramatsu, S.; Songsri, P.; Fujie, M. Alternative expression of a chitosanase gene produces two different proteins in cells infected with Chlorella virus CVK2. *Virology* **1997**, *14*, 361–368. [CrossRef] [PubMed]
81. Graves, M.V.; Meints, R.H. Characterization of the major capsid protein and cloning of its gene from algal virus PBCV-1. *Virology* **1992**, *188*, 198–207. [CrossRef]
82. Sugimoto, I.; Hiramatsu, S.; Murakami, D.; Fujie, M.; Usami, S.; Yamada, T. Algal-lytic activities encoded by Chlorella virus CVK2. *Virology* **2000**, *10*, 119–126. [CrossRef] [PubMed]
83. Fitzgerald, L.A.; Graves, M.V.; Li, X.; Feldblyum, T.; Hartigan, J.; van Etten, J.L. Sequence and annotation of the 314-kb MT325 and the 321-kb FR483 viruses that infect Chlorella Pbi. *Virology* **2007**, *20*, 459–471. [CrossRef] [PubMed]
84. Fitzgerald, L.A.; Graves, M.V.; Li, X.; Feldblyum, T.; Nierman, W.C.; van Etten, J.L. Sequence and annotation of the 369-kb NY-2A and the 345-kb AR158 viruses that infect Chlorella NC64A. *Virology* **2007**, *20*, 472–484. [CrossRef] [PubMed]
85. Fitzgerald, L.A.; Boucher, P.T.; Yanai-Balser, G.M.; Suhre, K.; Graves, M.V.; van Etten, J.L. Putative gene promoter sequences in the chlorella viruses. *Virology* **2008**, *25*, 388–393. [CrossRef] [PubMed]
86. Van Etten, J.L. Unusual life style of giant chlorella viruses. *Ann. Rev. Genet.* **2003**, *37*, 153–195. [CrossRef] [PubMed]
87. Wilson, W.H.; Schroeder, D.C.; Allen, M.J.; Holden, M.T.; Parkhill, J.; Barrell, B.G.; Churcher, C.; Hamlin, N.; Mungall, K.; Norbertczak, H.; et al. Complete genome sequence and lytic phase transcription profile of a Coccolithovirus. *Science* **2005**, *12*, 1090–1092. [CrossRef] [PubMed]

88. International Committee on Taxonomy of Viruses. Available online: http://www.ictvonline.org/taxonomyHistory.asp.taxnode_id=20153003&taxa_name=Iridoviridae (accessed on 22 September 2016).
89. Darai, G.; Delius, H.; Clarke, J.; Apfel, H.; Schnitzler, P.; Flugel, R.M. Molecular cloning and physical mapping of the genome of fish lymphocystis disease virus. *Virology* **1985**, *146*, 292–301. [CrossRef]
90. Williams, T.; Barbosa-Solomieu, V.; Chinchar, V.G. A decade of advances in Iridovirus research. *Adv. Virus Res.* **2005**, *65*, 174–248.
91. Jakob, N.J.; Muller, K.; Bahr, U.; Darai, G. Analysis of the first complete DNA sequence of an invertebrate iridovirus: Coding strategy of the genome of Chilo iridescent virus. *Virology* **2001**, *286*, 182–196. [CrossRef] [PubMed]
92. Chinchar, V.G.; Yu, K.H.; Jancovich, J.K. The molecular biology of frog virus 3 and other iridoviruses infecting cold-blooded vertebrates. *Viruses* **2011**, *3*, 1959–1985. [CrossRef] [PubMed]
93. Barray, S.; Devauchelle, G. Protein synthesis in cells infected by Chilo iridescent virus: Evidence for temporal control of three classes of induced polypeptides. *Virology* **1987**, *138*, 253–261.
94. D'Costa, S.M.; Yao, H.; Bilimoria, S.L. Transcription and temporal cascade in Chilo iridescent virus infected cells. *Arch. Virol.* **2001**, *146*, 2165–2178. [CrossRef] [PubMed]
95. D'Costa, S.M.; Yao, H.J.; Bilimoria, S.L. Transcriptional mapping in Chilo iridescent virus infections. *Arch. Virol.* **2004**, *149*, 723–742. [CrossRef] [PubMed]
96. Willis, D.B. DNA sequences required for trans activation of an immediate- early frog virus 3 gene. *Virology* **1987**, *161*, 1–7. [CrossRef]
97. Beckman, W.; Tham, T.N.; Aubertin, A.M.; Willis, D.B. Structure and regulation of the immediate-early frog virus 3 gene that encodes ICR489. *J. Virol.* **1988**, *62*, 1271–1277. [PubMed]
98. Willis, D.B.; Granoff, A. Transactivation of an immediateearly frog virus 3 promoter by a virion protein. *J. Virol.* **1985**, *56*, 495–501. [PubMed]
99. Pallister, J.; Goldie, S.; Coupar, B.; Hyatt, A. Promoter activity in the 59 flanking regions of the Bohle iridovirus ICP 18, ICP 46 and major capsid protein genes. *Arch. Virol.* **2005**, *150*, 1911–1919. [CrossRef] [PubMed]
100. Nalcacioglu, R.; Ince, I.A.; Vlak, J.M.; Demirbag, Z.; van Oers, M.M. The Chilo iridescent virus DNA polymerase promoter contains an essential AAAAT motif. *J. Gen. Virol.* **2007**, *88*, 2488–2494. [CrossRef] [PubMed]
101. Nalcacioglu, R.; Demirbag, Z.; Vlak, J.M.; van Oers, M.M. Promoter analysis of the Chilo iridescent virus DNA polymerase and major capsid protein genes. *Virology* **2003**, *317*, 321–329. [CrossRef] [PubMed]
102. Dizman, Y.A.; Demirbag, Z.; Ince, I.A.; Nalcacioglu, R. Transcriptomic analysis of Chilo iridescent virus immediate early promoter. *Virus Res.* **2012**, *167*, 353–357. [CrossRef] [PubMed]
103. Goorha, R. Frog virus 3 requires RNA polymerase II for its replication. *J. Virol.* **1981**, *37*, 496–499. [PubMed]
104. Goorha, R.; Willis, D.B.; Granoff, A. Macromolecular synthesis in cells infected by frog virus 3. VI. Frog virus 3 replication is dependent on the cell nucleus. *J. Virol.* **1977**, *21*, 802–805. [PubMed]
105. Goorha, R.; Murti, G.; Granoff, A.; Tirey, R. Macromolecular synthesis in cells infected by frog virus 3. VIII. The nucleus is a site of frog virus 3 DNA and RNA synthesis. *Virology* **1978**, *84*, 32–50. [CrossRef]
106. Baroudy, B.M.; Moss, B. Sequence homologies of diverse length tandem repetitions near ends of vaccinia virus genome suggest unequal crossing over. *Nucleic Acids Res.* **1982**, *25*, 5673–5679. [CrossRef]
107. Tidona, C.A.; Darai, G. Molecular anatomy of lymphocystis disease virus. *Arch. Virol. Suppl.* **1997**, *13*, 49–56. [PubMed]
108. Federici, B.A.; Bigot, Y.; Granados, R.R.; Hamm, J.J.; Miller, L.K.; Newton, I.; Stasiak, K.; Vlak, J.M. Family Ascoviridae. In *Virus Taxonomy: 8th Report of the International Committee on Taxonomy of Viruses*; Fauquet, C.M., Mayo, M.A., Maniloff, J., Desselberger, U., Ball, L.A., Eds.; Elsevier Academic Press: San Diego, CA, USA, 2005; pp. 261–265.
109. International Committee on Taxonomy of Viruses. Available online: http://www.ictvonline.org/taxonomyHistory.asp?taxnode_id=20151919&taxa_name=Ascoviridae (accessed on 22 September 2016).
110. Cheng, X.W.; Wang, L.; Carner, G.R.; Arif, B.M. Characterization of three ascovirus isolates from cotton insects. *J. Invertebr. Pathol.* **2005**, *89*, 193–202. [CrossRef] [PubMed]
111. Asgari, S.; Davis, J.; Wood, D.; Wilson, P.; McGrath, A. Sequence and organization of the Heliothis virescens ascovirus genome. *J. Gen. Virol.* **2007**, *88*, 1120–1132. [CrossRef] [PubMed]

112. Bigot, Y.; Rabouille, A.; Sizaret, P.Y.; Hamelin, M.H.; Periquet, G. Particle and genomic characterization of a new member of the Ascoviridae, *Diadromus pulchellus ascovirus*. *J. Gen. Virol.* **1997**, *78*, 1139–1147. [CrossRef] [PubMed]
113. Cheng, X.W.; Carner, G.R.; Arif, B.M. A new ascovirus from *Spodoptera exigua* and its relatedness to the isolate from *Spodoptera frugiperda*. *J. Gen. Virol.* **2000**, *81*, 3083–3092. [CrossRef] [PubMed]
114. Salem, T.Z.; Turney, C.M.; Wang, L.; Xue, J.; Wan, X.-F.; Cheng, X.-W. Transcriptional analysis of a major capsid protein gene from *Spodoptera exigua ascovirus 5a*. *Arch. Virol.* **2008**, *153*, 149–162. [CrossRef] [PubMed]
115. Zhao, K.; Cui, L.W. Molecular characterization of the major virion protein gene from the *Trichoplusia ni ascovirus*. *Virus Genes* **2003**, *27*, 93–102. [CrossRef] [PubMed]
116. Stasiak, K.; Renault, S.; Demattei, M.V.; Bigot, Y.; Federici, B.A. Evidence for the evolution of ascoviruses from iridoviruses. *J. Gen. Virol.* **2003**, *84*, 2999–3009. [CrossRef] [PubMed]
117. Chinchar, V.G.; Hyatt, A.; Miyazaki, T.; Williams, T. Family *Iridoviridae*: Poor viral relations no longer. *Curr. Top. Microbiol. Immunol.* **2009**, *328*, 123–170. [PubMed]
118. Piégu, B.; Asgari, S.; Bideshi, D.; Federici, B.A.; Bigot, Y. Evolutionary relationships of iridoviruses and divergence of ascoviruses from invertebrate iridoviruses in the superfamily Megavirales. *Mol. Phylogenet. Evol.* **2015**, *84*, 44–52. [CrossRef] [PubMed]
119. Zauberman, N.; Mutsafi, Y.; Halevy, D.B.; Shimoni, E.; Klein, E.; Xiao, C.; Sun, S.; Minsky, A. Distinct DNA exit and packaging portals in the virus *Acanthamoeba polyphaga mimivirus*. *PLoS Biol.* **2008**, *13*, 114. [CrossRef] [PubMed]
120. Xiao, C.; Kuznetsov, Y.G.; Sun, S.; Hafenstein, S.L.; Kostyuchenko, V.A.; Chipman, P.R.; Suzan-Monti, M.; Raoult, D.; McPherson, A.; Rossmann, M.G. Structural studies of the giant mimivirus. *PLoS Biol.* **2009**, *28*, e92. [CrossRef] [PubMed]
121. Rodrigues, R.A.; dos Santos Silva, L.K.; Dornas, F.P.; de Oliveira, D.B.; Magalhães, T.F.; Santos, D.A.; Costa, A.O.; de Macêdo Farias, L.; Magalhães, P.P.; Bonjardim, C.A.; et al. Mimivirus fibrils are important for viral attachment to the microbial world by a diverse glycoside interaction repertoire. *J. Virol.* **2015**, *89*, 11812–11819. [CrossRef] [PubMed]
122. Legendre, M.; Santini, S.; Rico, A.; Abergel, C.; Claverie, J.M. Breaking the 1000-gene barrier for Mimivirus using ultra-deep genome and transcriptome sequencing. *Virol. J.* **2011**, *4*, 8–99. [CrossRef] [PubMed]
123. Fischer, M.G.; Allen, M.J.; Wilson, W.H.; Suttle, C.A. Giant virus with a remarkable complement of genes infects marine zooplankton. *Proc. Natl. Acad. Sci. USA* **2010**, *9*, 19508–19513. [CrossRef] [PubMed]
124. Colson, P.; de Lamballerie, X.; Yutin, N.; Asgari, S.; Bigot, Y.; Bideshi, D.K.; Cheng, X.W.; Federici, B.A.; van Etten, J.L.; Koonin, E.V.; et al. "Megavirales", a proposed new order for eukaryotic nucleocytoplasmic large DNA viruses. *Arch. Virol.* **2013**, *158*, 2517–2521. [CrossRef] [PubMed]
125. Reteno, D.G.; Benamar, S.; Khalil, J.B.; Andreani, J.; Armstrong, N.; Klose, T.; Rossmann, M.; Colson, P.; Raoult, D.; La Scola, B. Faustovirus, an asfarvirus-related new lineage of giant viruses infecting amoebae. *J. Virol.* **2015**, *89*, 6585–6594. [CrossRef] [PubMed]
126. Philippe, N.; Legendre, M.; Doutre, G.; Couté, Y.; Poirot, O.; Lescot, M.; Arslan, D.; Seltzer, V.; Bertaux, L.; Bruley, C.; et al. Pandoraviruses: Amoeba viruses with genomes up to 2.5 Mb reaching that of parasitic eukaryotes. *Science* **2013**, *341*, 281–286. [CrossRef] [PubMed]
127. Legendre, M.; Bartoli, J.; Shmakova, L.; Jeudy, S.; Labadie, K.; Adrait, A.; Lescot, M.; Poirot, O.; Bertaux, L.; Bruley, C.; et al. Thirty-thousand-year-old distant relative of giant icosahedral DNA viruses with a pandoravirus morphology. *Proc. Natl. Acad. Sci. USA* **2014**, *111*, 4274–4279. [CrossRef] [PubMed]
128. Levasseur, A.; Andreani, J.; Delerce, J.; Bou Khalil, J.; Robert, C.; La Scola, B.; Raoult, D. Comparison of a modern and fossil pithovirus reveals its genetic conservation and evolution. *Genome Biol. Evol.* **2016**, *25*, 2333–2339. [CrossRef] [PubMed]
129. Legendre, M.; Lartigue, A.; Bertaux, L.; Jeudy, S.; Bartoli, J.; Lescot, M.; Alempic, J.M.; Ramus, C.; Bruley, C.; Labadie, K.; et al. In-depth study of *Mollivirus sibericum*, a new 30,000-y-old giant virus infecting Acanthamoeba. *Proc. Natl. Acad. Sci. USA* **2015**, *112*, 5327–5335. [CrossRef] [PubMed]
130. McLysaght, A.; Baldi, P.F.; Gaut, B.S. Extensive gene gain associated with adaptive evolution of poxviruses. *Proc. Natl. Acad. Sci. USA* **2003**, *23*, 15655–15660. [CrossRef] [PubMed]
131. Hughes, A.L.; Friedman, R. Poxvirus genome evolution by gene gain and loss. *Mol. Phylogenet. Evol.* **2005**, *35*, 186–195. [CrossRef] [PubMed]

132. Elde, N.C.; Child, S.J.; Eickbush, M.T.; Kitzman, J.O.; Rogers, K.S.; Shendure, J.; Geballe, A.P.; Malik, H.S. Poxviruses deploy genomic accordions to adapt rapidly against host antiviral defenses. *Cell* **2012**, *17*, 831–841. [CrossRef] [PubMed]
133. Dixon, L.K.; Chapman, D.A.; Netherton, C.L.; Upton, C. African swine fever virus replication and genomics. *Virus Res.* **2013**, *173*, 3–14. [CrossRef] [PubMed]
134. Portugal, R.; Coelho, J.; Höper, D.; Little, N.S.; Smithson, C.; Upton, C.; Martins, C.; Leitão, A.; Keil, G.M. Related strains of African swine fever virus with different virulence: Genome comparison and analysis. *J. Gen. Virol.* **2015**, *96*, 408–419. [CrossRef] [PubMed]
135. Huang, Y.; Huang, X.; Liu, H.; Gong, J.; Ouyang, Z.; Cui, H.; Cao, J.; Zhao, Y.; Wang, X.; Jiang, Y.; et al. Complete sequence determination of a novel reptile iridovirus isolated from soft-shelled turtle and evolutionary analysis of Iridoviridae. *BMC Genomics* **2009**, *14*, 224. [CrossRef] [PubMed]
136. Koonin, E.V.; Krupovic, M.; Yutin, N. Evolution of double-stranded DNA viruses of eukaryotes: From bacteriophages to transposons to giant viruses. *Ann. N. Y. Acad. Sci.* **2015**, *1341*, 10–24. [CrossRef] [PubMed]
137. Nasir, A.; Kim, K.M.; Caetano-Anolles, G. Giant viruses coexisted with the cellular ancestors and represent a distinct supergroup along with superkingdoms Archaea, Bacteria and Eukarya. *BMC Evol. Biol.* **2012**, *24*. [CrossRef] [PubMed]
138. Moss, B. Reflections on the early development of poxvirus vectors 2013. *Vaccine* **2013**, *6*, 4220–4222. [CrossRef] [PubMed]

AMERICAN SOCIETY FOR MICROBIOLOGY | Journal of Virology

The Large Marseillevirus Explores Different Entry Pathways by Forming Giant Infectious Vesicles

Thalita Souza Arantes,[a] Rodrigo Araújo Lima Rodrigues,[a] Ludmila Karen dos Santos Silva,[a] Graziele Pereira Oliveira,[a] Helton Luís de Souza,[a] Jacques Y. B. Khalil,[c] Danilo Bretas de Oliveira,[a] Alice Abreu Torres,[a] Luis Lamberti da Silva,[b] Philippe Colson,[c] Erna Geessien Kroon,[a] Flávio Guimarães da Fonseca,[a] Cláudio Antônio Bonjardim,[a] Bernard La Scola,[c] Jônatas Santos Abrahão[a]

Department of Microbiology, Institute of Biological Sciences, Unviversidade Federal de Minas Gerais, Belo Horizonte, Minas Gerais, Brazil[a]; Department of Cell and Molecular Biology, Ribeirão Preto Medical School, Universidade de São Paulo, Ribeirão Preto, São Paulo, Brazil[b]; URMITE CNRS UMR 6236–IRD 3R198, Aix Marseille Universite, Marseille, France[c]

ABSTRACT

Triggering the amoebal phagocytosis process is a *sine qua non* condition for most giant viruses to initiate their replication cycle and consequently to promote their progeny formation. It is well known that the amoebal phagocytosis process requires the recognition of particles of >500 nm, and most amoebal giant viruses meet this requirement, such as mimivirus, pandoravirus, pithovirus, and mollivirus. However, in the context of the discovery of amoebal giant viruses in the last decade, *Marseillevirus marseillevirus* (MsV) has drawn our attention, because despite its ability to successfully replicate in *Acanthamoeba*, remarkably it does not fulfill the >500-nm condition, since it presents an ~250-nm icosahedrally shaped capsid. We deeply investigated the MsV cycle by using a set of methods, including virological, molecular, and microscopic (immunofluorescence, scanning electron microscopy, and transmission electron microscopy) assays. Our results revealed that MsV is able to form giant vesicles containing dozens to thousands of viral particles wrapped by membranes derived from amoebal endoplasmic reticulum. Remarkably, our results strongly suggested that these giant vesicles are able to stimulate amoebal phagocytosis and to trigger the MsV replication cycle by an acidification-independent process. Also, we observed that MsV entry may occur by the phagocytosis of grouped particles (without surrounding membranes) and by an endosome-stimulated pathway triggered by single particles. Taken together, not only do our data deeply describe the main features of MsV replication cycle, but this is the first time, to our knowledge, that the formation of giant infective vesicles related to a DNA virus has been described.

IMPORTANCE

Triggering the amoebal phagocytosis process is a *sine qua non* condition required by most giant viruses to initiate their replication cycle. This process requires the recognition of particles of >500 nm, and many giant viruses meet this requirement. However, MsV is unusual, as despite having particles of ~250 nm it is able to replicate in *Acanthamoeba*. Our results revealed that MsV is able to form giant vesicles, containing dozens to thousands of viral particles, wrapped in membranes derived from amoebal endoplasmic reticulum. Remarkably, our results strongly suggest that these giant vesicles are able to stimulate phagocytosis using an acidification-independent process. Our work not only describes the main features of the MsV replication cycle but also describes, for the first time to our knowledge, the formation of huge infective vesicles in a large DNA viruses.

The discovery of the amoebal giant virus *Acanthamoeba polyphaga mimivirus* (APMV) in 2003 (1) raised new and exciting questions regarding the virosphere and boosted the hunt for new giant viruses. Owing to these efforts, an increasing number of remarkable giant viruses have been described (2–6).

Recent data suggest that giant viruses initiate their replication cycles after being phagocytosed by amoebas or other phagocytic cells (1, 7). This conclusion is well supported by classical studies which show that the phagocytosis process is triggered in *Acanthamoeba* by particles of >500 nm (8). Therefore, most of the giant viruses, such as mimivirus, pandoravirus, pithovirus, and mollivirus, meet this requirement (1–3, 5). *Marseillevirus marseillevirus* (MsV) particles, on the other hand, are formed by 250-nm icosahedral capsids that do not reach the 500-nm size threshold (6). Nonetheless, MsV still is able to successfully replicate in *Acanthamoeba*, raising the question of how the virus enters its host cell. After entry, a large and diffuse viral factory is assembled (2 to 4 h), wherein genome replication and virion morphogenesis occurs (6 to 8 h), and the virions are released from the cell within 24 h. Just like the mimivirus, MsV has fibers with globular ends on the surface, although they are shorter in length (~12 nm compared to ~125 nm of mimiviruses), and both have an internal membrane surrounding the nucleocapsid (6). However, the origins of the MsV inner membrane remain unknown (6). The first marseillevirus was isolated from a water sample collected from a cooling

Received 28 January 2016 Accepted 10 March 2016
Accepted manuscript posted online 16 March 2016
Citation Arantes TS, Rodrigues RAL, dos Santos Silva LK, Oliveira GP, de Souza HL, Khalil JYB, de Oliveira DB, Torres AA, da Silva LL, Colson P, Kroon EG, da Fonseca FG, Bonjardim CA, La Scola B, Abrahão JS. 2016. The large marseillevirus explores different entry pathways by forming giant infectious vesicles. J Virol 90:5246–5255. doi:10.1128/JVI.00177-16.
Editor: G. McFadden
Address correspondence to Bernard La Scola, bernard.la-scola@univ-amu.fr, or Jônatas Santos Abrahão, jonatas.abrahao@gmail.com.

tower in Paris, France, by culturing *Acanthamoeba castellanii* cells. Since then, marseillevirus-like organisms have been isolated from several environmental samples, with representatives from France, Tunisia, Senegal, Australia, and Brazil (6, 9–13).

Although these viruses were discovered almost a decade ago, little is known regarding their replication cycle. Thus, our objective was to perform a detailed study on the steps of the MsV replication cycle, specifically focusing on two fundamental questions: does MsV enter its amoeba host by phagocytosis, and if so, how does it stimulate the phagocytosis process while being smaller than 500 nm in size? Interestingly, our findings reveal that MsV is able to form giant vesicles containing dozens to thousands of viral particles. Using several approaches, it was possible to track the origins of these vesicles, as well as their important role in MsV biology and the maintenance of these viruses in the environment. Our results strongly suggest that these giant vesicles are remarkably able to stimulate amoeba phagocytosis by an acidification-independent process, successfully initiating the MsV replication cycle. Also, we observed that MsV entry may occur by phagocytosis of grouped particles (without surrounding membranes) or by an endosome-mediated pathway triggered by single particles. Taken together, our data not only thoroughly describe the main features of the MsV replication cycle but also provide the first report, to our knowledge, of the formation of giant infective vesicles as a way to boost the replicative success of a large DNA virus.

MATERIALS AND METHODS

Virus production, purification, and replication cycle analysis. *Acanthamoeba castellanii* cells (ATCC 30010) were cultivated in PYG medium supplemented with 7% fetal calf serum (FCS; Cultilab, Brazil), 25 mg/ml amphotericin B (Fungizone; Cristalia, São Paulo, Brazil), 500 U/ml penicillin, and 50 mg/ml gentamicin (Schering-Plough, Brazil). A total of 7×10^6 cells were infected with MsV at a multiplicity of infection (MOI) of 0.01 and incubated at 32°C. After the appearance of cytopathic effect, the cells and supernatant were collected and the viruses were then purified through ultracentrifugation with a 25% sucrose cushion at 36,000 × *g* for 2 h. After purification, the amoeba cells were infected with purified viruses at MOIs of 0.01 and 10 to evaluate the MsV replication cycle. Infected cells were fixed with 2.5% glutaraldehyde in a 0.1 M sodium phosphate buffer for 1 h at room temperature at various times postinfection. The amoebas were postfixed with 2% osmium tetroxide and embedded in EPON resin. Ultrathin sections then were analyzed under transmission electron microscopy (TEM; Spirit Biotwin FEI-120 kV).

Purification of vesicles. For the purification of the vesicles, the supernatant obtained from *A. castellanii* cells infected with MsV at an MOI of 0.01 was submitted to ultracentrifugation at 20,000 × *g* for 5 min. The pellet containing vesicles was collected and the supernatant containing only naked particles was discarded. After this purification, the samples were prepared for analysis by scanning electron microscopy (SEM), as previously described (14). Furthermore, we also evaluated if these vesicles could be phagocytosed by amoebas. This analysis was conducted under TEM. For the infection, 1×10^6 50% tissue culture infective doses ($TCID_{50}$) (15) of purified vesicles were added to a culture flask containing 7×10^6 cells of *A. castellanii*. One hour postadsorption the cells were fixed with 2.5% glutaraldehyde in a sodium phosphate buffer, 0.1 M, and analyzed by TEM as described above.

Entry assays. In this set of experiments, we evaluated different entry pathways that MsV explores in order to infect amoeba cells. First, we evaluated the endocytic pathway using chloroquine treatment. For this experiment, *A. castellanii* cells were infected with single particles of MsV or vesicles at an MOI of 10, plus chloroquine (Sigma) at a concentration of 50 μg/ml. Twenty-four hours postinfection, the treated and untreated cells were titrated using $TCID_{50}$ methods. In addition, we evaluated whether the inhibition of actin filaments and microtubules (related to phagocytosis) could decrease the viral titer. For this, *A. castellanii* cells were infected with particles of the MsV or vesicles at an MOI of 10 and further treated with cytochalasin D (Sigma) at a concentration of 2 μM. Twenty-four hours postinfection, the treated and untreated cells were titrated by $TCID_{50}$ methods.

In order to verify the impact of membrane transportation on the viral replication cycle, *A. castellanii* cells were infected with MsV at an MOI of 10 and treated with 10 μg/ml of brefeldin A (BFA). We observed four different infection periods, 1, 2, 4, and 8 h, that correspond to four different stages of the MsV replication cycle, namely, entry, membrane recruitment, early viral factory formation, and mature viral factories. The amoebas were then transferred to 96-well microplates containing 100 μl of PYG medium and maintained at 32°C for 24 h before being further titrated by $TCID_{50}$.

Biological properties of the vesicles. *A. castellanii* cells were infected with MsV at an MOI of 0.01. Forty-eight hours postinfection, the vesicles were purified as described above. A portion of the purified vesicles was treated with a lysis buffer at a ratio of 1:1 for 10 min for the release of viral particles present in the vesicles. The vesicles containing the viruses, and also the single particles, then were titrated using the $TCID_{50}$ method. After titration, 1×10^5 $TCID_{50}$ of each was used to infect new *A. castellanii* cells. The cells were observed daily, and 100 μl was collected after 24, 48, and 72 h. In addition, we evaluated the temperature resistance of vesicles and single particles. For this, we used 1×10^5 $TCID_{50}$ vesicles or single particles and submitted them to 70°C for 1, 3, 5, 7, and 10 min using an Eppendorf Thermomixer comfort apparatus. Seventy degrees was chosen due to previous data from our laboratory that indicated this temperature is a good choice for performing heat resistance assays of large/giant viruses. It is important to highlight that at room temperature (25°C), both MsV naked particles and vesicles remain infective for at least 2 months (data not published). The samples then were titrated in *A. castellanii* using $TCID_{50}$.

The origins of the internal membrane and the giant vesicles. To investigate the origins of the internal membrane and the giant vesicles formed by marseilleviruses, immunofluorescence microscopy and an immunoblotting assay were performed.

(i) Immunofluorescence microscopy. *A. castellanii* cells were grown on coverslips and infected with MsV (MOI of 10) for 1.5 and 4 h for endosome, endoplasmic reticulum (ER), and Golgi analysis. After infection, the cells were rinsed in cold phosphate-buffered saline (PBS) and fixed with 4% paraformaldehyde (PFA) in PBS for 10 min at room temperature (RT). After fixation, the cells were permeabilized with 0.2% Triton X-100 in 3% bovine serum albumin (BSA)–PBS for 5 min, followed by a rinse with 3% BSA–PBS three times. The cells then were stained for 1 h at room temperature with four specific primary antibodies: rabbit polyclonal anti-sorting nexin 2 (SNX2) (Santa Cruz Technology, USA) (16), goat polyclonal anti-GRP 78 (N-20) (Santa Cruz Technology, USA), mouse monoclonal anti-GM130 (BD Biosciences, USA), and mouse polyclonal anti-MsV (17). After incubation with secondary antibodies, fluorescently labeled cells were visualized using a Zeiss (LSM 510 META) microscope. The images were processed with LSM Image Browser and Adobe Photoshop (version 7.0) software.

(ii) Immunoblotting assay. Briefly, for protein extraction, electrophoresis, and immunoblotting of the infected cells, vesicles, and purified single particles (described above), the samples were disrupted on ice with a lysis buffer and centrifuged at 18,000 × *g* for 15 min at 4°C. The protein concentration was determined using Bio-Rad protein assay dye reagent concentrate number 5000006. Thirty micrograms of protein per sample was separated by electrophoresis on a 10% SDS polyacrylamide gel and transferred to polyvinylidene difluoride membranes. The membranes were incubated overnight at 4°C with anti-sorting nexin 2 (1:1,000), anti-GRP 78 (1:1,000), and anti-GM130 (1:1,000) antibodies. After washing, the membranes were incubated with peroxidase-conjugated anti-rabbit (1:5,000) and anti-goat (1:5,000) secondary antibodies. Immunoreactive

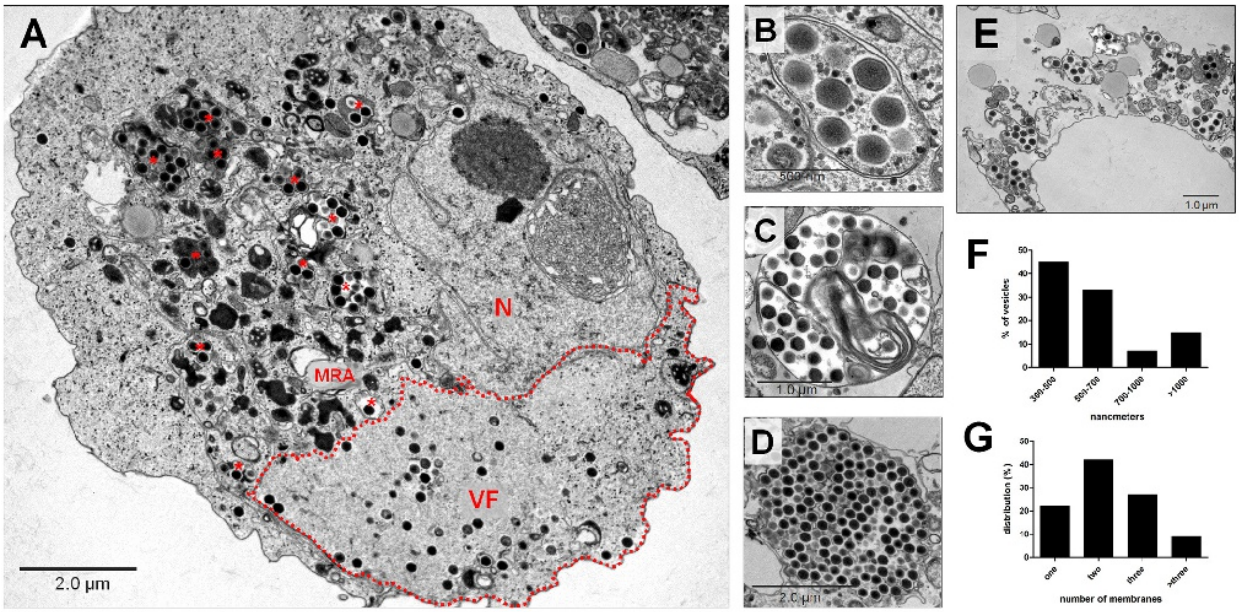

FIG 1 MsV forms a large viral factory and produces giant vesicles. (A) A TEM image of an *A. castellanii* cell infected with MsV exhibiting a large viral factory surrounded by membranes and vesicles (asterisks), with several viral particles, both inside and outside, often being found in vesicles. The dotted red line surrounds the viral factory. (B to D) TEM images demonstrating that the vesicles may contain one or more membranes and variable numbers of viruses. (E) A TEM image demonstrating a cell undergoing lysis, releasing a number of MsV vesicles. (F) Analyses of the size of the vesicles, in nanometers, found in the cytoplasm of an *A. castellanii* cell. (G) The distribution of the number of membranes present in the vesicles. For panels F and G, a total of 200 circular vesicles were considered. *, viral particles in vesicles; VF, viral factory; MRA, membrane-rich area; N, nucleus. All of the images were obtained 24 h postinfection at low MOI (0.01).

bands were visualized using a Luminata Forte Western horseradish peroxidase (HRP) substrate.

RESULTS

MsV viral factory observations. It was possible to clarify the various stages of the MsV replication cycle, which had so far remained poorly understood, through observations of *A. castellanii* cells at different times postinfection using transmission electron microscopy (TEM). Around 3 to 4 h postinfection we observed large viral factories, occupying 1/3 to 1/2 of the amoeba cytoplasm, all containing MsV particles in different stages of morphogenesis (Fig. 1A). At the edge of the viral factories it was possible to observe membrane-rich areas (MRA) (Fig. 1A) in which most of the mature viral particles were wrapped into large vesicles. These vesicles varied widely in terms of size and number of membranes (Fig. 1B, C, and D). By means of TEM, we also could observe some cells undergoing lysis, releasing a number of MsV vesicles (Fig. 1E). We noticed that the vesicles could measure from 300 nm up to >1,000 nm in diameter, depending on the amount of virus found within them. Most vesicles had an approximate size of 300 to 500 nm, representing 45% of the produced vesicles (Fig. 1F). Interestingly, we observed that the vesicles consisted of various numbers of membranes. By performing an analysis of infected amoebas containing vesicles, we evaluated the number of membranes present in each one. There were vesicles with only one membrane but also vesicles with three or more membranes. Vesicles with two membranes were the most prevalent, making up around 40% of the total (Fig. 1G).

The origins of vesicle membranes and their impact on viral replication. During the replication of MsV, we observed the recruitment and rearranging of cell membranes toward vesicle formation. In addition, we noted that the vesicles could consist of one or several membranes. In order to investigate the origins of these membranes, we performed immunofluorescence (IF) assays targeting three distinct parts of cellular membranes, namely, endoplasmic reticulum (ER; anti-GRP78), Golgi complex (anti-GM130), and endosome (anti-SNX2), as these structures have been described as being involved in the morphogenesis of a number of other viruses. We also used an anti-MsV polyclonal antibody. *A. castellanii* cells were infected with MsV. Three hours postinfection we could observe colocalization between the anti-GRP78 and anti-MsV targets, suggesting that the membranes of the vesicles originated from the ER (Fig. 2A). The colocalization between MsV vesicles and other analyzed cellular targets was not observed (data not shown). Only structures outside the particles were targeted, as we believe that the immunofluorescence permeabilization process is not efficient enough to allow the binding of antibodies to membranes inside the viral particle (to answer this question, we performed immunoblotting assays of purified particles as described below). It is also clear from Fig. 2A that vesicle formation is polarized within the cell, coinciding with the polarization of ER membranes at this specific moment of infection. The formation of ER membrane-rich areas during MsV infection could be further visualized by TEM (Fig. 2B).

After we confirmed the origins of the vesicle membranes, we evaluated the influence of BFA, a membrane transport inhibitor, during the MsV replication cycle and vesicle formation. A decrease of ~2 logs in viral titer was observed in treated cells compared to untreated cells (Fig. 2C). In addition, using TEM images,

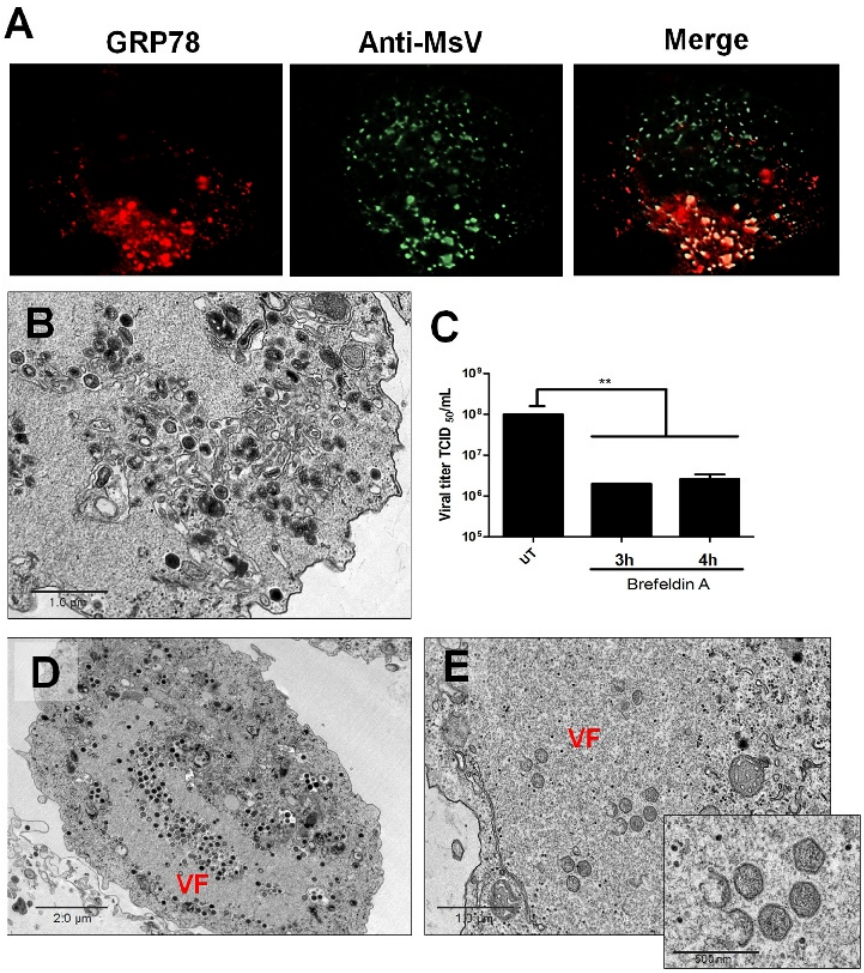

FIG 2 Membranes of MsV giant vesicles likely originate from ER. (A) Immunofluorescence microscopy showing the colocalization between anti-GRP78 and anti-MsV targets, suggesting that the membranes of the vesicles originate from the ER. (B) A TEM image of an *A. castellanii* cell 3 h postinfection, demonstrating an ER-rich area. (C) The impact of BFA on viral replication. After infected *A. castellanii* cells were treated with BFA, an ~2 log reduction in the viral titer was observed relative to untreated cells. The experiment was performed twice in duplicate. (D) TEM image of a cell not treated with brefeldin A, evidencing many viral particles within the viral factory. (E) TEM image of brefeldin A-treated cells (3 h of treatment) exhibiting a decrease in or absence of membranes around the viral factories as well as a significant reduction in the number of particles being assembled. **, $P < 0.001$; VF, viral factory.

we observed that treated cells exhibited a decrease/absence of membranes around the viral factories, as well as a significant reduction in the number of particles being assembled compared to untreated cells (Fig. 2D), suggesting that membranes are important not only to vesicle formation but also to particle morphogenesis (Fig. 2E).

Vesicle attachment and entry into amoebas. After establishing the origin of the vesicles, we then evaluated whether MsV vesicles could attach to and be phagocytosed by amoebas. Initially, to demonstrate that the viruses could be released within vesicles, we performed a scanning electron microscopy (SEM) analysis of these structures after they were purified from amoebas infected with MsV. The SEM images corroborated the existence of the extracellular vesicles (Fig. 3A). In addition, the results also demonstrated the efficacy of the purification method used. Considering that MsV particles are icosahedral and that most of the vesicles are spherical, we estimated the number of virus particles present within the vesicles, as they varied in size (300 to >1,000 nm in diameter). Using a mathematical model, we sought to obtain the most probable number of viral particles present in each vesicle. A logarithmic profile was achieved, and it was possible to estimate that >1,000 viral particles could exist inside a vesicle (Fig. 3B). A vesicle 1,100 nm in diameter hypothetically could contain ~100 MsV particles, for example (Fig. 3B).

In order to verify that the vesicles were able to attach to the host surface and stimulate phagocytosis, purified vesicles were incubated with *A. castellanii* cells for 10 min and further analyzed by SEM. The images demonstrated that an interaction between vesicles of different sizes and amoebae occurred (Fig. 3C to E). TEM analysis of the vesicles after 30 min of incubation with *A. castellanii* cells also was performed. It was possible to observe intact vesicles and many viruses spread throughout the cell cytoplasm (Fig. 3F

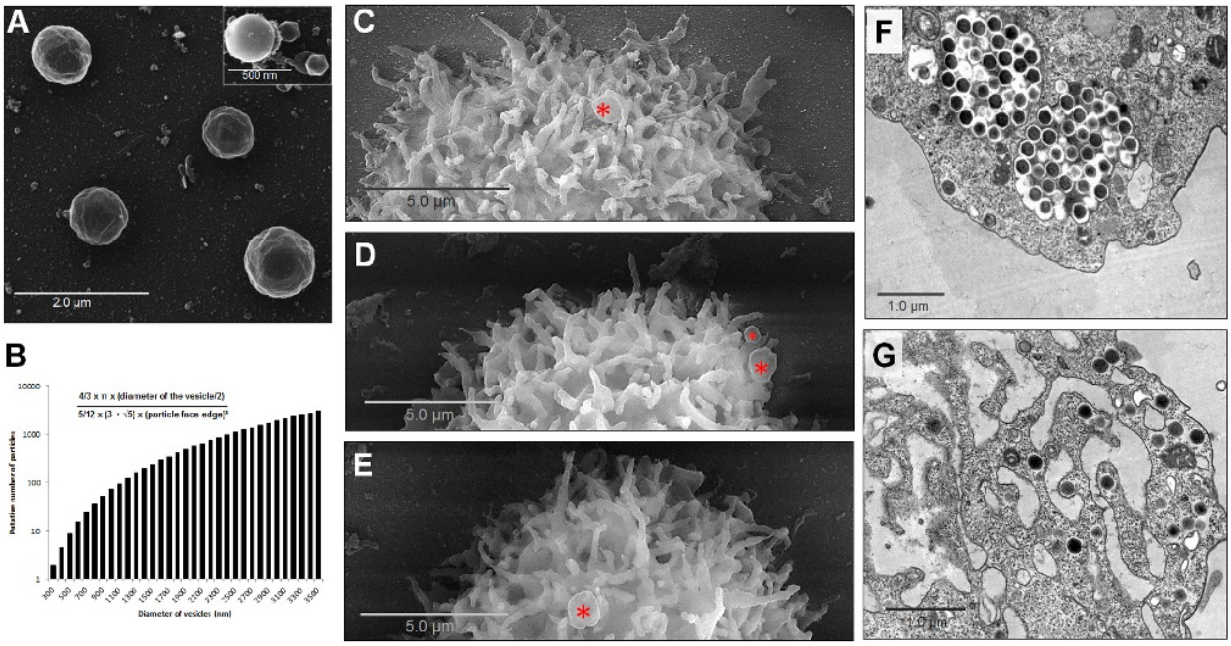

FIG 3 Giant vesicles contain several viral particles and promote phagocytosis. (A) SEM images of purified giant vesicles produced by MsV during its replication cycle. (Top right) Details of some particles close to a small vesicle. (B) A putative amount of viral particles inside vesicles of different sizes. Using a mathematical model, the number of particles per vesicle with diameters ranging from 300 to 3,500 nm was estimated. (C to E) Vesicles of different sizes attached to the surface of an *A. castellanii* cell. (F) A TEM image of intact giant vesicles inside an *A. castellanii* cell directly after penetration. The vesicles had more than one membrane. The external layer fused with the cell membrane, releasing the viruses surrounded by the inner membrane of the vesicles. (G) A TEM image of several dispersed viral particles inside an *A. castellanii* cell directly after penetration of a giant vesicle. In contrast to results shown in panel F, the giant vesicle likely had only one membrane that fused with the cell membrane, releasing the viruses directly into the cytoplasm of the cell. An asterisk indicates vesicles attached to amoebal surface; in panels C and E it is possible to see amoebal pseudopods attached to the vesicles. Both TEM images were obtained 1 h postinfection with the large vesicles.

and G). We believe that when a vesicle has only one membrane, it merges with the phagosome membrane and releases the viruses inside the cytoplasm of the amoeba (Fig. 3G). However, when a vesicle has several membranes, only the outer membrane merges with the phagosome membrane and the internal membranes remain intact, keeping the viruses inside the vesicle (Fig. 3F).

The origins of the inner membrane of MsV. Considering the results described above, a rational next step would be to perform immunoblotting assays of purified vesicles to confirm their origins. However, Boyer and colleagues (6) have previously hypothesized the existence of an MsV inner membrane. Therefore, to design this assay we would have to consider the possibility that this inner membrane has a different origin from that described for the membranes of the giant vesicles. Indeed, as described previously (6), during MsV morphogenesis we observed the incorporation of structures resembling membranes (Fig. 4A).

In order to confirm the origins of the giant vesicles and to investigate the origins of the MsV inner membrane, we performed immunoblotting assays of vesicles (membrane and particles), of particles released from vesicles (after detergent treatment), and of membranes purified from vesicles. Distinct parts of the cellular membranes were probed (ER, Golgi complex, and endosome). As expected, purified vesicle membranes were recognized only by the anti-ER marker antibody (GRP78). Remarkably, purified particles were recognized only by the anti-endosome marker antibody (SNX2). Finally, vesicles containing MsV particles (and the *A. castellanii* protein extract-positive control) were recognized both by anti-ER and anti-endosome antibodies. The anti-Golgi antibody (anti-GM130) only recognized the positive control (Fig. 4B). Therefore, these data suggest that the origin of the MsV inner membrane is endosomal.

Endosomes are recruited to early viral factories. To investigate how endosome membranes are incorporated in the viral factory, we infected *A. castellanii* cells with MsV, and after 90 min we performed IF assays using antibodies against MsV (anti-MsV) and an endosome marker (anti-SNX2). The colocalization between anti-SNX2 and anti-MsV reinforced our previous results and suggests that endosomes are recruited to the MsV viral factory during the early stages of infection (Fig. 4C).

Since the endosome participates in the formation of MsV particles, we performed TEM of infected cells in order to observe its location and participation in the MsV multiplication cycle. During the early stages (1, 2, and 3 h) of infection, we observed many endosomal vacuoles in the cytoplasm of the host cell surrounding an early membrane-rich viral factory (Fig. 4D, E, and F). Since these vacuoles are found near the viral factory region, they probably contribute to the morphogenesis of the viruses, likely contributing to the formation of the particle internal membrane, corroborating our previous data.

Vesicles versus particles: biological properties. Our next step was to evaluate if MsV giant vesicles confer any advantage compared to single viral particles. In order to measure the efficacy of

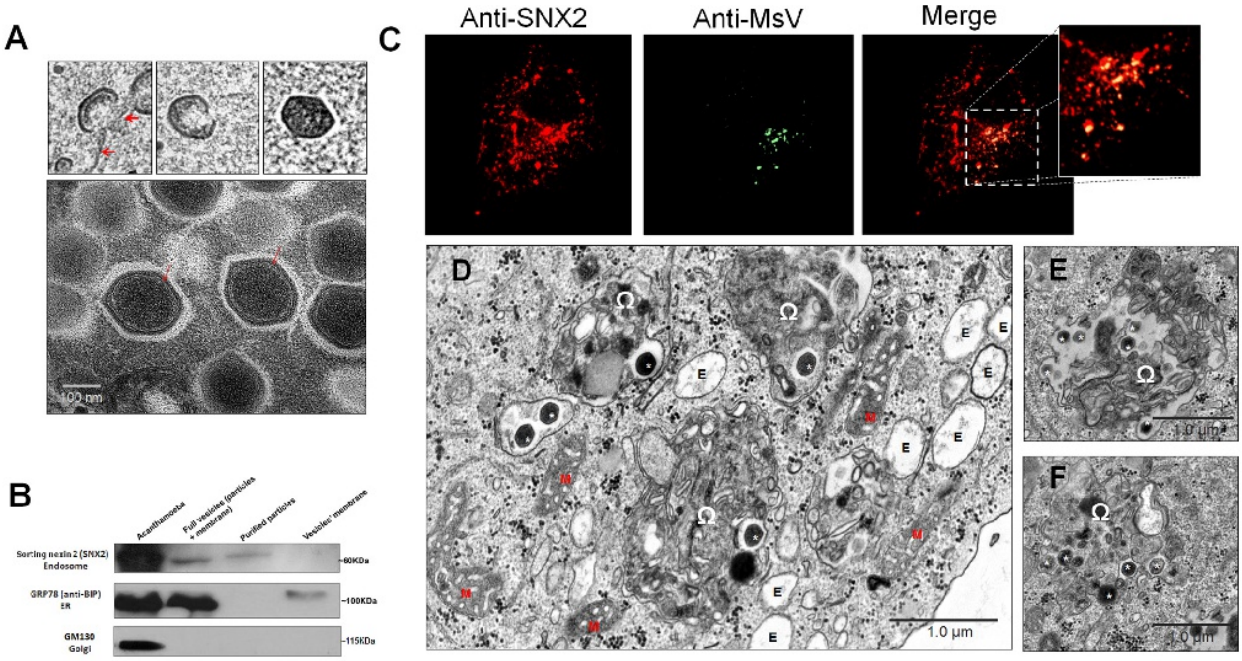

FIG 4 Marseilleviruses have an internal membrane that likely originates from the endosome. (A) TEM images of immature (inset) and mature MsV particles showing the crescent structure of the viral particles and the internal membrane surrounding the nucleocapsid (arrows). (B) The internal membrane originates from the endosome, while the giant vesicles originate from the ER. A specific endosome antibody (SNX2) recognized the full vesicles and the purified particles but not the vesicles' membrane, indicating that endosomal components are present only when the viral particles are present (60 kDa). Otherwise, a specific antibody to ER (GRP78) recognized the full vesicles and the vesicles' membrane but not the purified particles, demonstrating the ER origins of giant vesicles (100 kDa). Both antibodies recognized the *A. castellanii* structures. The anti-Golgi antibody (anti-GM130) recognized only the positive control. (C) Immunofluorescence microscopy corroborates the Western blotting data once MsV colocalizes with the endosomal components. (D) A TEM image of an *A. castellanii* cell infected with MsV, showing the presence of several endosomes (some containing viruses) and some membrane-rich areas containing viruses, probably originating from the endosome. (E and F) TEM images showing different membrane-rich areas containing viral particles. *, viral particles; M, mitochondria; E, endosome; Ω, membrane-rich area. TEM images were obtained 3 h postinfection.

vesicles and single particles in infecting *A. castellanii*, 1×10^5 $TCID_{50}$ of each (full vesicles and viruses, previously normalized as infectious entities) was incubated with *A. castellanii* cells. The cells were observed daily and collected 24, 48, and 72 h postinfection for further titration. It was possible to observe that the vesicles have a higher efficacy in terms of infection than the isolated viruses. For each evaluated time point the vesicles reached significantly higher titers. After 72 h the titer of the vesicles increased by ~2 logs, while the particles exhibited a lower increase of ~1.5 logs (Fig. 5A).

In order to investigate if giant vesicles confer any physical advantage to MsV compared to isolated particles, we simulated an extreme heat condition. After exposure to 70°C on multiple occasions, our findings showed the giant vesicles were significantly more resistant to this physical stress than the particles. Exposure to 70°C for 7 and 10 min completely eliminated the infectivity of isolated particles of MsV; however, some vesicles remained infectious under the same conditions, reaching ~1×10^2 $TCID_{50}$ (Fig. 5B). This result strongly suggests that giant vesicles confer a physical advantage to MsV.

Vesicles versus particles: entry. Based on our findings (Fig. 3C to G), i.e., the discovery of giant vesicles, we raised an interesting question regarding MsV entry: would vesicles be able to stimulate phagocytosis? To address this question, we designed additional experiments and compared the MsV entry pathways of giant vesicles and isolated particles.

Thus, *A. castellanii* cells were treated with chloroquine or with cytochalasin D and then infected with giant vesicles or isolated particles. Twenty-four hours postinfection the infected and treated cells were collected and the MsV titer determined. Chloroquine is a 9-aminoquinoline that prevents the acidification of the endosome and has a negative impact on the replication of some viruses that depend on this pathway (18). Cytochalasin D is a mycotoxin that promotes a variety of changes in cellular functions, including the destabilization of the cytoskeleton, and has been associated with the inhibition of phagocytosis (19).

Our results showed that treatment with chloroquine significantly impacted the titers of isolated particles ($P < 0.001$) but not (significantly) those of giant vesicles (Fig. 5C). On the other hand, cytochalasin D significantly decreased ($P < 0.01$) the titers of the cells infected with giant vesicles but not (significantly) those infected with isolated particles (Fig. 5D). Together, these results indicate that while isolated particles use an endosomal acidification-dependent entry pathway, giant vesicle entry is mediated via phagocytosis.

In addition, TEM images from amoebas infected with MsV corroborated our hypothesis that particle entry into the amoeba occurs via the endosome. It was possible to observe the viral par-

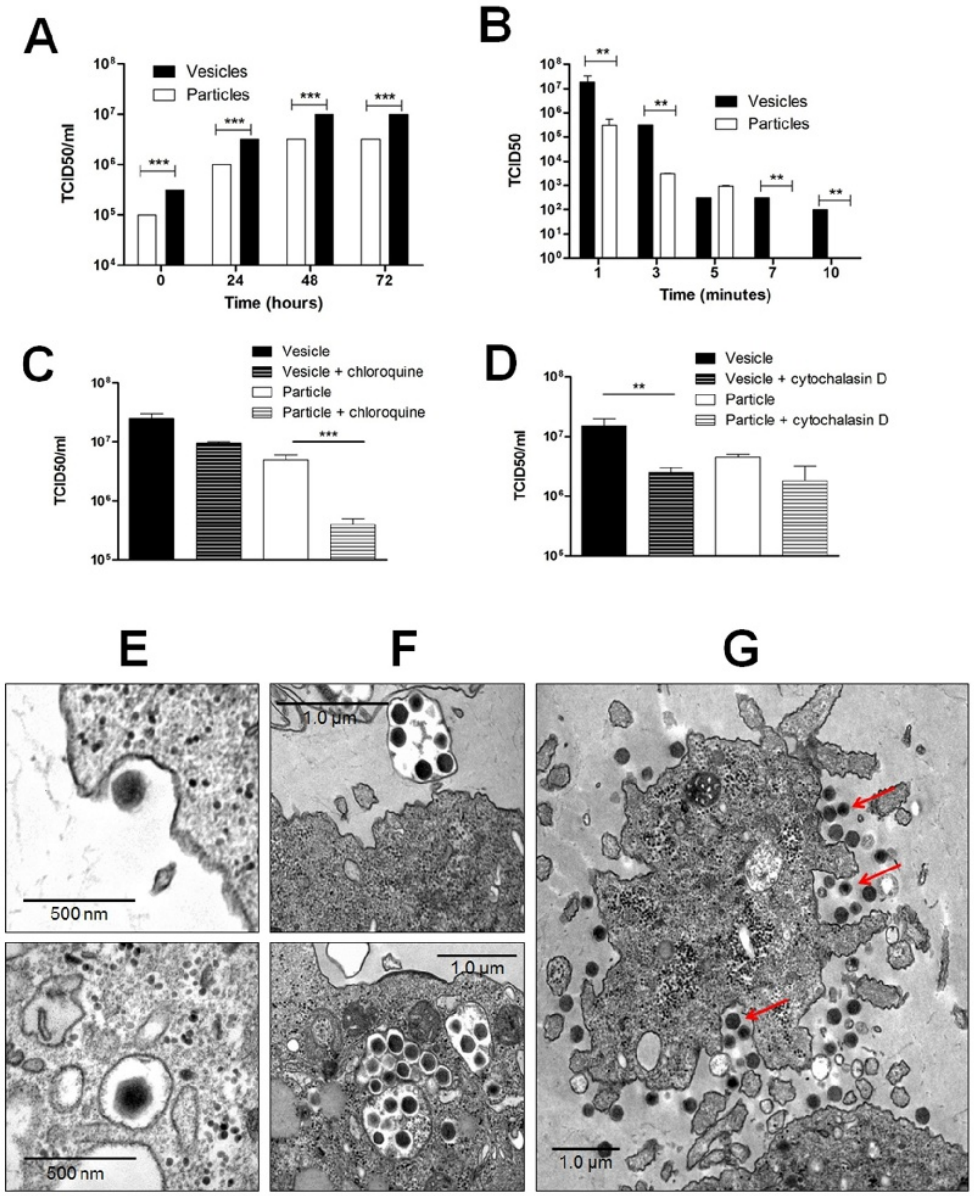

FIG 5 MsV entry into the host cell through different pathways. (A) Vesicles containing viruses provide a faster beginning to the replication cycle than single particles. (B) Vesicles confer longer-duration temperature resistance to MsV than single particles. (C and D) The effects of chloroquine and cytochalasin D on viral replication when viruses are isolated or found within vesicles. (E) TEM images of the MsV penetrating an *A. castellanii* cell using the endocytic pathway. (F) TEM images of giant vesicles penetrating an *A. castellanii* cell by phagocytosis. (G) A TEM image of grouped viral particles being engulfed by *A. castellanii* (arrows). The experiments were performed twice in duplicate. **, $P < 0.001$; ***, $P < 0.0001$. TEM images were obtained 1 h postinfection.

ticle interacting with the surface of the amoebae (Fig. 5E), and such interaction might occur through the short viral fibers found on the viral capsid. Moreover, after entry there were particles within the amoeba cytoplasm (Fig. 5E). Also, the TEM images corroborated the results from the cytochalasin D condition that vesicles can enter via phagocytosis, as it was possible to observe them both outside and inside the cell (Fig. 5F). Furthermore, it was possible to observe an aggregate of viral particles being engulfed by the cell, suggesting that phagocytosis of grouped particles is another virus entry route (Fig. 5G).

DISCUSSION

In 2013, Feng and colleagues described a pathogenic picornavirus able to acquire an envelope by hijacking cellular membranes (20). This represented a breakthrough in virology as, until then, a virus was considered either enveloped or nonenveloped, without the

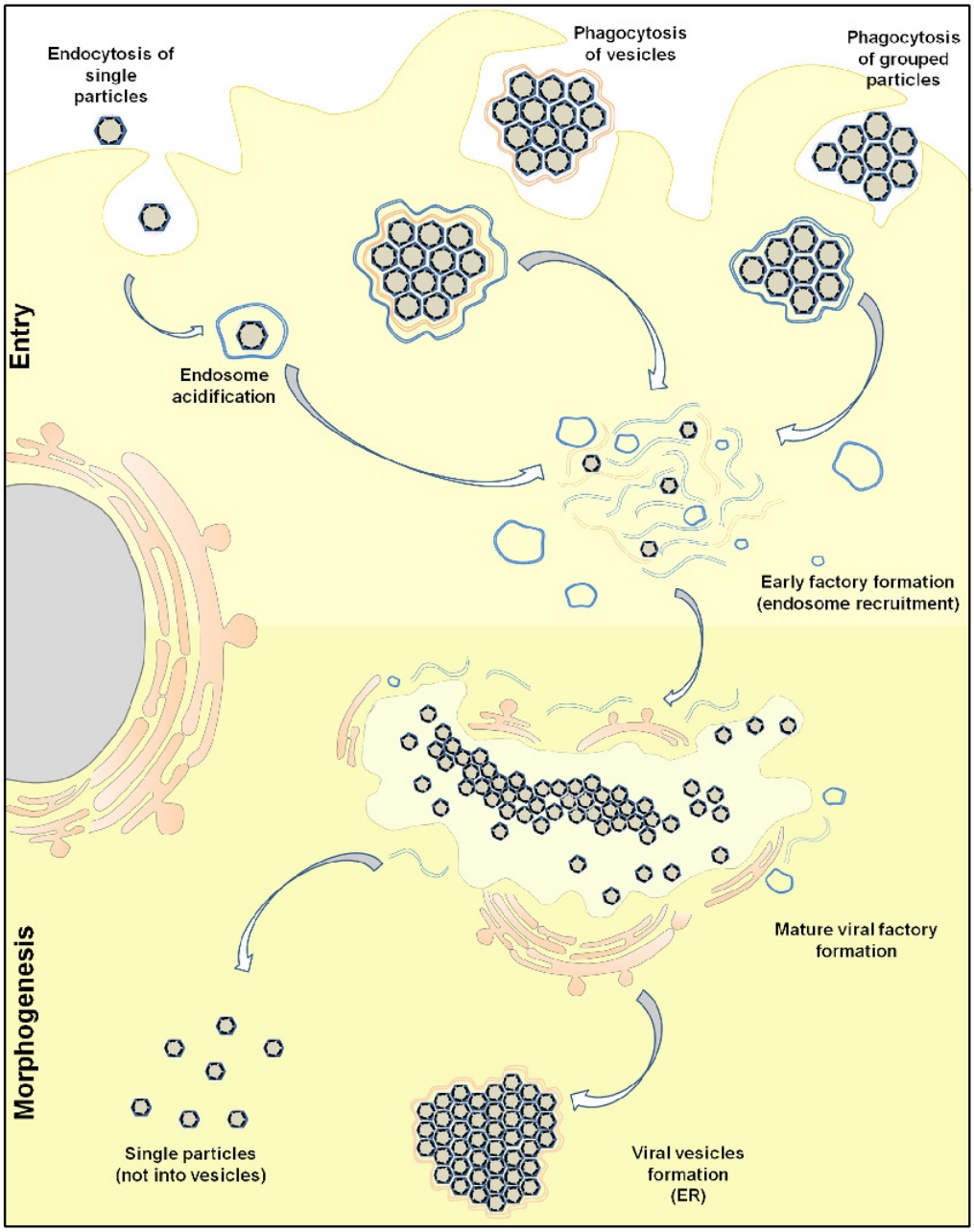

FIG 6 Models of MsV cycle replication. This model summarizes the replication cycle of MsV in *Acanthamoeba* cells. MsV can enter into the cell by different pathways, including endocytosis of single particles, phagocytosis of giant vesicles, and phagocytosis of grouped particles.

possibility of interchangeable states by the acquisition of membranes by the virus. A few other RNA viruses also are able to form infectious vesicles, which act mainly as a mechanism for escape from host immunity (21). Here, we describe for the first time, to our knowledge, a DNA virus, marseillevirus, that is able to induce the formation of giant vesicles while replicating within amoebas, its natural host.

Acanthamoeba species are unicellular protozoans that obtain nutrients through phagocytosis of microorganisms, including giant viruses (1, 22). Here, we have demonstrated that MsV, which is different from other amoebal viruses where a single particle can penetrate by phagocytosis, has developed an alternative mechanism to trigger this process, the formation of giant vesicles. The dispersion of pathogenic RNA viruses by vesicles was described as

useful in repelling specific antibodies, thus providing an important advantage to those viruses within their hosts (20, 21). Given the natural hosts of marseilleviruses, this does not seem to be applicable, as amoebas do not possess an adaptive immune system. However, this could be important if humans were their hosts, since marseilleviruses have already been described as putative human pathogens (17, 23). In addition, our results suggest that infection through vesicles evolved as a powerful mechanism to boost the replicative success of this virus within its natural hosts and/or its survival in the environment where they coexist. Indeed, we have demonstrated here that being wrapped inside vesicles may confer to the virus a number of advantages, including a greater efficiency of infection and the ability to stimulate phagocytosis. Therefore, these vesicles can facilitate the spread of the virus to other susceptible cells by collectively transferring multiple viral genomes into the cytoplasm (21). Also, we demonstrated that the vesicles confer to MsV resistance to high temperature. Considering the vesicle as an infectious entity and that each viral particle has the same heat stability, being wrapped within a membranous structure is an advantage for the species (in the case of MsV as the infectious agent), since more particles will remain infectious and grouped even under harsh conditions. In addition, the vesicle membranes could confer more resistance to wrapped particles. The giant vesicles observed in this study seem to have originated from the ER and can contain one or more membranes (Fig. 1) and up to 1,000 viral particles (Fig. 3). It seems that MsV modulates these membranes for the host cell in order to delimit a large viral factory where the vesicles are produced. The number of membrane layers in the vesicles can influence the entry of the virus into the cell. When the vesicles have only one layer, they can fuse with the cell membrane, releasing the viruses directly into the cytoplasm of the amoeba in a disorganized way. When more than one layer is present, fusion also occurs but the internal membranes remain intact, preserving the viruses within them. The large size of the vesicles makes them appropriate for phagocytosis. According to a study by Korn and Weisman, which evaluated the phagocytosis capacity of *Acanthamoeba* using latex beads of different sizes, particles smaller than 500 nm, such as those of MsV, were not phagocytosed unless they formed vesicles or particle agglomerations around the amoeba surface (8). Generally, giant viruses, such as mimivirus, pandoravirus, and pithovirus, enter into the host cell via phagocytosis, since they range in size from 750 nm to 1.5 μm (1–3). However, despite the relatively small size of marseilleviruses, they are able to enter into their host via phagocytosis using a mechanism never described before for large DNA viruses (Fig. 6).

In addition to the phagocytic pathway, marseilleviruses can enter into their host via endocytosis (Fig. 6). Macropinocytosis might be involved as well, but this should be investigated further (Fig. 5G and 6). A similar mechanism was observed in vaccinia virus (VACV), which can penetrate the cell in different ways, e.g., membrane fusion, macropinocytosis, or a low-pH-dependent endocytic route (24, 25). Another similarity between VACV and MsV is the presence of an inner membrane. In this study, we suggested that the inner membrane of MsV is acquired from the endosomes, although we believe that other sources cannot be ruled out. After penetration, it was possible to observe the accumulation of endosomal vacuoles near the viral factories (Fig. 4); therefore, when the particle was formed a membrane layer was incorporated into the viral capsid. Other large DNA viruses, such as *Paramecium bursaria* chlorella virus, African swine fever virus, and APMV, also acquire their inner membranes during the morphogenesis step, but these membranes have different origins (26). Altogether, our results fill in some of the gaps regarding the replication cycle of the marseilleviruses, providing some important biological information about these large viruses. Using several different approaches, we have demonstrated that MsV either can interact with the cell surface and enter through endocytosis or can be found inside giant vesicles that stimulate the phagocytosis mechanism. Finally, the discovery of giant viruses not only has brought to light their genomic complexity, with hundreds of new genes/proteins that are able to perform activities never before attributable to a virus, but also allowed us a glimpse into a microcosm of ecological interactions, where viruses are able, for example, to actively seek new hosts and habitats by adsorbing into other, more complex life forms, such as fungi and arthropods (14). Here, we have identified yet another possible ecological strategy for the release of a giant virus from its last host in vesicles that have the potential to boost its entry into another host, as well as to help it endure in the environment during an "interhost" period. Although rare, we can trace a parallel between this strategy and the type B inclusion body of cowpox virus, which also may represent a similar method of enhancing interhost resistance and infectivity (27). The investigation and discovery of new giant viruses is fundamental to uncovering new information about the biology of these amazing viruses and to better understand their biological interactions, both cellular and molecular, with their hosts.

ACKNOWLEDGMENTS

We thank our colleagues from Gepvig, Laboratório de Vírus, Centro de Microscopia da UFMG, and Aix Marseille Université for their excellent technical support.

We also thank the CAPES, FAPEMIG, and CNPq for their financial support.

We have no conflicts of interest to declare.

FUNDING INFORMATION

This work, including the efforts of Jonatas Santos Abrahao, was funded by MCTI | Conselho Nacional de Desenvolvimento Científico e Tecnológico (CNPq) (470645/2011-3).

REFERENCES

1. **La Scola B, Audic S, Robert C, Jungang L, de Lamballerie X, Drancourt M, Birtles R, Claverie JM, Raoult D.** 2003. A giant virus in amoebae. Science **299**:2033. http://dx.doi.org/10.1126/science.1081867.
2. **Philippe N, Legendre M, Doutre G, Couté Y, Poirot O, Lescot M, Arslan D, Seltzer V, Bertaux L, Bruley C, Garin J, Claverie JM, Abergel C.** 2013. Pandoraviruses: amoeba viruses with genomes up to 2.5 Mb reaching that of parasitic eukaryotes. Science **341**:281–286. http://dx.doi.org/10.1126/science.1239181.
3. **Legendre M, Bartoli J, Shmakova L, Jeudy S, Labadie K, Adrait A, Lescot M, Poirot O, Bertaux L, Bruley C, Couté Y, Rivkina E, Abergel C, Claverie JM.** 2014. Thirty-thousand-year-old distant relative of giant icosahedral DNA viruses with a pandoravirus morphology. Proc Natl Acad Sci U S A **111**:4274–4279. http://dx.doi.org/10.1073/pnas.1320670111.
4. **Reteno DG, Benamar S, Khalil JB, Andreani J, Armstrong N, Klose T, Rossmann M, Colson P, Raoult D, La Scola B.** 2015. Faustovirus, an asfarvirus-related new line age of giant viruses infecting amoebae. J Virol **89**:6585–6594. http://dx.doi.org/10.1128/JVI.00115-15.
5. **Legendre M, Lartigue A, Bertaux L, Jeudy S, Bartoli J, Lescot M, Alempic JM, Ramus C, Bruley C, Labadie K, Shmakova L, Rivkina E, Couté Y, Abergel C, Claverie JM.** 2015. In-depth study of Mollivirus sibericum, a new 30,000-y-old giant virus infecting Acanthamoeba. Proc

Natl Acad Sci U S A 112:E5327–E5335. http://dx.doi.org/10.1073/pnas.1510795112.

6. **Boyer M, Yutin N, Pagnier I, Barrassi L, Fournous G, Espinosa L, Robert C, Azza S, Sun S, Rossmann MG, Suzan-Monti M, La Scola B, Koonin EV, Raoult D.** 2009. Giant marseillevirus highlights the role of amoebae as a melting pot in emergence of chimeric microorganisms. Proc Natl Acad Sci U S A **106:**21848–21853. http://dx.doi.org/10.1073/pnas.0911354106.
7. **Ghigo E, Kartenbeck J, Lien P, Pelkmans L, Capo C, Mege JL, Raoult D.** 2008. Ameobal pathogen mimivirus infects macrophages through phagocytosis. PLoS Pathog **4:**e1000087. http://dx.doi.org/10.1371/journal.ppat.1000087.
8. **Weisman RA, Korn ED.** 1967. Phagocytosis of latex beads by Acanthamoeba. I. Biochemical properties. Biochemistry **6:**485–497.
9. **Thomas V, Bertelli C, Collyn F, Casson N, Telenti A, Goesmann A, Croxatto A, Greub G.** 2011. Lausannevirus, a giant amoebal virus encoding histone doublets. Environ Microbiol **13:**1454–1466. http://dx.doi.org/10.1111/j.1462-2920.2011.02446.x.
10. **Aherfi S, Boughalmi M, Pagnier I, Fournous G, La Scola B, Raoult D, Colson P.** 2014. Complete genome sequence of Tunisvirus, a new member of the proposed family Marseilleviridae. Arch Virol **159:**2349–2358. http://dx.doi.org/10.1007/s00705-014-2023-5.
11. **Lagier JC, Armougom F, Million M, Hugon P, Pagnier I, Robert C, Bittar F, Fournous G, Gimenez G, Maraninchi M, Trape JF, Koonin EV, La Scola B, Raoult D.** 2012. Microbial culturomics: paradigm shift in the human gut microbiome study. Clin Microbiol Infect **18:**1185–1193. http://dx.doi.org/10.1111/1469-0691.12023.
12. **Doutre G, Philippe N, Abergel C, Claverie JM.** 2014. Genome analysis of the first Marseilleviridae representative from Australia indicates that most of its genes contribute to virus fitness. J Virol **88:**14340–14349. http://dx.doi.org/10.1128/JVI.02414-14.
13. **Dornas FP, Khalil JY, Pagnier I, Raoult D, Abrahão J, La Scola B.** 2015. Isolation of new Brazilian giant viruses from environmental samples using a panel of protozoa. Front Microbiol **6:**1086.
14. **Rodrigues RA, Dos Santos Silva LK, Dornas FP, de Oliveira DB, Magalhães TF, Santos DA, Costa AO, de Macêdo Farias L, Magalhães PP, Bonjardim CA, Kroon EG, La Scola B, Cortines JR, Abrahão JSA.** 2015. Mimivirus fibrils are important for viral attachment to the microbial world by a diverse glycoside interaction repertoire. J Virol **89:**11812–11819. http://dx.doi.org/10.1128/JVI.01976-15.
15. **Reed LJ, Muench H.** 1938. A simple method of estimating fifty percent endpoints. Am J Hyg **27:**493–497.
16. **Haft CR, de la Luz Sierra M, Barr VA, Haft DH, Taylor SI.** 1998. Identification of a family of sorting nexin molecules and characterization of their association with receptors. Mol Cell Biol **18:**7278–72787. http://dx.doi.org/10.1128/MCB.18.12.7278.
17. **Popgeorgiev N, Michel G, Lepidi H, Raoult D, Desnues C.** 2013. Marseillevirus adenitis in an 11-month-old child. J Clin Microbiol **51:**4102–4105. http://dx.doi.org/10.1128/JCM.01918-13.
18. **Savarino A, Boelaert JR, Cassone A, Majori G, Cauda R.** 2003. Effects of chloroquine on viral infections: an old drug against today's diseases? Lancet Infect Dis **3:**722–727. http://dx.doi.org/10.1016/S1473-3099(03)00806-5.
19. **Koch G, Koch F.** 1978. The use of cytochalasins in studies on the molecular biology of virus-host cell interactions. Front Biol **46:**475–498.
20. **Feng Z, Hensley L, McKnight KL, Hu F, Madden V, Ping L, Jeong SH, Walker C, Lanford RE, Lemon SM.** 2013. A pathogenic picornavirus acquires an envelope by hijacking cellular membranes. Nature **496:**367–371. http://dx.doi.org/10.1038/nature12029.
21. **Altan-Bonnet G, Chen YH.** 2015. Intercellular transmission of viral populations with vesicles. J Virol **89:**12242–12244.
22. **Visvesvara GS, Moura H, Schuster FL.** 2007. Pathogenic and opportunistic free-living amoebae: Acanthamoeba spp., Balamuthia mandrillaris, Naegleria fowleri, and Sappinia diploidea. FEMS Immunol Med Microbiol **50:**1–26. http://dx.doi.org/10.1111/j.1574-695X.2007.00232.x.
23. **Popgeorgiev N, Boyer M, Fancello L, Monteil S, Robert C, Rivet R, Nappez C, Azza S, Chiaroni J, Raoult D, Desnues C.** 2013. Marseillevirus-like virus recovered from blood donated by asymptomatic humans. J Infect Dis **208:**1042–1050. http://dx.doi.org/10.1093/infdis/jit292.
24. **Senkevich TG, Ojeda S, Townsley A, Nelson GE, Moss B.** 2005. Poxvirus multiprotein entry-fusion complex. Proc Natl Acad Sci U S A **102:**18572–18577. http://dx.doi.org/10.1073/pnas.0509239102.
25. **Townsley AC, Weisberg AS, Wagenaar TR, Moss B.** 2006. Vaccinia virus entry into cells via a low-pH-dependent endosomal pathway. J Virol **80:**8899–8908. http://dx.doi.org/10.1128/JVI.01053-06.
26. **Milrot E, Mutsafi Y, Fridmann-Sirkis Y, Shimoni E, Rechav K, Gurnon JR, Van Etten JL, Minsky A.** 2016. Virus-host interactions: insights from the replication cycle of the large Paramecium bursaria chlorella virus. Cell Microbiol **18:**3–16. http://dx.doi.org/10.1111/cmi.12486.
27. **Kato S, Takahashi M, Kameyama S, Kamahora J.** 1959. A study of the morphological and cyto-immunological relationship between the inclusions of vaccinia, rabbitpox, vaccinia (variola origin) and vaccinia IHD and a consideration of the term "Guarnieri body." Biken's J **2:**343–363.

Mimiviruses: Replication, Purification, and Quantification

Jônatas Santos Abrahão,[1,3] Graziele Pereira Oliveira,[1,3] Lorena Christine Ferreira da Silva,[1] Ludmila Karen dos Santos Silva,[1] Erna Geessien Kroon,[1] and Bernard La Scola[2]

[1]Instituto de Ciências Biológicas, Departamento de Microbiologia, Laboratório de Vírus, Universidade Federal de Minas Gerais, Belo Horizonte-Minas Gerais, Brazil
[2]Unité de Recherche sur les Maladies Infectieuses et Tropicales Emergentes (URMITE), Aix-Marseille Université, Marseille, France
[3]These authors contributed equally to this work

The aim of this protocol is to describe the replication, purification, and titration of mimiviruses. These viruses belong to the *Mimiviridae* family, the first member of which was isolated in 1992 from a cooling tower water sample collected during an outbreak of pneumonia in a hospital in Bradford, England. In recent years, several new mimiviruses have been isolated from different environmental conditions. These giant viruses are easily replicated in amoeba of the *Acanthamoeba* genus, its natural host. Mimiviruses present peculiar features that make them unique viruses, such as the particle and genome size and the genome's complexity. The discovery of these viruses rekindled discussions about their origin and evolution, and the genetic and structural complexity opened up a new field of study. Here, we describe some methods utilized for mimiviruses replication, purification, and titration. © 2016 by John Wiley & Sons, Inc.

Keywords: mimiviruses • purification • replication • titration

How to cite this article:
Abrahão, J.S., Oliveira, G.P., Ferreira da Silva, L.C., dos Santos Silva, L.K., Kroon, E.G., and La Scola, B. 2016. Mimiviruses: replication, purification, and quantification. *Curr. Protoc. Microbiol.* 41:14G.1.1-14G.1.13.
doi: 10.1002/cpmc.2

INTRODUCTION

Mimiviruses are a group of recently discovered giant viruses that are distributed worldwide and infect amoeba of the *Acanthamoeba* genus and have been related to infections in a number of vertebrates. The first *Mimivirus* was isolated from a cooling tower water sample collected in a hospital in Bradford, England, during an outbreak of pneumonia in 1992 (La Scola et al., 2003). This isolate was named *Acanthamoeba polyphaga mimivirus* (APMV); due to its unique morphological and molecular features, it was included in a new viral family denominated *Mimiviridae*. The family *Mimiviridae* contains two genera: *Mimivirus* and *Cafeteriavirus* (King et al., 2012). Mimiviruses present peculiar features that make them unique viruses. One of the most notable characteristics is the 700-nm diameter particles; that size allows their retention on 0.2-μm filters which are commonly used in virus studies. The mimivirus particles are constituted of a core, an inner membrane, a capsid with semi-icosahedral symmetry, and external fibrils (Xiao et al., 2005). Members of the *Mimiviridae* family are composed of a double-stranded DNA genome of

Current Protocols in Microbiology 14G.1.1-14G.1.13, May 2016
Published online May 2016 in Wiley Online Library (wileyonlinelibrary.com).
doi: 10.1002/cpmc.2

~1.2 Mb that encodes more than 900 proteins, thereby surpassing the coding capacity of some bacteria (La Scola et al., 2003; Raoult et al., 2004; Moreira and Brochier-Armanet, 2008).

The *Mimiviridae* family was grouped with other families of giant virus known as nucleocytoplasmic large DNA viruses (NCLDVs) which include *Poxviridae*, *Asfarviridae*, *Iridoviridae*, *Ascoviridae*, *Phycodnaviridae*, and *Marseilleviridae*, leading to the proposition of the putative order "Megavirales" to group these families (Arslan et al., 2011). In addition, phylogenetic studies resulted in an exclusive clade for the giant viruses, distinct from Eukarya, Bacteria, and Archaea, generating the proposition of a fourth domain of life composed of the giant viruses (Boyer et al., 2010).

Due to the unique structure and genetic complexity of the mimiviruses, a new field of study was opened, and subsequently rekindled several debates regarding the definition of viruses, and their evolution and origin (Raoult and Forterre, 2008; Yamada, 2011).

Amoebae of the *Acanthamoeba* genus are the natural hosts of mimiviruses (La Scola et al., 2003). The APMV was first isolated from *A. polyphaga* culture, but it is also able to replicate in *A. castellanii*, *A. griffin*, *A. lenticulata*, and *A. quina* (La Scola et al., 2003; Claverie et al., 2009). Nevertheless, there is increasing evidence that these viruses have a wider host range, since APMV is internalized by different phagocyte cells (including human cells) and it has been shown that this virus can interact with the human interferon system (Ghigo et al., 2008; Silva et al., 2013). Mimivirus DNA has been detected in primates and bovines (Dornas et al., 2014a). A number of studies proposed that APMV could be pathogenic to humans and mice, and described the presence of antibodies against mimivirus in patients with nosocomial pneumonia (Raoult et al., 2006; Khan et al., 2007; Bousbia et al., 2013). Furthermore, mimiviruses have been isolated from samples collected from patients with pneumonia (Colson et al., 2013; Saadi et al., 2013a,b). It was also found that environmental exposure to mimivirus represents a risk factor in triggering autoimmunity to collagens (Shah et al., 2013).

Viruses belonging to the *Mimiviridae* family have been isolated from environments such as soil, air, aquatic environments, sewage treatment systems, hospital environments, and systems of ventilation and air conditioning, suggesting that they represent a ubiquitous group. The isolation reports were from England, France, Tunisia, U.S., Chile, and Brazil and also from oceans (La Scola et al., 2003; Arslan et al., 2011; Boughalmi et al., 2012; Legendre et al., 2012; Campos et al., 2014; Andrade et al., 2015; Santos Silva et al., 2015). Furthermore, metagenomic studies showed the presence of mimivirus DNA in the Sargasso Sea and other oceanic samples (Ghedin and Claverie, 2005; Monier et al., 2008; Yamada, 2011; Williamson et al., 2012). Mimiviruses and other giant viruses are an outstanding research field, and the rate of publications related to these viruses has increased since their discovery (Abrahão et al., 2014a).

This unit describes the methods utilized for replication (Basic Protocol 1), purification (Basic Protocol 2), and titration (Basic Protocol 3) of mimiviruses. Furthermore, it provides a procedure for *Acanthamoeba* cell maintenance (Support Protocol). Although there is evidence of mimivirus replication in human phagocytes (Ghigo et al., 2008; Silva et al., 2013), the *Acanthamoeba* sp. cell, mainly *A. castellanii*, is the preferred choice for mimivirus replication in the laboratory. Mimivirus purification is performed using sucrose cushions, which successfully increase the viral titer by concentrating the viral stock and removing non-viral elements. Although sucrose gradient methodology is commonly used for virus purification, for most biological and molecular experiments involving mimiviruses, the level of purification and titer obtained by pelleting through

a 24% sucrose cushion is sufficient. Although it is also possible to titrate mimiviruses using a plaque-forming unit assay (depending on the *Acanthamoeba* strain used), here we describe an end-point dilution assay.

CAUTION: Mimiviruses have been studied for a few years and many of their relationships with the environment and other hosts remain unclear. Furthermore, mimiviruses were initially associated with outbreaks of pneumonia and several studies reinforced the hypothesis of their clinical relevance. Although the role of mimiviruses as etiological agents of pneumonia is still under investigation, it is recommended that assays are done using a Class II biological safety cabinet. In addition, it is important to inactivate the viruses by autoclaving lab material containing viral residue before they are discarded. To clean the working area, a 70% ethanol solution can be used. Amoebae of the *Acanthamoeba* genus are the host for mimivirus propagation and titration. Although ubiquitous, these protists can cause opportunistic infections. Therefore, it is important to take precautions, such as not wearing contact lenses when handling these amoebae (Marciano-Cabral and Cabral, 2003). Despite the mimivirus particles being very stable in environmental and clinical substrates (Dornas et al., 2014b), it is recommended that the virus solutions are kept on ice while working. Although mimivirus particles are very stable when stored at −20°C, we recommend storing the purified virus stock at −80°C to avoid viral titer decrease.

MIMIVIRUS PRODUCTION

BASIC PROTOCOL 1

Mimiviruses can be replicated in large amounts of *Acanthamoeba* sp. culture to increase the virus stock. Mimiviruses should be produced in culture flasks containing *Acanthamoeba* sp. cultivated in peptone-yeast extract with glucose (PYG) medium. This medium has been shown to be efficient for mimivirus production and yielded titers that were ~6 logarithmic units higher than viral titers produced in Page's amoeba saline (PAS; Abrahão et al., 2014b). This protocol describes mimivirus production using *A. castellanii* cultures. However, this protocol can be used to produce mimivirus stocks in other amoeba species, such as *A. polyphaga*. After reaching confluence, the amoebae should be infected and incubated at 28°C until cytopathic effects (CPE) are induced, such as amoebae rounding, loss of motility, and lysis. To obtain efficient mimivirus replication, a multiplicity of infection (MOI) of 0.01 is recommended since low MOIs produce higher viral titers compared to high MOIs (Abrahão et al., 2014b). Supernatants from the infected amoeba should be collected and submitted to three cycles of freezing and thawing to release viruses from cells (Basic Protocol 2).

NOTE: It is recommended that the procedure be performed using sterile materials in a Class II Biosafety hood. *A. castellanii* cells can be obtained from the American Type Culture Collection (ATCC; ATCC 30234 and ATCC 30010).

Materials

Viral samples to be produced (a previously titrated seed pool; see Basic Protocol 3)
Acanthamoeba castellanii culture grown in tissue culture flasks (see Support Protocol)
Peptone-yeast extract with glucose (PYG) medium (see recipe)
Phosphate-buffered saline (PBS; see recipe)

Incubator (28° to 32°C)
150-cm^2 cell culture flasks
Refrigerated low-speed table-top centrifuge
50-ml conical centrifuge tubes
1.5-ml microcentrifuge tubes

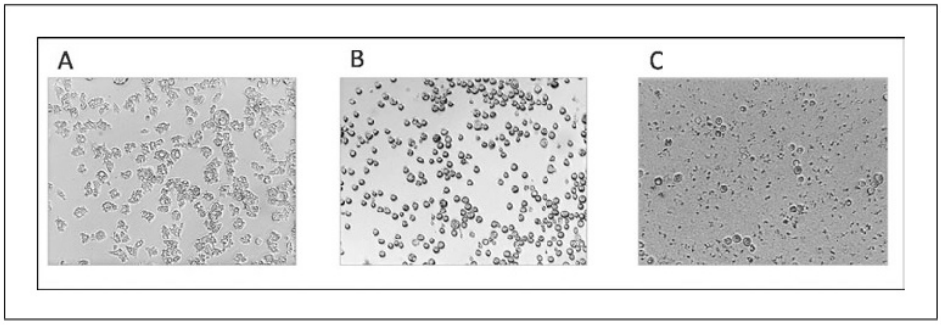

Figure 14G.1.1 Uninfected monolayer of *A. castellanii* (**A**). Mimivirus production in *A. castellanii* cells showing CPE at 48 hr (**B**) and 72 hr (**C**) post-infection.

37°C water bath
Inverted microscope

Mimivirus production in cultures of Acanthamoeba sp.

1. Add 7×10^6 *A. castellanii* cells in PYG medium to 150-cm^2 cell culture flasks (see Support Protocol).

   For biological assays, a total of six 150-cm^2 cell culture flasks is enough for mimivirus replication. However, the number of culture flasks can be increased according to necessity (e.g., production of virus for genome sequencing usually requires about twenty flasks).

2. Incubate at 28°C, 30 min to allow cells to adhere to the flasks.

   The cell culture flasks could be prepared 24 hr before infection. In this case, 150-cm^2 cell culture flasks should be prepared by seeding 3×10^6 A. castellanii per 150-cm^2 cell culture flask in 25 ml PYG medium and before the infection, cells should be counted to calculate the MOI.

3. Inoculate viral samples to be replicated, diluted in PBS, at MOI of 0.01.

   Low MOIs produce higher titers of infectious particles than high MOIs, since high MOIs may be related to a higher rate of defective particle formation.

4. Incubate at 28°C, ~72 hr.

   Check cells every day under the microscope to verify CPE (see Fig. 14G.1.1).

5. Collect supernatant and cell lysates using a pipet when CPE are observed in ~80% to 90% of cells.

   Typically, at MOI of 0.01, 48 hr after infection, all of the cells showed rounding and 72 hr after infection, ≥90% of the cells presented cell lysis; most of the cells have detached from the monolayer and lysed (see Fig. 14G.1.1).

6. Submit infected cells to three cycles of freezing at −80°C and thawing at room temperature to release the virus.

   To make the process faster, freezing could be performed in liquid nitrogen and thawing in a 37°C water bath. Alternatively, a hypotonic lysis buffer could be used to promote lysis of the remaining amoeba cells.

7. Freeze tubes in a −80°C freezer for storage until purification (*Basic Protocol 2*).

   If the virus will not be purified, the supernatant and cell lysates should be centrifuged at 600 × g for 5 min at 4°C. After that the debris should be discarded and the supernatant stored at −80°C.

MIMIVIRUS PURIFICATION

BASIC PROTOCOL 2

Sucrose cushions are sufficient to concentrate viral stocks, increase viral titer, and remove non-viral elements from the stock. For most of the biological and molecular experiments involving mimiviruses, including animal experimentation, this level of purification (sucrose cushion at 24%) is sufficient, and will be presented here. Also, if required, a simple filtration of virus-containing cell lysates through a 0.8-μm filter has been empirically tested, and shown to eliminate traces of the host genome.

In this protocol, the mimivirus-rich supernatants from the infected amoebae obtained during the mimivirus replication (Basic Protocol 1) were submitted to several rounds of homogenization in a Dounce, and purified by ultracentrifugation through a sucrose cushion (24%), followed by homogenization in PBS or Page's amoeba saline (PAS), and stored at −80°C.

Materials

Viral samples to be purified (see Basic Protocol 1)
24% sucrose solution (see recipe)
Phosphate-buffered saline (PBS; see recipe, or Page's amoeba saline [PAS; see recipe])

Dounce homogenizer, glass, with tight pestle
50-ml conical centrifuge tubes
Refrigerated low-speed table-top centrifuge
1.2-μm pore syringe filter
Ultracentrifuge (Sorvall Combi OTD or equivalent)
Beckman ultracentrifuge polypropylene tubes
0.6-ml microcentrifuge tubes

Mimivirus purification by sucrose cushion

1. Submit viral samples to be purified (see Basic Protocol 1) to 80 homogenization cycles in a Dounce homogenizer.

   Although not essential, this step is important to disrupt remaining amoeba cells and also to homogenize the solution.

2. Filter supernatant and cell lysates through a 1.2-μm syringe filter to remove amoeba debris.

   Although filtration allows purer viral stocks to be obtained, some particles may be retained in the filter, causing a decrease of viral titer.

3. Slowly layer 25 ml filtrate onto a 10-ml 24% sucrose cushion (see recipe) in ultracentrifuge tubes (see Fig. 14G.1.2).

   This protocol used a 24% sucrose cushion; a 22% sucrose cushion can also be used with success.

4. Balance centrifuge tubes.

5. Centrifuge at 35,250 × *g*, 30 min at 4°C in an ultracentrifuge.

   An easily visualized pellet will be formed (see Fig. 14G.1.2).

6. Homogenize pellet with a pipet in 500 μl PBS.

   This step should be performed on ice.

7. Store 5 to 10 μl aliquots (or in an appropriate volume according to specific needs) in 0.6-ml microcentrifuge tubes at −80°C; and then titrate virus (see Basic Protocol 3).

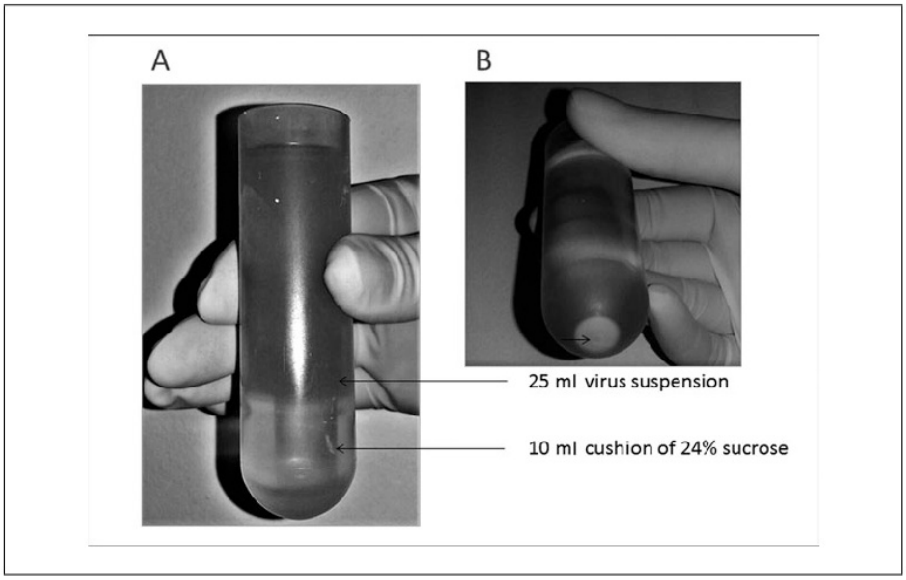

Figure 14G.1.2 Ultracentrifuge tube with 24% sucrose cushion prepared with virus overlay prior to centrifugation (**A**) and mimivirus pellet after ultracentrifugation (**B**).

BASIC PROTOCOL 3

MIMIVIRUS TITER CALCULATION BY END-POINT DILUTION ASSAY

End-point dilution assays are commonly performed to determine the viral titer of viruses that do not form plaques, such as mimiviruses, in *Acanthamoeba* sp. cells. This protocol describes the mimivirus end-point dilution assays. The procedure involves performing serial dilutions of the viral solution and inoculating in *A. castellanii* previously plotted on 96-well plates. After incubation, CPE are observed under an optical microscope and the titer ($TCID_{50}$) is calculated as described by Reed and Muench (1938).

Materials

Viral samples to be quantified
Acanthamoeba castellanii culture grown in tissue culture flasks (see Support Protocol)
Peptone-yeast extract with glucose (PYG) medium (see recipe)
Phosphate-buffered saline (PBS; see recipe, or Page's amoeba saline [PAS; see recipe])

Incubator (28°C)
96-well plates
75-cm^2 tissue culture flasks
Transfer pipet
1.5-ml microcentrifuge tubes (for serial dilutions of virus)
Inverted microscope

A. castellanii cells preparation

1. Setup 4×10^4 *A. castellanii* cells in 96-well plates in 100 µl PYG medium per well (see Support Protocol).
2. Prepare cells in PYG medium to a final volume of 11 ml for one 96-well plate.
3. Pipet 100 µl cell mixture into each well of a 96-well tissue culture plate.

	1	2	3	4	5	6	7	8	9	10	11	12
A	10^{-1}	10^{-2}	10^{-3}	10^{-4}	10^{-5}	10^{-6}	10^{-7}	10^{-8}	10^{-9}	10^{-10}	10^{-11}	Uninfected controls
B	10^{-1}	10^{-2}	10^{-3}	10^{-4}	10^{-5}	10^{-6}	10^{-7}	10^{-8}	10^{-9}	10^{-10}	10^{-11}	Uninfected controls
C	10^{-1}	10^{-2}	10^{-3}	10^{-4}	10^{-5}	10^{-6}	10^{-7}	10^{-8}	10^{-9}	10^{-10}	10^{-11}	Uninfected controls
D	10^{-1}	10^{-2}	10^{-3}	10^{-4}	10^{-5}	10^{-6}	10^{-7}	10^{-8}	10^{-9}	10^{-10}	10^{-11}	Uninfected controls
E	10^{-1}	10^{-2}	10^{-3}	10^{-4}	10^{-5}	10^{-6}	10^{-7}	10^{-8}	10^{-9}	10^{-10}	10^{-11}	Uninfected controls
F	10^{-1}	10^{-2}	10^{-3}	10^{-4}	10^{-5}	10^{-6}	10^{-7}	10^{-8}	10^{-9}	10^{-10}	10^{-11}	Uninfected controls
G	10^{-1}	10^{-2}	10^{-3}	10^{-4}	10^{-5}	10^{-6}	10^{-7}	10^{-8}	10^{-9}	10^{-10}	10^{-11}	Uninfected controls
H	10^{-1}	10^{-2}	10^{-3}	10^{-4}	10^{-5}	10^{-6}	10^{-7}	10^{-8}	10^{-9}	10^{-10}	10^{-11}	Uninfected controls

Figure 14G.1.3 Schematic figure to prepare 96-well plaque for mimivirus titration by end-point dilution assay.

One 75-cm^2 tissue culture flask, when confluent, contains ~1.5× 10^7 cells, and each well of the 96-well plate should be seeded with 4 × 10^4 A. castellanii. Therefore, a single 75-cm^2 tissue culture flask is needed to prepare four 96-well plates.

4. Incubate at 28°C, 30 min to adhere the cells.

   The 96-well plates could be prepared 24 hr before infection. In this case, the 96-well plates should be prepared by seeding 3 × 10^4 A. castellanii per well in 100 µl of PYG medium.

5. Visualize *A. castellanii* cells using a microscope.

   The cells should be 80% to 90% confluent.

Cell infection

6. If the sample to be titrated is directly derived from mimivirus production (see Basic Protocol 1), submit samples to three cycles of freezing and thawing to release viruses trapped in the cells. If the sample to be titrated is derived from mimivirus purification (Basic Protocol 2) dilute samples directly.

7. For each sample to be titrated, perform serial ten-fold dilutions (from 10^{-1} to 10^{-11}) of the virus final volume of 500 µl in PBS (or PAS), in microtubes.

   During the dilution it is important to pipet from the surface of the sample to be diluted and dispense the sample on the tube wall of the next tube. It is necessary to change tips between dilutions.

8. Then add directly onto the amoebae monolayer with 100 µl medium, 100 µl of each dilution to a single well in the plate, as shown in Figure 14G.1.3.

   Each dilution is usually titrated in duplicate.

9. Inoculate one row of each plate with PBS (or PAS) to serve as uninfected controls, as shown in Figure 14G.1.3.

10. Incubate samples at 28°C, 96 hr and observe CPE in an inverted microscope.

    It is recommended CPE be observed in each well daily.

    For mimiviruses the CPE are rounding, loss of motility, and cell lysis of amoebae.

11. Calculate titer as described by Reed and Muench (1938).

SUPPORT PROTOCOL

GROWTH AND PASSING OF *ACANTHAMOEBA* CULTURE

Amoebae of the *Acanthamoeba* genus are mimivirus hosts. The first mimivirus was originally isolated from *A. polyphaga*, but in the laboratory, the following can also be cultured: *A. castellanii*, *A. griffin*, *A. lenticulata*, and *A. quina* cultures. *A. polyphaga* or *A. castellanii* cells are the most widely used for mimivirus replication. In this protocol, the *A. castellanii* are cultivated at 28°C in PYG medium and subcultured until confluent cell monolayers are obtained. The amoebae should be counted when splitting.

Materials

Acanthamoeba castellanii cells (ATCC; ATCC 30234 and ATCC 30010)
Peptone-yeast extract with glucose (PYG) medium (see recipe)
Ice

Incubator (28°C)
25-, 75-, and 150-cm^2 tissue culture flasks
Neubauer chamber and glass cover (for cell counting)
1.5-ml microcentrifuge tubes
50-ml tubes
Inverted microscope

NOTE: Preparation of *A. castellanii* cultures: All solutions and equipment coming into contact with *A. castellanii* cultures must be sterile, and aseptic technique should be used accordingly.

1. Maintain *A. castellanii* cultures at 28°C in 75-cm^2 tissue culture flasks containing 15 ml PYG medium.

Cell splitting

2. Incubate cell culture flasks containing *A. castellanii* culture in an ice bath 5 min to detach the cells.
3. Gently knock flask to detach cells and observe under an inverted microscope
4. Determine cell count using a Neubauer chamber.

   For counting, a dilution of the cells should be prepared. Typically, the concentration range for a cell count with a Neubauer chamber is between 250,000 cells/ml and 2.5 million cells/ml. The Neubauer chamber should be loaded with 10 µl of the dilution with a micropipet.

5. Subculture cells in a new tissue culture flask, adding 100,000; 500,000; and 1,000,000 cells to 25-, 75-, and 150-cm^2 tissue culture flasks containing 5 ml, 15 ml, and 25 ml PYG medium, respectively, according to requirement.
6. Incubate at 28°C until cell confluence is reached.

   Perform cell splitting at least three times weekly.

   The same procedure should be used to prepare plates of cells for titration (see Basic Protocol 3).

REAGENTS AND SOLUTIONS

Use deionized, distilled water in all recipes and protocol steps unless noted otherwise. For common stock solutions, see APPENDIX 2A.

NOTE: Media recipes were calculated for 1 liter but can be modified for smaller or larger volumes.

NOTE: Solutions should be prepared in sterile ultrapure water.

Page's amoeba saline (PAS)

Solution A:
1.20 g NaCl
0.04 g $MgSO_4 \cdot 7H_2O$
1.42 g Na_2HPO_4
1.36 g KH_2PO_4
Dissolve in distilled water (dH_2O) to a final volume of 100 ml.
Solution B:
0.04 g $CaCl_2 \cdot 2H_2O$.
Dissolve in dH_2O to final volume of 100 ml.
For 1 liter:
Add 10 ml of solution A and 10 ml of solution B to 980 ml dH_2O.
Check pH and adjust to pH 6.91 if necessary, using NaOH 10 M or HCl 4 M.
Autoclave for 20 min.
Store at room temperature or at 4°C after opening for up to 6 months.

Peptone-yeast extract with glucose (PYG) medium

Solution A:
Dissolve the following components in 300 ml ultrapure H_2O:
0.98 g $MgSO_4 \cdot 7H_2O$
0.06 g $CaCl_2$
9.0 g glucose ($C_6H_{12}O_6$)
0.02 g ammonium iron(II) sulfate hexahydrate ($(NH_4)_2Fe(SO_4) \cdot 6H_2O$)
0.40 g $Na_2HPO_4 \cdot 7H_2O$
0.34 g KH_2PO_4
1.00 g sodium citrate tribasic dihydrate ($C_6H_5Na_3O_7 \cdot 2H_2O$)
Solution B:
Dissolve 20.0 g Bacto-peptone extract in 200 ml ultrapure H_2O.
Solution C:
Dissolve 2.0 g yeast extract in 200 ml ultrapure H_2O.
Combine solutions A, B, and C, mix well, and add ultrapure H_2O to a final volume of 1 liter. Check pH; adjust to pH 6.5 if necessary, using 10 M NaOH or 4 M HCl. Autoclave at 121°C for 20 min and allow to cool. Filter the medium; add fetal bovine serum, antibiotics, and fungicides to the medium at the following concentrations:
7% FBS
25 mg/ml amphotericin B
500 U/ml penicillin
50 mg/ml gentamicin
Store at 4°C for up to 6 months.

Phosphate-buffered saline (PBS)

For 1 liter:
8 g NaCl (137 mM)
1.44 g Na_2HPO_4 (10 mM)
0.2 g KCl (2.7 mM)
0.24 g KH_2PO_4 (2 mM)
Dissolve in 900 ml ultrapure H_2O.
Check pH and adjust to pH 7.4 if necessary, using NaOH 10 M or HCl 4 M.
Make up volume to 1 liter with ultrapure H_2O.
Autoclave in 500-ml bottles for 20 min.
Store at room temperature or at 4°C after opening for up to 6 months.

Sucrose, 24% (w/v)

For 1 liter:
240 g sucrose
Dissolve in 800 ml ultrapure H_2O, mixing well on a magnetic stirrer.
Adjust volume to 1 liter.
Prepare immediately or store in 250-ml aliquots at 4°C for up to 3 months.

COMMENTARY

Background Information

The first mimivirus was isolated in 1992 and has been investigated as a putative etiological agent of pneumonia (La Scola et al., 2003, 2005). However, its characterization as a virus occurred only in 2003. The study of this sample was delayed for a decade due to difficulty in characterization of the mimivirus, which was initially thought to be a bacterium. In addition, its size was unexpected for a viral particle, which may have delayed its isolation, consequent discovery, and study. Traditionally, viruses were thought to pass through 0.2-μm filters in which this virus is retained. The difficulty of characterizing the mimivirus was mainly due to the fact that these viruses have unique characteristics that differentiate them from most viruses described to date. Among these features are its extensive size (~700 nm) and genome (~1.2 million base pairs). These viruses show an extensive gene content that had not previously been attributed to any virus. These and other features make the mimivirus one of the most complex viruses described to date.

Electron microscopy was one of the main techniques responsible for solving the mystery surrounding the mimivirus. Because of their unique morphological features, microscopy has also been a very important tool in the characterization of these viruses. Since the discovery and characterization of the first *Mimivirus*, the search for mimiviruses has been conducted in different environments and clinical samples, and the mimivirus replication in the laboratory has been performed in amoebae of the *Acanthamoeba* genus, its natural host, as described in this section.

Mimivirus study is an open field for basic and applied studies. However, to improve research involving the characterization of these viruses as well as elucidating their clinical and environmental significance, it was necessary to establish and improve the protocols for their study; for example, to test and determine the best conditions for viral isolation and replication. Analyzing growth conditions, obtaining purified virus at high titers as well as searching for fast, efficient, and inexpensive viral production strategies are sine qua non points in the scientific routine, and are directly linked to further understanding the biology of viruses (Kusnetsov et al., 2010; Mutsafi et al., 2013), but require a standardization process. Most of the newly identified mimiviruses have been successfully replicated, purified, and titrated using the methods described here. However, due to the increasing number of *Mimivirus* isolates, it is necessary for these protocols to be routinely assessed for their suitability for new samples that have been isolated. The interest in *Mimivirus* continues to increase among researchers worldwide, creating the need to establish methods and descriptions to improve *Mimivirus* study and provide a basis for their study in the laboratory.

Critical Parameters and Troubleshooting

As in other cell cultures, the *Acanthamoeba* sp. cultures are very susceptible to contamination with bacteria, filamentous fungus, and yeast. To overcome this critical parameter and to minimize contamination, preventive measures such as the use of medium containing large amounts of antimicrobial agents have been taken (mainly when isolating viruses from environmental samples). However, in specific cases, the antimicrobial agents can be reduced or even eliminated.

All protocols described here involving cell culture must be performed in a biosafety cabinet and with aseptic technique. Furthermore it is essential that the cabinet and the work surfaces are cleaned with 70% ethanol. The PYG medium should be autoclaved and can be filtered after the autoclave step to remove salt crystals. Another critical point to consider in preparation of *Acanthamoeba* sp. cultures is the procedure in step 2 of the Support Protocol, in which the amoeba cultures are kept in an ice bath to aid detachment. It is essential that the time of 5 min is followed because amoeba cultures maintained in an ice bath for a longer time period could encyst due to physiological stress. A second critical parameter is the cultivation atmosphere because the *Acanthamoeba* culture should be incubated

without additional CO_2. It is essential that the plates and flasks containing *Acanthamoeba* sp. cultures be carefully maintained, completely sealed, and closed.

Mimivirus replication and titration by end-point dilution assays are very sensitive and reliable. However, the success of these techniques depends on the state of the *Acanthamoeba* sp. cultures used. During repeated subculture of *Acanthamoeba* sp., passage modifications may occur, which affect virus production. Therefore, we recommend *Acanthamoeba* sp. cultures be grown for no more than ten passages to try to reduce variability, and keep a stock of Acanthamoeba cysts to be excysted when necessary.

For mimivirus production and titration, it is necessary to prepare the culture plates and flasks in advance and wait for cells to adhere. Furthermore, at this step it is essential to seed a consistent number of cells because this is a critical parameter for titration by end-point dilution assays. The seeding of 4×10^4 cells per well in 96-well plates for mimivirus titration and 7×10^6 cells per culture flasks for mimivirus production is ideal when cells are infected on the same day. If necessary the cells can be prepared ~24 hr before infection, as described in step 2 of Basic Protocol 1 and step 4 of Basic Protocol 3. However, in this case, it is necessary to add a lower concentration of cells per well. One of the most important parameters for mimivirus production is the MOI. Thus, the cell count is a critical parameter to obtain an MOI of 0.01.

One of the critical parameters for mimivirus purification is the quality of the sample to be purified. It is therefore very important that the viral production protocol is carried out properly and that the viral titer is high enough. Furthermore, during the procedure of placing the virus over the sucrose solution, it is important not to disturb the sucrose solution. It is also important to handle the ultracentrifuge tube carefully after the addition of the viral solution.

Anticipated Results

After mimivirus production (from a viral seed pool; Basic Protocol 1) the titers obtained in the laboratory typically ranged between 10^6 and 10^7 $TCID_{50}$/ml. Also, after 48 to 72 hr of incubation, at an MOI of 0.01, ≥90% of the cells presented CPE with most of the cells having detached from the monolayer. The CPE most commonly observed in amoeba infected with mimivirus are amoebae rounding, loss of motility, and lysis (see Fig. 14G.1.1). The titers can be increased by purifying the produced virus. Viral purification by sucrose cushion (Basic Protocol 2) results in the formation of easily visualized pellets, as shown in Figure 14G.1.2. After viral purification, titers typically range between 10^9 and 10^{11} $TCID_{50}$/ml. As described, mimivirus can be titrated by the end-point dilution assay (Basic Protocol 3). When the growth and splitting of amoebae in culture are performed using the specific conditions and amoeba concentration indicated in Support Protocol (every 2 days), the amoebae monolayer quickly becomes confluent and can be counted, split, and used to prepare plates.

Time Considerations

It generally takes 1 to 2 hr to split and prepare the amoebae culture for infection. Preparation of the plate to perform titration generally takes 1 to 2 hr. For PYG medium preparation, a complete day is necessary, since the medium is autoclaved and only after it is cold should it be filtered. However, PYG medium can be prepared and stored at 4°C until use.

In successful experiments, it generally takes 4 days to propagate mimivirus (Basic Protocol 1), a single day for mimivirus purification (Basic Protocol 2), and another 5 days to determine the titer (Basic Protocol 3). The infection for mimivirus replication generally takes ~72 hr, since the infection is performed by the inoculation of the samples in the amoebae monolayer at adequate MOI. After mimivirus production, the sample can be purified on the same day or stored at −80°C until purification. Amoeba cells infected with mimivirus at an MOI of 0.01 generally show CPE 24 to 72 hr after infection. The time of incubation can vary among the different isolates of mimivirus. Samples with decreased rates of growth can be incubated as early as 72 hr. Then, in ~3 days, the virus can be collected.

Mimivirus purification (Basic Protocol 2) generally takes about 8 hr to perform. This protocol involves homogenizing with a Dounce tissue grinder, centrifugation, and 30 min of ultracentrifugation through a sucrose cushion. All of these steps can be performed in a single day.

The mimivirus titration of the viral sample by end-point dilution assay is done over several days (5 days), but the plates can be prepared and infected in about 30 min on the first day of the procedure (Basic Protocol 3). For example, on day 1, cells are seeded into a 96-well dish and incubation of ~30 min is maintained; after this, the virus is diluted and added to the plate. This process takes ~1 hour.

In this case, most of the time will be spent waiting for cell seeding. While the amoebae are being incubated to adhere to the plate, samples can be diluted for titration. The analyses and titer calculations can be performed in ~1 hr.

Acknowledgements

We thank our colleagues from Laboratório de Vírus of Universidade Federal de Minas Gerais and the research team of URMITE, Aix Marseille Université for their excellent support. We would also like to thank Conselho Nacional de Desenvolvimento Científico e Tecnológico (CNPq), Coordenação de Aperfeiçoamento de Pessoal de Nivel Superior (CAPES), Fundação de Amparo à Pesquisa do Estado de Minas Gerais (FAPEMIG), and Pro-Reitoria de Pesquisa da Universidade Federal de Minas Gerais (PRPq-UFMG) for the financial support.

Literature Cited

Abrahão, J.S., Dornas, F.P., Silva, L.C., Almeida, G.M., Boratto, P.V.M., Colson, P., La Scola, B., and Kroon, E.G. 2014a. Acanthamoeba polyphaga mimivirus and other giant viruses: An open field to outstanding discoveries. *Virol. J.* 11:120. doi: 10.1186/1743-422X-11-120.

Abrahão, J.S., Boratto, P.V.M., Dornas, F.P., Silva, L.C., Campos, R.K., Almeida, G.M., Kroon, E.G., and La Scola, B. 2014b. Growing a giant: Evaluation of the virological parameters for mimivirus production. *J. Virol. Methods* 207:6-11. doi: 10.1016/j.jviromet.2014.06.001.

Andrade, K.R., Boratto, P.V.M., Rodrigues, F.P., Silva, L.C., Dornas, F.P., Pilotto, M.R., La Scola, B., Almeida, G.M., Kroon, E.G., and Abrahão, J.S. 2015. Oysters as hot spots for mimivirus isolation. *Arch. Virol.* 160:477-82. doi: 10.1007/s00705-014-2257-2.

Arslan, D., Legendre, M., Seltzer, V., Abergel, C., and Claverie, J. 2011. Distant Mimivirus relative with a larger genome highlights the fundamental features of Megaviridae. *Proc. Natl. Acad. Sci. U.S.A.* 108:17486-17491. doi: 10.1073/pnas.1110889108.

Boughalmi, M., Saadi, H., Pagnier, I., Colson, P., Fournous, G., Raoult, D., and La Scola, B. 2012. High-throughput isolation of giant viruses of the Mimiviridae and Marseilleviridae families in the Tunisian environment. *Environ. Microbiol.* 53:344-353. doi: 10.1111/1462-2920.12068.

Bousbia, S., Papazian, L., Saux, P., Forel, J.M., Auffray, J.P., Martin, C., Raoult, D., and La Scola, B. 2013. Serologic prevalence of amoeba-associated microorganisms in intensive care unit pneumonia patients. *PLoS One* 8:e58111. doi: 10.1371/journal.pone.0058111.

Boyer, M., Madoui, M.A., Gimenez, G., La Scola, B., and Raoult, D. 2010. Phylogenetic and phyletic studies of informational genes in genomes highlight existence of a 4 domain of life including giant viruses. *PLoS One* 5:e15530. doi: 10.1371/journal.pone.0015530.

Campos, R.K., Boratto, P.V., Assis, F.L., Aguiar, E.R.G.R., Silva, L.C.F., Albarnaz, J.D., Dornas, F.P., Trindade, G.S., Ferreira, P.C.P., Marques, J.T., Roberts, C., Raoult, D., Kroon, E.G., La Scola, B., and Abrahao, J.S. 2014. Samba virus: A novel mimivirus from a giant rain forest, the Brazilian Amazon. *Virol. J.* 11:95. doi: 10.1186/1743-422X-11-95.

Claverie, J.M., Grzela, R., Lartigue, A., Bernadac, A., Nitsche, S., Vacelet, J., Ogata, H., and Abergel, C. 2009. Mimivirus and Mimiviridae: Giant viruses with an increasing number of potential hosts, including corals and sponges. *J. Invertebr. Pathol.* 101:172-180. doi: 10.1016/j.jip.2009.03.011.

Colson, P., La Scola, B., and Raoult, D. 2013. Giant viruses of amoebae as potential human pathogens. *Intervirology* 56:376-385. doi: 10.1159/000354558.

Dornas, F.P., Rodrigues, F.P., Boratto, P.V., Silva, L.C., Ferreira, P.C., Bonjardim, C.A., Trindade, G.S., Kroon, E.G., La Scola, B., and Abrahao, J.S. 2014a. Mimivirus circulation among wild and domestic mammals, Amazon Region, Brazil. *Emerg. Infect. Dis.* 20:469-472. doi: 10.3201/eid2003.131050.

Dornas, F.P., Silva, L.C., de Almeida, G.M., Campos, R.K., Boratto, P.V., Franco-Luiz, A.P., La Scola, B., Ferreira, P.C., Kroon, E.G., and Abrahão, J.S. 2014b. Acanthamoeba polyphaga mimivirus stability in environmental and clinical substrates: Implications for virus detection and isolation. *PLoS One* 9:e87811. doi: 10.1371/journal.pone.0087811.

Ghedin, E., and Claverie, J.M. 2005. Mimivirus relatives in the Sargasso sea. *Virol. J.* 2:62. doi: 10.1186/1743-422X-2-62.

Ghigo, E., Kartenbeck, J., Lien, P., Pelkmans, L., Capo, C., Mege, J.L., and Raoult, D. 2008. Ameobal pathogen mimivirus infects macrophages through phagocytosis. *PLoS Pathog.* 4:e1000087. doi: 10.1371/journal.ppat.1000087.

Khan, M., La Scola, B., Lepidi, H., and Raoult, D. 2007. Pneumonia in mice inoculated experimentally with *Acanthamoeba polyphaga mimivirus*. *Microb. Pathog.* 42:56-61. doi: 10.1016/j.micpath.2006.08.004.

King, A.M.Q., Adams, M.J., Carstens, E.B., and Lefkowitz, E.J. 2012. Virus Taxonomy: Classification and Nomenclature of Viruses: Ninth Report of the International Committee on Taxonomy of Viruses. Elsevier, New York.

Kusnetsov, Y.G., Xiao, C., Sun, S., Raoult, D., Rossmann, M., and McPherson, A. 2010. Atomic force microscopy investigation of the giant mimivirus. *Virology* 404:127-137. doi: 10.1016/j.virol.2010.05.007.

La Scola, B., Marrie, T.J., Auffray, J.P., and Raoult, D. 2005. Mimivirus in pneumonia patients. *Emerg. Infect. Dis.* 11:449-452. doi: 10.3201/eid1103.040538.

La Scola, B., Audic, S., Robert, C., Jungang, L., de Lamballerie, X., Drancourt, M., Birtles, R., Claverie, J.M., and Raoult, D. 2003. A giant virus in amoebae. *Science* 299:2033. doi: 10.1126/science.1081867.

Legendre, M., Arslan, D., Abergel, C., and Claverie, J.M. 2012. Genomics of Megavirus and the elusive fourth domain of Life. *Commun. Integr. Biol.* 5:102-106. doi: 10.4161/cib.18624.

Marciano-Cabral, F. and Cabral, G. 2003. *Acanthamoeba* spp. as agents of disease in humans. *Clin. Microbiol. Ver.* 16:273-307. doi: 10.1128/CMR.16.2.273-307.2003.

Monier, A., Larsen, J.B., Sandaa, R.A., Bratbak, G., Claverie, J.M., and Ogata, H. 2008. Marine mimivirus relatives are probably large algal viruses. *Virol. J.* 5:12. doi: 10.1186/1743-422X-5-12.

Moreira, D., and Brochier-Armanet, C. 2008. Giant viruses, giant chimeras: The multiple evolutionary histories of mimivirus genes. *BMC Evol. Biol.* 8:12. doi: 10.1186/1471-2148-8-12.

Mutsafi, Y., Shimoni, E., Shimon, A., and Minsky, A. 2013. Membrane assembly during the infection cycle of the giant mimivirus. *PLoS Pathog.* 9:5. doi: 10.1371/journal.ppat.1003367.

Raoult, D., Audic, S., Robert, C., Abergel, C., Renesto, P., Ogata, H., La Scola, B., Suzan, M., and Claverie, J.M. 2004. The 1.2-megabase genome sequence of mimivirus. *Science* 306:1344-1350. doi: 10.1126/science.1101485.

Raoult, D., and Forterre, P. 2008. Redefining viruses: Lessons from mimivirus. *Nat. Rev. Microbiol.* 6:315-319. doi: 10.1038/nrmicro1858.

Raoult, D., Renesto, P., and Brouqui, P. 2006. Laboratory infection of a technician by mimivirus. *Ann. Intern. Med.* 144:702-703. doi: 10.7326/0003-4819-144-9-200605020-00025.

Reed, L.J., and Muench, H., 1938. A simple method of estimating fifty percent endpoints. *Am. J. Hyg.* 27:493-497.

Saadi, H., Pagnier, I., Colson, P., Cherif, J.K., Beji, M., Boughalmi, M., Azza, S., Armstrong, N., Robert, C., Fournous, G., La Scola, B., and Raoult, D. 2013a. First isolation of *Mimivirus* in a patient with pneumonia. *Clin. Infect. Dis.* 57:127-134. doi: 10.1093/cid/cit354.

Saadi, H., Reteno, D.G., Colson, P., Aherfi, S., Minodier, P., Pagnier, I., Raoult, D., and La Scola, B. 2013b. Shan virus: A new mimivirus isolated from the stool of a Tunisian patient with pneumonia. *Intervirology* 56:424-429. doi: 10.1159/000354564.

Santos Silva, L.K., Arantes, T.S., Andrade, K.R., Lima Rodrigues, R.A., Miranda Boratto, P.V., de Freitas Almeida, G.M., Kroon, E.G., La Scola, B., Clemente, W.T., and Santos Abrahão, J. 2015. High positivity of mimivirus in inanimate surfaces of a hospital respiratory-isolation facility, Brazil. *Clin. Virol.* 66:62-65. doi: 10.1016/j.jcv.2015.03.008.

Shah, N., Hülsmeier, A.J., Hochhold, N., Neidhart, M., Gay, S., and Hennet, T. 2013. Exposure to mimivirus collagen promotes arthritis. *J. Virol.* 88:838-845. doi: 10.1128/JVI.03141-13.

Silva, L.C., Almeida, G.M., Oliveira, D.B., Dornas, F.P., Campos, R.K., La Scola, B., Ferreira, P.C., Kroon, E.G., and Abrahao, J.S. 2013. A resourceful giant: APMV is able to interfere with the human type I interferon system. *Microbes Infect.* 16:187-195. doi: 10.1016/j.micinf.2013.11.011.

Williamson, S.J., Allen, L.Z., Lorenzi, H.A., Fadrosh, D.W., Brami, D., Thiagarajan, M., McCrow, J.P., Tovchigrechko, A., Yooseph, S., and Venter, J.C. 2012. Metagenomic exploration of viruses throughout the Indian Ocean. *PLoS One* 7:e42047. doi: 10.1371/journal.pone.0042047.

Xiao, C., Chipman, P.R., Battisti, A.J., Bowman, V.D., Renesto, P., Raoult, D., and Rossmann, M.G. 2005. Cryo-electron microscopy of the giant mimivirus. *J. Mol. Biol.* 353:493-496. doi:10.1016/j.jmb.2005.08.060.

Yamada, T. 2011. Giant viruses in the environment: Their origins and evolution. *Curr. Opin. Virol.* 1:58-62. doi: 10.1016/j.coviro.2011.05.008.